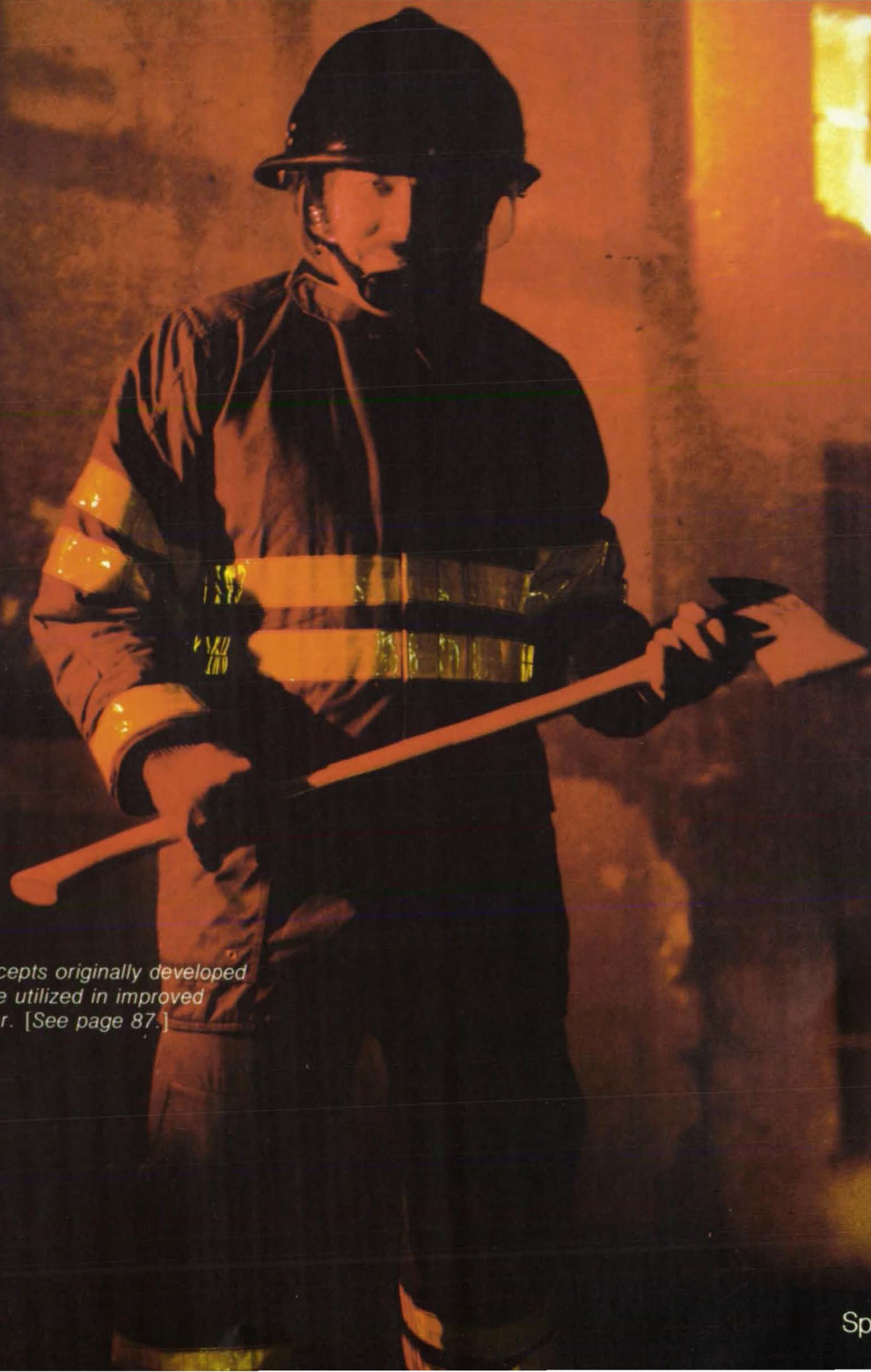


# NASA Tech Briefs

National  
Aeronautics and  
Space  
Administration



*Materials and design concepts originally developed for the space program are utilized in improved firefighters protective gear. [See page 87.]*

# About the NASA Technology Utilization Program

The National Aeronautics and Space Act of 1958, which established NASA and the United States civilian space program, requires that "The Administration shall provide for the widest practicable and appropriate dissemination of information concerning its activities and the results thereof."

To help carry out this objective, NASA's Technology Utilization (TU) Program was established in 1962. Now, as an element of NASA's Technology Transfer Division, this program offers a variety of valuable services to help transfer aerospace technology to nonaerospace applications, thus assuring American taxpayers maximum return on their investment in space research; thousands of spinoffs of NASA research have already occurred in virtually every area of our economy.

The TU program has worked for engineers, scientists, technicians, and businessmen; and it can work for you.

## NASA Tech Briefs

*Tech Briefs* is published quarterly and is free to engineers in U.S. industry and to other domestic technology transfer agents. It is both a current-awareness medium and a problem-solving tool. Potential products . . . industrial processes . . . basic and applied research . . . shop and lab techniques . . . computer software . . . new sources of technical data . . . concepts . . . can be found here. The short section on New Product Ideas highlights a few of the potential new products contained in this issue. The remainder of the volume is organized by technical category to help you quickly review new developments in your areas of interest. Finally, a subject index makes each issue a convenient reference file.

## Further Information on Innovations

Although some new technology announcements are complete in themselves, most are backed up by Technical Support Packages (TSP's). TSP's are available without charge and may be ordered by simply completing a TSP Request Card found at the back of this volume. Further information on some innovations is available for a nominal fee from other sources, as indicated. In addition, Technology Utilization Officers at NASA Field Centers will often be able to lend necessary guidance and assistance.

## Patent Licenses

Patents have been issued to NASA on some of the inventions described, and patent applications have been submitted on others. Each announcement indicates patent status, if applicable.

## Other Technology Utilization Services

To assist engineers, industrial researchers, business executives, city officials, and other potential users in applying space technology to their problems, NASA sponsors Industrial Applications Centers. Their services are described on page A7. In addition, an extensive library of computer programs is available through COSMIC, the Technology Utilization Program's outlet for NASA-developed software.












## Applications Program

NASA conducts applications engineering projects to help solve public-sector problems in such areas as safety, health, transportation, and environmental protection. Applications teams, staffed by professionals from a variety of disciplines, assist in this effort by working with Federal agencies and health organizations to identify critical problems amenable to solution by the application of existing NASA technology.

## Reader Feedback

We hope you find the information in *NASA Tech Briefs* useful. A reader-feedback card has been included because we want your comments and suggestions on how we can further help you apply NASA innovations and technology to your needs. Please use it; or if you need more space, write to the Director, Technology Transfer Division, P. O. Box 8757, Baltimore/Washington International Airport, Maryland 21240.

National  
Aeronautics and  
Space  
Administration

NASA TU Services	A3	Technology Utilization services that can assist you in learning about and applying NASA technology.	
New Product Ideas	A9	A summary of selected innovations of value to manufacturers for the development of new products.	
Tech Briefs	1	<b>Electronic Components and Circuits</b>	
	13	<b>Electronic Systems</b>	
	21	<b>Physical Sciences</b>	
	33	<b>Materials</b>	
	43	<b>Life Sciences</b>	
	49	<b>Mechanics</b>	
	73	<b>Machinery</b>	
	85	<b>Fabrication Technology</b>	
	111	<b>Mathematics and Information Sciences</b>	
	Subject Index	115	Items in this issue are indexed by subject; a cumulative index will be published yearly.

*COVERS: The photographs on the front and back covers illustrate developments by NASA that have resulted in nonaerospace spinoffs. Further information on the Firefighters Protective Gear may be found in "Improved Clothing for Firefighters" (MFS-25546) on page 87 of this issue of NASA Tech Briefs. To find out about the Heated Transparent Materials, Circle 89 on the TSP Request Card.*

## *About This NASA Publication*

NASA Tech Briefs, a quarterly publication, is distributed free to qualified U.S. citizens to encourage commercial application of U.S. space technology. For information on publications and services available through the NASA Technology Utilization Program, write to the Director, Technology Transfer Division, P. O. Box 8757, Baltimore/Washington International Airport, Maryland 21240.

"The Administrator of National Aeronautics and Space Administration has determined that the publication of this periodical is necessary in the transaction of the public business required by law of this Agency. Use of funds for printing this periodical has been approved by the Director of the Office of Management and Budget."

## *Change of Address*

If you wish to have NASA Tech Briefs forwarded to your new address, use one of the Subscriptions cards enclosed in the back of this volume of NASA Tech Briefs. Be sure to check the appropriate box indicating change of address.

## *Communications Concerning Editorial Matter*

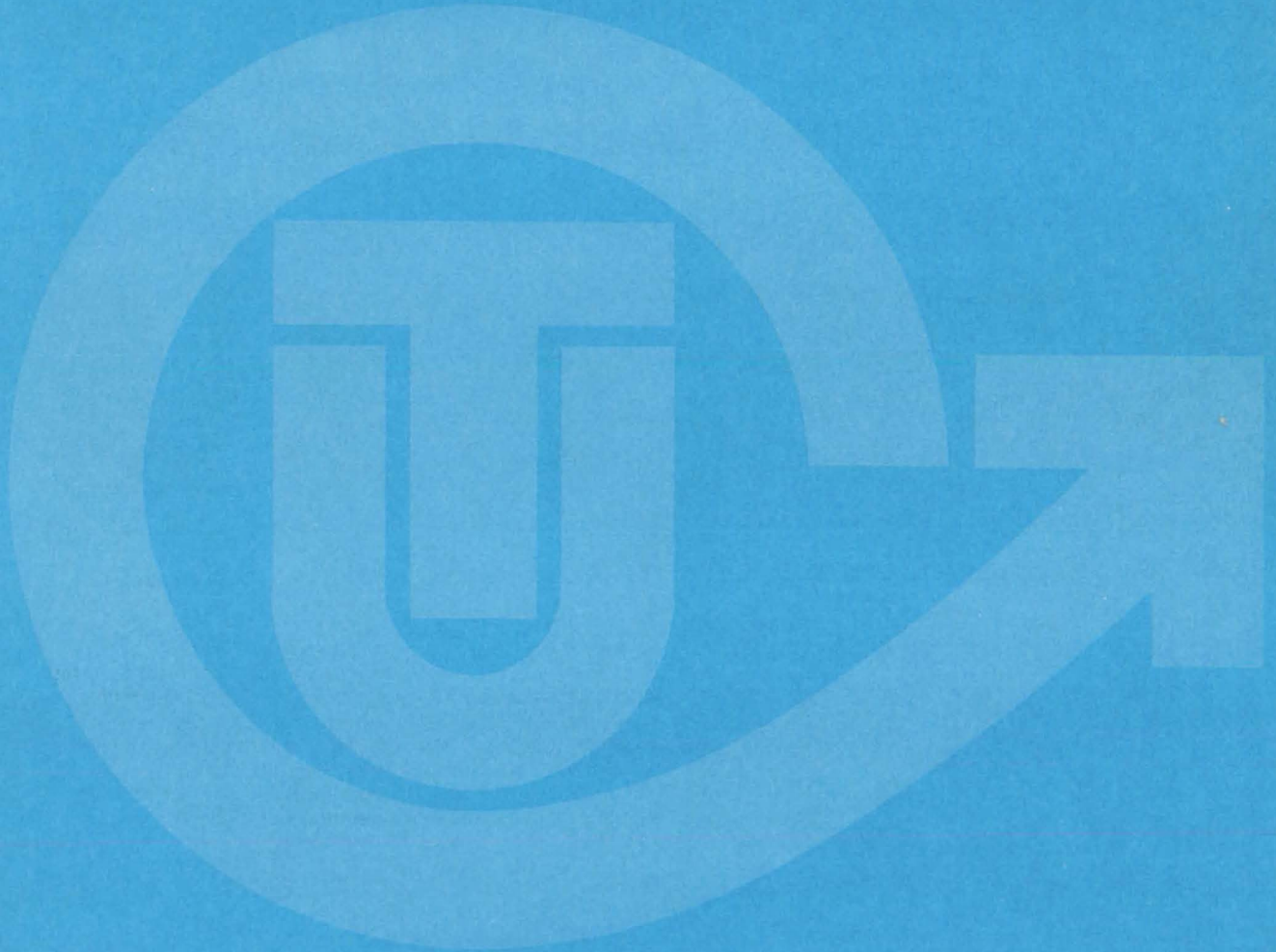
For editorial comments or general communications about NASA Tech Briefs, you may use the Feedback card in the back of NASA Tech Briefs, or write to: The Publications Manager, Technology Transfer Division (ETD-6), NASA Headquarters, Washington, DC 20546. Technical questions concerning specific articles should be directed to the Technology Utilization Officer of the sponsoring NASA Center (addresses listed on page A4).

## *Acknowledgements*

NASA Tech Briefs is published quarterly by the National Aeronautics and Space Administration, Technology Utilization Branch, Washington, DC: Administrator: **Robert A. Frosch**; Director, Technology Transfer Division: **Floyd I. Roberson**; Publications Manager: **D. W. Orrick**. Prepared for the National Aeronautics and Space Administration by **Logical Technical Services Corp.**: Editor-in-Chief: **Jay Kirschenbaum**; Art Director: **Ernest Gillespie**; Senior Editor: **Jerome Rosen**; Chief Copy Editor: **Oden Browne**; Staff Editors: **Donald Blattner**, **Larry Grunberger**, **Ted Selinsky**, **George Watson**; Graphics: **Concetto Auditore**, **Luis Martinez**, **Janet McCrie**; Editorial & Production: **Richard Johnson**, **Jeanne Bonner**, **Cintra Maharaj**, **Barbara Mauney**, **Vincent Susinno**, **John Tucker**, **Ernestine Walker**.

This document was prepared under the sponsorship of the National Aeronautics and Space Administration.. Neither the United States Government nor any person acting on behalf of the United States Government assumes any liability resulting from the use of the information contained in this document, or warrants that such use will be free from privately owned rights.

# NASA TU SERVICES



---

# NASA TECHNOLOGY UTILIZATION NETWORK

---

## ★ TECHNOLOGY UTILIZATION OFFICERS

*Stanley A. Miller*  
**Ames Research Center**  
Code 204-10  
Moffett Field, CA 94035  
(415) 965-6471

*Gussie Anderson*  
**Hugh L. Dryden Flight Research Center**  
Code OD/TU Office - Room 2015  
Post Office Box 273  
Edwards, CA 93523  
(805) 258-3311, Ext. 787

*Donald S. Friedman*  
**Goddard Space Flight Center**  
Code 702.1  
Greenbelt, MD 20771  
(301) 344-6242

*John T. Wheeler*  
**Lyndon B. Johnson Space Center**  
Code AT-3  
Houston, TX 77058  
(713) 483-3809

*U. Reed Barnett*  
**John F. Kennedy Space Center**  
Code PT-SPD  
Kennedy Space Center, FL 32899  
(305) 867-2780

*John Samos*  
**Langley Research Center**  
Mail Stop 139A  
Hampton, VA 23665  
(804) 827-3281

*Harrison Allen, Jr.*  
**Lewis Research Center**  
Mail Code 7-3  
21000 Brookpark Road  
Cleveland, OH 44135  
(216) 433-4000, Ext. 6422

*Ismael Akbay*  
**George C. Marshall Space Flight Center**  
Code AT01  
Marshall Space Flight Center, AL 35812  
(205) 453-2224

*Leonard A. Ault*  
**NASA Headquarters**  
Code ETD-6  
Washington, DC 20546  
(202) 755-2244

*Aubrey D. Smith*  
**NASA Resident Office-JPL**  
4800 Oak Grove Drive  
Pasadena, CA 91103  
(213) 354-6420

*Gilmore H. Trafford*  
**Wallops Flight Center**  
Code OD  
Wallops Island, VA 23337  
(804) 824-3411, Ext. 201

## ● INDUSTRIAL APPLICATIONS CENTERS

**Aerospace Research Applications Center**  
1201 East 38th Street  
Indianapolis, IN 46205  
*John M. Ulrich, director*  
(317) 264-4644

**Computer Software Management and Information Center (COSMIC)**  
Suite 112, Barrow Hall  
University of Georgia  
Athens, GA 30602  
*Robert L. Brugh, director*  
(404) 542-3265

**Kerr Industrial Applications Center**  
Southeastern Oklahoma State University  
Durant, OK 74701  
*James Harmon, director*  
(405) 924-0121, Ext. 413

**NASA Industrial Applications Center**  
701 LIS Building  
University of Pittsburgh  
Pittsburgh, PA 15260  
*Paul A. McWilliams, executive director*  
(412) 624-5211

**New England Research Applications Center**  
Mansfield Professional Park  
Storrs, CT 06268  
*Daniel Wilde, director*  
(203) 486-4533

**North Carolina Science and Technology Research Center**  
Post Office Box 12235  
Research Triangle Park, NC 27709  
*James E. Vann, director*  
(919) 549-0671

**Technology Applications Center**  
University of New Mexico  
Albuquerque, NM 87131  
*Stanley Morain, director*  
(505) 277-3622

**NASA Industrial Applications Center**  
University of Southern California  
Denny Research Building  
University Park  
Los Angeles, CA 90007  
*Robert Mixer, acting director*  
(213) 743-6132

## ■ STATE TECHNOLOGY APPLICATIONS CENTERS

**NASA/University of Florida State Technology Applications Center**  
311 Weil Hall  
University of Florida  
Gainesville, FL 32611  
*Ronald J. Thornton, director*  
Gainesville: (904) 392-6760  
Orlando: (305) 275-2706  
Tampa: (813) 974-2499

**NASA/University of Kentucky State Technology Applications Program**  
109 Kinkead Hall  
University of Kentucky  
Lexington, KY 40506  
*William R. Strong, manager*  
(606) 258-4632



## ◆ PATENT COUNSELS

*Robert F. Kempf*  
*Asst. Gen. Counsel for patent matters*  
**NASA Headquarters**  
 Code GP-4  
 400 Maryland Avenue, SW.  
 Washington, DC 20546  
 (202) 755-3954

*Darrell G. Brekke*  
**Ames Research Center**  
 Mail Code: 200-11A  
 Moffett Field, CA 94035  
 (415) 965-5104

*Paul F. McCaul*  
**Hugh L. Dryden Flight Research Center**  
 Code OD/TU Office - Room 2015  
 Post Office Box 273  
 Edwards, CA 93523  
 (213) 354-2734

*John O. Tresansky*  
**Goddard Space Flight Center**  
 Mail Code: 204  
 Greenbelt, MD 20771  
 (301) 344-7351

*Marvin F. Matthews*  
**Lyndon B. Johnson Space Center**  
 Mail Code: AM  
 Houston, TX 77058  
 (713) 483-4871

*James O. Harrell*  
**John F. Kennedy Space Center**  
 Mail Code: SA-PAT  
 Kennedy Space Center, FL 32899  
 (305) 867-2544

*Howard J. Osborn*  
**Langley Research Center**  
 Mail Code: 279  
 Hampton, VA 23665  
 (804) 827-3725

*Norman T. Musial*  
**Lewis Research Center**  
 Mail Code: 500-311  
 21000 Brookpark Road  
 Cleveland, OH 44135  
 (216) 433-4000, Ext. 346

*Leon D. Wofford, Jr.*  
**George C. Marshall Space Flight Center**  
 Mail Code: CC01  
 Marshall Space Flight Center, AL 35812  
 (205) 453-0020

*Monte F. Mott*  
**NASA Resident Office-JPL**  
 Mail Code: 180-601  
 4800 Oak Grove Drive  
 Pasadena, CA 91103  
 (213) 354-2700

## ▲ APPLICATION TEAMS

*William N. Fetzner, director*  
**Advisory Center for Medical  
 Technology and Systems**  
 University of Wisconsin  
 1500 Johnson Drive  
 Madison, WI 53706  
 (608) 263-2735

*Edmund R. Bangs, director*  
**IIT Research Institute**  
 10 West 35th Street  
 Chicago, IL 60616  
 (312) 567-4191

*Doris Rouse, director*  
**Research Triangle Institute**  
 Post Office Box 12194  
 Research Triangle Park, NC 27709  
 (919) 541-6256

*Tom Anyos, director*  
**SRI International**  
 333 Ravenswood Avenue  
 Menlo Park, CA 94026  
 (415) 326-6200, Ext. 2864

*Eugene Schmidt, program coordinator*  
**Stanford University School of Medicine**  
 Cardiology Division  
 Biomedical Technology Transfer  
 703 Welch Road, Suite E-4  
 Palo Alto, CA 94304  
 (415) 497-5353

*David MacFadyen, project director*  
**Technology + Economics**  
 2225 Massachusetts Avenue  
 Cambridge, MA 02140  
 (617) 491-1500

---

## TECHNOLOGY UTILIZATION OFFICERS

Technology transfer experts can help you apply the innovations in NASA Tech Briefs.

---

**The Technology Utilization Officer** at each NASA Field Center is an applications engineer who can help you make use of new technology developed at his center. He brings you NASA Tech Briefs and other special publications, sponsors conferences, and arranges for expert assistance in solving technical problems.

### Technical assistance,

in the form of further information about NASA innovations and technology, is one of the services available from the TUO. Together with NASA scientists and engineers, he can often help you find and implement NASA technology to meet your specific needs.

**Technical Support Packages (TSP's)** are prepared by the center TUO's. They provide further technical details for articles in NASA Tech Briefs. This additional material can help you evaluate and use NASA technology. You may receive most TSP's free of charge by using the TSP Request Card found at the back of this issue.

**Technical questions about articles** in NASA Tech Briefs are answered in the TSP's. When no TSP is available, or you have further questions, contact the Technology Utilization Officer at the center that sponsored the research [see page A4].



---

## NASA INVENTIONS AVAILABLE FOR LICENSING

Over 3,500 NASA inventions are available for licensing in the United States — both exclusive and nonexclusive.

---

### Nonexclusive licenses

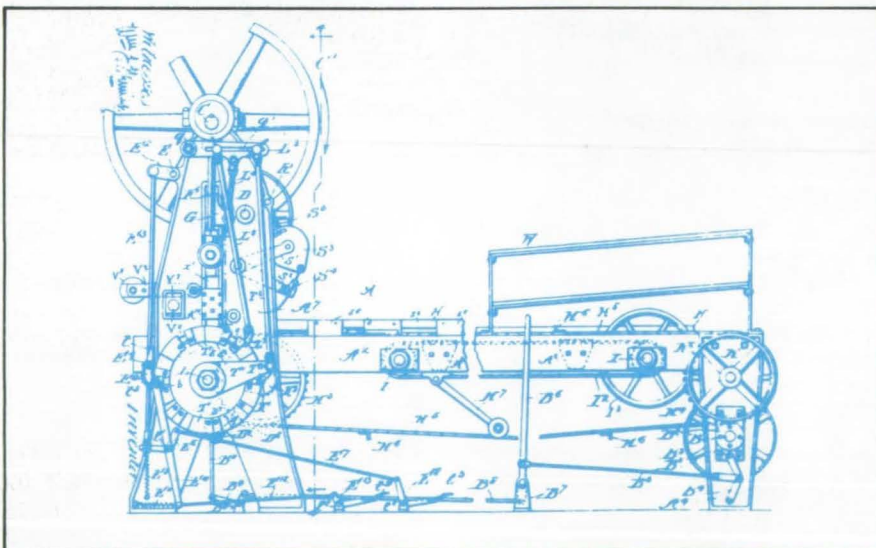
for commercial use of NASA inventions are encouraged to promote competition and to achieve the widest use of inventions. They must be used by a negotiated target date but are usually royalty-free.

### Exclusive licenses

may be granted to encourage early commercial development of NASA inventions, especially when considerable private investment is required. These are generally for 5 to 10 years and usually require royalties based on sales or use.

### Additional licenses available

include those of NASA-owned foreign patents. In addition to inventions described in NASA Tech Briefs, "NASA Patent Abstract Bibliography" (PAB), containing abstracts of all NASA inventions, can be purchased from National Technical Information Service, Springfield, VA 22161. The PAB is updated semiannually.



### Patent licenses for Tech Briefs

are frequently available. Many of the inventions reported in NASA Tech Briefs are patented or are under consideration for a patent at the time they are published. The current patent status is described at the end of the article; otherwise, there is no statement about patents. If you want to know more about the patent program or are interested in licensing a particular invention, contact the Patent Counsel at the NASA Field Center that sponsored the research [see page A5]. Be sure to refer to the NASA reference number at the end of the Tech Brief.



---

## APPLICATION TEAMS

Technology-matching and problem-solving assistance to public-sector organizations

---

### Application engineering projects

are conducted by NASA to help solve public-sector problems in such areas as safety, health, transportation, and environmental protection. Some application teams specialize in biomedical disciplines; others, in engineering and scientific problems. Staffed by professionals from various disciplines, these teams work with other Federal agencies and health organizations to



identify critical problems amenable to solution by the application of existing NASA technology.

### Public-sector organization

representatives can learn more about application teams by contacting a nearby NASA Field Center Technology Utilization Office [see page A4].

---

## INDUSTRIAL APPLICATIONS CENTERS

Computerized access to nearly 10 million documents worldwide

---

### Computerized information retrieval

from one of the world's largest banks of technical data is available from NASA's network of Industrial Applications Centers (IAC's). The IAC's give you access to 1,800,000 technical reports in the NASA data base and to more than 10 times that many reports and articles found in 140 other computerized data bases.

### The major sources include:

- 750,000 NASA Technical Reports
- Selected Water Resources Abstracts
- NASA Scientific and Technical Aerospace Reports
- Air Pollution Technical Information Center
- NASA International Aerospace Abstracts
- Chem Abstracts Condensates
- Engineering Index
- Energy Research Abstracts
- NASA Tech Briefs
- Government Reports Announcements

and many other specialized files on food technology, textile technology, metallurgy, medicine, business, economics, social sciences, and physical science.

### The IAC services

range from tailored literature searches through expert technical assistance:



- **Retrospective Searches:** Published or unpublished literature is screened, and documents are identified according to your interest profile. IAC engineers tailor results to your specific needs and furnish abstracts considered the most pertinent. Complete reports are available upon request.
- **Current-Awareness Searches:** IAC engineers will help design a program to suit your needs. You will receive selected monthly or quarterly abstracts on new developments in your area of interest.

- **Technical Assistance:** IAC engineers will help you evaluate the results of your literature searches. They can help find answers to your technical problems and put you in touch with scientists and engineers at appropriate NASA Field Centers.

### Prospective clients

can obtain more information about the services offered by NASA IAC's by contacting the nearest IAC [see page A4] or by checking the IAC box on a TSP Request Card in this issue.

---

## STATE TECHNOLOGY APPLICATIONS CENTERS

Technical information services for industry  
and state and local government agencies

---

**Local government and industry** in Florida and Kentucky can utilize the services of NASA's State Technology Applications Centers (STAC's). The STAC's differ from the Industrial Applications Centers described on page A7, primarily in that they are integrated into existing state technical assistance programs and serve only

the host state, whereas the IAC's serve multistate regions.

**Many data bases,** including the NASA base and several commercial bases, are available for automatic data retrieval through the STAC's. Other services such as document retrieval and special

searches are also provided. (The STAC's normally charge a fee for their services.)

**To obtain information** about the services offered by NASA STAC's, write or call the STAC in your state [see page A4].

---

## COSMIC®

An economical source of computer programs  
developed by NASA and other government agencies

---

### A vast software library

is maintained by COSMIC — the Computer Software Management and Information Center. COSMIC gives you access to approximately 1,600 computer programs developed for NASA and the Department of Defense and selected programs for other government agencies. Programs and documentation are available at reasonable cost.

### Available programs

range from management (PERT scheduling) to information science (retrieval systems) and computer operations (hardware and software). Hundreds of engineering programs perform such tasks as structural analysis, electronic circuit design, chemical analysis, and the design of fluid systems. Others determine building energy requirements and optimize mineral exploration.

### COSMIC services

go beyond the collection and storage of software packages. Programs are checked for completeness; special announcements and an indexed software catalog are prepared; and programs are reproduced for distribution. Customers are helped to

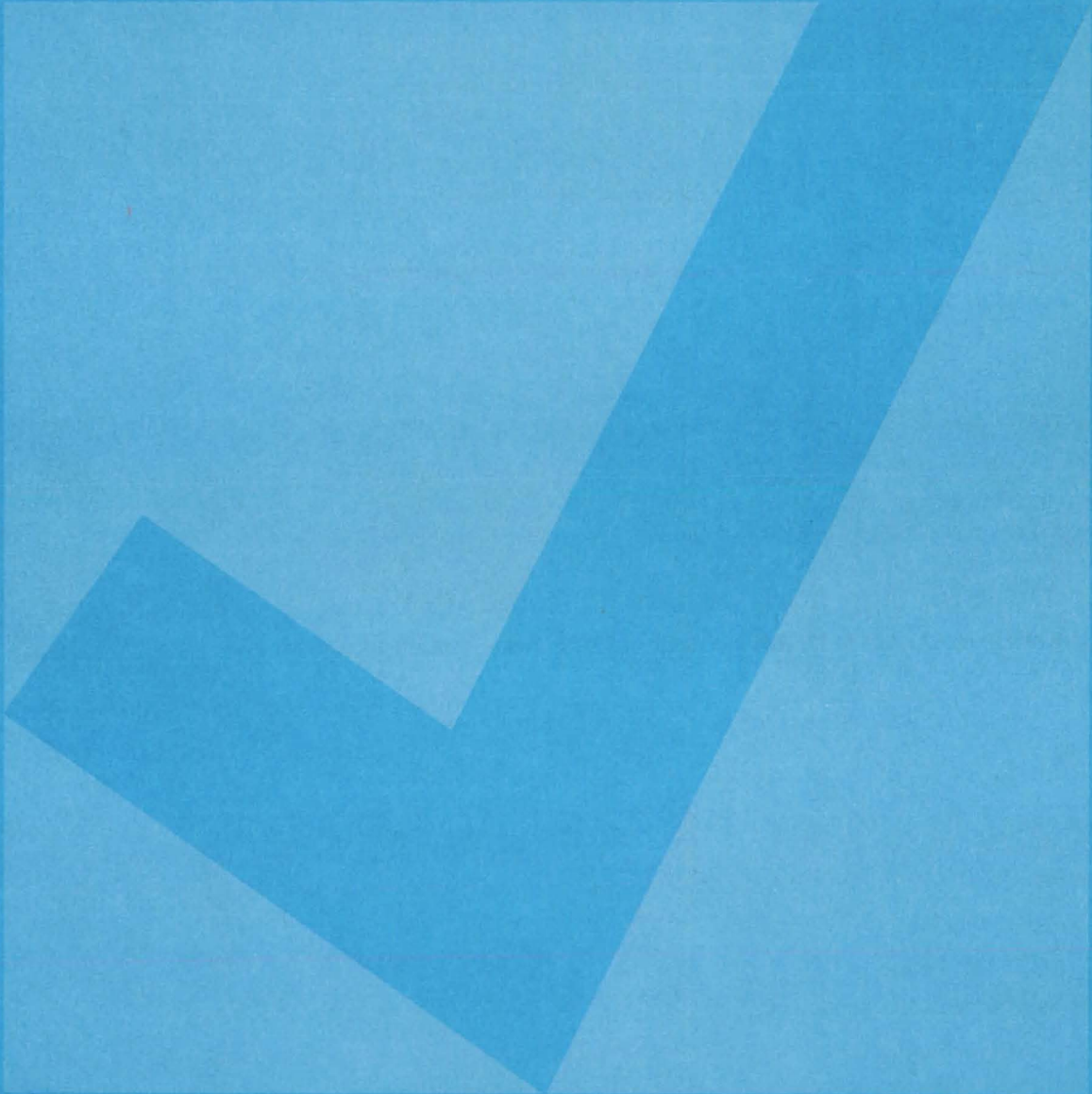


identify their software needs; and COSMIC follows up to determine the successes and problems and to provide updates and error corrections. In some cases, NASA engineers can offer guidance to users in installing or running a program.

### Information about programs

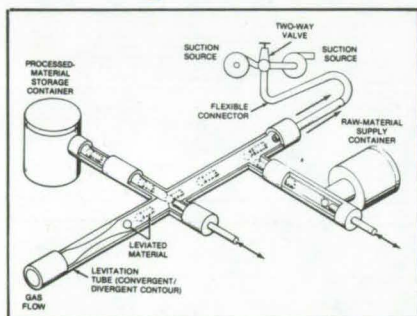
described in NASA Tech Briefs articles can be obtained by completing the COSMIC Request Card at the back of this issue. Just circle the letters that correspond to the programs in which you are interested.

# NEW PRODUCT IDEAS



**NEW PRODUCT IDEAS** are just a few of the many innovations described in this issue of NASA Tech Briefs and having promising commercial applications. Each is discussed further on the referenced page in the appropriate section in this issue. If you are interested in developing a product from these or other NASA innovations, you can receive further technical information by requesting the TSP referenced at the end of the full-length article or by writing the Technology Utilization Office of the sponsoring NASA center (see page A4). NASA's patent-licensing program to encourage commercial development is described on page A6.

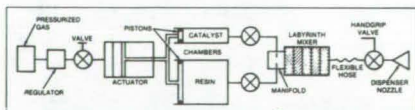
## Levitor for Containerless Processing



Aerodynamic forces support objects in a new levitator that could be used for containerless processing of materials. The levitator is a tube containing converging and diverging sections on the upstream and downstream sides of a constriction. The gas flow and pressure in the tube are regulated so that aerodynamic forces suspend material at the downstream end of the diverging section. A tube in the downstream section sucks gas from the main tube or blows gas into it to influence the position of the material. The unique shape of the tube makes the aerodynamic forces on the object greater than its weight. (See page 105.)

## Adhesives Mixer/ Applicator

Two-part adhesives, such as an epoxy resin and its catalyst, are stored, mixed, and dispensed by a self-contained portable applicator.

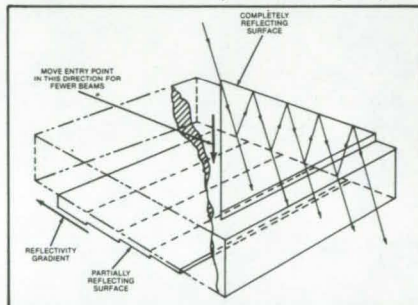


The adhesive/components are stored in concentric chambers. Compressed nitrogen gas forces the components from the chambers and into a static labyrinth-path mixer. There they combine into a homogeneous paste as they flow to the dispensing nozzle. The

operator stops the flow by releasing the handgrip. (See page 77.)

## Beam Splitter Intensities Are Preselected

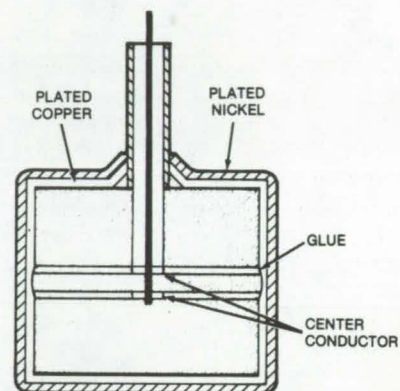
The light beams emanating from a new beam splitter all have the same intensity or can have predetermined intensities. It could be used in fluid-flow measurements, aerosol sizing, and other applications in interferometry and holography. The beam splitter is a block of optically clear material with two parallel polished faces. Some of the area of one face is coated with a totally reflecting layer;



the opposite face is overcoated with a metallic layer of stepped thickness. An input beam reflects between the polished faces, and a portion of the beam emerges at each reflection from the stepped surface. (See page 23.)

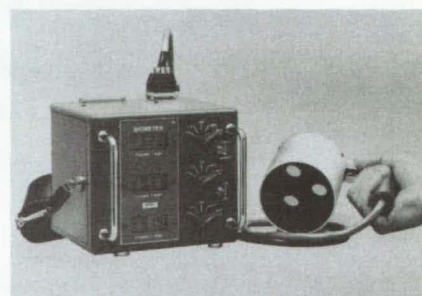
## Sealed Strip Line for Extreme Temperatures

A new strip line for microwave circuits is strong, light, and weather-proof. It can withstand temperatures ranging from  $-300^{\circ}$  to  $+600^{\circ}$  F and has good electrical characteristics. It is made by an inexpensive plating technique. The new strip line could be used in airborne-radar front ends and feed networks; it could also be adapted for underwater applications. The strip-line circuit consists of an inner conductor, a dielectric, and an



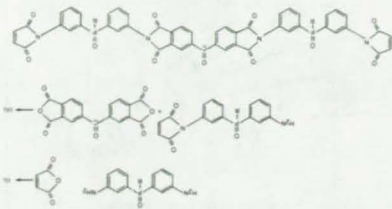
outer conductor, in a structure similar to a coaxial transmission line. The outer conductor is plated around the dielectric on all four sides, producing a unibody construction that is hermetically sealed. (See page 108.)

## Portable Radiometer Monitors Plant Growth



A hand-held radiometer measures visible and infrared energy reflected from plant canopies. The reflectance in three measured bands correlates closely with chlorophyll content, leaf area, and leaf water content — all measures of plant growth and development. Mobile and easy to use for repeated measurements, the radiometer probe is held over the plant canopy, range switches are set, and the measurements are recorded. The radiometer consists of two modules, a hand-held detector and a readout-and-control module. (See page 47.)

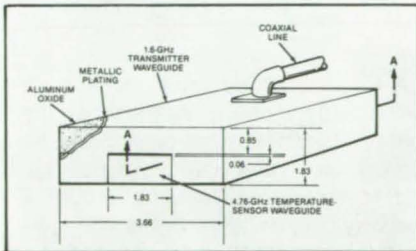
## Improved Fire-Resistant Resins for Laminates



New fire-resistant phosphorus-containing resins may be used as adhesives and as matrix material for graphite fiber-reinforced lightweight composites. The resins resist solvents, chemicals, and fire, being virtually incombustible in pure oxygen at 300° C. By using different components for the resin, as well as mixtures of components, some mechanical properties of the laminates can be selectively altered. The resins are formed from bisimides containing main-chain phosphorus and olefinic end groups. The bisimides are thermally polymerized to form the resins and laminates.

(See page 37.)

## Compact Dual-Mode Microwave Antenna

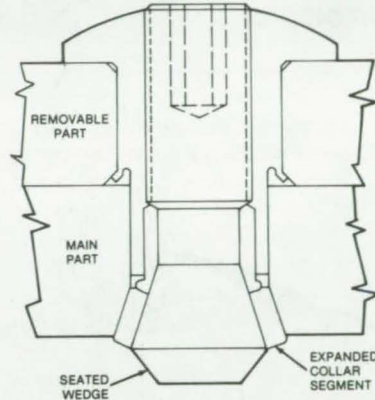


A compact dual-mode antenna can be used for both heating and for temperature sensing in special applications. The new antenna heats an object by irradiating it with microwaves. Temperature is sensed by measuring the intensity of microwaves radiated from the hot object. Differences in temperature as small as 0.1° C were detected when the antenna was used for cancer research. The transmitter is a single-ridged waveguide. A rectangular waveguide within the ridge of the transmitter is the receiver. The outside dimensions of the antenna are just 3.66 cm in width by 1.83 cm in thickness.

(See page 6.)

## Blind Fastener Is Easy To Install

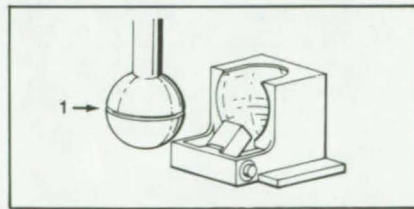
Panels, sheets, doors, and other structures could be easily attached to and removed from a mating part by a proposed new fastener. It could be used even if only one side of the assembly is accessible. The hardware is permanently anchored in the removable part, and its protruding end is inserted into a hole in the mating part.



When a wedge pin is rotated, a segmented collar presses against the bottom surface of the assembly, clamping the two parts together. To disengage the parts, the wedge pin is unscrewed.

(See page 80.)

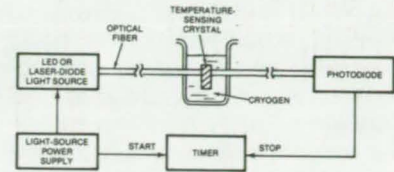
## Ball-and-Socket Joint Can Be Disassembled



Quick assembly and disassembly of structural elements are made possible by a new ball-and-socket joint. The new coupling could be used to put together temporary structures, such as scaffolding, camping equipment, and trade-show displays. It is reusable over many connect/disconnect cycles and can accommodate many assembly configurations. The basic joint consists of a laterally latching socket and a ball-ended, mounted fitting. The spring-loaded latch in the socket retains the ball. The coupling is disengaged by simply depressing the latch and extracting the ball.

(See page 82.)

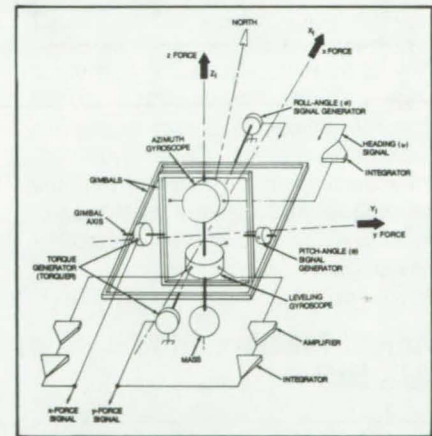
## Fiber-Optic, Semiconductor Temperature Gage



A new cryogenic temperature gage is based on optical principles, rather than electrical, as in previous sensors. The new sensor thus minimizes the danger of electrically ignited explosions in hazardous cryogens such as hydrogen and oxygen. It should also be useful for handling noncryogenic liquids in aircraft, automobiles, boats, and other applications. Accurately measuring the optical band edge of a crystal is the key to measuring temperature with the new sensor. Fiber optics carry light to and from the immersed crystal.

(See page 55.)

## Less-Costly Inertial Guidance

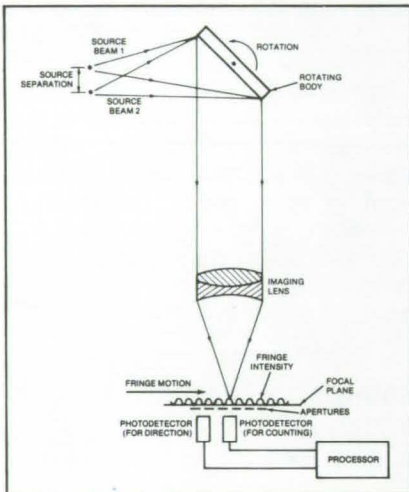


Small and large aircraft can benefit from a new, less-costly, inertial navigation system that uses two gimbal-mounted gyroscopes. The system is insensitive to yaw, roll, and aircraft pitch and is accurate to within 1 nautical mile after a 1-hour mission. Microprocessor controlled, it simultaneously displays the aircraft position, velocity, heading, and attitude. Signals generated by the two gyroscopes are used to calculate the displayed parameters. The microprocessor and supporting electronics are all readily-available commercial electronics.

(See page 51.)

## Interferometer Accurately Measures Rotation Angle

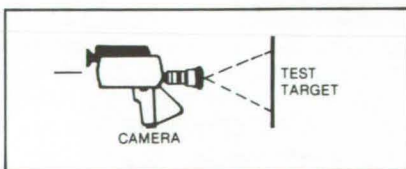
An optical interferometer developed at Goddard Space Flight Center could be the basis for a sensitive, nonintrusive tachometer. By analyzing the interference fringes produced by two coherent light beams reflected off a rotating object, angular velocity and angular position are measured to an accuracy of better than 1 microradian. The two beams are derived from a conventional Helium/Neon laser.



They combine to produce a moving fringe pattern. The speed of fringe motion is sensed and converted to a measurement of the speed of rotation. Small translational movement of the object does not affect the measurements.

(See page 58.)

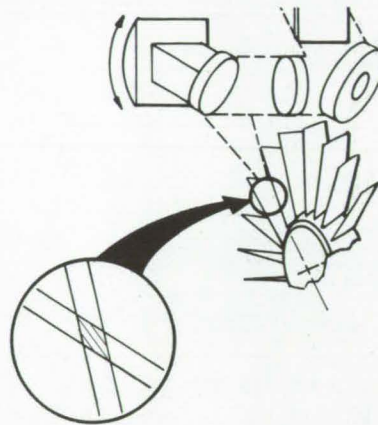
## Optical Memory Stores $10^{12}$ Bits



Large storage capacity and high read and write rates are possible with a new optical mass memory. Data are stored on fiches, each of which holds  $10^9$  bits. In under 10 seconds, any of the 1,000 fiches, which are stored in a carousel, can be retrieved. The

memory has separate recorder and reproducer modules, with a separate laser to write on or read from the fiche. Data are input into the memory with a standard television camera, and the output is displayed on a television monitor. The system read rate is 5 megabits per second, and the write rate is 30 megabits per second. (See page 15.)

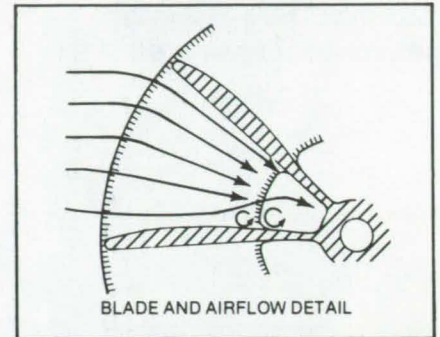
## High-Speed Laser Anemometer



A new laser anemometer rapidly maps the gas velocities between the rotating blades of turbomachinery. It can be used with many types of turbines and should be applicable to other gas-flow situations. The system measures the velocities of small seed particles entrained in the gas flow. A minicomputer sorts the data and graphically displays the velocity profile, a histogram of the distribution of measurements, and the conditions of the run. (See page 52.)

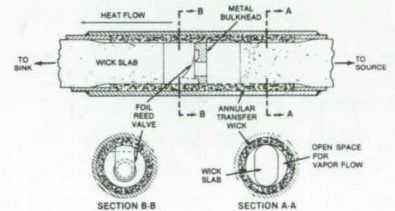
## Aerodynamics Improve Wind Wheel

As a result of proposed aerodynamic refinements, the power output and efficiency of a wind-wheel electric-power generator would increase. Modifications to the wind wheel



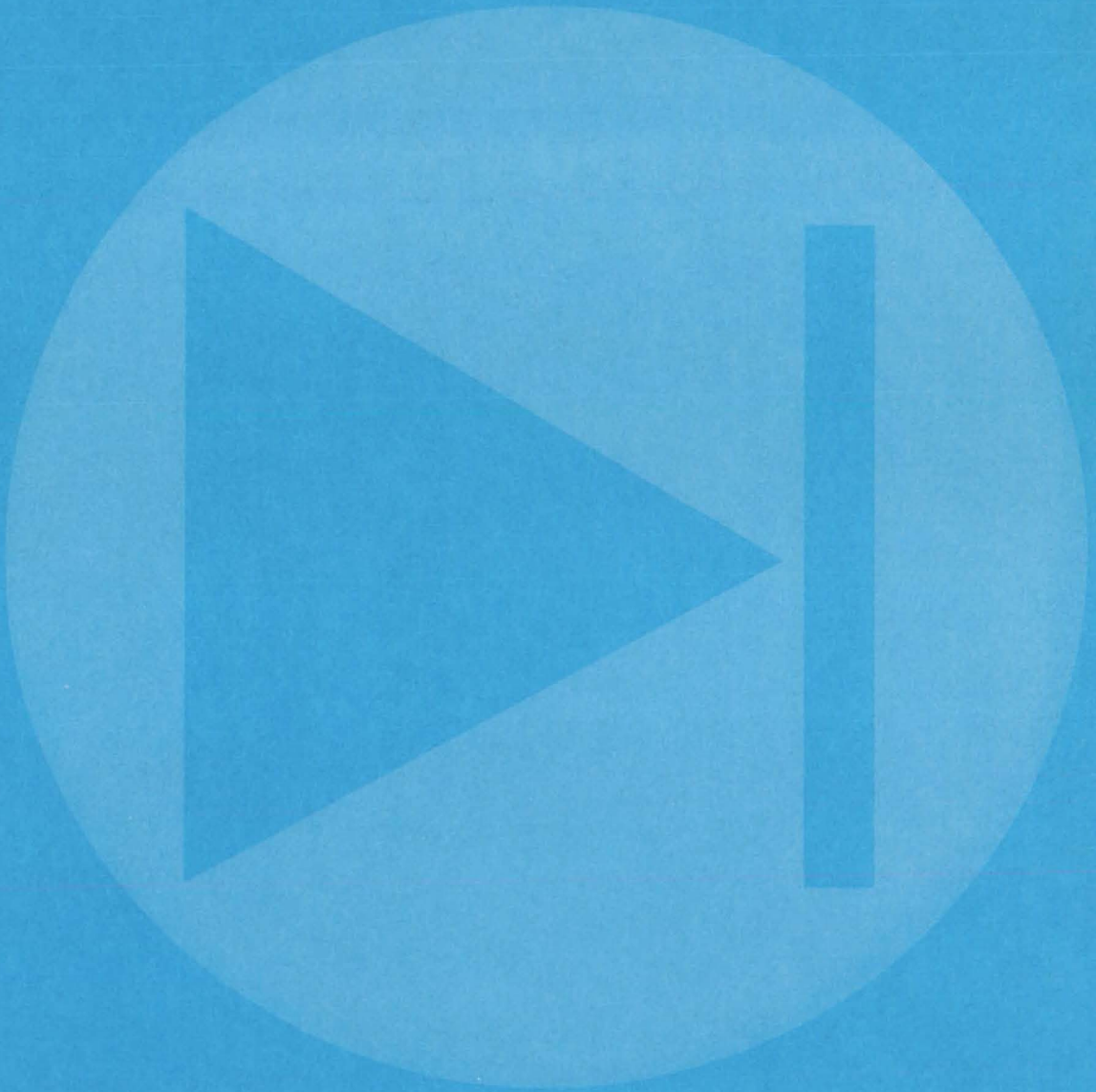
improve performance without increasing its size or the number of moving parts. Streamlined ducting and airfoil blades smooth the wind-wheel airflow. The airfoil keeps the boundary-layer airflow attached, reduces wind deceleration, and increases mass flow through the generator. Venting flaps on a duct guide accelerate airflow along the blades, and guide vanes direct wind into the blades. (See page 78.)

## One-Way Heat Pipe



A metal-foil reed valve shuts off a heat pipe if the sink is warmer than the source. The new heat pipe could be used to cool electronic components and for other applications requiring one-way heat transfer. In the conducting direction, the reed flexes open at a pressure differential that is small compared to the capillary pressure limit of the wicking. In the insulating direction, with the sink warmer than the source, the reed is forced closed, and the heat-pipe fluid returns to the source side through an annular transfer wick. When this occurs, the wick on the sink side of the valve dries out, and the heat pipe ceases to conduct. (See page 61.)

# Electronic Components and Circuits



## Hardware, Techniques, and Processes

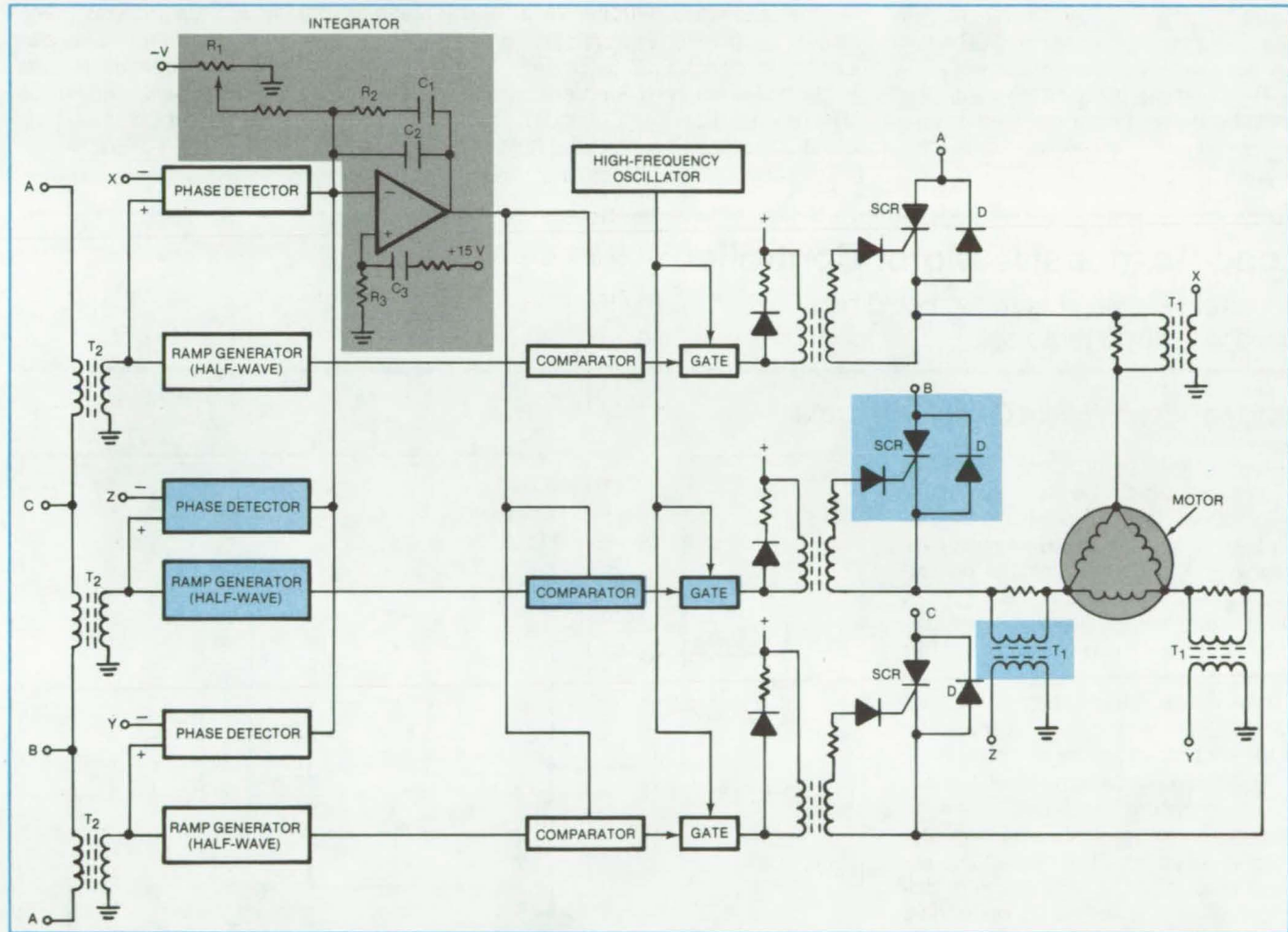
- 3 Three-Phase Power-Factor Controller
- 4 Load-Responsive Motor Controller
- 5 Power-Factor Controller With Regenerative Braking
- 6 Compact Dual-Mode Microwave Antenna
- 7 Resistors Improve Ramp Linearity
- 8 Spike-Free Automatic Level Control
- 8 Improved Model for MOS Breakdown
- 9 Rotary Transformer Seals Power In
- 10 Multilayer, Front-Contact Grid for Solar Cells
- 11 Log-Output Signal Processor Scans Eight Decades
- 12 High-Frequency Gated Oscillator



# Three-Phase Power-Factor Controller

Improved feedback control overcomes the instabilities of earlier systems.

Marshall Space Flight Center, Alabama



**A Three-Phase Power-Factor Controller**, shown here in its half-wave version, develops a control signal for each motor winding. As the motor loading decreases, the rms value of applied voltage is decreased by the feedback-control circuit. Power consumption is therefore lower than in unregulated operation.

A modified power-factor controller employs a phase detector for each of the three phases of a delta-connected induction motor. The phase-difference sum is the basis for control. The 20-Hz bandwidth of the feedback signal is sufficient to compensate for the instabilities present in previous systems. [See "Improved Power-Factor Controller" (MFS-25323) on page 133 of *NASA Tech Briefs*, Vol. 5, No. 2.]

The circuit has been developed in full- and half-wave versions. The half-wave circuit is shown in the figure. Power to each leg of the motor is supplied during the positive half cycle

through a silicon controlled rectifier (SCR) and during the negative half cycle through a parallel diode, D. Current in each leg is sampled by transformer T<sub>1</sub> shunted by a small resistor.

The transformer outputs X, Y, and Z are each fed to one of the two inputs of a phase detector, while a sample of the corresponding powerline phase is fed to the other phase-detector input through transformer T<sub>2</sub>. The output of each phase detector is a positive rectangular pulse with duration that is nearly proportional to the phase difference between the line voltage and the motor current. The basic control signal,

consisting of the combined phase-detector outputs, is therefore a series of pulses with a repetition rate of 180 Hz for a standard 60-Hz line.

The control signal is applied to the inverting input of an operational amplifier, together with a negative dc voltage from potentiometer R<sub>1</sub>. The integrator feedback elements R<sub>1</sub>, C<sub>1</sub>, and C<sub>2</sub> are chosen so that the 180-Hz component is suppressed, while signals up to about 20 Hz in response to changes in motor loading are passed. The output of this circuit is therefore smooth except for low-frequency indications of deviation

(continued on next page)

from the power factor or phase angle commanded by the value of  $R_1$ .

The control signal is compared with a line-synchronized ramp voltage in each comparator. When the two signals are equal, the comparator actuates a gate to pass a high-frequency (typically, 10-kHz) signal that triggers the associated SCR. As the phase angle increases (power factor decreases) as with lower motor loading, the SCR turns on later and for a shorter interval.

The operation of the phase controller must be delayed for a few seconds after power is first applied, to allow the

motor to reach operating speed. Initially,  $C_3$  charges through  $R_3$  to supply a positive signal to the noninverting input of the amplifier. The positive signal overrides any signal at the inverting input for several seconds, thereby causing full power to be applied during that time.

While each SCR fires once per cycle in the half-wave version described above, each Triac (or equivalent) gate-controlled switch fires twice per cycle in the full-wave system. The essential difference is that phase, ramp, and trigger signals must be provided for both

half cycles. When properly adjusted, both versions give power-factor regulation as a function of loading, without significant motor instability.

*This work was done by Frank J. Nola of Marshall Space Flight Center. For further information, Circle 1 on the TSP Request Card.*

*This invention is owned by NASA, and a patent application has been filed. Inquiries concerning nonexclusive or exclusive license for its commercial development should be addressed to the Patent Counsel, [see page A5]. Refer to MFS-25535.*

## Load-Responsive Motor Controller

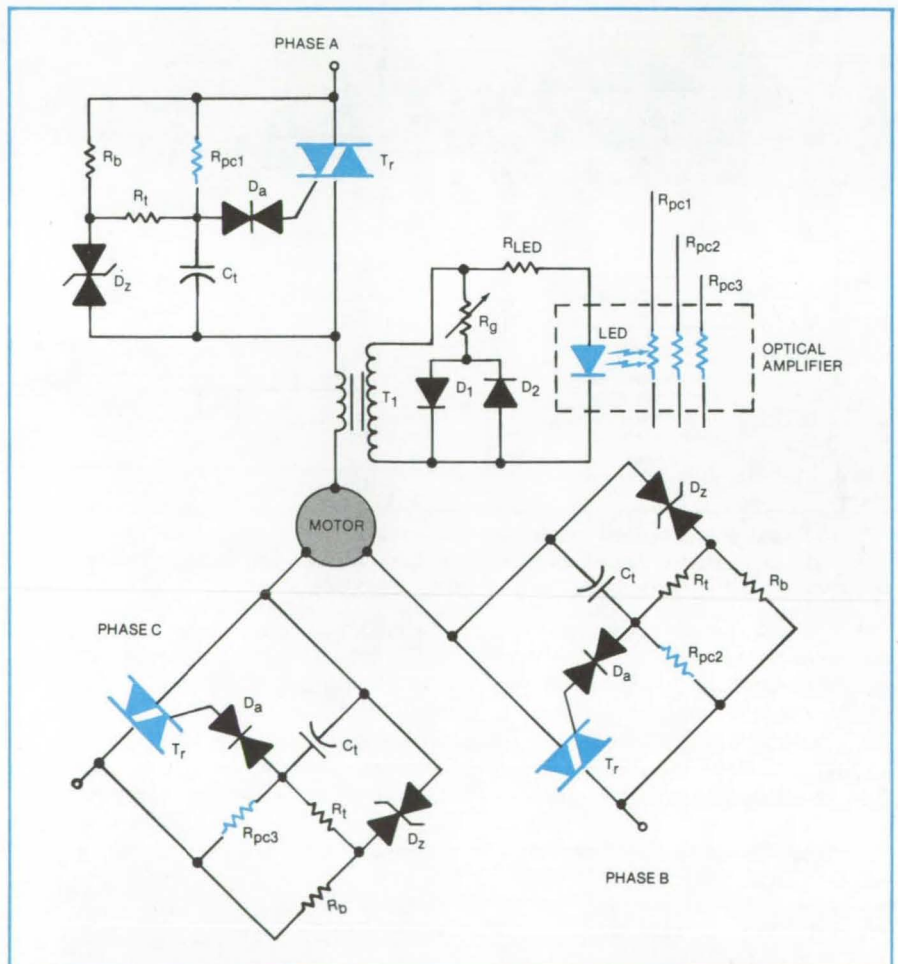
A current-sensing controller could be used with small motors.

### Marshall Space Flight Center, Alabama

A new circuit controls the voltage applied to a three-phase induction motor in response to the magnitude of current, so as to reduce power consumption when the motor is idling or operating at less than full load. The circuit is simpler and less expensive than phase-sensing power-factor controllers [for example, see the preceding article "Three-Phase Power-Factor Controller" (MFS-25535)], and it performs adequately for fractional-horsepower motors.

The three-phase version of the circuit is shown in the figure. A single-phase controller would use only the "phase A" portion. The rms voltage applied to each phase (whether Y- or delta-connected) is varied by controlling the firing angle of a Triac switch. The firing angle is determined by the interaction of resistors  $R_b$  and  $R_t$ , photocell  $R_{pc}$ , and capacitor  $C_t$ . When  $C_t$  is charged to the trigger voltage of Diac switch  $D_a$ , part of the charge fires the Triac switch into conduction.

The resistance in the control circuit, and hence the capacitor charging time, is determined by the motor current in one of the phases. The current is sensed by transformer  $T_1$ , which applies a voltage to a light-emitting diode. Light from the diode varies the resistances of the three photocells, which determine the "on" time of the Triacs. Resistor  $R_g$  sets the gain relationship between motor current and Triac switch firing angle. It is adjusted for



The **Power Saver** is shown in its three-phase version. Current in one of the phases is sensed to control the firing delay of the Triac switches in response to motor loading. The circuit saves power at reduced loads.

minimum power usage at the motor rated torque.

If there is no load,  $R_{PC}$  is large, and the combination of  $R_B$ , back-to-back Zener diodes  $D_Z$ , and resistor  $R_T$  establishes the no-load firing angle. The firing delay (off time of the Triac switch) must not exceed  $60^\circ$  (2.78 milliseconds) in the three-phase system, so that at least two Triac switches remain conducting at all times. In practice, a delay of 2.6 milliseconds is used, to allow for parameter variations.

The back-emf varies among individual motors. The circuit insures against changes in no-load firing angle with changes in back-emf: When a Triac

switch stops conducting, the difference between the applied emf and the back-emf appears across the  $R_B/D_Z$  combination. The Zener diode conducts and so establishes a voltage reference for charging  $C_T$  through  $R_T$ . This voltage is independent of the back-emf, and it establishes the 2.6-millisecond maximum firing delay.

The control circuit decreases the rms applied voltage to match decreases in motor load over the entire torque range. This considerably decreases power consumption in motors operating at a fraction of their rated torques. Tests on a commercial

1/3-horsepower (250-watt) single-phase motor showed power savings ranging from 75 percent at no load to 0.8 percent at full load. In a typical application with varying loads, savings would be expected in the range of 2 to 15 percent.

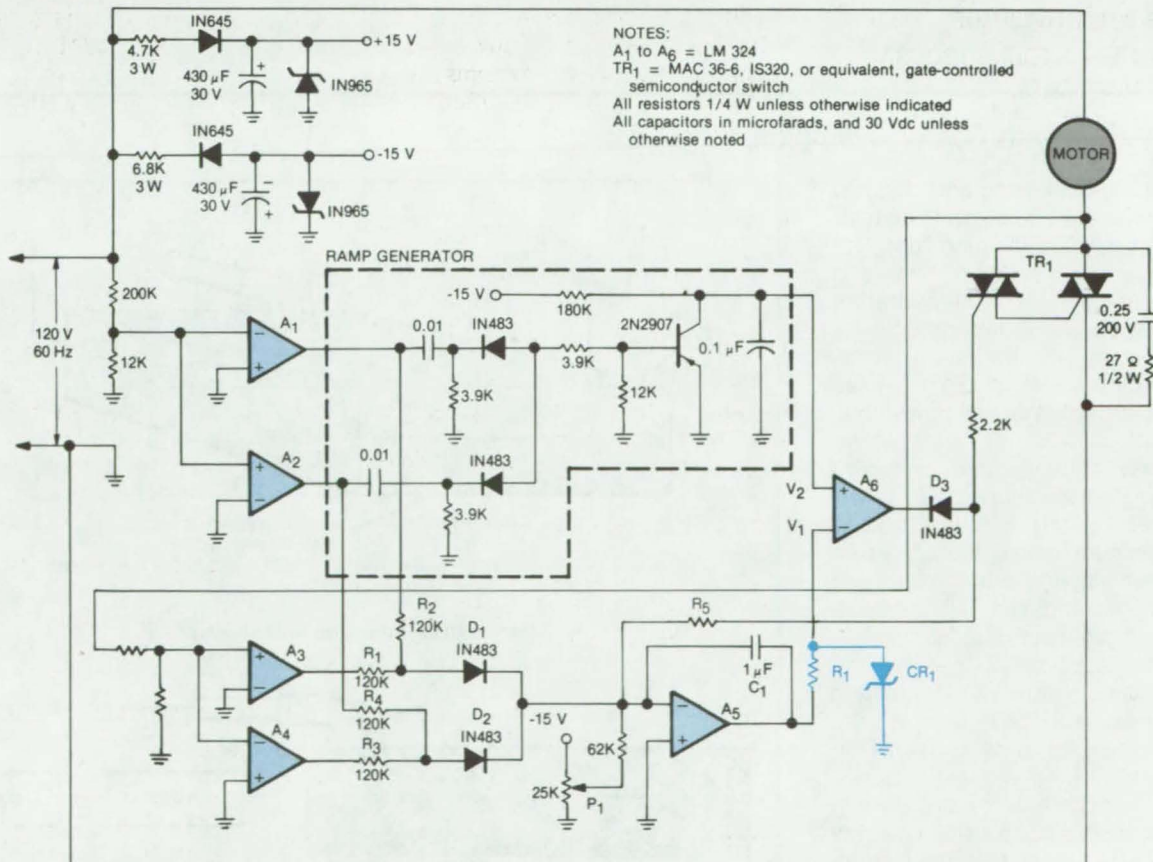
This work was done by Teddy M. Edge of **Marshall Space Flight Center**. For further information, Circle 2 on the TSP Request Card.

Inquiries concerning rights for the commercial use of this invention should be addressed to the Patent Counsel, Marshall Space Flight Center [see page A5]. Refer to MFS-25560

## Power-Factor Controller With Regenerative Braking

Regenerative braking gives additional energy savings.

Marshall Space Flight Center, Alabama



The **Modified Power-Factor Motor Controller** also functions as a phase-angle generator control for regenerative braking. The addition of resistor  $R_1$  and Zener diode  $CR_1$  allows the controller to change automatically to the generator mode when the load attempts to overspeed the motor.

(continued on next page)

A modified power-factor motor-control circuit operates the motor as a phase-controlled generator when the load attempts to turn at higher than synchronous speed. [Also see the related article, "Improved Power-Factor Controller" (MFS-25323), on page 133 of *NASA Tech Briefs*, Vol. 5, No. 2.]

An induction motor is required to act at times as a brake. This is needed, for example in a "down" escalator loaded with people, in an elevator in descent, or in an oil pump on the downward stroke. The circuit modification allows the power-factor controller to save energy in the motoring mode and to convert automatically to an induction-generator controller in the generating, or braking, mode.

A power-factor controller for a single-phase induction motor is shown in the figure. The voltage across semiconductor switch TR<sub>1</sub> senses the phase

angle between the line voltage and the motor current. The circuit measures the interval between the voltage and current zero crossings and develops a voltage proportional to this interval at the inverting input of A<sub>5</sub>. A negative voltage from the 25K potentiometer is also fed to the input, so that the output of A<sub>5</sub> measures the departure of the phase angle from a preset value. This error voltage is compared with a line-synchronized ramp voltage in A<sub>6</sub>, the output of which determines the firing point of the switch.

If the load attempts to turn the motor faster than the synchronous speed, the output of A<sub>5</sub> is further reduced, thus decreasing even more the interval during which the switch is on. Ultimately, the switch is held in its off state, effectively disconnecting the line from the motor. The motor then does not offer any braking, nor does it feed energy back into the line.

With the addition of R<sub>1</sub> and CR<sub>1</sub>, the Zener voltage of CR<sub>1</sub> prevents the output of A<sub>5</sub> from retreating below a minimum value, the value for motor idling. The switch fires during at least some small interval. Once the switch is on, the gate loses control until the current decreases to zero. The more the load tries to outrun the motor, the longer will be the interval during which the switch remains on, and more power will be returned to the line from the load. Thus, the addition of the two components saves energy through power-factor control in both the driving and braking modes.

*This work was done by Frank J. Nola of Marshall Space Flight Center. No further documentation is available.*

*Inquiries concerning rights for the commercial use of this invention should be addressed to the Patent Counsel, Marshall Space Flight Center [see page A5]. Refer to MFS-25477.*

## Compact Dual-Mode Microwave Antenna

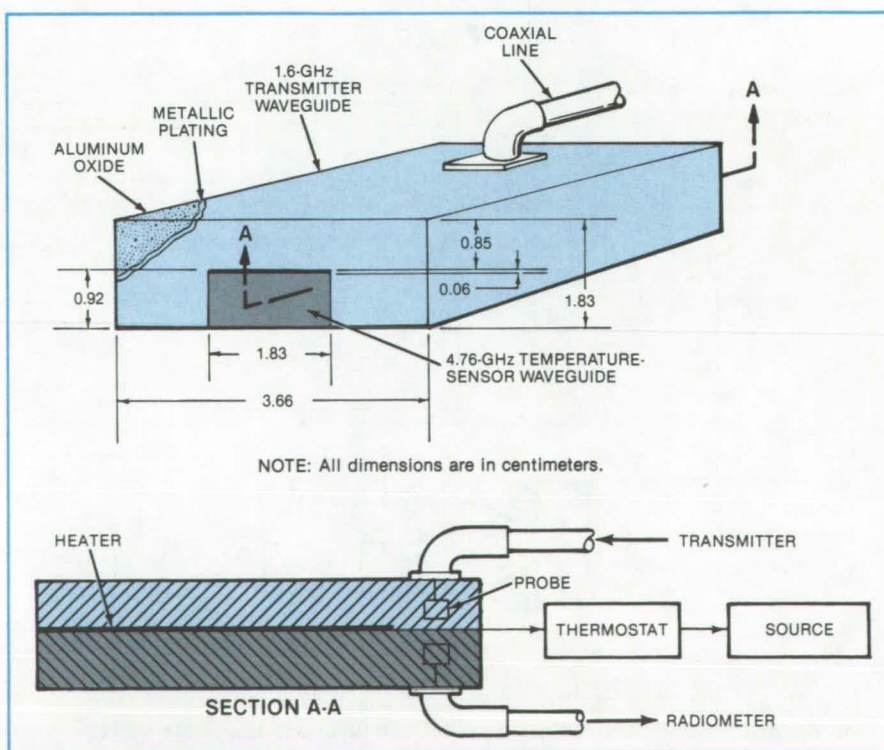
It heats and measures temperature simultaneously.

*Langley Research Center, Hampton, Virginia*

A compact dual-mode antenna, just 3.66 cm wide by 1.83 cm in thickness, is used both for heating and for thermographic detection of tumors in cancer research. The temperature sensor operates independently or simultaneously with the heater. Temperature differences of 0.1° C have been detected. Maximum power output is 25 W.

The new antenna uses an open-ended, single-ridged waveguide as the transmitter (heater). It is constructed from aluminum oxide, then covered with a three-layer metallic plating of nickel, copper, and gold. This combination of a ridged waveguide and dielectric loading substantially reduces the antenna size. An antenna size close to the tumor size gives better temperature detection and improved focusing of the heating.

The dual-mode antenna is shown in the figure. It consists of a single-ridged-waveguide, 1.6-GHz transmitting antenna and a 4.76-GHz rectangular-waveguide temperature sensor within the ridge of the transmitting antenna. Microwave power is supplied via a



The **Compact Dual-Mode Antenna** includes a 1.6-GHz transmitter and a 4.76-GHz receiver. A strip heater between the antennas controls the temperature of the device.

coaxial line through the probe to the ridged-waveguide transmitting antenna. Microwaves received by the temperature-sensing antenna are picked up by another probe and transmitted through another coaxial line to a sensitive radiometer. A conventional thin-sheet heater is between the antennas. It is controlled by a proportional thermostat to keep the dual-mode antenna at human body temperature.

The temperature-sensing antenna receives at 4.76 GHz. This frequency gives increased resolution at small temperature differences, which is important in locating small tumors.

The heating-antenna design frequency is 1.6 GHz, (Antennas having

frequencies of 915 and 430 MHz are being constructed for deeper penetration of microwaves.) It is a simple single-ridge TE<sub>10</sub>-mode waveguide reduced in size by dielectric loading. The two antennas are isolated from each other by the cutoff characteristics of the temperature-sensing antenna and other filtering, which form a high-pass filter. Because the human body is a variable match, the transmitter includes a reflectometer to measure incident and reflected power levels.

When uncoupled from a human body, the low-impedance heater antenna has a large mismatch with air, about 12 to 1. This open-circuited condition

gives a measured radiation 2.54 cm from the antenna with the heater at full power of less than 0.4 mW/cm<sup>2</sup>. That is well within Government safety standards, which allow 10 mW/cm<sup>2</sup> regardless of frequency.

This work was done by Kenneth L. Carr of Microwave Associates, Inc., for **Langley Research Center**. For further information, Circle 3 on the TSP Request Card.

Title of this invention has been waived under the provisions of the National Aeronautics and Space Act [42 U.S.C. 2457(f)], to the Microwave Associates, Inc., South Avenue, Bldg. 7, Burlington, Massachusetts 01803. LAR-12784

## Resistors Improve Ramp Linearity

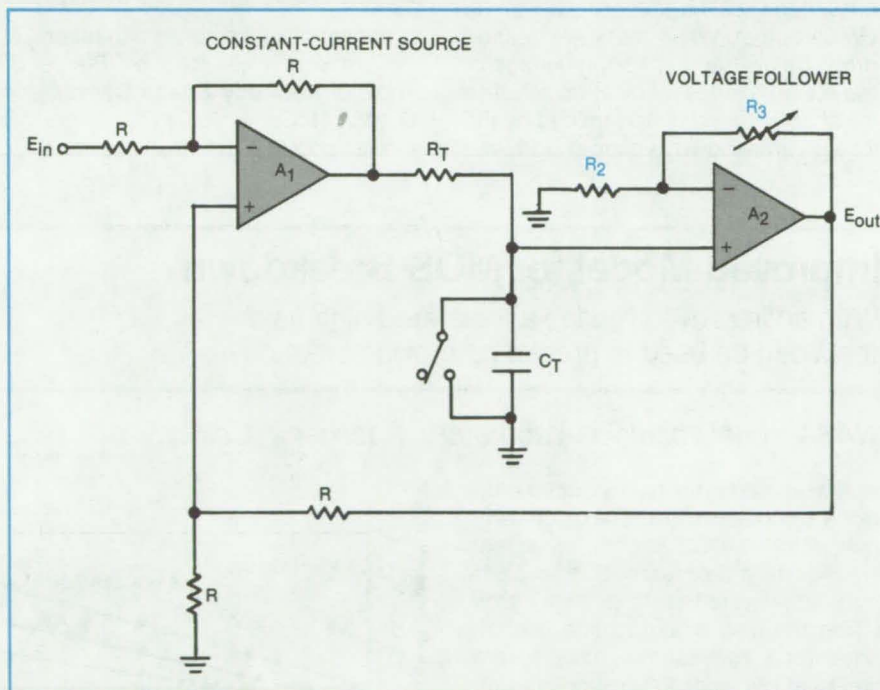
Bootstrap integrator is improved by two resistors.

Goddard Space Flight Center, Greenbelt, Maryland

A simple modification to the bootstrap ramp generator gives a more linear output over longer sweep times. The new circuit adds just two resistors, one of which is adjustable. The modification cancels nonlinearities due to variations in the load on the charging capacitor and due to changes in the charging current as the voltage across the capacitor increases. Since linear ramps are a key part of many analog and digital circuits, the new sweep circuit should find wide application.

In the simple bootstrap integrator, the voltage developed across the charging capacitor is fed back to the constant-current source through a voltage follower. This feedback neutralizes the effect of the capacitor voltage on the constancy of the charging current. However, changes in the load on the capacitor can alter the charging rate. That load consists of the capacitor leakage resistance and the input impedance of the voltage follower, both of which are affected by temperature, frequency, and other factors.

In the modified circuit (see figure), A<sub>2</sub> is changed from a voltage follower to a noninverting amplifier, resistor R<sub>2</sub> is fixed, and R<sub>3</sub> is varied until the linearity of the output signal is a maximum. When the circuit equations



A Feedback Circuit Utilizing Two Operational Amplifiers produces a linear voltage ramp. R<sub>3</sub> is adjusted experimentally to optimize the ramp output.

are analyzed, it is found that the circuit is optimized if  $R_3/R_2 = Y_1/Y_{RT}$ , where Y<sub>1</sub> and Y<sub>RT</sub> are the admittances of the unknown varying load and of resistor R<sub>T</sub>, respectively.

This work was done by Leonard L. Kleinberg of **Goddard Space Flight Center**. For further information, Circle 4 on the TSP Request Card. GSC-12635

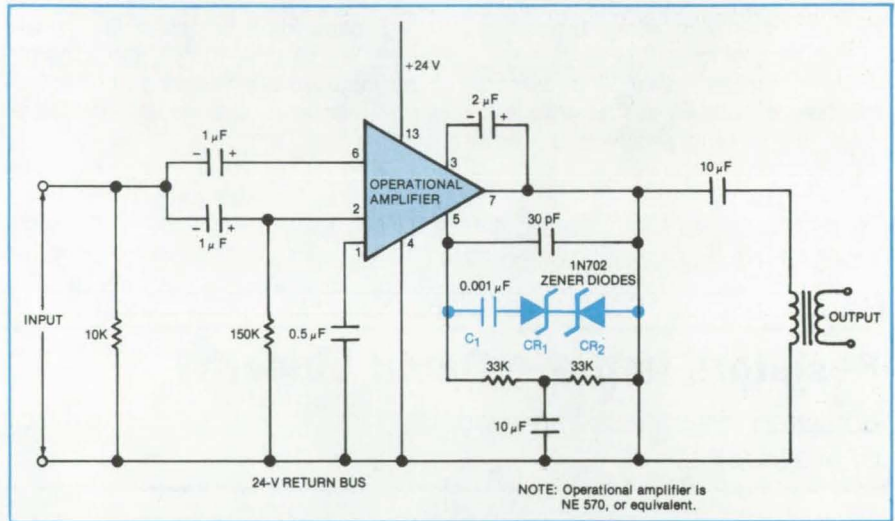
# Spike-Free Automatic Level Control

Zener diodes absorb signal overshoots.

*John F. Kennedy Space Center, Florida*

A new automatic-level-control circuit protects against signal "overshoot." In conventional level-control circuits, the gain is varied according to the average of the input signal. Since the gain is highest when there is no signal, the first part of an incoming signal is amplified at maximum gain until the automatic control takes over. As a result, a sharp peak, or overshoot, appears at the output.

In the new circuit, two Zener diodes, connected back-to-back in series with a capacitor, feed back a signal that reduces the circuit gain when a signal is first applied (see figure). The overshoot voltage spike causes the voltage across the Zeners to exceed their breakdown voltages. When this happens, the diodes turn on, preventing the voltage spike from appearing at the circuit output. When the spike voltage drops below the breakdown voltage of the Zener diodes, they turn off. The initial output level is determined by the Zener breakdown voltage and the



**Zener Diodes and a Series Capacitor** prevent voltage spikes (caused by a sudden increase in the input level) from appearing at the output.

capacitance of the series capacitor.

This work was done by Pierce C. Toole of Kennedy Space Center and D. M. McCarthy of PRC Corp. No further documentation is available.

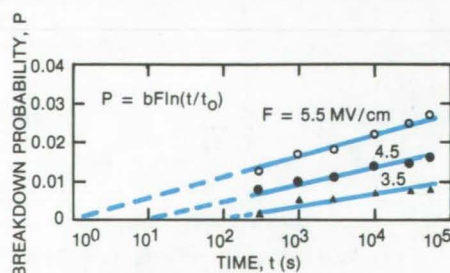
Inquiries concerning rights for the commercial use of this invention should be addressed to the Patent Counsel, Kennedy Space Center [see page A5]. Refer to KSC-11170

# Improved Model for MOS Breakdown

With an improved model, accelerated high-field tests can be used to predict gate-oxide breakdown.

*NASA's Jet Propulsion Laboratory, Pasadena, California*

A new model for field-induced gate-oxide breakdown in metal-oxide-semiconductor (MOS) structures agrees well with high-field test data. It thus permits accelerated tests at high fields. Using the new model to interpret the data, tests that normally take several weeks at low fields to accumulate sufficient statistics can be completed in only a few hours at high fields. [The previous model is described in "Model for MOS Field-Time-Dependent Breakdown" (NPO-14701) on page 145 of NASA Tech Briefs, Vol. 5, No. 2.]



The **Breakdown Probability Data** for three values of the applied field  $F$  are well fitted by the model when the exponent  $n$  in the field-dependent factor  $F^n$  equals 1.

The principal mechanism in MOS breakdown is mobile-ion emission from the metal/oxide interface, which occurs during the application of a positive gate-bias field. This breakdown is related to the clustering of the emitted ions at localized defect sites in the oxide/silicon interface. With clustering, much smaller ion densities than normally associated with ion-charge instabilities can initiate breakdown.

In the improved model, the field-time-dependent breakdown probability is multiplied by a field-dependent factor

$F^n$ , where  $F$  is the applied electric field. The factor  $F^n$  is an approximation. (The previous model corresponds to setting  $n$  equal to zero.) It may possibly be the dominant term of a more complicated expression. The value of  $n$  is determined empirically.

The field-dependent factor arises from such effects as:

- A higher field supplies a higher power input at a defect site where the current density has been enhanced by ion clustering. This higher power increases the probability of thermal runaway leading to breakdown.
- The lowering of the Schottky barrier

with increased field permits ion emission from deeper traps. If the occupied density of these traps increases at deeper levels, it will lead to a positive value of  $n$ .

- Electron trapping in low-energy states increases with the applied field. In conjunction with the strained  $\text{SiO}_2$  structure near the silicon interface, this could enhance ion clustering.
- The applied field will further reduce the barrier at a clustering site by Schottky or Fowler-Nordheim mechanisms.

The exponent  $n$  was determined from measurements of breakdowns vs.

time in arrays of MOS capacitors. At each of three fields (up to  $5.5 \times 10^6$  V/cm), 1,782 capacitors were monitored for breakdown for times up to 15 hours. The breakdown data were least-squares fitted to the model for  $n = 0, 0.5, 1,$  and  $2$ . The value  $n = 1$  gave the smallest standard error of estimate. Two other smaller sets of data also gave the best fit for  $n = 1$ .

*This work was done by Seung P. Li and Joseph Maserjian of Caltech for NASA's Jet Propulsion Laboratory. For further information, Circle 5 on the TSP Request Card. NPO-14850*

## Rotary Transformer Seals Power In

An enclosed airgap efficiently transfers ac power across a rotating interface.

*Goddard Space Flight Center, Greenbelt, Maryland*

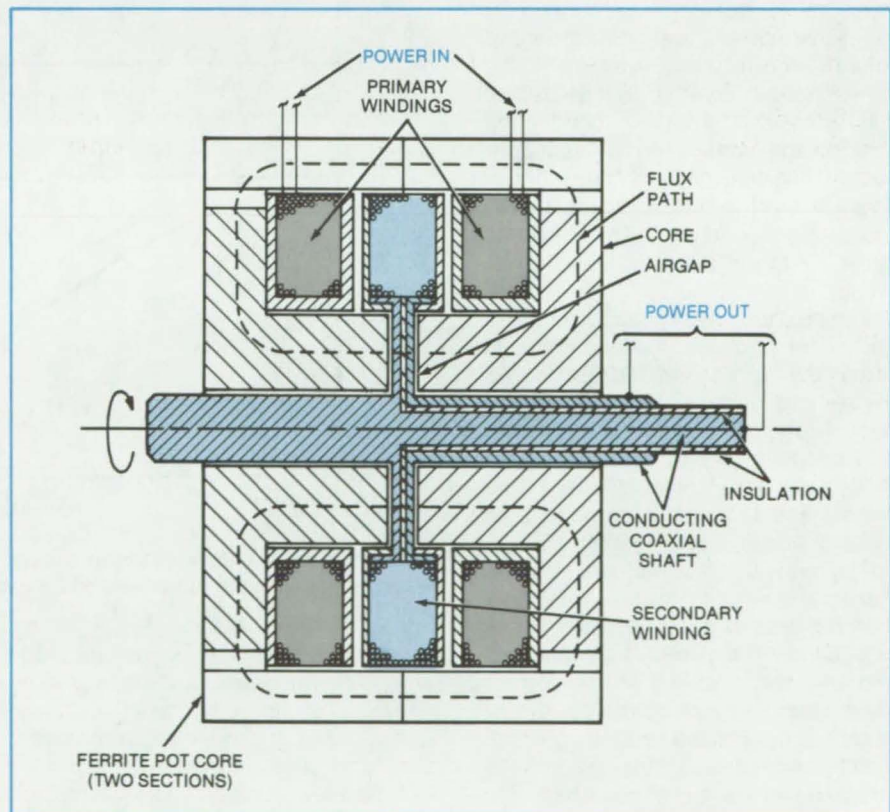
A rotary transformer originally developed for spacecraft transfers electrical power from a stationary primary winding to a rotating secondary without sliding contacts and with very little leakage of electromagnetic radiation. The transformer has a very small airgap within a magnetically permeable core. Since the gap is completely shielded, magnetic flux is coupled from the primary to the secondary.

As shown in the figure, the transformer actually has two stationary primary windings connected in parallel. The secondary, mounted on a shaft that extends out of the housing, rotates between the two windings of the primary.

The magnetic field set up by the primary current follows closed loops through the surrounding magnetic shield and across a narrow airgap where the hub of the secondary passes through the magnetic core. Changes in the primary current induce voltages in the secondary, as in a conventional transformer.

The transformer core is assembled from two half sections. The halves butt squarely against each other, so that electromagnetic flux does not escape through the joint between them.

(continued on next page)



The Rotary Transformer primary and secondary windings are surrounded by a ferromagnetic core that confines magnetic flux. Regardless of the angular position or velocity of the secondary, the flux coupling between the primary and secondary is substantially constant.

The shaft of the secondary is composed of electrically-conducting inner and outer parts separated by an insulator. Electrical contact is made from the secondary winding, through the shaft, to external leads.

This work was done by Philip A. Studer and John Paulkovich of **Goddard Space Flight Center**. For further information, Circle 6 on the TSP Request Card.

This invention is owned by NASA, and a patent application has been

filed. Inquiries concerning nonexclusive or exclusive license for its commercial development should be addressed to the Patent Counsel, Goddard Space Flight Center [see page A5]. Refer to GSC-12595.

## Multilayer, Front-Contact Grid for Solar Cells

New concept significantly increases cell efficiency at high output powers.

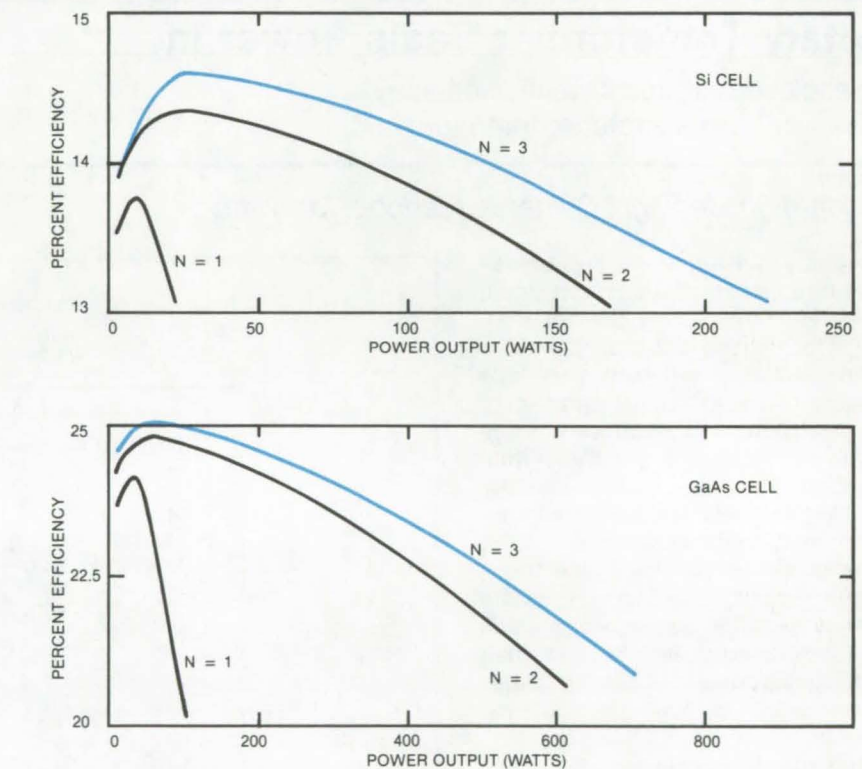
Langley Research Center, Hampton, Virginia

A proposed multilayer, front-contact grid structure for solar cells optimizes the collection of photogenerated current with minimum power losses. It is constructed of several layers of conducting grids. The finest grid layer makes ohmic contact to the front surface of the cell. Its function is to collect the photogenerated current from the active layer and prevent excessive power losses due to lateral voltage drop in the active layer. This ohmic contact layer is constructed of fine, densely-distributed conducting lines on the surface of the semiconductor. The thickness of the gridlines on each layer is built up to about the width of the gridlines. This helps to minimize series resistance and shadowing.

The next grid layer is made of thicker and wider gridlines. Its function is to collect the current from the first grid. As the second layer has lower resistance per unit length than the previous layer, it can conduct current over larger distances without significant losses. The two adjacent layers interconnect on multiple points of intersection.

The third layer is constructed of even thicker and wider conducting segments than the second grid layer. Its function is to collect the current from the second level and enable it to flow toward the contact with less power loss than if it were flowing on the second layer. Additional layers are constructed, with the last grid layer carrying the current into the current output lead.

The number of grid levels, the thickness of the gridlines on each level, and the number of gridlines on each level are determined by optimizing power



**Efficiency Versus Power Output** curves show the calculated behavior for Si and GaAs solar cells with optimized grid structure using one, two, and three grid layers. N is the number of grid layers.

output. Optimization is a tradeoff among power losses due to lateral voltage drop in the active layer, resistive losses in the gridline itself, contact-resistance losses, and shadowing losses. Optimization curves illustrated in the figure indicate a significant efficiency increase with multiple layers.

The calculated behavior for Si and GaAs cells indicates that, with the multiple-layer concept, peak efficiency can

occur at higher output-power levels. Because of this, higher solar concentrations can be applied to solar-cell arrays.

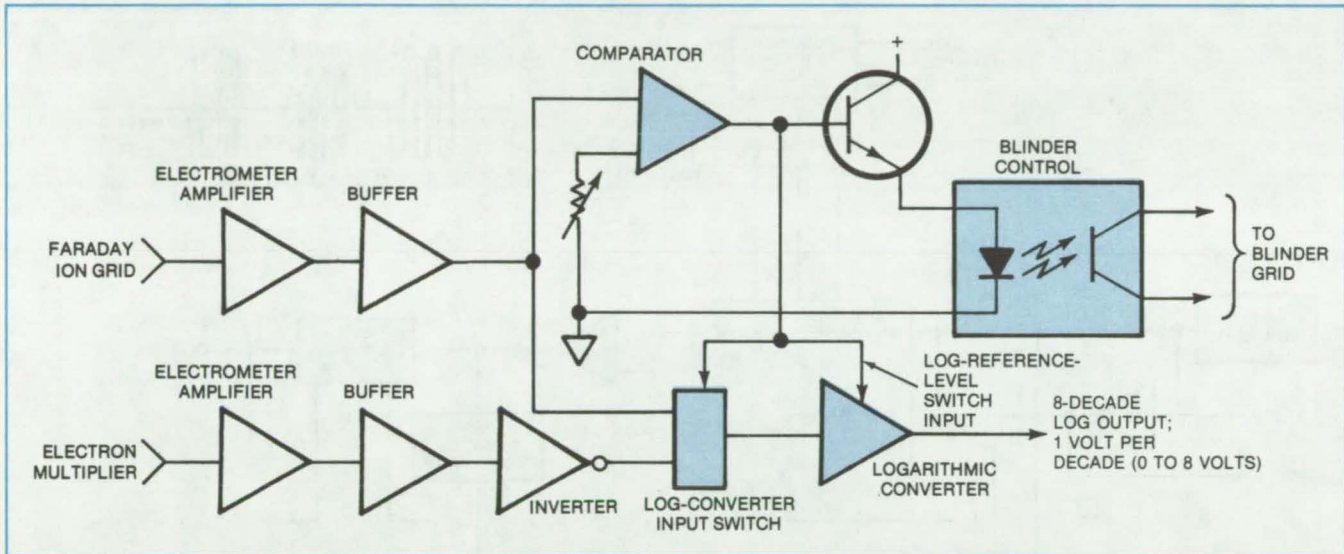
This work was done by A. G. Milnes and A. Flat of Carnegie-Mellon University for **Langley Research Center**. For further information, Circle 7 on the TSP Request Card. LAR-12613



# Log-Output Signal Processor Scans Eight Decades

Processor combines logarithmic output with automatic range switching.

Ames Research Center, Moffett Field, California



The **Logarithmic-Output Signal Processor** has automatic range switching and continuous readout over eight decades. The comparator output switches the logarithmic converter to the detector of interest and enables the blinder grid to protect the more-sensitive detector when operating in the high-input range.

A proposed logarithmic amplifier handles input currents that vary over eight decades of dynamic range. Originally developed to process the wide-ranging signals from two linear-response detectors in a mass spectrometer, the circuit features automatic range switching and overload protection for the more-sensitive detector. It could be used to process any wide-varying signal that is to be read on a limited-range recording device, such as a strip-chart recorder.

When using a mass spectrometer to analyze gas samples, there is usually a problem displaying on one scale the output current for the dominant species and the much smaller currents for trace components. Often these signals differ by many orders of magnitude. In the mass-spectrometer soil analyzer for which the new circuit is to be used, the range variation is eight decades, and the currents come

from two detectors: a Faraday ion screen and an electron multiplier.

The new processor automatically switches to the appropriate detector for the range being examined. The amplified detector signal is fed to a logarithmic converter, the output of which increases by 1 volt for each decade of increase in input voltage. Thus, the entire  $10^8$  of dynamic range can be displayed on an X/Y recorder or other display operating in the range of 0 to 8 volts.

The current from each detector develops a voltage across a feedback resistor. That voltage is amplified by a low-noise electrometer amplifier and then by a buffer amplifier. The electron-multiplier buffer is followed by an inverter so that the output voltages are positive for both detectors. The detector-grid transparencies, feedback resistors, and electron-multiplier gain are chosen so that the

amplified electron-multiplier output is  $10^3$  times the Faraday output for the same mass-spectrometer current.

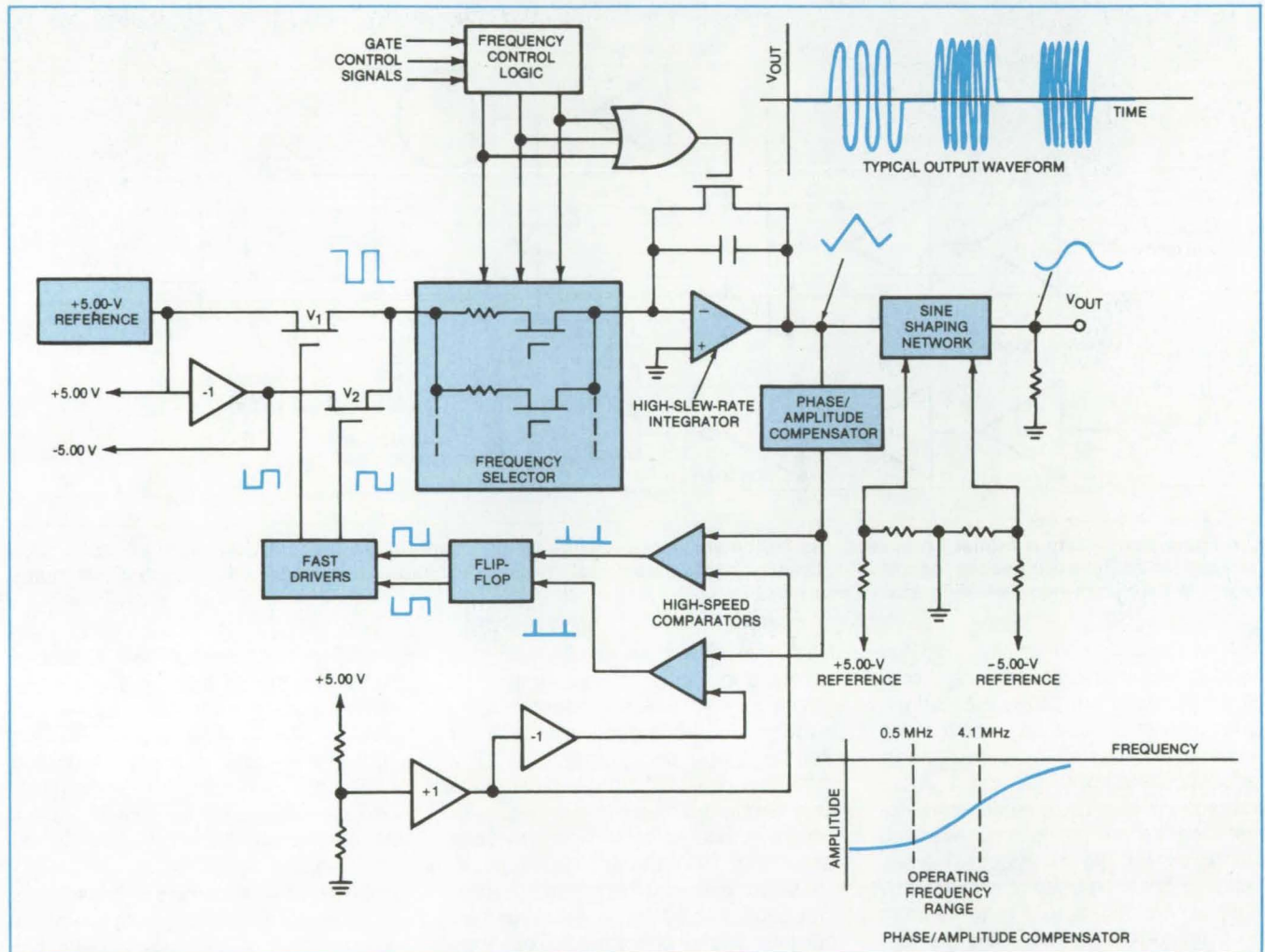
When the Faraday signal exceeds 10 mV (ion current exceeds  $1.38 \times 10^{-12}$  ampere), a comparator circuit enables a blinder grid to protect the electron multiplier. In this mode, the Faraday signal is fed to the log amplifier. An ion current of  $1.38 \times 10^{-12}$  to  $1.38 \times 10^{-9}$  ampere results in an output of 5 to 8 volts. When the Faraday signal is less than 10 mV, the blinder grid is disabled, and the log amplifier is switched to receive the electron-multiplier signal. An ion current of  $1.38 \times 10^{-17}$  to  $1.38 \times 10^{-12}$  ampere results in a log output of 0 to 5 volts in this mode.

*This work was done by Jeffrey L. Hayden of Martin Marietta Aerospace for Ames Research Center. For further information, Circle 8 on the TSP Request Card.*  
ARC-11293

# High-Frequency Gated Oscillator

High-speed circuit elements generate burst frequencies in the megahertz range.

Lyndon B. Johnson Space Center, Houston, Texas



This **Gated Oscillator** develops burst frequencies of 0.5, 1.25, 2.0, 3.0, 3.58, and 4.1 MHz for the Space Shuttle CCTV system. Amplitude and frequency control are better than 2 percent.

A new gated oscillator generates bursts of high-frequency sine waves, square waves, and triangular waves in response to control signals. Each burst starts at zero phase, with tight tolerances on signal amplitude and frequency. Frequencies in the megahertz range are made possible by using high-speed comparators and a high-speed flip-flop as a fast-response threshold detector.

As shown in the figure, a 5.00-volt reference signal, chopped by two MOS transistor switches, generates a precise square wave. The square wave is integrated and fed as a triangular wave to a phase/amplitude compensator that offsets any delay in the feedback path.

Two high-speed comparators compare the triangular wave to positive and negative 5.00-volt references. The fast pulses developed by the comparators clock a high-speed flip-flop, which produces square waves at the MOS transistor gate inputs.

The frequency, amplitude, and rise time of the output signal are controlled by using stable reference voltages and fast MOS switching transistors with low "on" resistance. The transistors are bulk-biased (by voltages  $V_1$  and  $V_2$ ) to equalize their switching thresholds.

High-speed drivers couple the low-level digital outputs of the flip-flop to the MOS transistors, while maintaining

short rise times (less than 10 nanoseconds) and edge coincidence of the two square waves (180° out of phase). Input coupling to the drivers is through Zener diodes; the output coupling is inductive. The circuit output frequency is selected by changing the resistance at the input to the integrator.

This work was done by Clement A. Berard of RCA Corp. for **Johnson Space Center**. For further information, including a detailed schematic of the gated oscillator, Circle 9 on the TSP Request Card.  
MSC-18634

# Electronic Systems



**Hardware,  
Techniques, and  
Processes**

- 15 Optical Memory Stores  $10^{12}$  Bits
- 16 New Algorithms Manage Fourfold Redundancy
- 17 Graphics-System Color-Code Interface
- 18 Solar-Powered Supply Is Light and Reliable
- 19 Improved Phase-Lock Detector

**Books and Reports**

- 20 Advanced Technologies for Commercial Airplanes

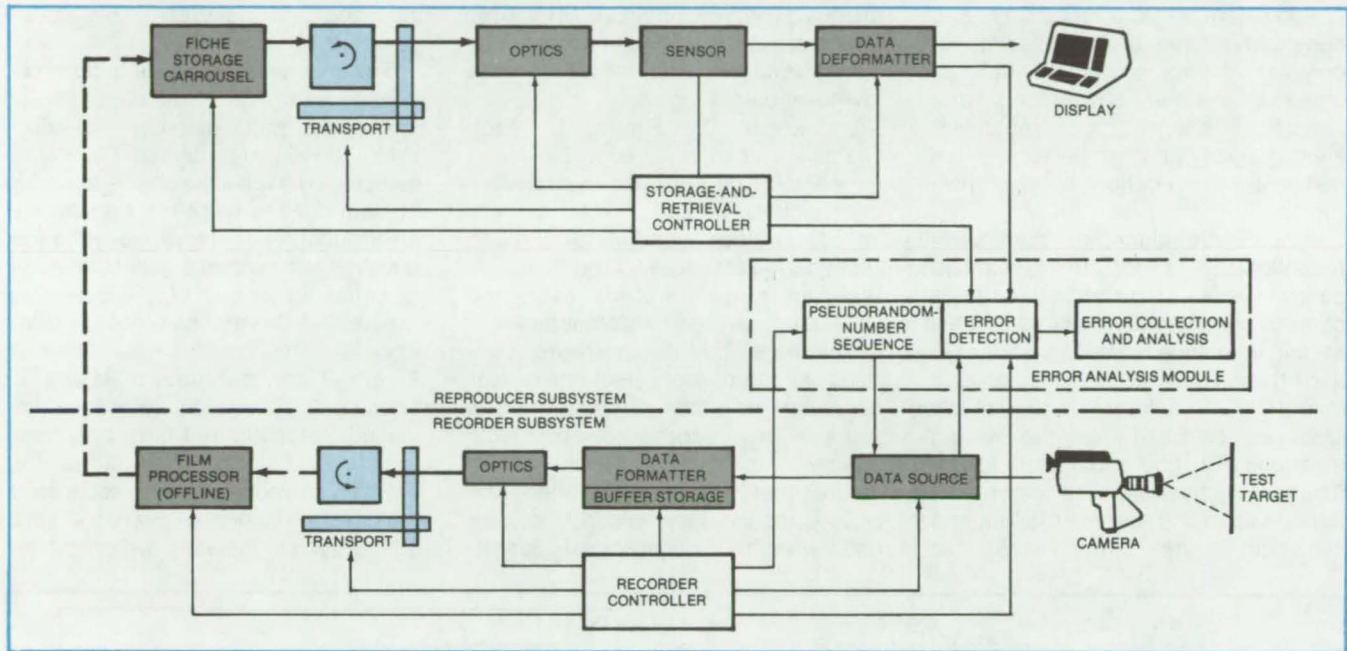
**Computer Programs**

- 20 Short-Circuited Power Networks

# Optical Memory Stores $10^{12}$ Bits

Data are stored at 30 megabits/s by a laser writing on silver halide film.

Marshall Space Flight Center, Alabama



The **Optical Mass Memory** has separate recorder (write) and reproducer (read) modules. Data are recorded on fiches, which are stored in a carrousel. A particular fiche is retrieved from the carrousel by a transporter in under 10 seconds.

Digital data are stored as spots on silver halide film in a  $10^{12}$ -bit optical memory now under development. Read rates of 5 megabits per second and write rates of 30 megabits per second are made possible by acoustic/optic components that deflect and modulate a focused laser beam as it scans the film frames, called fiches. The input to the optical memory is a standard television camera. A television monitor at the memory output displays the stored video images when they are retrieved from fiches.

The optical memory in the  $10^{12}$ -bit system (see figure) consists of 1,000 fiches, each holding  $10^9$  bits. A rotating carrousel stores the fiches, allowing them to be retrieved one at a time by a transporter for reading. Data are recorded on the film in lines containing 330 data bits each, although such overhead as format and synchronization information raises the actual number of spots to 792 per line.

In the recorder, or write portion of memory, the analog video signal from the television camera is converted to

digital data, formatted, and transferred to a buffer electronic memory until  $10^6$  bits are stored: This is equivalent to one TV frame.

When the buffer is filled, the data are read out and transferred to the fiche. A He/Cd laser beam is acoustic/optically modulated by the data. The beam is expanded and projected through an acoustic/optic beam deflector (AOBD). The AOBD sweeps the beam across an acoustic traveling-wave lens, which focuses the beam to a moving spot. Stationary optics image the spot onto the fiche.

In the reproducer, or memory reader, an AOBD and lenses deflect and focus a He/Ne laser beam, which sweeps along the line being read on the fiche. Light that passes through the fiche is focused onto a detector. The data are decoded, stored in a buffer memory, and eventually converted to an analog signal for readout on the television monitor.

The fiche data format arranges the data in 36 annular tracks. Each track consists of many 1.11-mm radial lines,

each of which contains 330 user data bits (ten 33-bit words). The fiche is translated laterally for access to the desired track; it is rotated about its center to sweep the desired lines through the writing or reading stations in the recorder or reproducer.

Instead of the television camera source, the input to the optical memory can also be taken from a pseudorandom sequence generator. The pseudorandom strings are used as reference data to check the system bit-error rate. Error rates below 1 in  $10^6$  bits are anticipated.

A He/Ne laser is used in the reproducer because it is less expensive than the He/Cd laser and is compatible with the detector sensitivity; He/Ne lasers are not powerful enough for use in the recorder, given the higher writing speed and the low film sensitivity at the He/Ne wavelength (632.8 nm).

*This work was done by Harris Corp. for Marshall Space Flight Center. For further information, Circle 10 on the TSP Request Card. MFS-25456*

# New Algorithms Manage Fourfold Redundancy

Quad selection filter rejects data from null-failed and hardover-failed units.

Lyndon B. Johnson Space Center, Houston, Texas

Redundant sensors, actuators, and computers improve the reliability of complex control systems, such as those in nuclear powerplants and aircraft. If one or more redundant elements fail, another takes over so that normal operation is not interrupted.

A new set of algorithms continually reconfigures a fourfold-redundant control system to minimize the effects of failed components. Sensors that fail at full amplitude (hardover failures) and those that drop to near-zero output (null failures) are rapidly identified, removed from the system electronically, and substituted for by functioning sensors. The algorithms tolerate up to one hardover failure and two null failures among the four

channels — an improvement over previous systems, which had difficulty distinguishing a null failure from a low-level output signal.

As shown in Figure 1, each redundant channel of each sensor is connected to a separate multiplexer/demultiplexer (MDM). The MDM's are linked to four computers through redundant data buses. The result is that data from each of four paths end up in each of the four computers.

The selection-filter software contains algorithms that select one of four channels as the primary control signal. The algorithms and logic change, depending on the number of failures that have been identified. The quad-selection-filter algorithms are used when four channels are operat-

ing and no failures have been detected.

The four selection-filter inputs obtained from the redundant sensor channels are processed by mid-value-select (MVS) algorithms. The signal selected by each algorithm is bounded on both sides by two other signals. The MVS function instantly reconfigures any time the median signal falls above or below either one of the other two signals, as in the case of a failed channel. This condition is shown in Figure 2 for a hardover failure of channel 3. The quad selection filter instantly reconfigured from channel 3 to channel 2 at the time of the failure.

Figure 2 also shows the response to the dual null failures of channels 3 and 2. The system instantly switches from

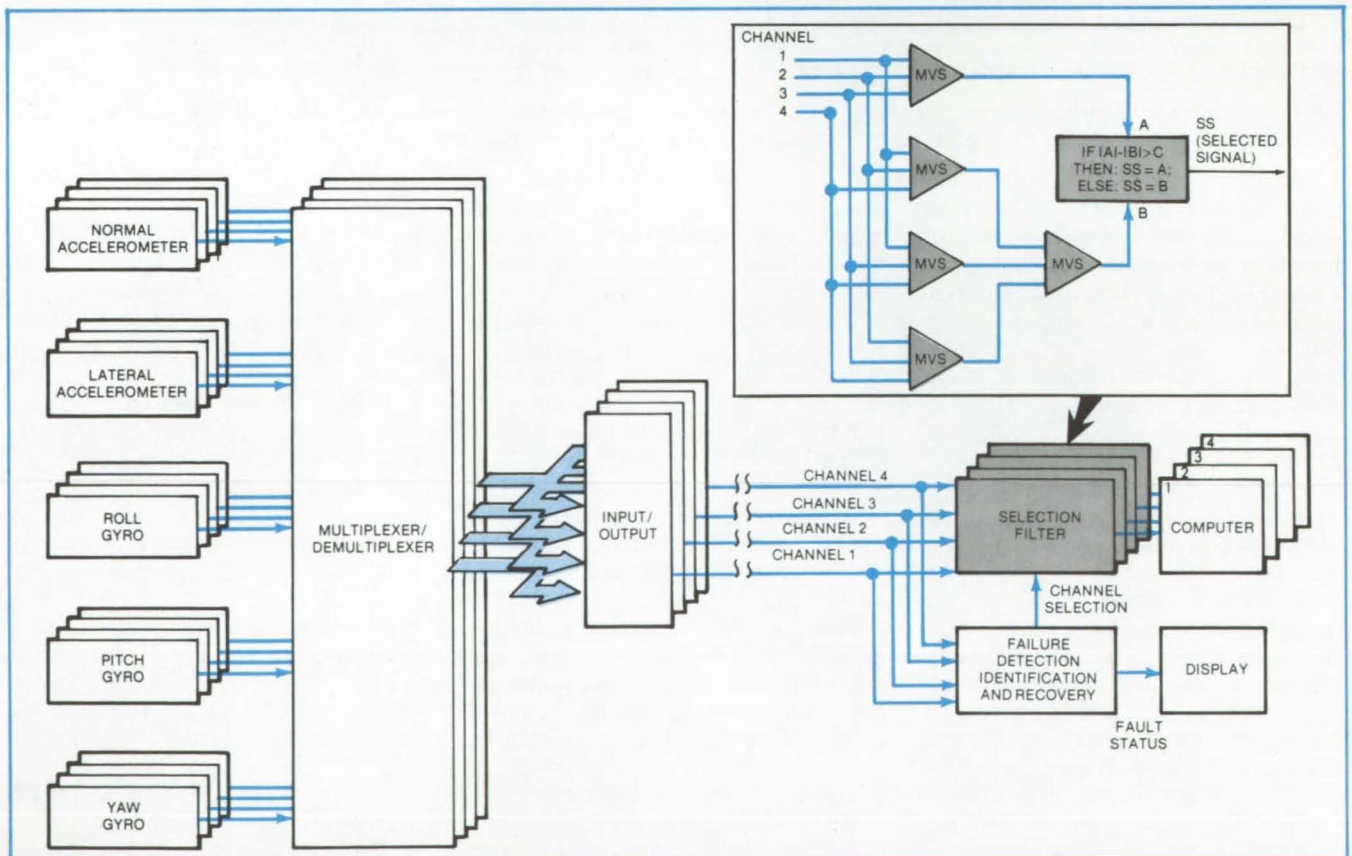


Figure 1. **Fourfold Redundant Control** for the Space Shuttle flight-control system includes a selection filter that electronically identifies and removes failed components. The filter uses mid-value-select algorithms, each monitoring three sensor signals, to select a failure-free data signal.

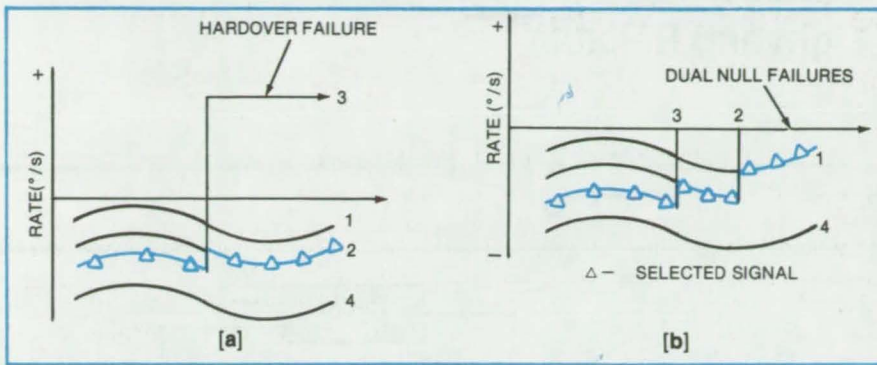


Figure 2. Instant Reconfigurations around a hardover failure (a) and around dual null failures (b) are shown in these time histories.

3 to 2 at the time of the first null failure and then switches from channel 2 to channel 1 at the second null failure.

This work was done by Hendrik C. Gelderloos of Honeywell, Inc., for Johnson Space Center. For further information, Circle 11 on the TSP Request Card.

This invention is owned by NASA, and a patent application has been filed. Inquiries concerning nonexclusive or exclusive license for its commercial development should be addressed to the Patent Counsel, Johnson Space Center [see page A5]. Refer to MSC-18498.

## Graphics-System Color-Code Interface

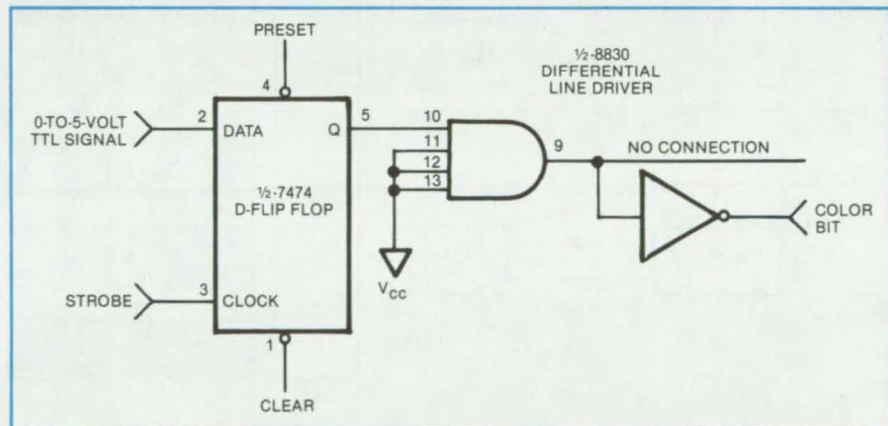
Hardware and software interface a graphics computer to a color monitor.

Langley Research Center, Hampton, Virginia

A circuit originally developed for a flight simulator interfaces a computer graphics system with a color monitor. The subsystem is intended for a particular display computer (AGT-130, ADAGE Graphics Terminal) and a specific color monitor (beam penetration tube — Penetron).

Previously, the images were displayed on a green-phosphor monitor. With the new circuit, they are presented in five colors, with only minor changes necessary to existing programs. The interface does not interfere with other input/output operations of the computer and does not require revision of the existing operating-system software.

The graphics computer transmits the color for each picture element as a 5-bit code; on the computer transfer bus, each bit is either +2.7 volts or -2.7 volts. The color-code interface converts this transfer-bus logic to transistor-transistor logic (TTL — i.e., 0 volt or +5 volts) and strobes it into a 5-bit storage register. From there, the code is sent through TTL differential line drivers to the color monitor, which interprets it as one of the five available colors (red, orange, amber, yellow, or green). The selected color code remains until a new one is sent to the



**Store-and-Transmit Channel** is one of five in the graphics/color-monitor interface. Adding the 5-bit color code to existing graphics programs requires minimal programming effort.

color-code interface. One of the five channels is shown in the figure.

Because the operating program has no provision for outputting data from the computer transfer bus, the code is formed in a working register and transferred to the instruction register over the transfer bus. This transfer operation also causes a strobe signal to occur at the precise time required for loading the data into the storage register of the color transmitter.

The color-code transmitter hardware consists of the logic converter

that changes transfer-bus logic to TTL, a data buffer register, an address decoder, and five TTL differential line drivers. One FORTRAN subroutine is added to the computer-graphics library. A call to the subroutine activates the color-code transmission.

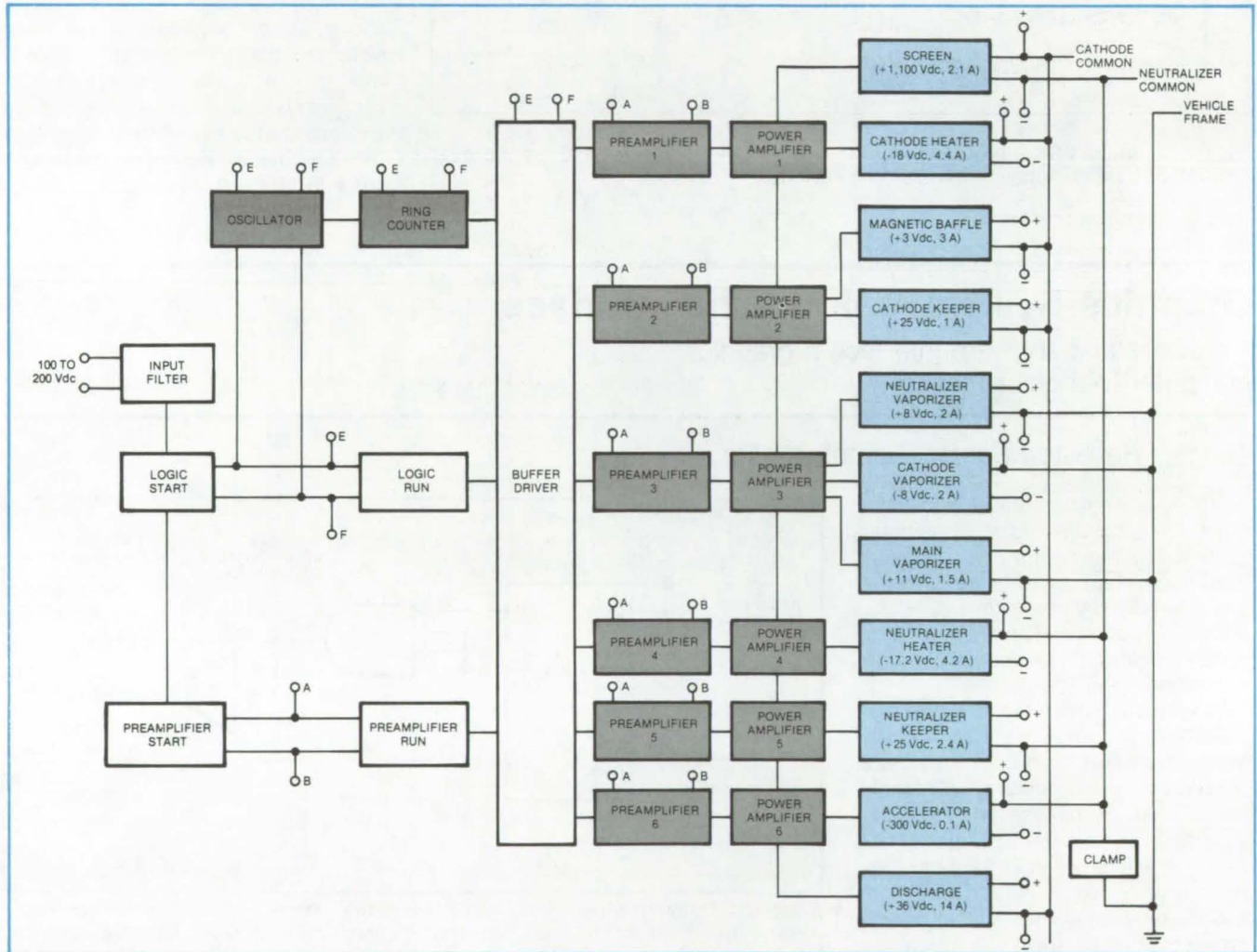
This work was done by John S. Tulppo of Sperry Rand Corp. for Langley Research Center. For further information, Circle 12 on the TSP Request Card.

LAR-12646

# Solar-Powered Supply Is Light and Reliable

A lightweight circuit delivers 11 different dc supply voltages.

Marshall Space Flight Center, Alabama



The **Multiphase Power Processor** supplies 11 dc voltages. CMOS integrated circuits reduce power consumption to about 250 W, while the processor delivers over 3 kW.

A dc supply originally intended for use in solar-powered spacecraft propulsion is lightweight and very reliable. It operates from the 100- to 200-volt output of solar panels to produce 11 different dc voltages, with a total demand of 3,138 watts.

A block diagram of the system is shown in the figure. The 2-MHz master-oscillator signal is divided by ripple and ring counters to produce six 10.4-kHz square waves with overlapping phases. The signals drive six preamplifiers fol-

lowed by six power amplifiers. The power-amplifier outputs are coupled through toroidal-core transformers (not seen in the figure) to rectifiers that produce the final dc voltages.

The connection of the secondaries of the transformers is unique. Each has two windings, designated S<sub>1</sub> and S<sub>2</sub>. The S<sub>1</sub> windings are connected in series and then to the S<sub>2</sub> windings, which are also wired in series. This reduces the voltage on any secondary.

The resulting ac waveform is recti-

fied using diodes and SCR's to produce the "screen" voltage supply and the "discharge" voltage supply. It has inherent redundancy since the failure of a preamplifier or amplifier reduces the output by only one-sixth. The other low-voltage power supplies are derived using conventional circuits from the secondary windings of the individual output transformers.

With the exception of specially wound inductors and transformers, the system uses readily available compo-



nents. A conceptual flight configuration estimated from a breadboard prototype would contain 428 parts and would weigh no more than 60 lb (27 kg). Power dissipation in the box would be about 250 watts.

This work was done by Albert E. Willis, Harrison Garrett, John M. Gould, and Jack Matheny of **Marshall Space Flight Center**. For further information, including a detailed schematic, Circle 13 on the TSP Request Card.

Inquiries concerning rights for the commercial use of this invention should be addressed to the Patent Counsel, [see page A5]. Refer to MFS-25430.

## Improved Phase-Lock Detector

The in-phase and quadrature signals in a phase-locked loop share common circuit elements.

Lyndon B. Johnson Space Center, Houston, Texas

A modification to the Costas loop lock detector promises to minimize errors in determining when the loop is locked to the incoming carrier signal. The detector,

used in a low-signal-to-noise communication carrier demodulator, previously produced errors due to an imbalance between the in-phase (I) and quadrature (Q)

channels. By using a single set of circuit elements for both channels, the errors are now minimized. In the modified arrangement, the I and Q products are switched in and out by a dither control.

Figure 1 shows a conventional Costas lock detector operating with a phase-locked loop. The detector computes the difference  $I^2 - Q^2$  and compares it with a threshold to determine whether the loop is phase-locked. Any difference in the mixers, filters, and square-law detectors of the two channels creates an error in the computation.

The detector of Figure 2 minimizes the errors by using the same mixer, filter, and square-law detector to determine I and Q. A dither control, or switch, connects the I and Q channels alternately to the common detection elements; only the 90° phase shifter is not common to both I and Q estimates. The errors due to asymmetry between the duration of the I and Q cycles of the dither, and to the lack of coherence between mixer switching and comparator switching, can be made very small compared to the unbalance between two detector chains. The dither rate need only be large enough to have many cycles in a detection interval (i.e., in the time constant of the output low-pass filter).

The dither-balanced detector is being used on the Shuttle Ku-band radar/communication-subsystem forward communication link to determine that the loop demodulator has phase-locked to the proper signal. It can be used to improve detection probability and reduce false alarm probability for any loop that must acquire a signal with a low signal-to-noise ratio.

This work was done by Leonard M. Bronstein of Hughes Aircraft Co. for **Johnson Space Center**. For further information, Circle 14 on the TSP Request Card.  
MSC-18797

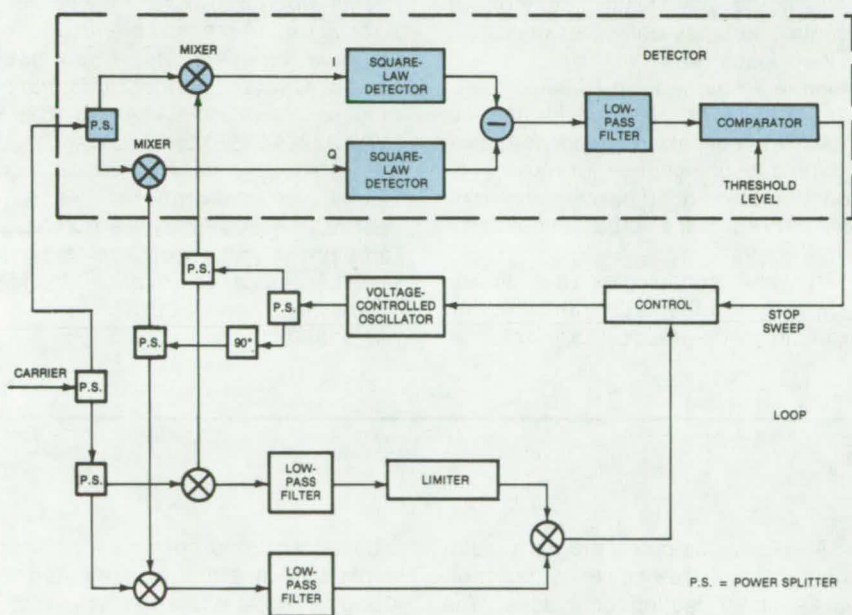


Figure 1. The **Locking Detector** in this conventional phase-locked loop has separate in-phase (I) and quadrature (Q) channels and therefore is subject to false locking due to erroneous levels caused by unbalance of the channel elements.

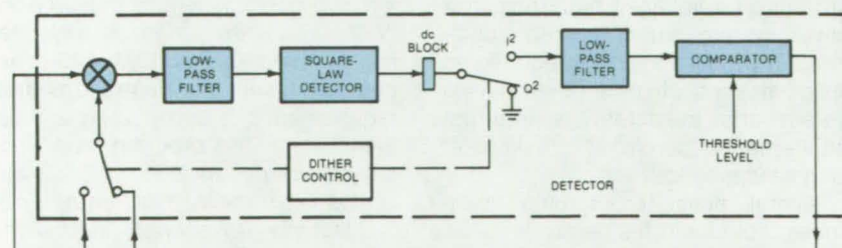


Figure 2. The **Single Detection Channel** in this modified arrangement is used alternately by in-phase (I) and quadrature (Q) signals, under the control of a dither switch. By eliminating errors caused by unbalance of the I and Q channels, this dither-balanced detector reduces false locking.

## Books and Reports

These reports, studies, and handbooks are available from NASA as Technical Support Packages (TSP's) when a Request Card number is cited; otherwise they are available from the National Technical Information Service.

### Advanced Technologies for Commercial Airplanes

Report evaluates potential in large and small aircraft.

What advanced electrical and electronic spacecraft technologies can be applied in commercial airplanes? A 263-page report addresses this question; describes the new technologies, the airplanes, the tradeoffs, and the methods of evaluation; and concludes that the major beneficiary would be an advanced wide-body transport (500-passenger). In particular, fuel consumption would be greatly reduced. Smaller airplanes, although suitable for the application of several new technologies, would benefit less.

The report discusses a study in which technologies used in the Space Shuttle were evaluated for their poten-

tial in commercial transports. These technologies include:

- Fly-by-wire flight control and stability augmentation, in which signals are transmitted over wires to actuators at the control devices (the present generation of transports, in contrast, transmits commands by mechanical or hydraulic lines);
- Computer monitoring and management of vehicle systems;
- The integration of avionics (flight controls, navigation systems, and displays) into a few computers; and
- Digital multiplexing of control and data signals.

In addition, the study evaluated several technologies that are not now used in the Space Shuttle but are being considered for it:

- All-electric power for actuation of control surfaces and other needs,
- Fiber optics, and
- Ring laser gyros for navigation.

The evaluations were performed on three hypothetical airplanes: a 500-passenger subsonic airliner for transcontinental routes, a 50-passenger short-haul aircraft, and a 30-passenger commuter aircraft.

The new technologies save significant weight in the large transport. For example, fly-by-wire control will reduce

takeoff weight by 971 lb (440 kg). Moreover, fly-by-wire control will help to stabilize supercritical wing designs and similar aerodynamic innovations, which further reduce takeoff weight by 5,060 lb (2,300 kg) and cut fuel consumption because of their aerodynamic efficiency.

Fly-by-wire control, digital multiplexing, and similar technologies are not now cost-effective in the smaller aircraft [about 40,000 lb (18,150 kg) and under]. An all-electric power system for actuators, however, may offer immediate advantages in all three types of aircraft. Not only will the all-electric system reduce takeoff weight [18,700 lb (8,500 kg) in the large airplane] but it will also reduce the costs of design, parts, and maintenance.

*This work was done by Lockheed Aircraft Co., Airsearch Manufacturing Co., and Honeywell Inc. for Johnson Space Center. Further information may be found in NASA CR-163576 [N80-32375/NSP], "Application of Advanced Electric/Electronic Technology to Conventional Aircraft" [\$21.50]. A copy may be purchased [prepayment required] from the National Technical Information Service, Springfield, Virginia 22161. MSC-18982.*

## Computer Programs

These programs may be obtained at very reasonable cost from COSMIC, a facility sponsored by NASA to make new programs available to the public. For information on program price, size, and availability, circle the reference letter on the COSMIC Request Card in this issue.

### Short-Circuited Power Networks

Program computes currents and voltages in shorted single-line or three-phase networks.

A NASA computer program automatically analyzes power-system networks under faulted conditions. The program is general enough to calculate single-line-to-ground faults and three-phase-to-ground faults.

Short-circuit calculations provide the design engineer with an idea of the currents and voltages occurring in a power system during faulted conditions. The information is required to design an adequate protective relaying system and to determine interrupt requirements for circuit breakers at each switching location.

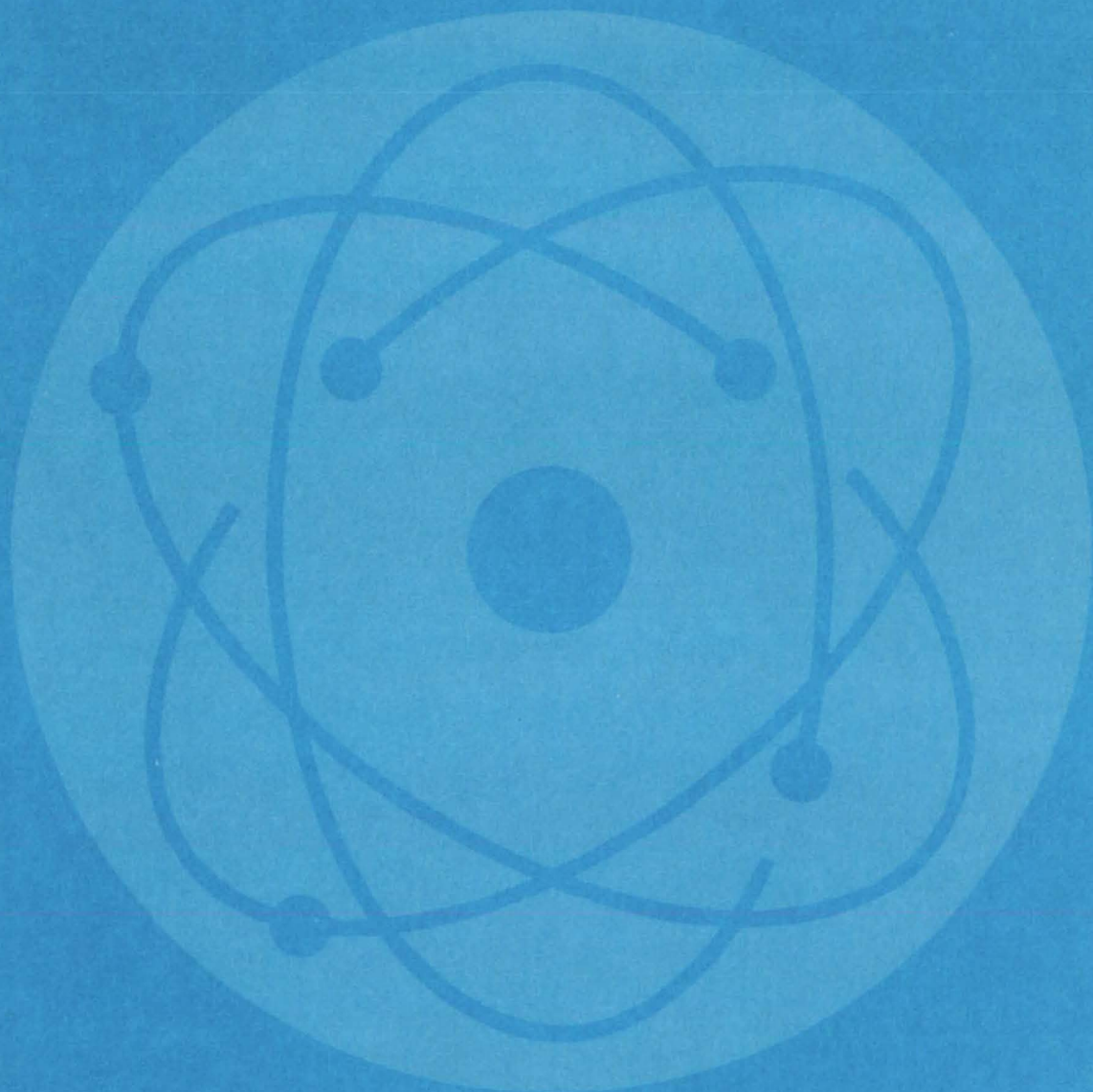
Several novel programming techniques automate the analysis while reducing computing time and storage requirements. Network trees systematically and automatically select the

independent loop currents. The loop-impedance matrix is generated by using topological relationships. Matrix generation by set-theoretical rules avoids the conventional matrix-multiplication approach, which can require extensive computing resources for the analysis of large systems.

The program is written in FORTRAN IV for batch execution. It has been implemented on an IBM 370-series computer with a central memory requirement of approximately 270K of 8-bit bytes. The program was originally developed in 1973.

*This program was written by Tedja S. Oepomo of Rockwell International Corp. for Johnson Space Center. For further information, Circle J on the COSMIC Request Card. MSC-18977*

# Physical Sciences



## Hardware, Techniques, and Processes

- 23 Beam Splitter Intensities Are Preselected
- 24 Sequential-Impulse Generator Uses Fiber Optics
- 25 New Energy-Saving Technologies Use Induction Generators
- 26 Temperature Controller for a Solar Furnace
- 27 Baffle Keeps Solar Energy in Receiver

## Books and Reports

- 27 Pyramidal-Reflector Solar Heater
- 28 Solar Water Heater Installation Package
- 28 Motel DHW Retrofit — Dallas, Texas
- 29 Solar Hot Water for Motor Inn— Texas City, Texas
- 29 Solar-Energy System for a Commercial Building — Topeka, Kansas
- 29 Solar-Heated Water at a Motel — Mobile, Alabama
- 30 Solar-Heated Public Library — Troy, Ohio
- 30 Solar-Cooled Classroom Building — Columbus, Ohio
- 30 Solar-Heated and Cooled Office Building — Columbus, Ohio
- 31 Solar Hot Water for an Industrial Laundry — Fresno, California
- 31 Solar-Water-Heater Design Package

## Computer Programs

- 32 Energy-Systems Economic Analysis

## Beam Splitter Intensities Are Preselected

One light beam is split into several beams with predetermined intensities.

*Marshall Space Flight Center, Alabama*

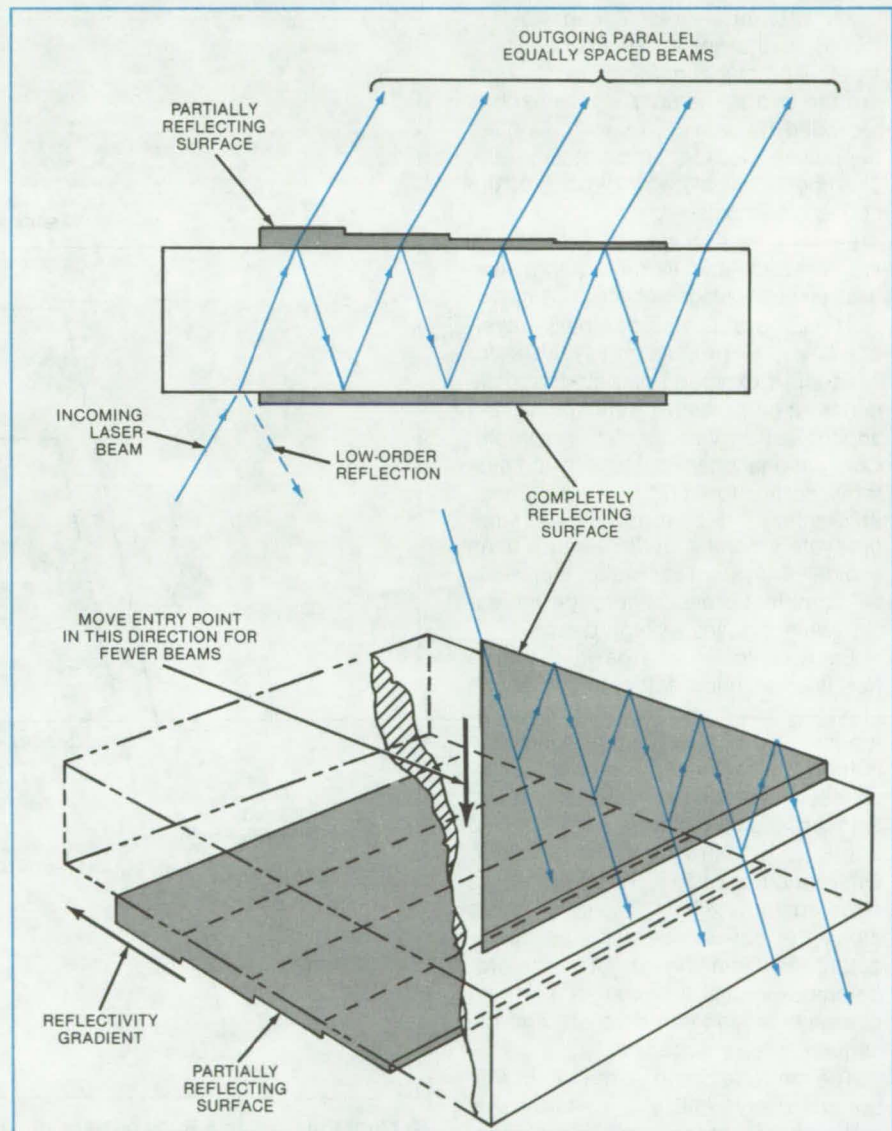
The light beams emanating from a beam splitter developed at Marshall Space Flight Center all have the same intensity. Attenuation and transmission losses, which weaken the beams from a conventional beam splitter, are compensated for in the new design by a partially reflecting coating that has a step-function reflectivity gradient. By adjusting the gradient, the relative intensities can be changed to other (nonunity) values.

The new beam splitter, shown in the figure, is a block of optically clear material with two parallel polished faces. Some of the area of one surface is coated with a totally reflecting layer, which may be metal or dielectric. On the opposite surface, a metal coating of stepped thickness offers a different reflectivity at each step. The width and spacing of the reflecting zones are chosen to accommodate the angle of incidence of the input beam and the desired spacing of the output beams.

The input beam enters through the uncoated area of the partially coated surface and reflects back and forth between the coatings on the polished faces, as in a conventional beam splitter. A portion of the beam emerges at each reflection from the partially reflecting surface.

The relative intensities of the emerging beams depend on the index of refraction of the block, the angle of incidence of the input beam, and the attenuation and reflectivity at each point of reflection. By controlling the thickness of the coating deposited on the partially reflecting surface, the output intensity ratios are controlled. In the example shown in the figure, there are five output beams of equal intensity. If refractive and dissipative effects are ignored, the first through the fifth steps must have reflectivities of  $4/5$ ,  $3/4$ ,  $2/3$ ,  $1/2$ , and  $0$ , respectively.

The number of output beams is varied by moving the point of entry along the diagonal line shown in the figure. The number of reflections (and, therefore, of output beams) increases or decreases as the entry point is made more or less distant from the last



In the **Manifold Beam Splitter**, a sequence of partial internal reflections produces multiple output beams. The relative intensities of the output beams depend on the reflectivities of the steps in the partially reflecting surface.

beam exit. To maintain constant beam intensities when changing the number of beams, the input-beam intensity is changed accordingly. The new beam splitter could find application in two-phase fluid-flow measurements, aerosol sizing, security systems, photogrammetry, laser-Doppler velocimetry, interferometry, and holography.

*This work was done by Warren Campbell and Robert B. Owen of*

**Marshall Space Flight Center.** For further information, Circle 16 on the TSP Request Card. MFS-25312

*This invention is owned by NASA, and a patent application has been filed. Inquiries concerning nonexclusive or exclusive license for its commercial development should be addressed to the Patent Counsel, Marshall Space Flight Center [see page A5]. Refer to MFS-25312.*

# Sequential-Impulse Generator Uses Fiber Optics

A train of impulses are laser-triggered.

NASA's Jet Propulsion Laboratory, Pasadena, California

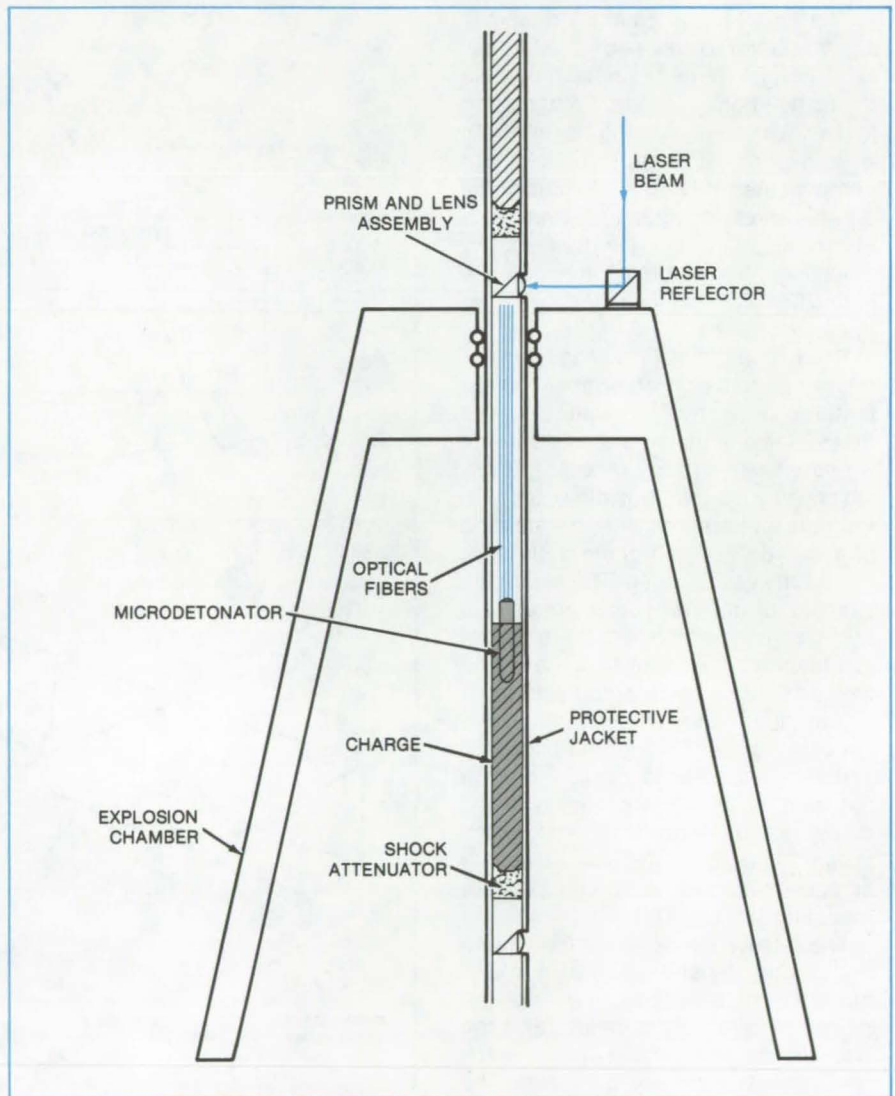
An apparatus fires a long train of explosive charges in rapid succession, safely and dependably. The charges are fed into a chamber where each is exploded by a microdetonator ignited by pulses from a laser outside the chamber. Possible applications of the sequential-impulse generator are in creating shock waves for aerodynamics research and in generating electrical power by magnetohydrodynamics.

The apparatus was originally developed as a propulsion system for spacecraft exploring planets that have dense, high-pressure atmospheres — Jupiter and Venus, for example. Conventional chemical propulsion systems do not function well in such an environment. In contrast to the chemical systems, the specific impulse of an explosive system actually increases with ambient pressure for high molecular-weight gases at high density.

Each explosive charge in the train has its own microdetonator, which is connected by an optical-fiber bundle to a prism and lens (see figure). The train is fed from a coil into the chamber by an indexing mechanism. The prism and lens of a given charge are stopped briefly at the entrance to the chamber, where a pulse of light from the laser is directed into the lens. The light travels along the optical fibers to the microdetonator, igniting it. The microdetonator ignites the charge. The next charge is moved into position, and the sequence is repeated.

The microdetonators, manufactured commercially, utilize a material that includes lead styphnate. This detonator is readily ignited by laser energy but is relatively insensitive to other stimuli. It is therefore safer to use than other detonators. It is estimated that the apparatus can operate at a rate of 100 explosions per second. With laser pulses 30 ns long, the time for initiation of an explosion varies no more than 0.17  $\mu$ s.

Because the charge is actuated when it is separated from the top and walls of the chamber, the erosion of these surfaces by the repeated explo-



**A Light Pulse From a Ruby or Neodymium-Glass Laser enters the miniature optics of the repetitive-detonation apparatus. Traveling along a bundle of optical fibers, the light strikes the laser-sensitive microdetonator, and the charge explodes. The apparatus then advances the next charge in the train into position.**

sions is minimized. A shock attenuator at the base of a charge prevents it from being set off when the preceding charge in the train detonates.

The laser-detonation concept could be adapted to the generation of plane shock waves. With a branched optical-fiber bundle, multiple points on an explosive sheet would be initiated by a single laser pulse. The explosion-initi-

ation period has a small variation; thus the sheet will detonate simultaneously across its surface, generating a plane shock wave.

*This work was done by Lien C. Yang of Caltech for NASA's Jet Propulsion Laboratory. For further information, Circle 17 on the TSP Request Card. NPO-14939*

## New Energy-Saving Technologies Use Induction Generators

An induction motor, mechanically driven to act as a generator, delivers power to an ac line.

*Marshall Space Flight Center, Alabama*

Two energy-saving technologies tested recently at Marshall Space Flight Center use an induction motor operated in reverse (as an induction generator). In the first, energy that is ordinarily dissipated during load testing of machinery is recovered and returned to the powerline. In the second, the efficiency of a wind-driven induction generator is improved, and the useful range of windspeed is broadened. Both technologies take advantage of the ac voltage developed across the terminals of an induction motor when it is rotated at higher-than-synchronous speed in the direction it normally turns when power is applied.

Figure 1 shows such an induction machine coupled to the output of another motor that is being tested for its performance under varying load. Other devices that can be tested this way are combustion engines, transmissions, gear trains, and other mechanical linkages. The generator recoups much of the test energy that otherwise would be dissipated as heat (in a dynamometer, for example) and returns it to the ac powerline. The mechanical energy must rotate the induction machine at higher-than-synchronous speed. The ac line regulates the frequency and output voltage.

To vary the load, the generator is connected to the ac line through a variable transformer. The load that the generator presents to the motor varies with the applied voltage on the generator and can be precisely controlled from zero to rated load by adjusting the variable transformer. Losses in the transformer are low, and the energy returned to the ac line is essentially equal to the energy applied to the shaft of the induction generator multiplied by its efficiency. A variable load can also be obtained by using a gate-controlled semiconductor switch or two silicon-controlled rectifiers to disconnect the generator from the powerline for a portion of each cycle.

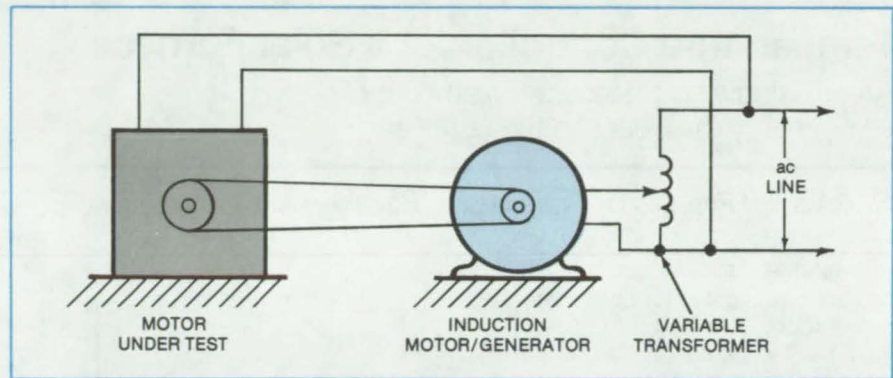


Figure 1. When the **Load on a Motor Being Tested** is an induction generator, much of the energy supplied to the motor can be returned to the ac line. The variable transformer controls the load applied to the motor. (The pulley ratio is chosen to make the generator run faster than its synchronous speed.) Although the system shown is for a single-phase motor, it is also applicable to three-phase motors by using a three-phase variable transformer. Approximately 70 percent of the drive energy was returned to the line in tests of a three-phase motor.

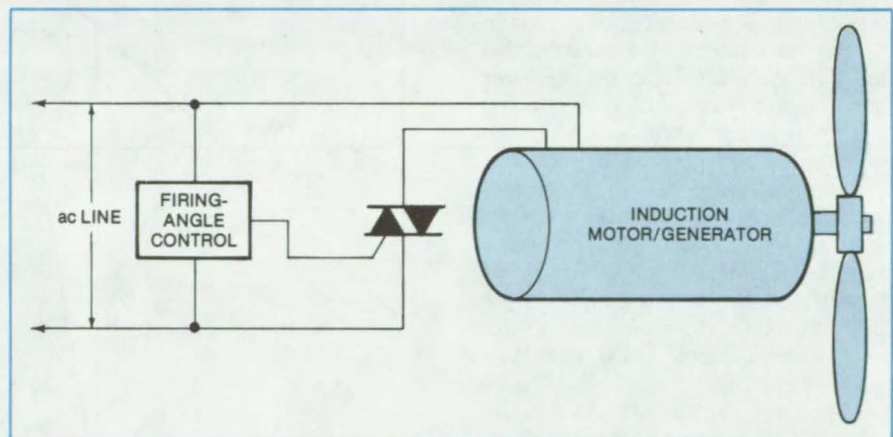


Figure 2. A **Wind-Driven Induction Generator** is made more efficient by controlling its output with a solid-state switch and firing-angle control circuit. Low-load losses of a 1/2-horsepower (375-watt) generator were reduced this way from 220 to 75 W, with no sacrifice of full-load power.

In applying the induction generator to convert wind energy to electrical energy, a primary problem is maintaining good efficiency over a broad range of windspeeds. The system is designed for a given maximum wind velocity, and the generator must be decoupled or disconnected from the line above that velocity to prevent damage. Also, a minimum windspeed is required to drive the generator to synchronous

speed to offset the inherent losses in the generator. The generator also is disconnected from the line at a minimum wind velocity to prevent it from consuming power.

The NASA-developed power-factor controller circuit [see "Energy Saving in ac Generators" (MFS-25302) on page 134 of *NASA Tech Briefs*, Vol. 5, No. 2] is an approach to maximizing performance at high and low wind-

speeds. As shown in Figure 2, a gate-controlled semiconductor switch is installed between the powerline and the wind-driven induction machine. A firing-angle control circuit regulates the switch "on" time so that the

generator is connected only for a portion of each cycle. The minimum on time occurs at low wind velocity; and for maximum windspeed, the switch is on continuously.

*This work was done by Frank Nola of Marshall Space Flight Center. For further information, Circle 18 on the TSP Request Card. MFS-25513*

## Temperature Controller for a Solar Furnace

An adjustable shield varies the amount of solar energy that reaches the receiver.

*NASA's Jet Propulsion Laboratory, Pasadena, California*

A relatively-simple movable shield has been suggested for controlling the temperature of a solar furnace. The temperature modulator can be set to have the collected solar energy fully "on," fully "off," or at any intermediate level.

The solar furnace for testing materials at 3,000° F (1,650° C) is shown in the figure. A parabolic mirror concentrates Sunlight into the receiver. The shade plate that blocks insolation at the back of the receiver produces a shade zone in the center of the collector. No radiation is returned to the receiver from the shade zone; only rays falling on other areas of the reflecting surface are directed back toward the receiver.

The proposed solar-flux modulator would be interposed between the receiver and the reflector. The modulator is a circular plate with the same outside diameter as the shade plate and the same aperture diameter as the receiver. Three positions of the modulator plate are illustrated:

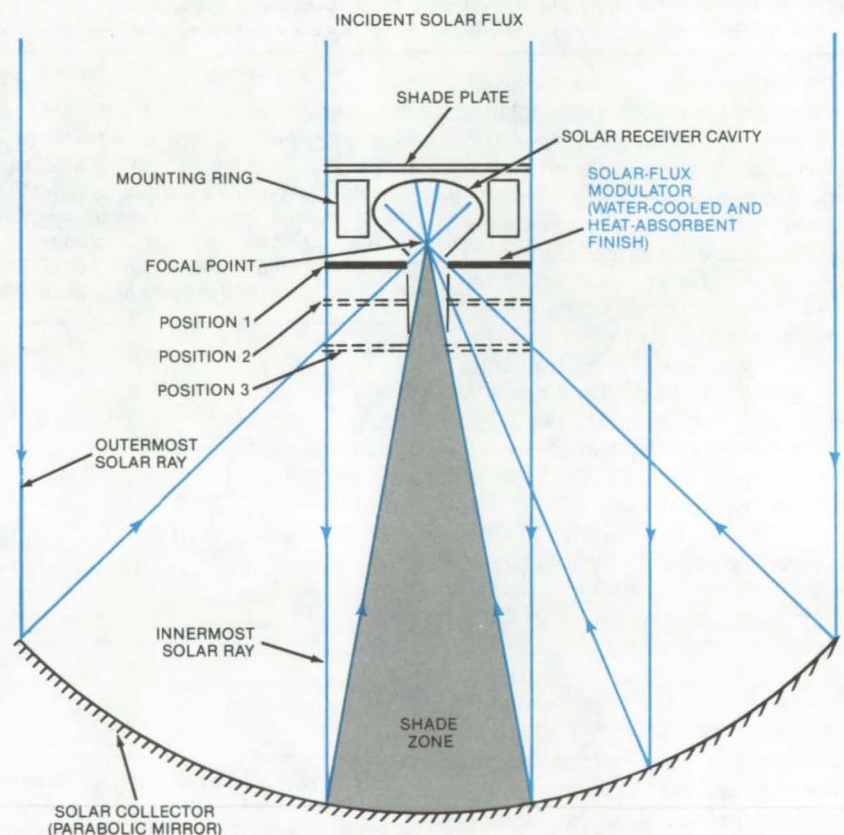
- At position 1, which is closest to the receiver, all of the rays from outside of the shade zone pass through the aperture of the modulator and into the receiver.
- At position 2, some of the rays that are reflected from the mirror are blocked by the modulator plate and thus are prevented from reaching the receiver.
- At position 3, where the modulator plate is farthest from the receiver, all rays are blocked from passing to the receiver aperture and cavity.

Any modulator position between 1 and 3 can be selected by operating an actuator mechanism, thereby control-

ling the solar power entering the receiver.

*This work was done by Allan R. McDougal and Robert R. Hale of Caltech for NASA's Jet Propulsion Laboratory. For further information, Circle 19 on the TSP Request Card.*

*Inquiries concerning rights for the commercial use of this invention should be addressed to the Patent Counsel, NASA Resident Office-JPL [see page A5]. Refer to NPO-15388.*



**The Position of the Modulator Plate** would be adjusted to vary the flux into the receiver cavity from fully on (position 1) to fully off (position 3).



## Baffle Keeps Solar Energy in Receiver

Mirror structure in solar concentrator reduces heat loss by reflection and reradiation.

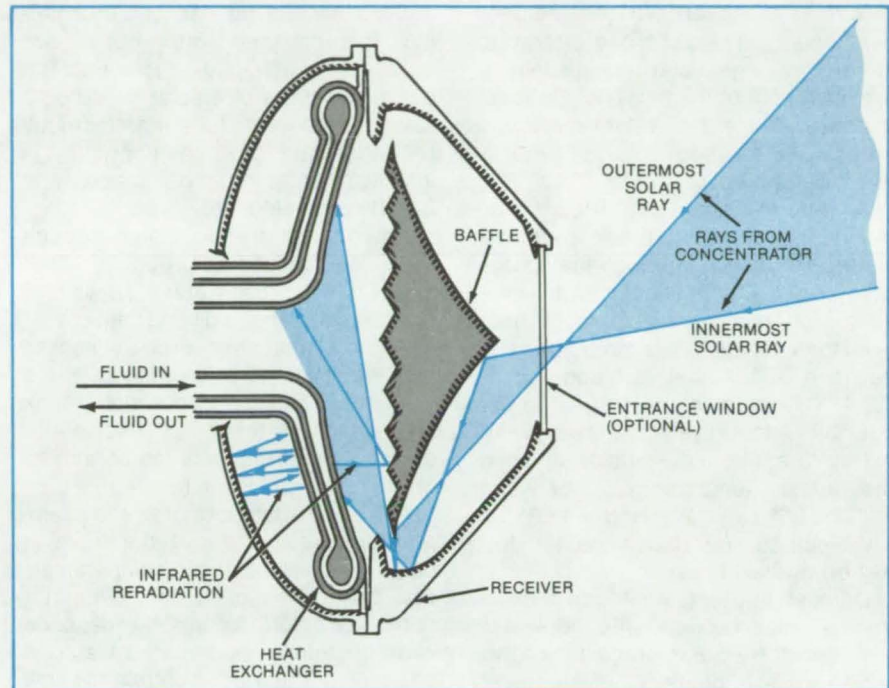
NASA's Jet Propulsion Laboratory, Pasadena, California

The efficiency and internal temperature of a concentrating solar collector could be increased by a baffle within the solar-energy receiver. According to the baffle concept, most of the solar energy that enters the receiver would be retained, rather than reflected or reradiated and lost.

Ordinarily, a part of the energy directed into a receiver by a concentrator is reflected back through the mouth of the receiver. In addition, part of the solar energy absorbed by the receiver heat exchanger is reradiated as infrared energy.

The new baffle would be interposed between the mouth of the receiver and the heat exchanger (see figure). Its forward surface is contoured and coated with a reflective material so that, in combination with the mirrored receiver wall, it directs incoming solar radiation to the heat exchanger. The back surface of the baffle is grooved and coated so that infrared rays emitted by the heat exchanger are reflected back to the exchanger. Since the back surface of the heat exchanger also emits infrared, the back portion of the receiver is also mirrored to reduce heat loss.

The baffle and receiver wall can be water-cooled to protect them from damage by high temperatures. An optional entrance window seals the



**A Baffle Reflects Entering Rays** back and forth in this solar-concentrator receiver until they reach the heat exchanger. Similarly, infrared energy reradiated by the heat exchanger is prevented from leaving the receiver. The surfaces of the baffle and the inside wall of the receiver are polished and highly reflective at solar and infrared wavelengths.

cavity to control its atmosphere for material testing or for use as a hot-gas-engine heat exchanger. Heat loss due to infrared absorption by the baffle and the cavity walls could be held to less than 10 percent.

*This work was done by Allan R. McDougal and Robert R. Hale of Caltech for NASA's Jet Propulsion Laboratory. For further information, Circle 20 on the TSP Request Card. NPO-15387*

## Books and Reports

These reports, studies, and handbooks are available from NASA as Technical Support Packages (TSP's) when a Request Card number is cited; otherwise they are available from the National Technical Information Service.

### Pyramidal-Reflector Solar Heater

Motor-driven reflector compensates for seasonal changes in the Sun's altitude.

Design data for a solar-heating and domestic hot-water system based on pyramidal optics are contained in a recently issued report. The system has flat-plate absorbers mounted on the north side of an attic interior. A skylight

window on the south-facing roof admits Sunlight into the attic, which is lined with mirrors that reflect the light to the absorbers. The reflectors are the inner surfaces of a pyramid lying on its side with the window at its base and the absorber plates in a cross-sectional plane near its apex.

The mirror on the floor of the attic is hinged near the collector and can be raised at its south (window) edge by a winch and cables. This hinged panel is raised slowly at its south edge at a rate of about 2 inches (5 cm) per week. The movement compensates for the

change in the altitude of the Sun with the seasons, ensuring that maximum sunlight is directed into the collector. The angular position of the panel ranges from a low of 10° for the December Sun to a high of 45° for the June Sun.

The Sunrays are focused on copper absorber panels through which water is circulated to absorb the incident heat energy. The absorbed energy is stored in a large water tank, usually in the basement of the dwelling. Optional accessories for the system include a fireplace-heat recovery unit and a window-heat recovery unit.

A water-to-air heat exchanger transfers heat directly from the solar-heated water to air flowing through the household ducts. A combination water-and-air-source heat pump extracts heat from the water when its temperature is between 40° F (4.4° C) and 85° F (29.4° C) and transfers the heat to the duct air. Alternatively, the heat pump extracts heat from the outside air when the outside temperature is between 10° and 65° F (-12.2° and +18.3° C). An electrical resistance heater furnishes auxiliary heat.

Domestic water is heated by a heat-transfer loop between the hot-water tank and the solar storage tank. The hot-water tank contains an electrical immersion heater for auxiliary heat.

The report describes the system and gives information on typical installation arrangements, dimensions, and ratings. It provides guidance on installation, sizing, and specification writing. A control schematic and a piping and wiring diagram are included.

*This work was done by Wormser Scientific Corp. for **Marshall Space Flight Center**. Further information may be found in DOE/NASA CR-161202 [N80-33865/NSP], "Design Data Brochure for a Pyramidal Optics Solar System" [\$6]. A paper copy may be purchased [prepayment required] from the National Technical Information Service, Springfield, Virginia 22161. The report is also available on microfiche at no charge. To obtain a microfiche copy, Circle 21 on the TSP Request Card.*  
MFS-25571

## Solar Water Heater Installation Package

Guide is based on experience with units in Arizona and California.

Installation guidelines for a commercial solar-powered water heater are contained in a 48-page document. The system consists of a solar collector, a solar-heated-water tank, an electrically-heated water tank, and controls. It is installed at sites in Tempe, Arizona, and San Deigo, California.

Potable water is circulated through the collector and returned to either tank. Collector-loop water is drawn only from the solar-heated-water tank.

Automatic control circuitry senses the temperatures of the collector, the solar tank, and the conventional tank and compares them with each other and with three reference temperatures: the highest- and lowest-allowable conventional-tank temperatures and a temperature set just above the freezing point. As a result of these comparisons, the control switches the circulator pump on or off, signals the cascade valve to return solar-heated water to one tank or the other, controls the flow of electrical power to the conventional heater, and drains the collector loop if its temperature approaches the freezing point.

The report describes the water-heating system, its installation (covering collector orientation and mounting and plumbing and wiring), operating instructions, and maintenance procedures. An analysis of possible hazards from pressure, electricity, toxicity, flammability, gas, hot water, and steam are also included.

*This work was done by Elcam, Inc., for **Marshall Space Flight Center**. Further information may be found in DOE/NASA CR-161562 [N80-33866/NSP], "Installation Package for a Sunspot Cascade Solar Water Heating System" [\$8]. A paper copy may be purchased [prepayment required] from the National Technical Information Service, Springfield, Virginia 22161. The report is also available on microfiche at no charge. To obtain a microfiche copy, Circle 22 on the TSP Request Card.*  
MFS-25573

## Motel DHW Retrofit — Dallas, Texas

Lavatory and shower water for 100 rooms and laundry-room water are preheated by solar energy.

A solar-energy system designed to provide 65 percent of the total domestic-hot-water (DHW) demand for a 100-room motel in Dallas, Texas, is the subject of a report that is now available. The system is retrofit, and storage-tank size was limited to 1,000 gallons (3,785 l) by the size of the room where it is located. Pumps and plumbing are located as near as possible to the steel tank to conserve space and minimize heat-transfer losses. Immediately below storage is the motel laundry room.

Liquid flat-plate collectors are mounted on the roof just above the storage-tank room. They drain automatically into storage when the collector-loop pump is not running. Freeze protection is insured by check valves that prevent hot moist air from rising through the pipe and condensing in the collectors. The storage tank is vented to the atmosphere.

Heat is transferred from storage to the motel DHW tanks through a tube-and-shell exchanger. Collector-loop water is pumped from the storage tank through the shell side; and DHW is pumped through the tube side.

All pumps are controlled by differential temperature settings, and pressure gages are installed across each pump so flow rates can be set and read periodically. The combination of flow rates derived from the gages with temperature measurements can be used to assess system performance.

*This work was done by Day's Inn of America, Inc., for **Marshall Space Flight Center**. Further information may be found in DOE/NASA CR-161569 [N81-10524/NSP], "Solar Hot Water System Installed at Day's Inn Motel, Dallas, Texas [Forrest Lane]" [\$6.50]. A paper copy may be purchased [prepayment required] from the National Technical Information Service, Springfield, Virginia 22161. The report is also available on microfiche at no charge. To obtain a microfiche copy, Circle 23 on the TSP Request Card.*  
MFS-25580

## Solar Hot Water for Motor Inn — Texas City, Texas

Roof collectors meet 63 percent of the total demand.

A final report describes a solar domestic-hot-water heater installation at LaQuinta Motor Inn, Texas City, Texas. The heater furnishes 63 percent of the total hot-water load of the new 98-unit inn. It employs flat-plate collectors circulating a mixture of 30 percent ethylene glycol antifreeze in water. Balancing valves regulate the flow to the solar panels. The system capacity is  $3.67 \times 10^8$  Btu/yr ( $3.87 \times 10^{11}$  J/yr).

Eleven banks of nine collectors each are mounted on the roof of the inn. Total collector area is 2,100 ft<sup>2</sup> (195 m<sup>2</sup>). The collector array feeds a 2,500-gal (9.5-m<sup>3</sup>) storage tank constructed of insulated steel and located outdoors, next to the inn air-conditioner cooling tower. The tank contains two heat exchangers: one to transfer heat from the collector solution to the storage tank and the other to transfer heat from the storage tank to domestic hot water. The two heat exchangers provide double-wall separation between the ethylene glycol and the hot-water system. A recirculating pump improves the heat transfer between the heat exchangers and the hot water. To avoid freezing in the recirculating line, the pump was modified to turn on when the ambient temperature drops to 32° F (0° C) or below.

When the temperature in the storage tank is at least 15° F (8.3° C) hotter than the water in the inn conventional electric water heater, a temperature-differential controller activates the pump to transfer solar heat to the building hot-water system. The pump is turned off when the storage-tank temperature is only 5° F (2.8° C) higher than that of the water in the electric heater.

The report presents a description of the system, drawings and photographs of the collectors, operation and maintenance instructions, manufacturers' specifications for pumps, and an engineer's report on performance. Placed in operation in the summer of 1978, the system has performed as expected and has been operating satisfactorily.

This work was done by LaQuinta Motor Inns, Inc., for Marshall Space Flight Center. Further information may be found in DOE/NASA CR-161605

[N81-15460/NSP], "Solar Domestic Hot Water System Installed at Texas City, Texas — Final Report" [\$6.50]. A paper copy may be purchased [prepayment required] from the National Technical Information Service, Springfield, Virginia 22161. The report is also available on microfiche at no charge. To obtain a microfiche copy, Circle 24 on the TSP Request Card. MFS-25614

## Solar-Energy System for a Commercial Building — Topeka, Kansas

Solar heating and cooling are integrated into an energy-efficient building design.

Solar energy for space heating, cooling, and domestic hot water at a 5,600-square-foot (520-square-meter) Topeka, Kansas, commercial building is supplied by evacuated-tube liquid collectors. The solar-energy system, described in a recent report, is expected to provide 74 percent of the annual cooling load, 47 percent of the heating load, and 95 percent of the domestic hot-water load.

The system was included in the building design to maximize energy conservation. The array of 72 collectors has a total area of 1,068 ft<sup>2</sup> (99.2 m<sup>2</sup>). Ethylene glycol solution circulates through the collectors and a tube-in-shell heat exchanger. Water heated in the exchanger is used for space heating, supplying heat to the absorption chillers, or for heating domestic hot water.

Energy is stored in a 1,100-gallon (4,200-liter) tank. A heat-rejection system protects the collector loop by dumping excess heat to the atmosphere when the collector outlet temperature exceeds 280° F (138° C).

An error in the control system resulted in freezing damage to the heat exchanger and collector tubes during an episode of cold weather; however, simple modification to the control eliminated the problem. Other concerns, investigated include mechanical protection for the fragile collector tubes and possible damage from stagnation temperatures and thermal shock during maintenance or draining of the collector system.

This work was done by Kaw Valley State Bank and Trust Co. for Marshall Space Flight Center. Further information may be found in DOE/NASA CR-161595 [N81-14393/NSP], "Solar Heating, Cooling, and Domestic Hot Water System Installed at Kaw Valley State Bank and Trust Company, Topeka, Kansas — Final Report" [\$15.50]. A paper copy may be purchased [prepayment required] from the National Technical Information Service, Springfield, Virginia 22161. The report is also available on microfiche at no charge. To obtain a microfiche copy, Circle 25 on the TSP Request Card. MFS-25609

## Solar-Heated Water at a Motel — Mobile, Alabama

Approximately two-thirds of the total annual hot-water load are supplied by solar energy.

A solar-assisted hot-water system for a new 122-unit motor inn in Mobile, Alabama, generates more than half the energy needed for hot-water heating at the motel each year. The motel is a low-rise, two-story building with a flat roof supporting the solar panels. A final report on this installation includes data on system operation and verification, design philosophy, and problems encountered and solutions.

The system consists of 93 flat-plate collectors, a 2,500-gallon (9,500-liter) insulated storage tank located outdoors, heat exchangers, and controls. It is protected from freezing by an ethylene glycol collector fluid. Two heat-exchanger tube bundles are installed in the storage tank; the upper heat exchanger extracts heat for the domestic hot-water system, and the lower exchanger transfers heat from the collectors. These exchangers provide a double-wall separation between the ethylene glycol solution and the domestic hot water.

Electronic thermometers, measuring the temperatures at 22 locations, monitor the system performance. Two solar-loop pumps, each sized for 100 percent of the system requirements, are controlled by a temperature-

(continued on next page)



differential controller with an alternator for equal usage of the pumps.

The system began operation in the summer of 1979 and performed as designed, except for a few minor piping leaks, until the property was struck by a hurricane later in the year. Flying debris damaged the roof and the solar panels. After it was repaired, the system remained in satisfactory operation.

*This work was done by LaQuinta Motors Inns, Inc., for Marshall Space Flight Center. Further information may be found in DOE/NASA CR-161587 [N81-13461/NSP], "Solar Hot Water System Installed at Mobile, Alabama — Final Report" [\$6.50]. A paper copy may be purchased [prepayment required] from the National Technical Information Service, Springfield, Virginia 22161. The report is also available on microfiche at no charge. To obtain a microfiche copy, Circle 26 on the TSP Request Card. MFS-25603*

## **Solar-Heated Public Library — Troy, Ohio**

An attractive solar-heating system is interfaced with building heating and air-conditioning.

A report on the installation, operation, and performance of a solar-heating system installed at the Troy-Miami County Public Library in Troy, Ohio, is now available. The solar retrofit system complements a passive solar-energy system and interfaces with the existing heat, ventilation, and air-conditioning systems. Recommendations for future installations are included in the report.

The library building, located in the downtown area of the city, has a floor area of over 23,000 square feet (2,100 m<sup>2</sup>). The roof-mounted solar-collector array forms a highly visible addition to the building. Tubular collectors minimize freeze danger even though the circulating fluid is water. An animated schematic public educational display on a wall of the main-floor lobby allows visitors to monitor the operation of the system.

Several problems were at first encountered with the installation and

operation of the solar-heating components. For example, some air binding problems, aggravated by low flow rates, were encountered as the collectors were being filled. Additional air bleeds were added to solve the problem.

*This work was done by the Troy-Miami County Public Library for Marshall Space Flight Center. Further information may be found in DOE/NASA CR-161588 [N81-12545/NSP], "Solar Heating System Installed at Troy, Ohio — Final Report" [\$17]. A paper copy may be purchased [prepayment required] from the National Technical Information Service, Springfield, Virginia 22161. The report is also available on microfiche at no charge. To obtain a microfiche copy, Circle 27 on the TSP Request Card. MFS-25601*

## **Solar-Cooled Classroom Building — Columbus, Ohio**

Advanced, evacuated tubular collectors supply solar energy for heating and cooling of a university building.

The solar-energy heating and cooling system of a new classroom/administration building, the "Phase V Building" in Columbus, Ohio, is described in a recently released report. Evacuated tubular collectors are used, so that temperatures sufficient for absorption chilling are reached in the solar loop. The report includes site files; specification references; drawings; and installation, operation, and maintenance instructions.

The maximum number of solar collectors that could be mounted on the roof, a total of 128 modules, is used in the solar-heating system. They are expected to provide 79 percent of the total annual heating requirements of the three-level building and 27 percent of the summer cooling.

Each solar-collector module consists of 24 individual tubes with an integral manifold. Water is the recommended heat-transfer fluid because of its low cost and good thermal performance. The low-loss construction of the tubular collectors makes antifreeze unnecessary in most cases. Emergency freeze protection for the Phase V

Building system is provided by the circulation of city water through the collectors or by draining.

The solar-collection system services independently-operated air handlers: Mixed-mode operation is possible, with one unit heating while the other is cooling. Storage is provided by an underground tank. Excessive collector temperatures can be purged into the cooling tower of the chilling system. Performance information for the solar-heating system is on display in the lobby, through a computerized video monitor and recording system.

*This work was done by the Columbus Technical Institute for Marshall Space Flight Center. Further information may be found in DOE/NASA CR-161589 [N81-12544/NSP], "Solar Heating and Cooling System Installed at Columbus, Ohio — Final Report" [\$14]. A paper copy may be purchased [prepayment required] from the National Technical Information Service; Springfield, Virginia 22161. The report is also available on microfiche at no charge. To obtain a microfiche copy, Circle 28 on the TSP Request Card. MFS-25597*

## **Solar-Heated and Cooled Office Building — Columbus, Ohio**

Energy for space heating, cooling, and domestic hot water is supplied by concentrating collectors.

A final report documents the solar-energy system installed in a Columbus, Ohio, office building to provide space heating, space cooling, and domestic hot water. Building floor area is 25,000 ft<sup>2</sup> (2,300 m<sup>2</sup>). Collectors mounted on the roof track the Sun and concentrate its rays on fluid-circulating tubes. Collected energy is distributed to the hot-water-fired absorption chiller and space-heating and domestic-hot-water preheating systems.

The system employs sensor heads and a microprocessor-based controller to keep solar radiation concentrated on the collection tubes. The collector array comprises 11 rows of 4 panels each, with individual rows controlled independently.

Drive motors move the collectors in the acquisition mode until a threshold flux is sensed on one of the sensors. At that point the collector is incremented until the flux beam is centered. The tracking mode is then entered to maintain beam centering.

The solar-energy system provides about 7 percent of the building thermal-energy demand. The seasonal collector-field efficiency is about 20 percent, based on total solar radiation. The original Sun-tracking controls performed poorly because of differences in sensitivity to bright and overcast days, which made adjustment difficult. These controls and the wakeup sensor for beginning collector operation, which also performed below normal, were replaced by better-adjusted new models. The final report on this system includes details of these replacements; operation, installation, and performance data; and site information, photographs, component specifications, and as-built drawings.

*This work was done by Columbia Gas System Service Corp. for Marshall Space Flight Center. Further information may be found in DOE/NASA CR-161603 [N81-14394/NSP], "Solar Heating, Cooling and Domestic Hot Water System Installed at Columbia Gas System Service Corporation, Columbus, Ohio — Final Report" [\$11]. A paper may be purchased [prepayment required] from the National Technical Information Service, Springfield, Virginia 22161. The report is also available on microfiche at no charge. To obtain a microfiche copy, Circle 29 on the TSP Request Card. MFS-25608*

## Solar Hot Water for an Industrial Laundry — Fresno, California

A large solar-water-heating-system retrofit uses lightweight collectors.

An integrated wastewater-heat-recovery system and solar preheating system to supply part of the hot-water requirements of an industrial laundry in Fresno, California, is described in a recent report. Problems encountered in constructing and operating the

system and recommended solutions are included along with system description and performance data. The  $2.6 \times 10^9$ -Btu/year ( $2.7 \times 10^{12}$ -joule/year) design output of the solar preheating subsystem makes it one of the largest industrial solar-water-heating installations in the DOE/NASA program.

The wastewater-heat-recovery subsystem is responsible for a 35 to 40 percent reduction in energy for process water heating. In the "normal" operating mode a pump circulates water from the wastewater storage pit through a tube-and-shell heat exchanger to heat the incoming city water. In the "weekend" mode excess heat from the storage tank is transferred to the wastewater for a hot start at the end of a weekend or holiday.

Low roof strength imposed a serious limit on solar-collector weight, and contracting difficulties were initially encountered in obtaining a large number of lightweight collector panels. The flat-plate liquid collectors used measure 6,528 square feet (606 square meters) and interconnect with the wastewater-heat-recovery subsystem. Water storage, heat exchangers, controls, plumbing, and a gas-fired auxiliary boiler complete the system.

Problems encountered in the course of the project include stagnation damage to the collectors (from excessive heating) before they were filled, dust accretion on the panels necessitating weekly cleaning, control and instrumentation difficulties, and funding delays. An acceptance test plan, test results, and corrective actions are part of the system report. Despite degraded collector performance, the heat-recovery and solar-energy system reduces the estimated annual energy consumption for hot water at the site by more than half.

*This work was done by Aratex Services, Inc., for Marshall Space Flight Center. Further information may be found in DOE/NASA CR-161537 [N80-32851/NSP], "Solar Hot Water Demonstration Project of Red Star Industrial Laundry, Fresno, California — Final Report" [\$8]. A paper copy may be purchased [prepayment required] from the National Technical Information Service, Springfield, Virginia 22161. The report is also*

*available on microfiche at no charge. To obtain a microfiche copy, Circle 30 on the TSP Request Card. MFS-25550*

## Solar-Water-Heater Design Package

Specifications and drawings are presented for a 75-gal/d system.

Information on a solar domestic-hot-water heater is contained in a 146-page design package. Included are performance specifications, schematics, solar-collector drawings, and drawings of control parts.

The system installed at sites in Tempe, Arizona, and San Diego, California, consists of a solar collector, storage tanks, automatic control circuitry, and an auxiliary heater. Data-acquisition equipment at the sites monitors the day-by-day performance.

Design specifications are for delivery of 75 gallons (283 l) of hot water per day at a minimum temperature of 140° F (60° C). The projected hot-water heating load is  $1.79 \times 10^6$  Btu/month ( $1.9 \times 10^6$  kJ/month), with no more than 30 percent of that energy drawn from the auxiliary heater. The maximum electrical power to operate the control circuits and other components (exclusive of the two 4.5-kW heating elements) is 150 W. System life expectancy is at least 10 years.

*This work was done by Elcam, Inc. for Marshall Space Flight Center. Further information may be found in DOE/NASA CR-161558 [N80-33867/NSP], "Design Package for Solar Domestic Hot Water System" [\$12.50]. A paper copy may be purchased [prepayment required] from the National Technical Information Service, Springfield, Virginia 22161. The report is also available on microfiche at no charge. To obtain a microfiche copy, Circle 31 on the TSP Request Card. MFS-25574*



## Computer Programs

These programs may be obtained at very reasonable cost from COSMIC, a facility sponsored by NASA to make new programs available to the public. For information on program price, size, and availability, circle the reference letter on the COSMIC Request Card in this issue.

### Energy-Systems Economic Analysis

Costs of purchasing, installing, and operating are estimated for the projected lifetime of the system.

The Energy Systems Economic Analysis (ESEA) program is a flexible analytical tool for the rank ordering of alternative energy systems. The basic ESEA approach is to derive an estimate of those costs incurred as a result of purchasing, installing, and operating an energy system. These costs, suitably aggregated into yearly costs over the lifetime of the system, are divided by the expected yearly energy output to determine the bus-bar energy cost. ESEA may be applied to a variety of energy systems and owners, from utility-owned fossil-fuel or solar/electric systems to individual-owned residential energy systems.

When planning an energy system, it is important to have a standard and consistent method of establishing and combining relevant economic parameters to support the comparison of different systems. A standard technique is particularly desirable for determining the commercial attractiveness of alternative designs.

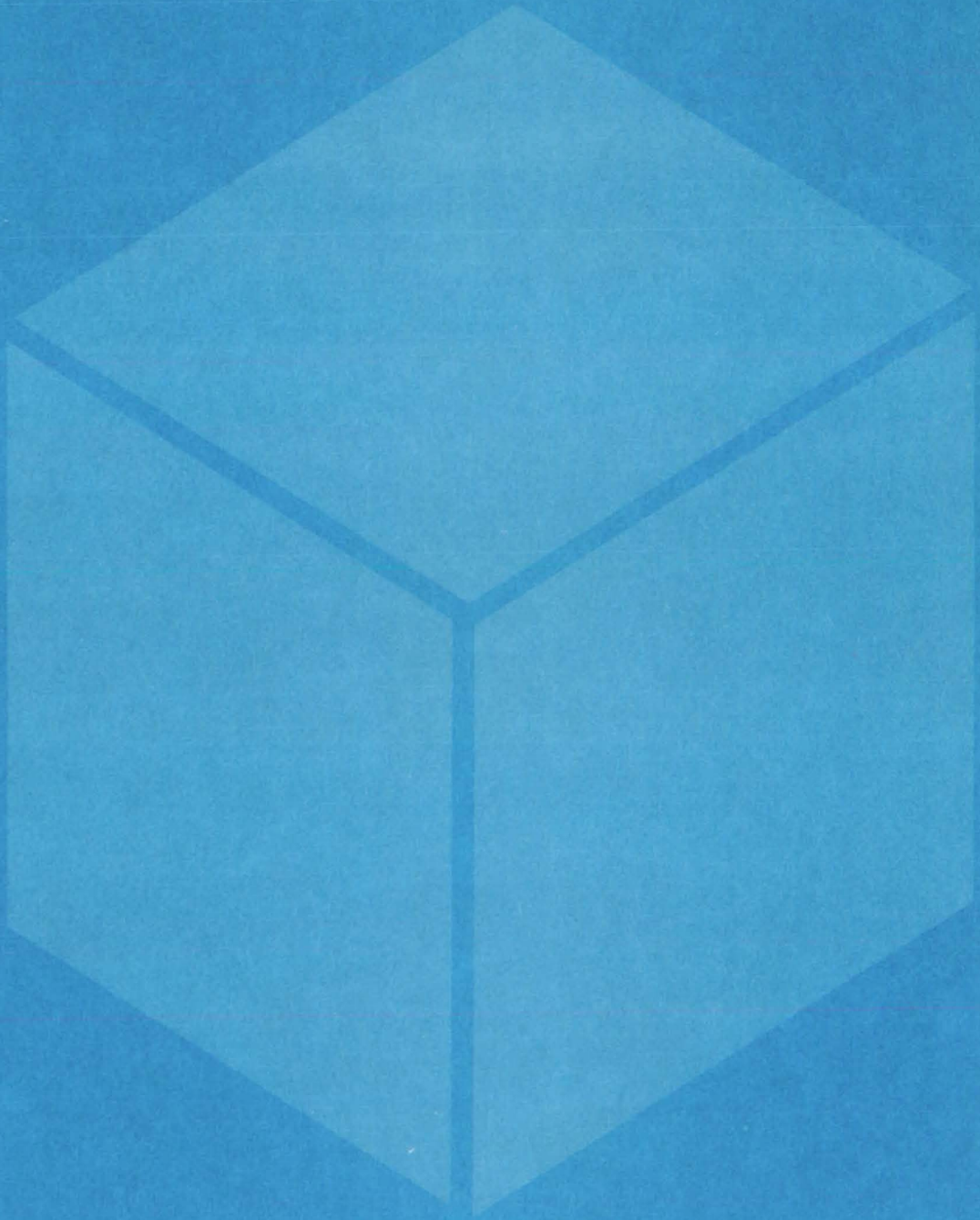
The ESEA analyzes the cost of energy generated by a given energy system (excluding transmission and distribution costs) based on an established economic model for energy systems. Inputs to the model consist of technical and cost data describing the energy system to be analyzed, escalation rates applicable to various categories of system-resultant cost, and pertinent characteristics of the financial environment. The system description data detail the basic costs of the system purchase, installation, and operation. These data also describe the system performance characteristics. The escalation rates determine the conversion of stated costs into current-year dollars over the analysis period. The financial-environment data influence the total costs of system ownership.

ESEA allows for the inclusion of tax preference factors in the form of accelerated depreciation and investment tax credits. The program first determines the discount rate and computes the capital recovery factor and the fixed charge rate. Next the input costs data are analyzed to compute the present values of cash flows, capital investment, and recurrent costs. All of these factors are employed to determine an annualized system-resultant cost. Finally, the life-cycle cost, net present value, and bus-bar energy cost are computed. ESEA may be run for several energy systems so that side-by-side comparisons of the results may be performed.

ESEA is written in FORTRAN IV for batch execution and has been implemented on a UNIVAC 1108 computer with a central memory requirement of approximately 20K of 36-bit words. It was developed in 1979.

*This program was written by James Doane of the Solar Energy Research Institute and Marie L. Slonski and Chester S. Borden of Caltech for NASA's Jet Propulsion Laboratory. For further information, Circle A on the COSMIC Request Card. NPO-15097*

# Materials



**Hardware,  
Techniques, and  
Processes**

- 35 Preparation of Perfluorinated Imidoamidoxime Polymers
- 36 Synthesis of Perfluorinated Polyethers
- 36 Synthesis of Fire-Extinguishing Dawsonites
- 37 Improved Fire-Resistant Resins for Laminates
- 38 Elastomer-Toughened Polyimide Adhesives
- 39 Viscoelastic Properties of Polymer Blends
- 40 Two-Stage Combustor Reduces Pollutant Emissions
- 41 Deformation-Induced Anisotropy of Polymers
- 42 Plasma Deposition of Amorphous Silicon



# Preparation of Perfluorinated Imidoylamidoxime Polymers

A two-reaction low-temperature process yields elastomers with excellent resistance to heat and chemicals.

Ames Research Center, Moffett Field, California

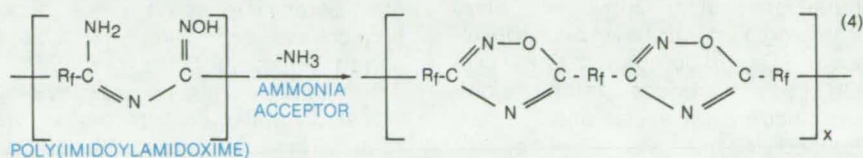
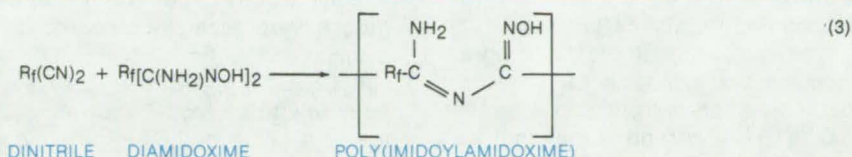
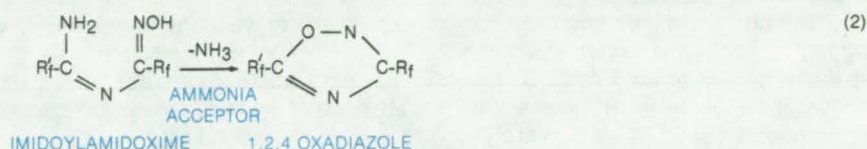
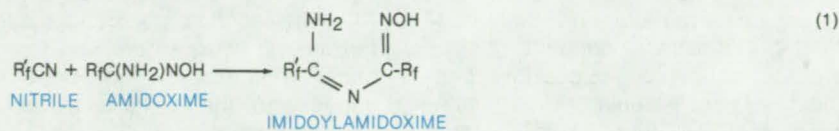
Perfluorinated imidoylamidoxime polymers with excellent resistance to heat, chemicals, and solvents are prepared by condensing a perfluorinated nitrile with a perfluorinated amidoxime in vacuum or inert atmosphere from 20° to 70° C. When both reactants are difunctional, oligomeric or polymeric products are obtained. After cyclization of the imidoylamidoxime groups to 1,2,4-oxadiazole linkages, the process yields the highly resistant elastomers. Competing side reactions are inhibited by the low processing temperature.

The manufacturing process starts at the reaction of either a perfluoroalkyl or perfluoroalkylether nitrile with a perfluoroalkyl or perfluoroalkyl ether amidoxime at temperatures in the range from 20° to 70° C, which produces an imidoylamidoxime (see figure, reaction 1). The imidoylamidoxime is then cyclized (reaction 2) to a 1,2,4-oxadiazole by heating in the presence of an ammonia acceptor at temperatures within the range of 40° to 100° C.

When dinitriles and diamidoximes are substituted for the monofunctional compounds in reactions (1) and (2), oligomeric and polymeric materials are obtained, in which either imidoylamidoxime or 1,2,4-oxadiazole linkages are involved depending on which reaction has produced them (see figure, reactions 3 and 4).

Addition reaction 1 or 3, is carried out in an inert atmosphere or in a vacuum, preferably at a temperature within the range of 20° to 70° C for a period of 24 to 240 hours. The proportion of reactions can vary from equimolarity to an excess of the nitrile of up to 200 percent. The excess is recoverable after completion of the reaction. Cyclization reaction 2 or 4 takes place in an inert atmosphere or in vacuum, preferably at a temperature within the range of 40° to 100° C, in the presence of an acid compound that acts as an ammonia acceptor.

The substituents  $R_f$  and  $R'_f$  in the nitriles and amidoximes can be identical or different. They are selected



**A Two-Step Reaction Sequence** yields either 1,2,4-oxadiazoles [reactions (1) and (2)] or polymers with 1,2,4-oxadiazole linkages [reactions (3) and (4)].

from the monovalent perfluoroalkyl and perfluoroalkylether radicals represented by the general formulas:

- $C_nF_{2n+1}$
- $C_2F_5(OCF_2CF_2)_nOCF_2-$
- $C_3F_7O(CF(CF_3)CF_2O)_nOCF(CF_3)-$

or, when dinitriles and diamidoximes are required, from such bivalent radicals as:

- $-(CX_2)_p-$
- arylene, and
- $-CFY(OCF_2CFY)_mO(CX_2)_pO(CFYCF_2O)_nCFY-$

Here p ranges from 2 to 8 when X is fluorine and from 2 to 18 when X is hydrogen, Y is fluorine or a trifluoromethyl group or an assortment of such substituents, and (m + n) ranges from 2 to 7.

The imidoylamidoximes can serve either as chain stoppers or cross-link index diluters in certain polymerization reactions; or when they are oligomeric or polymeric, they can be converted to

useful polyoxadiazoles. Such heat- and chemical-resistant polymers (when suitably compounded with fillers, extenders, and modifiers) can be used in applications in which high stability, impermeability to liquids and gases, and good plasticity are advantageous; e.g., as adhesives, caulking compounds, channel sealants, and fuel-tank liners.

This work was done by Robert W. Rosser of Ames Research Center and Reinhold H. Kratzer, Kazimiera J. L. Paciorek, and Thomas I. Ito of Ultrasystem, Inc. For further information, Circle 32 on the TSP Request Card.

This invention is owned by NASA, and a patent application has been filed. Inquiries concerning nonexclusive or exclusive license for its commercial development should be addressed to the Patent Counsel, Ames Research Center [see page A5]. Refer to ARC-11267.

---

## Synthesis of Perfluorinated Polyethers

New materials may be used as sealants or elastomers in extreme environment.

---

*Ames Research Center, Moffett Field, California*

Long-chain perfluoropolyethers containing functional pendent groups were investigated as possible candidates for new sealants and elastomers that will function in extreme environments. Of specific interest was the development of materials exhibiting high thermal and oxidative stability at temperatures around 400° C, low-temperature flexibility with glass transition at about -50° C, and hydrolytic stability as well as compatibility with metals and resistance to fuels.

The major thrust of this program involved the synthesis of long-chain perfluoroethers with functional groups (-C ≡ CH, -CN, and -CF<sub>2</sub>I) that was followed by investigating methods necessary to convert these compounds into stable cross-linked polymers for sealant application. Two promising systems have been developed: (1) perfluoropolytriazines with -CN pendent groups (terephthalonitrile-oxide cross-linking) and (2) perfluoropolytriazines with -CF<sub>2</sub>I pendent groups (thermally or photochemically curing). Both systems are based on a polyimidoylamidine prepolymer derived from HFPO (hexafluoropropylene oxide) oligomers.

Samples of polytriazines with pendent nitrile groups were generally prepared using EDAF (ether diacylfluoride) polyimidoylamidine dissolved in Freon-E4, or an equivalent, and added dropwise to a stirred mixture of [NC(CF<sub>2</sub>)<sub>3</sub>CO]<sub>2</sub>O and (CF<sub>3</sub>CO)<sub>2</sub>O.

After the reaction mixture was stirred for about 8 hours at ambient temperature, trifluoroacetic anhydride was added and the mixture stirred for another 8 hours.

The resulting mixture was heated at 60° C under vacuum to remove the solvent. An IR spectrum of the residual viscous material showed the absence of imidoylamidine groups and the presence of triazine groups.

Polytriazines with -CF<sub>2</sub>I pendent groups were generally prepared using a mixture of C<sub>3</sub>F<sub>7</sub>OCF(CF<sub>3</sub>)COF and ICF<sub>2</sub>CF<sub>2</sub>O(CF<sub>2</sub>)<sub>5</sub>OCF(CF<sub>3</sub>)COF added slowly to a Freon-E4, or an equivalent, solution of EDAF polyimidoylamidine and dry sodium fluoride. After stirring the mixture for about 8 hours at ambient temperature, HFPO (hexafluoropropylene oxide)-dimer acylfluoride was added and the mixture stirred for several hours.

The reaction mixture was washed repeatedly with water to remove the acids formed. The organic layer was separated, dissolved in Freon-113, or an equivalent, and passed over a column of neutral alumina to remove any traces of acid. The solvent was removed under vacuum, leaving the polytriazine.

The resulting polytriazines were cross-linked with pendent -CF<sub>2</sub>I groups by either (a) a low-temperature curing process by placing the samples on a rotary evacuated evaporator and irradiating with ultraviolet lamp for 100

hours or (b) a high-temperature curing process by heating the samples in a flask in the same evacuated evaporator using an oil bath at 200° to 230° C for 60 hours. In both cases, elastomeric gum was produced with a glass-transition temperature of about -60° C.

Results have shown that the properties of the final cross-linked polymer will depend largely on the molecular distribution of the polyimidoylamidine prepolymer. Consequently, further studies should concentrate on the formation of that prepolymer to determine whether high-molecular-weight (about 32,000 molecular weight) polyimidoylamidine can be prepared reproducibly so that the corresponding polytriazine with -CN or -CF<sub>2</sub>I pendent groups will yield a usable sealant on curing.

*This work was done by Robert W. Rosser of Ames Research Center and Theodore Psarras of PCR Research and Development. For further information, Circle 33 on the TSP Request Card.*

*This invention is owned by NASA, and a patent application has been filed. Inquiries concerning nonexclusive or exclusive license for its commercial development should be addressed to the Patent Counsel, Ames Research Center [see page A5]. Refer to ARC-11241.*

---

## Synthesis of Fire-Extinguishing Dawsonites

Nonaqueous synthesis under pressure converts dawsonites into fire-extinguishing chemicals.

---

*Ames Research Center, Moffett Field, California*

A simple nonaqueous process synthesizes sodium or potassium, dawsonites effective against hydrocarbon fuel fires. The fire-extinguishing alkali metal dawsonites are prepared using a

finely-pulverized equimolar mixture of hydrogen carbonate, or carbonates, and aluminum hydroxide heated for 1 to 6 hours under carbon dioxide pressure. The process adds another

useful application to the dawsonite family, already used for SO<sub>2</sub> absorption, as drying agents and inhibitors for gaseous organic compounds susceptible to polymerization, and as stomachal antacids.

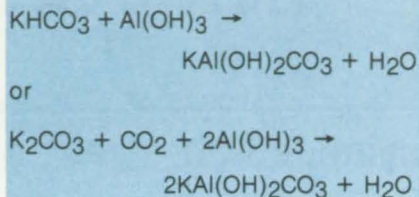
The six-step synthesis is carried out by:

1. intimately mixing approximately equimolar quantities of finely-divided, 90- $\mu\text{m}$ , aluminum hydroxide with a finely divided salt selected from the class consisting of hydrogen carbonates or carbonates of sodium or potassium;
2. placing the mixture in an open-top inert-metal container;
3. placing the container into a pressurized reactor;
4. sweeping the air from the container and pressurizing the container with carbon dioxide at about 120 to 360 psig ( $828 \times 10^3$  to  $2,484 \times 10^3$   $\text{N/m}^2$ );
5. heating the pressurized container at a temperature within  $150^\circ$  to

$250^\circ$  C for a period of about 1 to 6 hours; and

6. cooling the reactor, depressurizing at about  $50^\circ$  C, ambient temperature.

The chemical reactions in this process, using potassium (sodium or ammonium may be substituted for potassium) as an example, are:



The product  $\text{KAl}(\text{OH})_2\text{CO}_3$  can be pulverized by crushing and ball-milling

to a desired particle size and mixed with 1 percent by weight of a solid flow agent such as hydrophobic fumed silica powder to improve the flow properties. The synthesized dawsonites can be stored in a plastic bag inside a sealed metal container until needed since they do not hydrate.

This work was done by Robert L. Altman of **Ames Research Center**. For further information, Circle 34 on the TSP Request Card.

This invention is owned by NASA, and a patent application has been filed. Inquiries concerning nonexclusive or exclusive license for its commercial development should be addressed to the Patent Counsel, Ames Research Center [see page A5]. Refer to ARC-11326.

## Improved Fire-Resistant Resins for Laminates

Phosphorus-containing resins can be used in graphite or cloth composites.

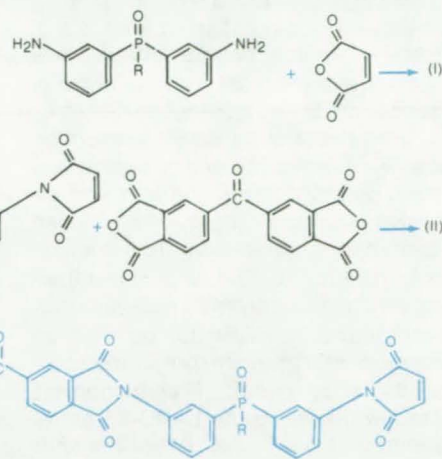
Ames Research Center, Moffett Field, California

Fire-resistant resins for fabricating laminates with inorganic fibers, especially graphite fibers, are formed from bisimides containing main-chain phosphorus and olefinic end groups. The bisimides are thermally polymerized to form resins and laminates virtually incombustible in pure oxygen at  $300^\circ$  C. Graphite cloth laminates made with these resins have shown  $800^\circ$  C char yields greater than 90 percent by weight in nitrogen.

Improved flame-resistant materials for laminates have been sought for greater safety in such places as aircraft cabins. Phosphorus-containing compounds have reduced flammability and increased adhesion; however, previous formulations have nonetheless remained somewhat flammable. The new resins are suitable for many applications requiring good adhesion and excellent resistance to heat, fire, solvents, and chemicals. They may be used as adhesives and as matrix material for fiber-reinforced lightweight composites.

The formation of bisimide begins with the condensation of an unsaturated cyclic aliphatic dibasic acid anhydride (typically, maleic anhydride) with a phosphorus-containing

aromatic diamine (a bis(aminophenyl) alkyl phosphine oxide). Some of the monoimide that is formed in this first reaction can also be condensed with an aromatic dianhydride (typically, benzophenonetetracarboxylic acid dianhydride) to produce a larger polymerizable molecule (see figure). The condensation reactions (reactions I



**A Polymerizable Bisimide** is formed in a sequence of condensation reactions. The resulting molecule contains two imide end groups attached to phosphine oxide groups and an aromatic dianhydride group in the middle. R represents a methyl, ethyl, or phenyl group. Polymers formed by addition reactions of such molecules exhibit excellent flame resistance.

and II in the figure) take place preferably in a polar solvent such as dimethyl formamide. The product monomer is generally isolated by pouring the reaction mixture in a nonsolvent liquid.

In fabricating a typical composite, a graphite cloth is impregnated with a  
(continued on next page)

solution of a bismaleimide in dimethyl formamide, then dried in an oven at 160° to 170° C. The dried prepregs are stacked to the desired thickness and pressed between aluminum plates coated with polytetrafluoroethylene release film. Curing by addition polymerization takes place at 232° C and 125 psi (8.6x10<sup>5</sup> N/m<sup>2</sup>) for 95 minutes. After pressing, postcuring is done at 300° C for 70 minutes.

Some of the mechanical properties of the laminates formed from these resins may be selectively altered by using different unsaturated anhydride components and different phosphine oxide components, as well as mixtures of these components. The properties may also be altered somewhat by varying the processing parameters.

This work was done by George M. Fohlen and John A. Parker of **Ames**

**Research Center** and Indra K. Varma of the National Research Council. For further information, Circle 35 on the TSP Request Card.

This invention is owned by NASA, and a patent application has been filed. Inquiries concerning nonexclusive or exclusive license for its commercial development should be addressed to the Patent Counsel, Ames Research Center [see page A5]. Refer to ARC-11321.

## Elastomer-Toughened Polyimide Adhesives

Rubber-modified resins are useful for high-temperature applications.

Langley Research Center, Hampton, Virginia

Addition polyimides are currently under consideration as high-temperature adhesives for bonding composite materials and such metals as titanium. These thermoset polyimides cure by an addition reaction involving unsaturated end groups that causes them to be highly cross-linked, insoluble, and extremely brittle. Elastomer toughening (the incorporation of small amounts of rubber into the polymer matrix) has been one of the most successful methods for modifying polymer toughness.

The effects of added elastomers on the T<sub>g</sub>, thermal stability, adhesive lap-shear strength, T-peel strength, and adhesive fracture energy have been studied for a high-temperature addition polyimide, LARC-13. LARC-13 is a thermoset addition polyimide adhesive currently used by NASA for bonding an experimental graphite/polyimide composite wing panel. The monomers used in preparing the LARC-13 adhesive resin are 3,3',4,4'-benzophenone tetracarboxylic dianhydride (BTDA), 3,3'-methylenedianiline (MDA), and nadic anhydride (NA).

The four elastomers studied were used "as received." Silastic® LS-420 is a solid fluorosilicone rubber that was obtained from Dow Corning. Sylgard® 184 resin, also from Dow Corning, is a low-viscosity, colorless liquid elastomer. The highly viscous aromatic amine-terminated butadiene/acrylonitrile (ATBN) is an experimental elastomer obtained from B. F. Goodrich, and the aromatic amine-terminated silicone (ATS) is a low-viscosity liquid elastomer

Adhesive	T-Peel Strength N/m (lb/in.) Samples Unaged		T-Peel Strength N/m (lb/in.) Samples Aged 500 h at 505 K	
	RT	505 K	RT	505 K
LARC-13	230 (1.3)	510 (2.9)	330 (1.9)	—
LARC-13/Silastic®	1,520 (8.7)	910 (5.2)	1,140 (6.5)	—
LARC-13/Sylgard®	540 (3.1)	960 (5.5)	490 (2.8)	440 (2.5)
LARC-13/ATBN	960 (5.5)	680 (3.9)	530 (3.0)	420 (2.4)
LARC-13/ATS	1,490 (8.5)	1,090 (6.2)	790 (4.5)	1,020 (5.8)

**T-Peel Strengths of Adhesive/Titanium Bonds** are compared for LARC-13 with and without elastomer additives. (RT=room temperature.)

obtained from Bergston and Associates.

The LARC-13 polyamic acid adhesive resin was prepared using glass-distilled dimethylformamide (DMF) solvent at a concentration of 50 percent solids by weight (w/w). The Silastic and Sylgard silicone rubbers were physically blended with the LARC-13 to produce solutions with elastomer contents of 15 percent w/w. The amine-terminated rubbers ATBN and ATS were chemically reacted into the prepolymer backbone.

Elastomer-containing LARC-13 solutions were prepared for use as adhesives by adding 30 percent w/w aluminum powder filler. The resins were brush-coated onto a 112 E-glass (1100 finish) cloth, which was tightly

stretched over an aluminum frame. The scrim cloth was dried between coats in a forced-air oven at 333 K; and, after the final fourth coat, the cloth was B-staged for 1 hour at 373 K and 1/2 hour at 453 K.

Each of the four rubber-modified resins displays a separate T<sub>g</sub> for the elastomer phase at low temperature and a T<sub>g</sub> at high temperature due to the LARC-13. Although the decomposition temperatures of unaged specimens are close together, LARC-13 is more thermally stable than the rubber-modified resins. However, after the adhesives are aged for 500 hours at 505 K, the LARC-13/Sylgard is the most thermally stable resin.

The elastomers sacrifice some of the elevated-temperature lap-shear strength of LARC-13. The high-temperature strengths of adhesives prepared with silicone elastomers, however, improve after aging at 505 K. All four rubber additives increase the T-peel strength of LARC-13, as shown in the table, indicating an increase in toughness. A sixfold to sevenfold increase in the unaged, room temperature peel strength of the base resin is achieved

with the LARC-13/Silastic and LARC-13/ATS formulations. The ambient and elevated-temperature fracture toughness of LARC-13 is improved threefold to fivefold with the ATBN and ATS rubbers, while Sylgard 184 increases the fracture toughness only slightly.

Few adhesives are available that can be used for long-term exposure at elevated temperatures of 505 K and above. The incorporation of these ATBN and silicone rubbers should in-

crease the utility of LARC-13 for selected high-temperature applications.

*This work was done by Anne K. St. Clair and Terry L. St. Clair of Langley Research Center. For further information, Circle 36 on the TSP Request Card.*

*Inquiries concerning rights for the commercial use of this invention should be addressed to the Patent Counsel, Langley Research Center [see page A5]. Refer to LAR-12775.*

## Viscoelastic Properties of Polymer Blends

"Entanglement" model predicts viscosity, shear modulus, and other properties.

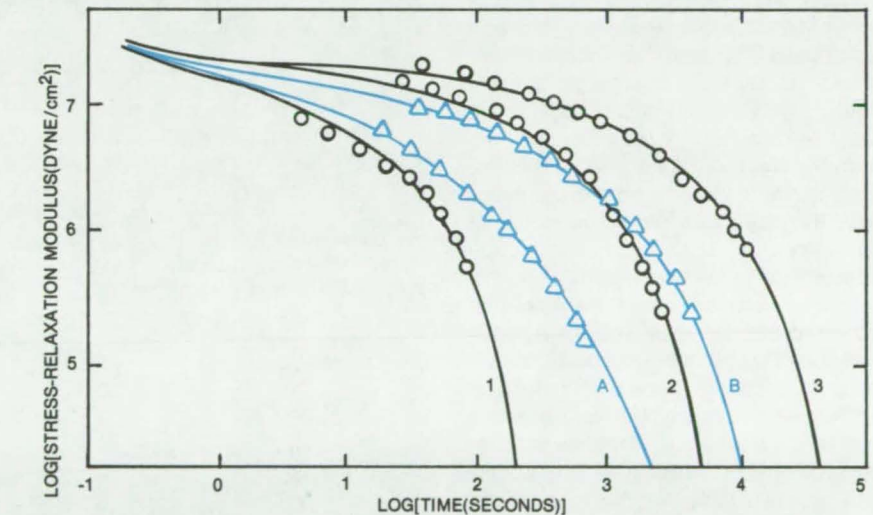
NASA's Jet Propulsion Laboratory, Pasadena, California

Viscosity, shear modulus, and other viscoelastic properties of multicomponent polymer blends are predicted from the behavior of the individual components, using a mathematical model. The properties predicted for three-component blends of the commercially important polymer polystyrene agree well with experimental data.

The model is an extension of a two-component-blend model based on the Rouse-Bueche-Zimm theory of polymer viscoelasticity. The extension assumes that the probabilities of forming the various possible intracomponent and intercomponent entanglements among the polymer molecules are proportional to the relative abundances of the components.

The model postulates that polymer molecules interact and entangle, forming a transient, three-dimensional network. The entanglement probabilities are expressed in terms of the total number of submolecules of a component, which in turn depend on the relative abundances of the components in the blend.

Matrix equations of motion containing the frictional coefficients are solved for each component to determine the relaxation times of that component. Since the frictional coefficients of the entanglements depend on the composition of the blend, the relaxation times are valid only for the assumed composition. Linear viscoelastic properties, such as the relaxation modulus, dynamic moduli, steady-state shear compliance, and zero-shear



**Stress-Relaxation-Moduli** are shown for monodisperse polystyrene components (1, 2, and 3) of three different molecular weights and for two three-component blends (A and B) of those components. The components 1, 2, and 3 have molecular weights of  $1.10 \times 10^5$ ,  $2.33 \times 10^5$ , and  $3.90 \times 10^5$ , respectively. The 1:2:3 weight composition of blend A is 0.8:0.1:0.1; that of blend B is 0.33:0.33:0.33.

viscosity, are calculated from the relaxation times.

Calculations have been done for two types of three-component blends. In the first type, all three components are long enough to form entanglements in their pure states. The second type of blend includes a component too short to form entanglements. Most polydisperse blends contain such short, low-molecular-weight fractions.

The stress-relaxation moduli of three monodisperse polystyrene samples and of two three-component blends were measured and compared to the

values predicted by the model (see figure). Although the average molecular weight of blend B is comparable to the molecular weight of the intermediate component 2, their stress-relaxation behaviors are different, as shown by the crossing of the two sets of data. The model predicts the crossing.

*This work was done by Su D. Hong, Jovan Moacanin, Mitchell Shen, and David Soong of Caltech for NASA's Jet Propulsion Laboratory. For further information, Circle 37 on the TSP Request Card. NPO-14924*

## Two-Stage Combustor Reduces Pollutant Emissions

A proposed precombustion stage in gas turbines would reduce  $\text{NO}_x$ , CO, and hydrocarbon emissions.

NASA's Jet Propulsion Laboratory, Pasadena, California

By controlling the fuel-to-air ratio of local reactants, pollutant emissions would be minimized in a proposed two-stage combustor for gas-turbine engines. It would use a fuel-rich partial-oxidation stage and an air-rich combustion stage to reduce emissions of nitrogen oxide ( $\text{NO}_x$ ), carbon monoxide (CO), and hydrocarbons. The combustor fuel-lean burning limit would be extended simultaneously.

One previous approach for reducing thermally-generated nitrogen oxides is to incorporate fuel-lean burning in the primary heat-release zone of a single-stage combustor. However, fuel-lean blowout (LBO) limits are closely approached, lowering the margin of combustor stability and raising the emissions of carbon monoxide and unburned hydrocarbons. Moreover, if fuels containing nitrogen are used, the nitrogen may be converted to oxides of nitrogen even under fuel-lean conditions.

In the proposed design, a substantial portion of the fuel is partially oxidized in a precombustion stage under fuel-rich conditions prior to final combustion with excess air. The fuel-lean blowout limit of the final stage would be extended, and the conversion of fuel-bound nitrogen to molecular nitrogen would be minimized.

In the first-stage reactions of the two-stage combustor (see Figure 1), the engine fuel is premixed and preheated at fuel-to-air equivalence ratios of 2 or more to maximize the conversion of raw hydrocarbons to hydrogen ( $\text{H}_2$ ) and CO and to maximize the conversion of any fuel-bound nitrogen to molecular nitrogen. The increased hydrogen content lowers the lean-flammability limit, and there is evidence that the precombustion inhibits the production of  $\text{NO}_x$  in the final combustion stage. Mixing the product gas with engine air not used in the first stage, prior to final combustion, reduces peak final flame temperatures, thus reducing  $\text{NO}_x$  emissions.

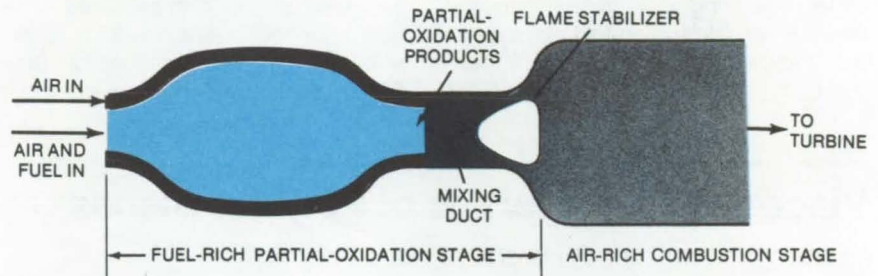


Figure 1. A Fuel-Rich Partial-Oxidation Stage and an Air-Rich Combustion Stage would reduce pollutant emissions in a two-stage combustor. In the first stage, engine fuel is premixed and preheated to oxidize partially the raw hydrocarbons to carbon monoxide and hydrogen. The partially oxidized mixture is combined in the second stage, just prior to combustion, with the air not used in the first stage.

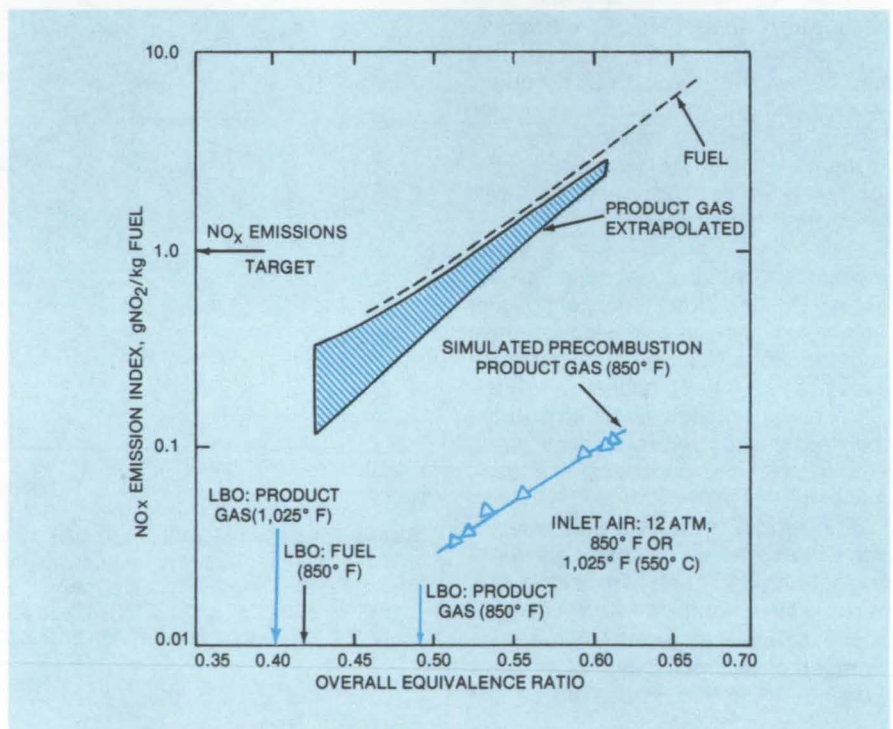


Figure 2.  $\text{NO}_x$  Emissions Are Reduced when a simulated precombustion product gas is used to fuel a combustor that is normally fed straight fuel. The results for the simulated product gas at 850° F are the color line. When extrapolated to temperatures expected for an actual product gas, the data give the results in the color envelope, which are still below that for the fuel-fired combustor. Reductions in emissions of CO and HC are also observed.

In experiments, a simulated precombustion product gas was supplied from a bottled source. The bottled gas was used in a combustor and operated under inlet conditions that approximate

typical turbofan aviation engines — i.e., 850° F (455° C) and 12 atm ( $1.2 \times 10^6 \text{ N/m}^2$ ). The composition of the bottled gas simulated that of the gas products that would be generated

by a fuel-rich partial-oxidation stage; however, the temperature of the actual product gas from a first-stage combustor would be about 2,100° F (1,150° C). When the combustor was

operated with the simulated fuel gas, pollutant products decreased (see Figure 2).

This work was done by Richard M. Clayton of Caltech for NASA's Jet Pro-

pulsion Laboratory. For further information, Circle 38 on the TSP Request Card.  
NPO-14911

## Deformation-Induced Anisotropy of Polymers

A theoretical relationship describes the anisotropy of thermal expansivity produced by large deformations.

NASA's Jet Propulsion Laboratory, Pasadena, California

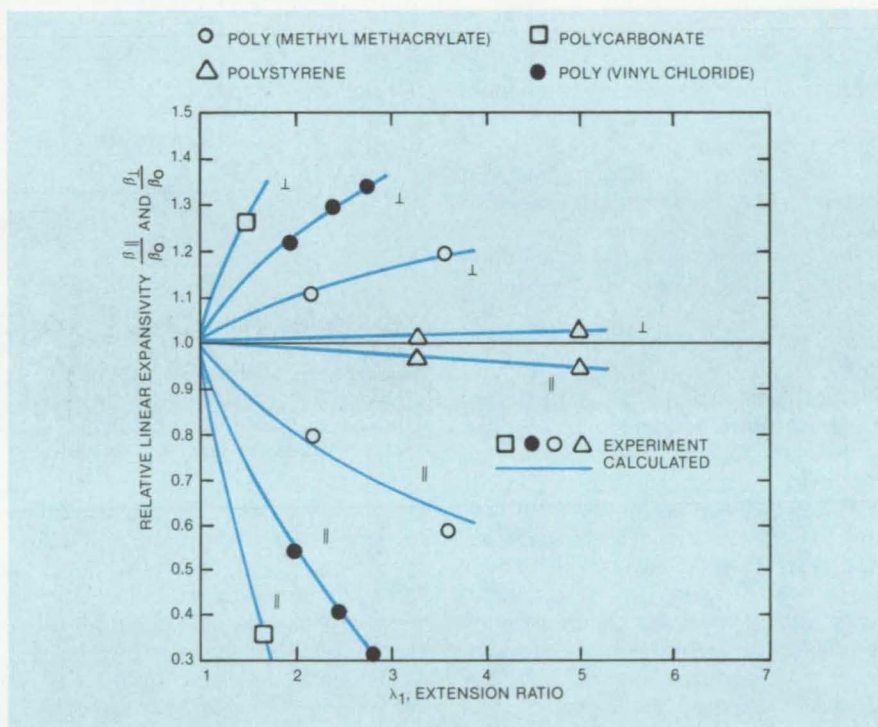
A new theory calculates anisotropies induced by large deformations in polymers. While the theory was developed primarily for calculating the anisotropy of thermal expansivity, it is also applicable to thermal conductivity, elastic moduli, and other properties.

When an isotropic solid is deformed, the thermal expansivity becomes anisotropic to an extent that depends on the degree of deformation. It is of particular interest to know the expansion coefficients in directions perpendicular and parallel to the axis of stretching.

The theory assumes that in the isotropic state, the long polymer chains are randomly coiled and not oriented in a particular direction. They acquire an orientation when the material is deformed. As the average molecular orientation increases with the deformation, the properties of the bulk material exhibit the averaging of the microscopic anisotropies of the oriented molecular segments.

The induced anisotropic thermal expansivity is expressed as a tensor. Each element of the expansivity tensor is expressed as the derivative of a scalar function with respect to an element of the strain tensor. The scalar function is similar to the distribution function for the chain orientation, which depends, in turn, on the deformation gradient.

The original isotropy of the undeformed material is incorporated into the equations by making the scalar function equally dependent upon the deformations along each of the principal axes of the system. The tensor



Relative Thermal Expansivities After Stretching were calculated and measured for four common polymers. Shown here are the ratios of expansivity after stretching to expansivity before stretching, as observed parallel ( $\parallel$ ) and perpendicular ( $\perp$ ) to the axis of stretching.

equations are solved and turn out to depend on a single unknown parameter. The latter is then evaluated from measurements of the thermal expansion coefficient measured either perpendicular or parallel to the stretch in a uniaxial experiment. The result can then be used to calculate the uniaxial response in the other direction or the general response in the multiaxial deformations.

Equations are obtained for uniaxial stretching, pure shear deformations, and for equal biaxial deformations. A comparison of theoretical predictions and experimental observations on different polymers is shown in the figure for the uniaxial case.

This work was done by Steven T. J. Peng and Robert F. Landel of Caltech for NASA's Jet Propulsion Laboratory. For further information, Circle 39 on the TSP Request Card.  
NPO-15325

## Plasma Deposition of Amorphous Silicon

Plasma-jet process produces highly adherent films on glass or aluminum.

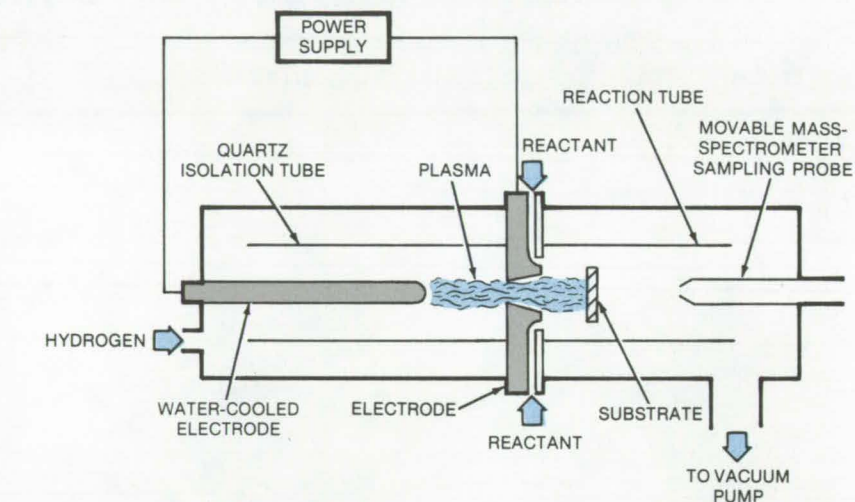
*NASA's Jet Propulsion Laboratory, Pasadena, California*

Strongly adhering films of silicon are deposited directly on such materials as Pyrex and Vycor (or equivalent materials) and aluminum by a non-equilibrium plasma jet. The amorphous silicon films are formed by the decomposition of silicon tetrachloride ( $\text{SiCl}_4$ ) or trichlorosilane ( $\text{SiHCl}_3$ ) in the plasma. The plasma-jet technique can also be used to deposit an adherent silicon film on aluminum from silane ( $\text{SiH}_4$ ) and to dope such films with phosphorus.

The ability to deposit silicon films on such readily available, inexpensive substrates could eventually lead to lower cost photovoltaic cells (although photovoltaic properties have not been demonstrated for these films). The glass substrate is particularly attractive, since it provides structural support and a protective transparent cover for the silicon.

In the nonequilibrium plasma-jet apparatus, the reactant ( $\text{SiCl}_4$ ,  $\text{SiHCl}_3$ , or  $\text{SiH}_4$ ) is introduced downstream from a plasma arc between two electrodes (see figure). A continuous flow of hydrogen furnishes the ions for the plasma, which extends through a central orifice in the downstream electrode into a reaction chamber. There, the reactant gas decomposes in the high-energy plasma, depositing silicon on substrate plates near the plasma nozzle. The other reaction products pass out of the reaction chamber.

Depositions were carried out under various conditions, typically at plasma voltages and currents up to 800 volts and 2.1 amperes, respectively; plasma-jet temperatures up to 850 K



**Amorphous Silicon Deposits** on a substrate positioned in a reaction tube, close to the nozzle-electrode of the plasma jet. Typical film thicknesses are 0.5 and 1.1  $\mu\text{m}$  for 3 and 6 minute exposures, respectively, to  $\text{SiCl}_4$  reactant. For the  $\text{SiHCl}_3$  reactant, silicon deposits at the faster rate of 4  $\mu\text{m}\cdot\text{min}^{-1}$ .

at the jet stagnation point; and a plasma-jet velocity up to 2,600 meters per second. The upstream discharge pressure varied up to 75 torr and the downstream reaction-chamber pressures reached 18 torr.

To deposit silicon from  $\text{SiH}_4$  on aluminum, it is necessary to mount the substrate in a holder that both heats and applies a voltage to the aluminum. The substrate is thus an electrode that, at 550 K, quickly accumulates an adherent film.

For depositing doped silicon film on aluminum, the same substrate holder is used. Mounted about 20 mm from the downstream side of the jet nozzle and heated to 550 K, the aluminum

substrate serves as the cathode.  $\text{SiH}_4$  is fed through the reactant nozzle, and a mixture of argon, hydrogen, and phosphine ( $\text{PH}_3$ ) is fed through the jet nozzle. Phosphorus dopant then deposits on the substrate with the silicon. The phosphorus concentration can be regulated to give a wide range of film resistivity. In experiments, the resistivity of the silicon could be reduced up to 950 times by plasma-jet doping.

*This work was done by Hartwell F. Calcote of Aerochem Research Laboratories, Inc., for NASA's Jet Propulsion Laboratory. For further information, Circle 40 on the TSP Request Card.*  
NPO-14954



# Life Sciences



**Hardware,  
Techniques, and  
Processes**

- 45 Algorithms Could Automate Cancer Diagnosis
- 46 Constraint-Free Measurement of Metabolic Rate
- 47 Portable Radiometer Monitors Plant Growth
- 48 Chemical Growth Regulators for Guayule Plants

# Algorithms Could Automate Cancer Diagnosis

Cell atypia would be quantified by computer analysis of digitized images.

Lyndon B. Johnson Space Center, Houston, Texas

Five new algorithms are a complete statistical procedure for quantifying cell abnormalities from digitized images. The procedure could be the basis for automated detection and diagnosis of cancer. When atypical bronchial cells from the sputum of cigarette smokers were analyzed, for example, the levels of carcinogenesis assigned by the algorithms agreed with those assigned by visual classification.

The objective of the procedure is to assign each cell an atypia status index (ASI), which quantifies the level of abnormality. For squamous cell carcinogenesis, the ASI runs from 0.5 to 5.5. Integer values correspond to the standard classification categories:

1. Metaplasia,
2. Mild Atypia,
3. Moderate Atypia,
4. Severe Atypia, and
5. Carcinoma.

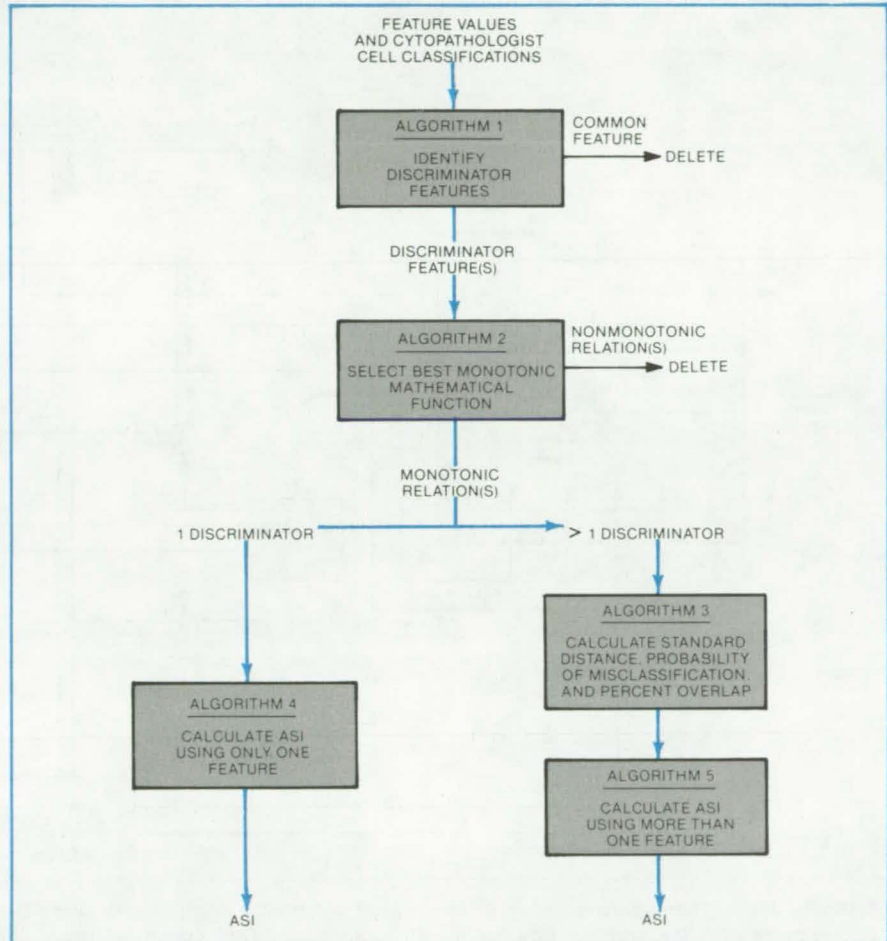
An ASI assignment is made by first measuring key cell features on a digitized image. Among possible significant features are:

- the area of cytoplasm,
- the nucleus/cytoplasm area ratio, and
- the nucleus/cytoplasm boundary.

The algorithm selects those features that are significant indicators of cell atypia and calculates the ASI from the measurements.

The flow chart in the figure shows the sequence of algorithms. Algorithm 1 determines which cell features are statistically significant. It looks at feature measurements for a cell population that has already been separated into the five groups by visual analysis. Those features for which the overlap between adjacent groups is less than 70.7 percent are considered significant.

Algorithm 2 discards any discriminator feature for which the cell-group means are not monotonically related to cell-group number. For each remaining feature, it checks through a set of 16 functions until it finds one that can be used to transform the



The **Image-Analysis Flow Chart** shows the procedure for determining cell ASI from information contained in cytological and feature data. ASI values calculated for cells extracted from the sputum of male cigarette smokers correlated at between 94 and 99 percent with visual cytopathologic classifications.

group means into a linear relationship with group number. To be accepted, the transformation must produce a correlation coefficient greater than 0.98.

Once the discriminating features are found, cells for which the atypia is not known are analyzed by algorithms 4 or 3 and 5, to determine the ASI values. If a feature is found such that the distance between adjacent groups exceeds 4 standard-deviation units, the ASI is calculated by algorithm 4 based on that feature alone, with an expected misclassification rate less than 2 percent. If no such single

feature exists, the ASI is calculated by algorithms 3 and 5 in a manner that takes into account the correlations between all the discriminator features.

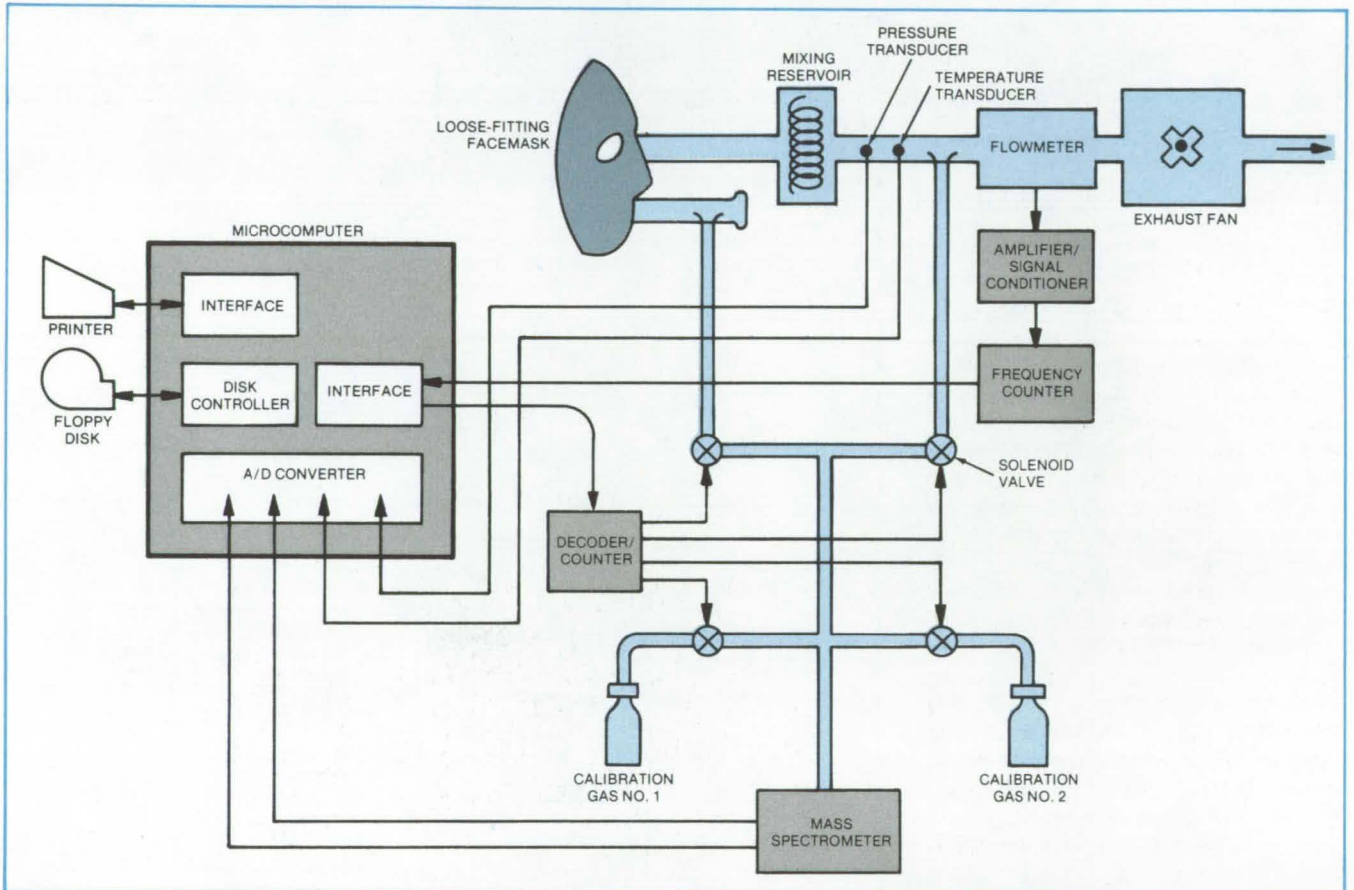
It is possible that ASI values will be accurate and economical enough to allow diagnoses to be made quickly and accurately by computer processing of laboratory specimens extracted from patients.

This work was done by Anwar A. Baky and Don G. Winkler of Northrop Services, Inc., for **Johnson Space Center**. For further information, Circle 41 on the TSP Request Card. MSC-18764

# Constraint-Free Measurement of Metabolic Rate

Microcomputer analysis technique allows breathing to be monitored by a comfortable loose-fitting mask.

Lyndon B. Johnson Space Center, Houston, Texas



**Metabolic Rate Measurement** using a loose mask for breath sampling is possible with microcomputer control of the mass spectrometer and the turbine flowmeter. An analog-to-digital converter reads the signals from the spectrometer and the flowmeter.

Conventional spirometer measurements of metabolic rate require the subject to wear a tight-fitting mask and nose clamp. However, by using hardware and software originally developed for manned spacecraft, metabolism is now measured while the subject wears only a loose-fitting mask. This more-comfortable, less-restrictive measurement technique uses the speed, accuracy, and control capabilities of a microcomputer.

Metabolic rate is calculated from two respiratory parameters: oxygen consumption and carbon dioxide production. In the new system,  $O_2$  consumed and  $CO_2$  produced are measured for a test subject by drawing a fairly constant flow of ambient air through the loose mask and mixing it with the subject's

expired air. The flow is controlled by an exhaust fan.

A mass spectrometer determines the concentrations of the gases in the inspired and expired air. These concentrations, as well as temperature, pressure, and ambient-air flow rate, are monitored by the microcomputer (see figure). The computer programs (written in FORTRAN and stored on a floppy disk) automatically calibrate the equipment, control the sampling of the measured parameters, calculate the volumes of the gases, and display the results on the printer.

Since the apparatus is software-controlled, the system is able to reanalyze quickly the ambient air during each 60-second measurement cycle. Errors due to drift of ambient conditions are

thus minimized. The software also rapidly corrects for the dilution of the exhaled gases by the ambient air — a feature that makes the "open" system practical.

The analog measurements of gas concentrations from the mass spectrometer and of temperature and pressure are fed to the computer through an analog-to-digital (A/D) converter. A parallel interface board is the communication link from the flowmeter to the computer and from the computer to the solenoid valve controls that select which gas (calibration gas No. 1, calibration gas No. 2, exhaled, or ambient) is analyzed by the mass spectrometer.

The use of two calibration gases generates a slope and an intercept for a linear equation, which is solved in real

time. This technique tends to cancel individual equipment errors and reduces the requirements for precise calibration of hardware. To reduce error further, the equipment is calibrated over the range of expected results rather than the entire range of capability. The experimental results are printed out as they are computed.

Because the mask imposes minimum interference to the subject undergoing testing, it can be used to measure respiratory responses to such activities as treadmill exercise. The mask can be worn for long periods with little discomfort.

This work was done by Kenneth L. Koester of Technology Inc. for **Johnson Space Center**. Further informa-

tion [including hardware and software details] may be found in NASA CR-160893 [N81-14614/NSP], "Special Report on the Metabolic Rate Measurement System" [\$8]. A copy may be purchased [prepayment required] from the National Technical Information Service, Springfield, Virginia 22161. MSC-18885

## Portable Radiometer Monitors Plant Growth

Chlorophyll content, leaf area index, and leaf water content can be quickly and easily measured.

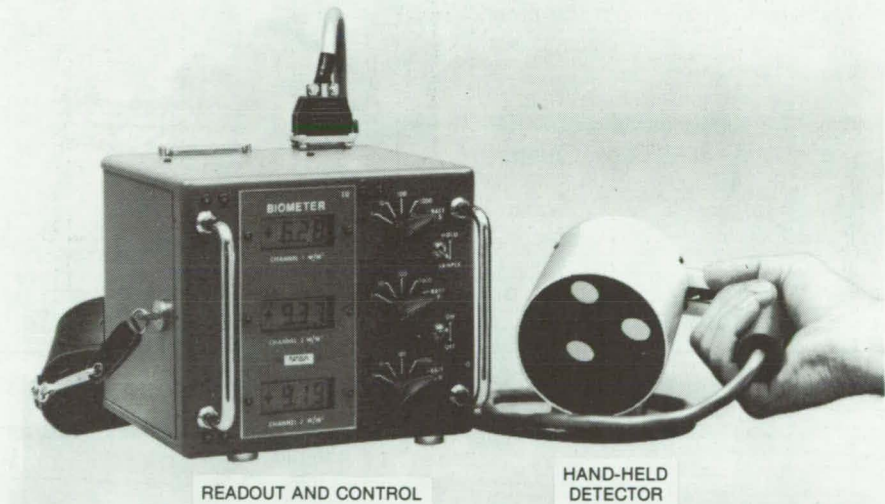
*Goddard Space Flight Center, Greenbelt, Maryland*

A three-band hand-held spectral radiometer measures electromagnetic energy reflected from plant canopies in the visible and infrared portions of the spectrum. It is mobile and easy to use for rapid, repeated measurements. The radiometer probe is simply held level over the plant canopy, the readout range switches are set, and the measurements are recorded.

The instrument measures in the red (0.63 to 0.69  $\mu\text{m}$ ), photographic infrared (0.76 to 0.90  $\mu\text{m}$ ), and near infrared (1.55 to 1.75  $\mu\text{m}$ ). The reflectances of plant canopies in these three spectral regions correlate closely with chlorophyll content, leaf area index, and leaf water content, respectively. The measurements therefore relate to plant growth and development.

The radiometric accuracy is 1 part in 1,000 ( $\sim 10$  bits) with a total range of 1,000,000 (20 bits). This translates into a power range from 1 milliwatt to 1 kilowatt per square meter within the optical band pass. The radiometric sampling occurs 4 times per second.

The new spectral radiometer (see figure) consists of two modules — a hand-held detector module and a readout-and-control module — that are connected by a cable. The detector module contains a lead sulfide sensor and two silicon radiation sensors. It also contains preamplifiers, a "zero" adjustment for the lead sulfide sensor channel, a sample-and-hold switch, a trigger switch for activating the radiometer, and a handle. Each sensor is covered by a collimation tube and an interference



The **Three-Band Hand-Held Spectral Radiometer** is portable and simple to operate. Three sensors monitor three separate bands of radiation reflected from crops. These reflectances correlate closely with chlorophyll content, leaf area index, and leaf water content. Extensive field tests have been successfully conducted on alfalfa, corn, soybeans, and winter-wheat crops.

filter. The field-of-view of each collimator is about 24°; it can be reduced by attaching an aperture plate. A lightproof housing encases the module.

The radiometer measurements are read on three liquid-crystal displays on the readout-and-control module. This module also contains a battery-pack power supply, a sample-and-hold switch, and range controls, in addition to associated electronics and switches. (The sample-and-hold switch can be operated from either of the modules.) The readout module has

sufficient space to accommodate a 1,000- to 2,000-entry digital memory, now under development.

This work was done by Compton J. Tucker III and Lee D. Miller of **Goddard Space Flight Center**. Further information may be found in NASA TM-80641 [N80-27674/NSP]. "The GSFC Mark-II Three Band Hand-Held Radiometer" [\$6]. A copy may be purchased [prepayment required] from the National Technical Information Service, Springfield, Virginia 22161. GSC-12412

## Chemical Growth Regulators for Guayule Plants

Experiments on a small American rubber plant seek chemicals that promote growth.

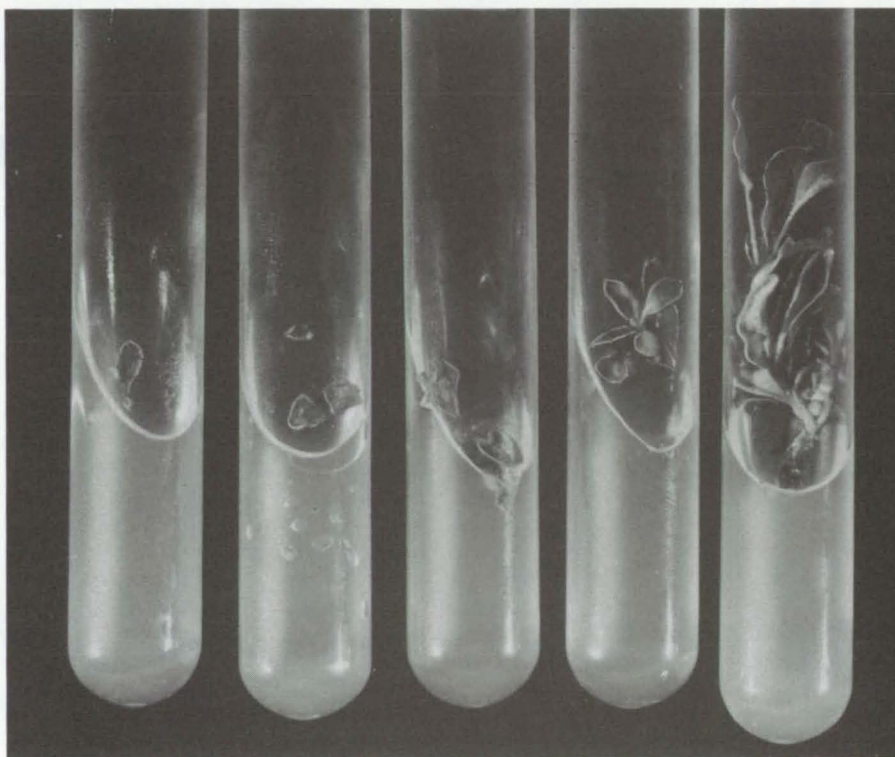
NASA's Jet Propulsion Laboratory, Pasadena, California

The possibility of artificially propagating the guayule rubber plant is encouraged by recent NASA experiments on tissue-culture growth. Preliminary results indicate that a class of compounds that promotes growth in soil may also promote growth in a culture medium.

Guayule (*Parthenium argentatum*) is a shrub native to Mexico and the Southwestern United States. It has been cultivated for its latex, used in making polyisoprene rubber. Unlike the latex of the rubber tree, the guayule latex is dispersed throughout the plant. Consequently, the whole plant is harvested and processed.

In previous experiments, chemical regulators induced a 400-percent increase in yield. [See "Chemical Agent Boosts Natural-Rubber Output" (NPO-14185) on page 376 of *NASA Tech Briefs*, Vol. 3, No. 3.] This increase is not sufficient to attain production goals, however, since the unenhanced yield of guayule rubber is only 700 to 1,000 lb per acre (0.007 to 0.01 kg per m<sup>2</sup>). Consequently, the propagation of whole guayule plants from tissue culture is sought as a way to increase production.

In experiments to determine the optimum conditions for tissue-culture growth, attention was given to the effect of 2-(3,4-dichlorophenoxy)-triethylamine [triethylamine (TEA) derivative] as a growth hormone. Explants for tissue cultures were obtained from the shoots and stems of guayule plants. Segments 0.5 to 2 cm long were placed in agar mediums in slanted test tubes and grown under controlled lighting, temperature, and humidity. Constituents of the mediums — including various nutrients and hormones — were varied to determine the effects on the growth of calluses and shoots.



**Test Tubes Containing Guayule-Tissue Cultures** were used in experiments to test the effects of chemical-growth regulators. The shoots in tubes 4 and 5 grew in response to the addition of 2-(3,4-dichlorophenoxy)-triethylamine to the agar medium.

Callus formation in stem segments usually showed cell division in the pith and cambium, primarily above and occasionally below the agar line. In the figure, tubes 1 and 2 contain callus growth. In tube 3, calluses and shoots developed. The luxuriant growth of shoots in tubes 4 and 5 is due to the addition of TEA derivative.

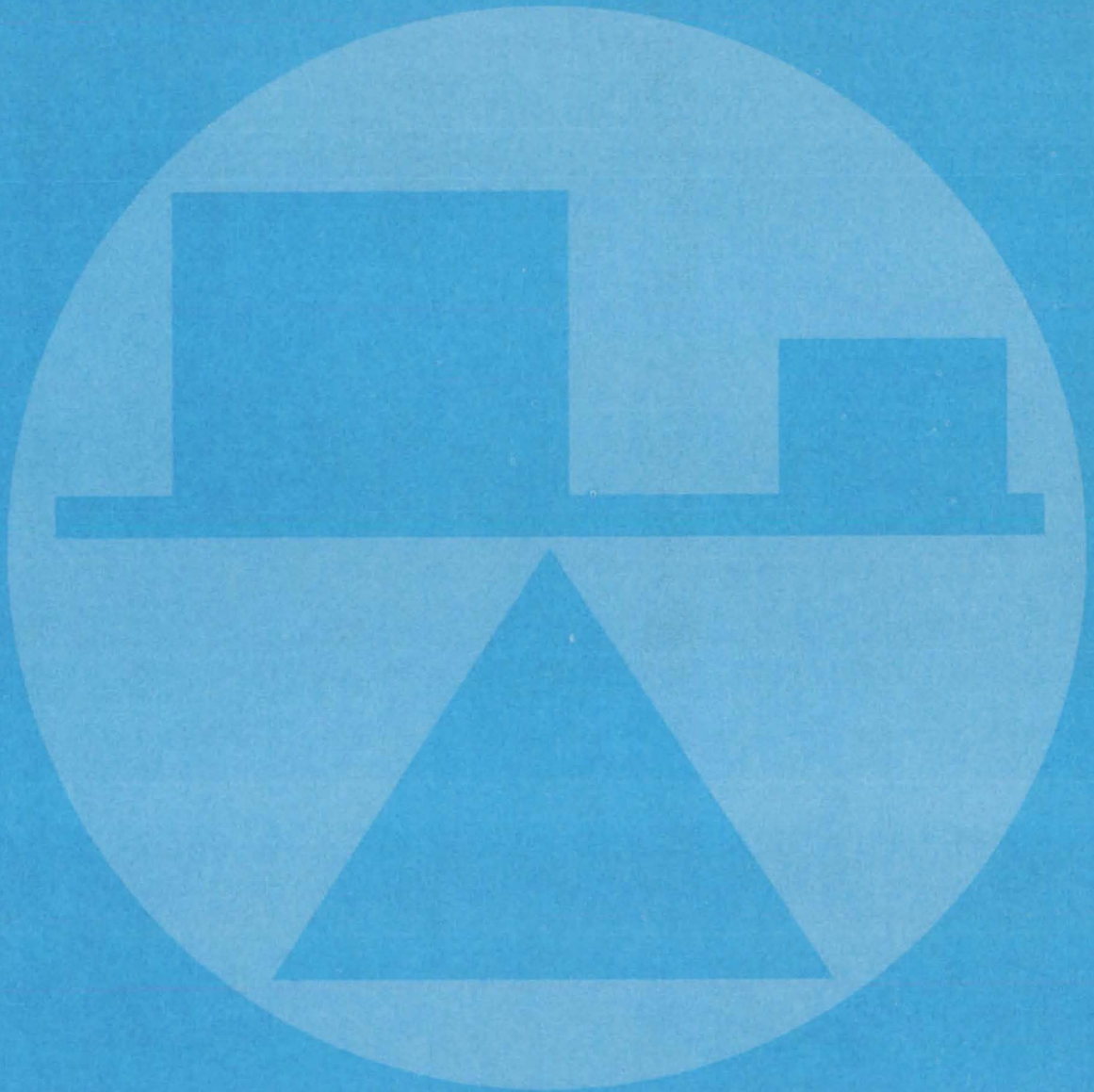
Shoot formation was greatest at 10 mg/l of TEA derivative and somewhat independent of the levels of the other hormones tested. Callus formation was strongly inhibited at that level, while lower and higher concentrations of TEA

derivative promoted callus formation. Further experiments are needed to define the effect of the TEA derivative.

This work was done by Minoo N. Dastoor, Wayne W. Schubert, and Gene R. Petersen of Caltech for NASA's Jet Propulsion Laboratory. For further information, Circle 42 on the TSP Request Card.

Inquiries concerning rights for the commercial use of this invention should be addressed to the Patent Counsel, NASA Resident Legal Office-JPL [see page A5]. Refer to NPO-15213.

# Mechanics



## Hardware, Techniques, and Processes

- 51 Less-Costly Inertial Guidance
- 52 High-Speed Laser Anemometer
- 53 Correcting for Background in Flowing Plasma Measurements
- 54 Dual-Laser Schlieren System
- 55 Fiber-Optic, Semiconductor Temperature Gage
- 56 Detecting Cracks on Inner Surfaces
- 56 Viscous Torques on a Levitating Body
- 57 Adhesive-Bonded Tab Attaches Thermocouples to Titanium
- 58 Interferometer Accurately Measures Rotation Angle
- 59 Ultrasonic Transducer Analyzer
- 60 Far-Field Antenna Pattern From a Near-Field Test
- 61 Heat Pipe Blocks Return Flow
- 62 Nozzle Modification Suppresses Flow Transients
- 62 Microcomputer Checks Butt-Weld Accuracy
- 63 Self-Correcting Electronically-Scanned Pressure Sensor
- 64 Lacquer Reveals Impact Damage in Composites
- 65 Measuring Cyclic-Stress Properties of Pressure Vessels
- 66 Matching of Apparent-Strain Characteristics
- 67 Pressure Switch Is a Low-Cost Battery Indicator
- 68 Pulsed Phase-Locked-Loop Strain Monitor
- 69 Strain-Gaged Bolts Are Easily Prepared
- 70 Load-Displacement Measurement on Pin-Loaded Specimens

## Computer Programs

- 70 Heat-Energy Analysis for Solar Receivers
- 71 Program for Analysis and Resizing of Structures
- 71 Unsteady Subsonic Loadings Due to Control-Surface Motion
- 72 Aerodynamics of Sounding-Rocket Geometries
- 72 Aeroelastic Analysis for Rotorcraft



# Less-Costly Inertial Guidance

Pendulum-based system uses only two gyros and no accelerometers.

Ames Research Center, Moffett Field, California

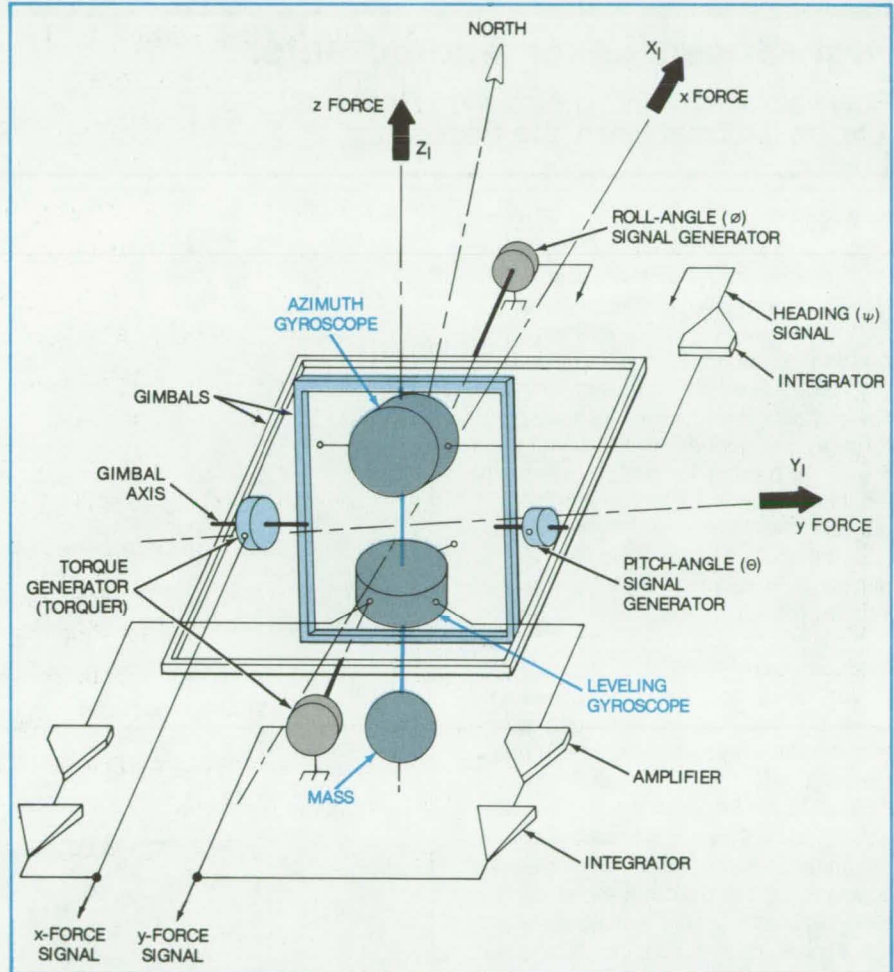
A microprocessor-controlled inertial navigation system is based upon a pendulous two-axis gimbal assembly. It is considerably simpler and less costly than conventional platform or strap-down inertial guidance and is therefore especially appropriate for small aircraft. Only two modern miniature dry tuned-rotor gyroscopes are used — one of just modest precision, and no accelerometers are required. The microprocessor and supporting electronics are readily-available commercial components.

As shown in the figure, the assembly has an outer gimbal (which is strapped to the longitudinal axis of the craft) and an inner gimbal that supports a two-degree-of-freedom leveling gyroscope and a heading (azimuth) gyroscope. A mass supported along the common axis of the two gyroscopes lowers the center of gravity of the assembly to below the geometrical center.

With lowered center of gravity, the instrument responds to forces as would a two-axis pendulum. The aircraft in motion is subjected to forces that can be resolved into components along the axes of a locally-level coordinate frame  $X_I, Y_I, Z_I$  ( $Z_I$  passes through Earth's center). When the torques due to the level forces tend to displace the pendulum, a servosystem restores it to alignment with the local vertical. The servo signals generated by the leveling gyroscope are amplified and fed to torque generators on the gimbal axes. The signals are a direct measure of the applied force components in the local coordinate frame.

In addition to determining the components of applied force, the instrument also determines the aircraft pitch and roll angles ( $\theta$  and  $\phi$ ) by processing the outputs from signal generators on the gimbal axes. The heading angle  $\psi$  between true north and the  $X_I$  axis, is determined by a signal from the azimuth gyro.

The gyro signals are handled by the microprocessor, which also receives such input data as initial position. The direction of true north and the initial



**Two Gyroscopes Mounted in Gimbals** yield signals that allow the calculation of velocity, position, and attitude of an aircraft. The mass lowers the center of gravity of the gimbal-and-gyro assembly to below the intersection of their axes. The combination acts as a two-axis pendulum. The rate signals from the leveling gyroscope are integrated, amplified, and fed to gimbal torquers to restore the pendulum to alignment with the local vertical.

heading are determined in a relatively-straightforward calibration sequence while the aircraft is on the ground.

The microprocessor performs the following operations on the x-force and y-force signals:

- Converts them from force components in the local frame of reference to components in geographical coordinates,
- Solves the standard navigation equations to determine longitudinal and lateral velocities, and

- Integrates the velocities to find the aircraft position.

The microprocessor also compensates for drift-rate errors and Earth rotation-rate errors. If required, a correction for gimbal bearing friction can be programmed.

The azimuth gyroscope can have a drift-rate uncertainty 10 times greater than that of the leveling gyroscope. The higher accuracy is needed in the leveling unit because it supplies the two force components. For example, for an

(continued on next page)

accuracy of only 1 nautical mile (1.9 km) after a 1-hour mission, the gyroscopes should have random drift rates of 0.1°/hour and 0.01°/hour, respectively. The system output simultaneously displays the vehicle position, velocity, heading, and attitude.

This work was done by Shmuel J. Merhav of the National Research Council for **Ames Research Center**. For further information, Circle 43 on the TSP Request Card.

This invention has been patented by NASA [U.S. Patent No. 4,244,215].

Inquiries concerning nonexclusive or exclusive license for its commercial development should be addressed to the Patent Counsel, Ames Research Center [see page A5]. Refer to ARC-11257.

## High-Speed Laser Anemometer

Flow velocities within the rotating blades of rotating turbomachinery are mapped.

Lewis Research Center, Cleveland, Ohio

A new high-speed laser anemometer system rapidly and efficiently maps the gas-flow velocities within the rotating blade rows of turbomachinery. Small seed particles entrained in the gas flow fluoresce when they pass through the probe volume, which is the fringe pattern formed by intersecting laser beams. The transit time of the particles is obtained by the use of suitable optics (see Figure 1), a photomultiplier tube, and an electronic signal processor. As shown in Figure 2, the data are then sent to a minicomputer.

Very accurate shaft-angle position data are obtained by a unique electronic shaft-angle encoder [see "Electronic Shaft-Angle Encoder" (LEW-12832) in *NASA Tech Briefs*, p. 444, Vol. 2, No. 4] and are also sent to the minicomputer. The minicomputer sorts the data and plots the results in a near-real-time graphic display. Since the probe volume can be accurately positioned, it is possible to map rapidly almost the entire volume between the blades of a rotating turbomachine. Typically, a velocity profile, derived from 30,000 measurements along 1,000 sequential circumferential positions covering 20 blade passages, can be mapped for a set radial and axial position in less than a minute. The graphic display, updated every 5 to 15 seconds, includes the velocity profile along a circumferential measurement line and a histogram of the distribution of the measurements along the 1,000 circumferential positions. The conditions of the run are displayed by alphanumeric characters.

In previous systems, the measurement process was time-gated, and

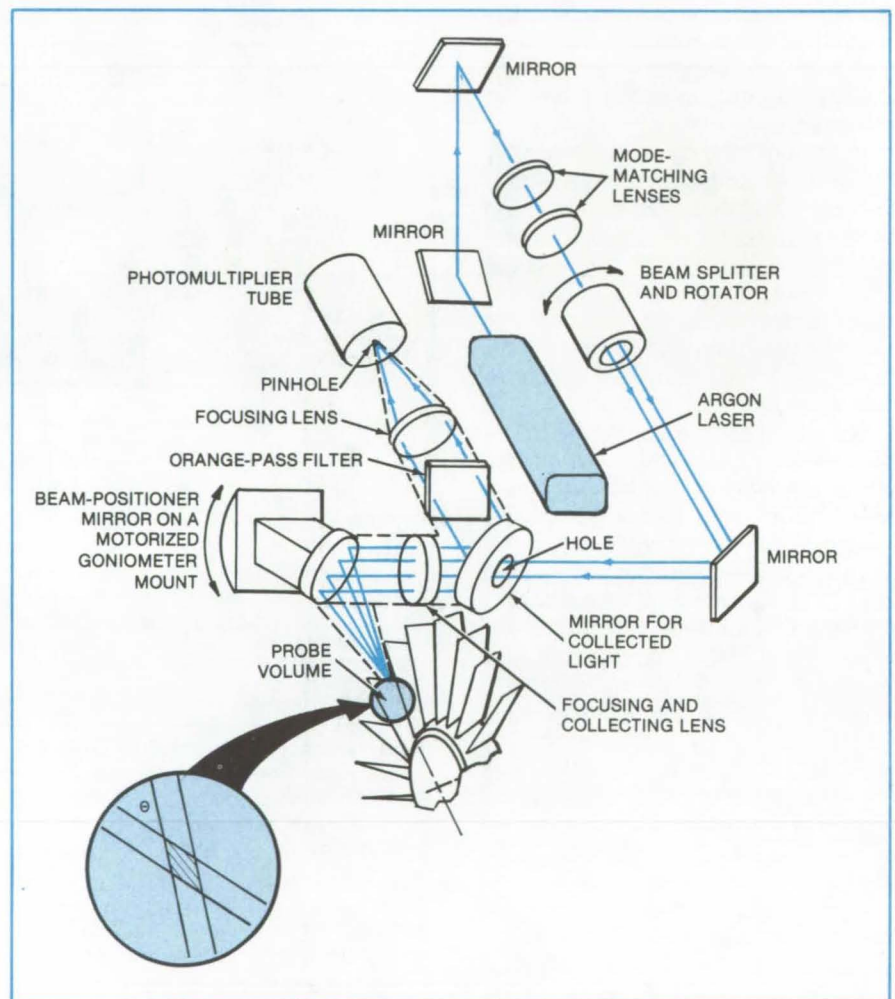


Figure 1. The **Anemometer Optics** form fringe patterns in a probe volume. When small seed particles in a flowing gas pass through the probe volume, they fluoresce.

hence only a small number of circumferential positions could be obtained during a measurement period. Thus, the building up of a map was a very long and laborious task.

This new system produces excellent maps quickly, easily, and economically. The graphic display allows a virtually-real-time image of an operating machine. This anemometer sys-

tem can be used with many types of turbomachinery, including those used in aeronautical and automotive turbines, and in electric-power production. The system should also be applicable to a variety of other gas-flow situations.

This work was done by J. A. Powell, A. J. Strazisar, and R. G. Seasholtz of Lewis Research Center. Further information may be found in NASA TM-79320 [N80-14375/NSP], "Efficient Laser Anemometer for Intra-Rotor Flow Mapping in Turbomachinery" [\$5]. A copy may be purchased [prepayment required] from the National Technical Information Service, Springfield, Virginia 22161.

This invention has been patented by NASA [U.S. Patent No. 4,171,522]. Inquiries concerning nonexclusive or exclusive license for its commercial development should be addressed to the Patent Counsel, Lewis Research Center [see page A5]. Refer to LEW-13527.

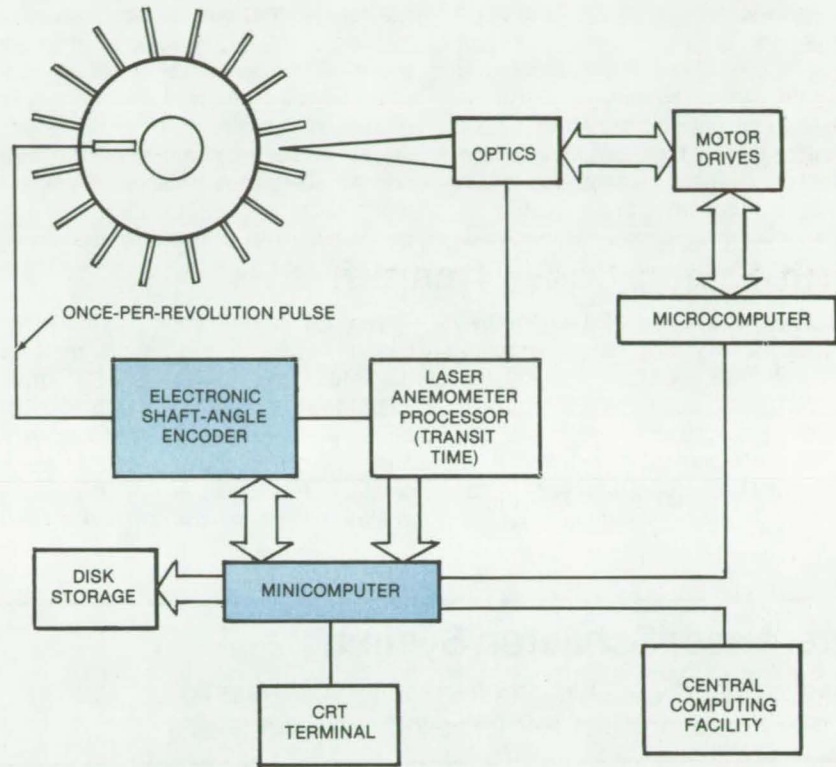


Figure 2. A **Minicomputer** sorts the position data obtained from an electronic shaft-angle encoder and plots the gas-flow velocities within the rotating blade rows of turbomachinery.

## Correcting for Background in Flowing Plasma Measurements

Langmuir-probe end effect allows measurements independent of background plasma.

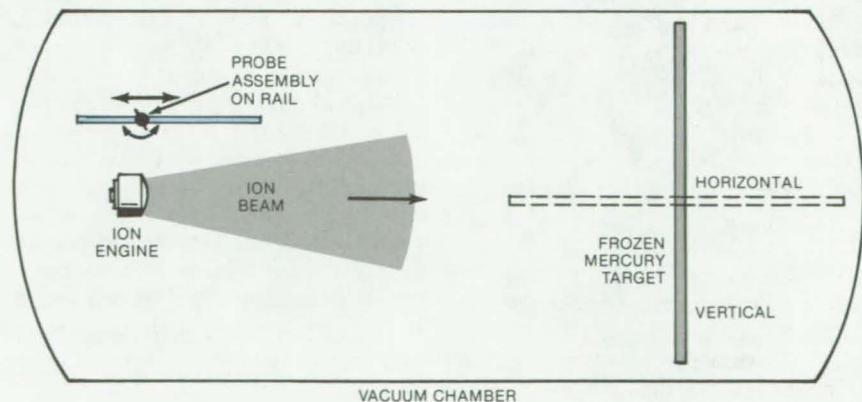
NASA's Jet Propulsion Laboratory, Pasadena, California

A simple mechanical arrangement of a movable Langmuir probe maps the flow of a low-energy plasma in the vicinity of an ion-beam source. The setup corrects for "background" ions produced when the beam strikes the target.

The new measurement setup aids NASA research on mercury-ion engines for spacecraft. Along with the primary ion beam, such engines also produce a low-energy plasma that can surround the spacecraft and interfere with its operation.

Efforts to study the plasma have been plagued by the masking effect of neutral atoms sputtered from the target struck by the ion beam: The sputtered atoms flow upstream, where they are converted to ions by the

(continued on next page)



A **Movable Langmuir Probe** measures charge-exchange plasma density and flow in the vicinity of an ion engine. The angular dependence of probe current is utilized to determine the plasma flow direction at the probe location. By rotating the target, the data are shown to be independent of the target-sputtered ions.

primary beam, in a charge-exchange interaction. Target emission does not occur in space, but it interferes with accurate measurements on Earth. A rotatable target demonstrates the insensitivity of the Langmuir-probe end effect to these background ions.

The measurement apparatus is mounted in a vacuum chamber (see figure) with walls that are cooled by liquid nitrogen. The ion engine (or other ion source) at one end of the chamber aims its beam at a frozen mercury target at the opposite end of the chamber. The probe moves along a rail parallel to the beam, and it can be rotated in the plane of the beam axis.

The target can be rotated so that it is horizontal instead of vertical. When it is

horizontal, the end of the chamber instead of the target is exposed to the beam. Although some steel is sputtered from the end wall, the number of neutral atoms coming from the downstream end of the chamber is considerably smaller. Thus measurements are made with the target alternately perpendicular and parallel to the beam axis, so that its effect can be determined.

The Langmuir probe is made of tungsten wire 5 mils (0.13 mm) in diameter. The probe is 450 times longer than its diameter. In the vacuum chamber, the probe is moved to various positions along the rail. At each position, the probe is set at various angles, and the ion current is recorded

at each setting.

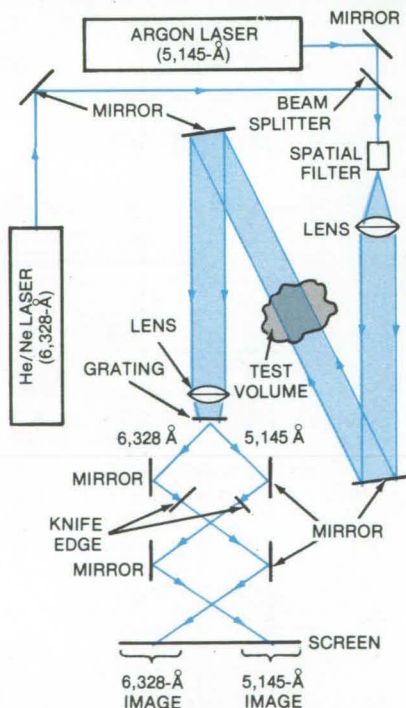
The shape of the curve of ion current versus probe angle depends on the plasma density and flow velocity. The curves can therefore be used to determine these quantities at various locations in the chamber. The plasma flow direction at the probe location is determined from the angular position of the probe where the peak ion current produced by the end effect is obtained.

*This work was done by Melvin R. Carruth, Jr., of Caltech for NASA's Jet Propulsion Laboratory. For further information, Circle 44 on the TSP Request Card. NPO-15332*

## Dual-Laser Schlieren System

Two laser beams enable simultaneous visualization of mutually-perpendicular refractive-index gradients.

Marshall Space Flight Center, Alabama



The **Dual-Laser Schlieren System** employs two lasers of different wavelengths and two perpendicular knife edges. The simultaneous side-by-side images on the screen display mutually-perpendicular refractivity gradients in the test volume. One gradient is in the plane of the page, normal to the optical axis; the other is normal to the page and to the axis.

A proposed schlieren system uses two lasers and two knife edges to simultaneously view perpendicular refractive-index gradients in a test volume. It is an improvement over conventional schlieren systems, which monitor the gradient along only one axis. Although the system was originally developed to monitor materials-processing experiments in space, it should find application wherever there is a need to study two-dimensional temperature, pressure, concentration, or other gradients related to the index of refraction.

In the modified system, shown schematically in the figure, two laser beams separated in wavelength by at least 1,000 Å are combined at a beam splitter. The composite beam is expanded, collimated, and then passed through the test volume. The emergent light is focused by a second lens and is

passed through a transmission grating that separates the laser beams.

Each of the beams is focused on one of two perpendicular knife edges. In the figure, one knife edge is in the plane of the page, normal to the optical axis; the other is normal to the page and to the axis. The images on the screen are thus a side-by-side display of the perpendicular refractivity gradients at the object point in the test volume.

*This work was done by Robert B. Owen and William K. Witherow of Marshall Space Flight Center. For further information, Circle 45 on the TSP Request Card.*

*This invention is owned by NASA, and a patent application has been filed. Inquiries concerning nonexclusive or exclusive license for its commercial development should be addressed to the Patent Counsel, Marshall Space Flight Center [see page A5]. Refer to MFS-25315.*

# Fiber-Optic, Semiconductor Temperature Gage

A "safe" temperature gage for explosive liquids is based on optical transmission.

Lyndon B. Johnson Space Center, Houston, Texas

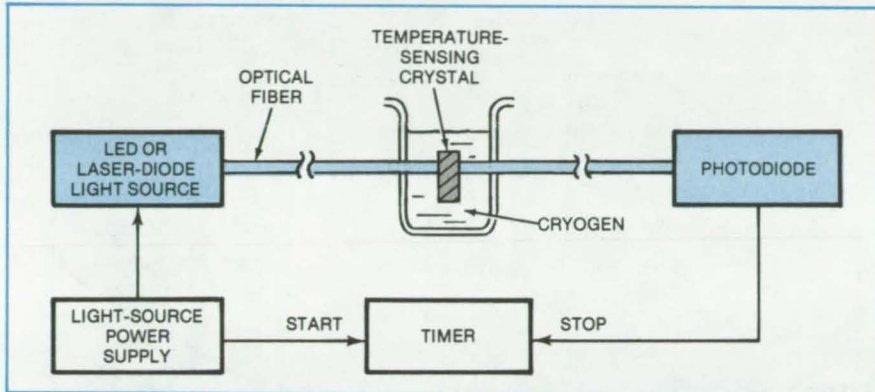


Figure 1. An Optical Fiber Carries Light to a Sensing Crystal immersed in a cryogen. The light, which originates in a swept-wavelength light source, is transmitted to a second optical fiber when its wavelength exceeds the absorption band edge of the sensing crystal.

A semiconductor crystal inserted between input and output optical fibers is the temperature-sensing element in a new approach to measuring the temperature of cryogenics. Since no electrical components are immersed in the liquid, the new sensor minimizes the danger of electrically ignited explosions in hazardous cryogenics such as oxygen and hydrogen. The gage also should be useful for handling noncryogenic liquids in aircraft, automobiles, boats, and water tanks.

Accurately measuring the band edge of the sensing crystal is the key to measuring temperature with the new sensor. Using the apparatus shown in Figure 1, a swept-wavelength light beam is initiated in an LED or a laser diode. Light transmission to a photodiode detector is controlled by the absorption band edge of the sensing crystal — wavelengths shorter than the band edge of the crystal are absorbed; those longer are transmitted.

When the power supply turns on the light source, it also sends a signal to start a timer. The wavelength of the light from the LED or laser diode increases linearly as the source is heated (see Figure 2), either directly from the power-supply current or indirectly from a

separate heater. At some point after the light source is turned on, the wavelength of its transmitted light increases beyond the absorption band edge of the sensing crystal. Light then passes through the crystal, to the second optical fiber, and on to the photodiode, which sends a signal to stop the timer. The elapsed time is a measure of the band-edge wavelength, which is related to the crystal and cryogen temperatures. The apparatus is calibrated so that the elapsed time is converted directly to a temperature reading.

Any of several light-transmitting crystals can be considered for the temperature gage, so long as the position of the optical-absorption (or transmission) edge is a well-defined function of temperature. For a temperature range of 4 to 135 K, in the gage under development, an InP crystal is the sensing crystal and GaAs is the laser-diode material.

This work was done by Madan Sharma of TRW, Inc., for Johnson Space Center. Further information may be found in NASA CR-160448 [N80-17848/NSP], "Fiber-Optic Instrumentation Final Report, Technical Report A001: Cryogenic Sensor Model Description" [\$11]. A copy may be purchased [prepayment required] from the National

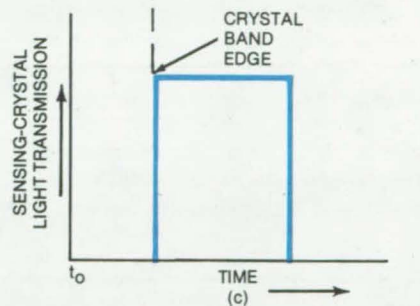
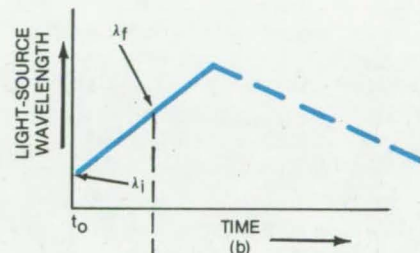
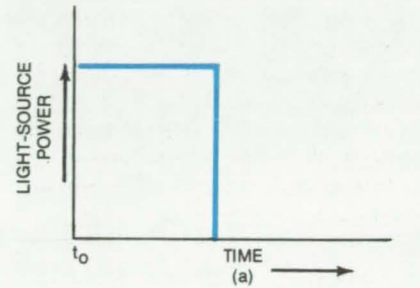


Figure 2. A Power Pulse (a) turns on the light source so that a beam of linearly increasing wavelength (b) is transmitted. At a wavelength that corresponds to the absorption band edge of the sensing crystal (c), a timer is stopped.

Technical Information Service, Springfield, Virginia 22161.

This invention is owned by NASA, and a patent application has been filed. Inquiries concerning nonexclusive or exclusive license for its commercial development should be addressed to the Patent Counsel, Johnson Space Center [see page A5]. Refer to MSC-18627.

---

## Detecting Cracks on Inner Surfaces

A silicone mold picks up fluorescent dye from cracks and pores.

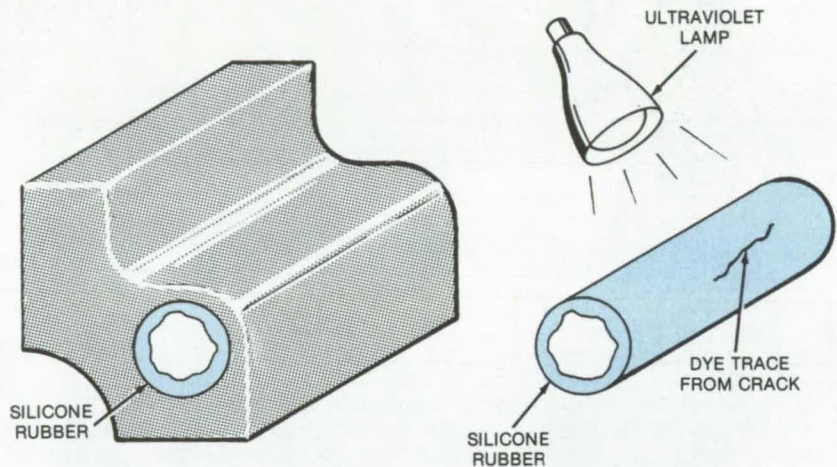
---

### Marshall Space Flight Center, Alabama

Microscopic cracks or flaws in the surface of a workpiece are often detected with fluorescent dye. The dye is spread over the surface to be inspected and then washed off. When the piece is then viewed under ultraviolet light, a glow is seen from dye trapped in any flaws.

This inspection technique has been extended to visually inaccessible areas, such as the surface inside the drilled or reamed hole in the machine part shown in the figure. After the fluorescent dye is spread on the inner surface and then wiped away, a silicone rubber compound is applied to the surface. Dye that has entered surface defects is absorbed into the silicone, which is then cured and is peeled away. Ultraviolet light beamed on the mold makes the absorbed dye glow, showing the locations of cracks and pores that previously were undetectable.

The intensity of the fluorescence gives a rough indication of the depth of the defect, because a deeper crack bleeds more dye into the silicone than a shallow crack does. The greater concentration of dye produces a higher intensity of emitted fluorescent light, so intensity is a clue to crack depth.



The **Silicone Rubber Mold** picks up fluorescent dye from cracks on the inner surface of the machine part on the left. When the cured mold is removed from the part and exposed to ultraviolet light (right), the dye fluoresces to reveal the presence of the cracks.

This fluorescent inspection procedure is fast, inexpensive, and simple to perform. A plaster reproduction of the inspected surface can be made from the silicone impression.

*This work was done by A. B. Sax of Rockwell International Corp. for Mar-*

**shall Space Flight Center.** *No further documentation is available.*

*Inquiries concerning rights for the commercial use of this invention should be addressed to the Patent Counsel, Marshall Space Flight Center [see page A5]. Refer to MFS-19575.*

---

## Viscous Torques on a Levitating Body

Measured and predicted torques due to acoustic waves are in good agreement.

---

### NASA's Jet Propulsion Laboratory, Pasadena, California

New analytical expressions for the viscous torque generated by orthogonal sound waves agree well with experiment. It is now possible to calculate the torque on an object levitated in a fluid. Levitation has applications in containerless materials processing, coating, and fabrication of small precision parts.

Nonzero time-averaged acoustic torques due to Bernoulli forces were first proposed by Lord Rayleigh in 1882. However, torques are also produced by viscosity when there are two orthogon-

al waves, even on such smooth, symmetric objects as spheres.

For the thin disk shown in the figure, for example, the torque about the z axis was calculated for plane acoustic waves incident along the x and y axes, with identical frequency, and a phase shift between them (as measured at a specified point in space).

The sound waves cause the fluid particles to move in elliptical paths and induce an azimuthal circulation in the boundary layer, giving rise to a time-

averaged torque. The graph shows the time-averaged acoustic/viscous torque for various phase shifts, as calculated and as measured on an actual disk.

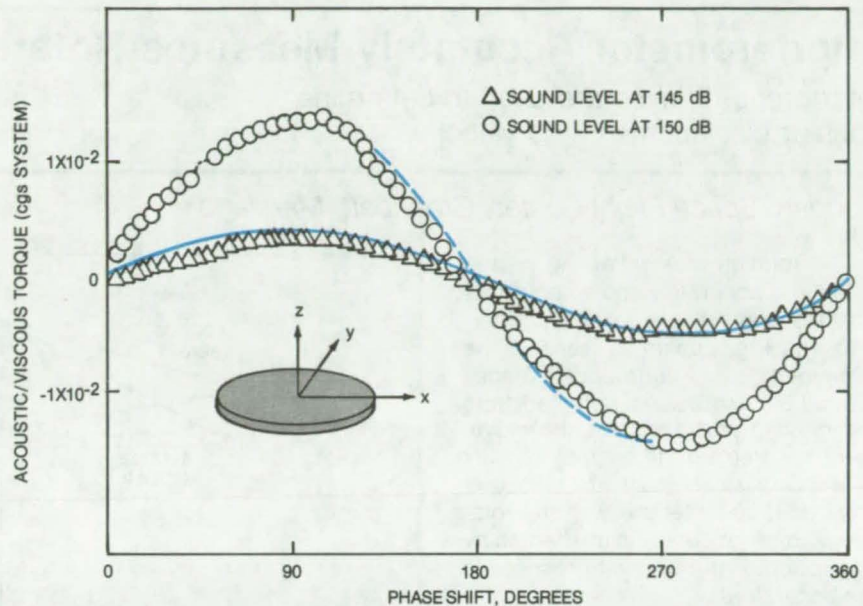
The theory requires some simplifying assumptions. It considers only axisymmetric bodies smaller than the sound wavelength, and it assumes small-amplitude motions in the fluid. The fluid is treated as inviscid everywhere except in a thin boundary layer on the surface of the object. Pressure gradients are neglected in the viscous boundary lay-

er. Normal and tangential velocities are assumed to vanish at the surface of the object.

The velocity field is treated mathematically as the sum of two fields, one of which satisfies the inviscid-fluid wave equation. The other satisfies the viscous-fluid wave equation and has an amplitude that rapidly decreases with distance away from the surface. The coupled equations of motion are solved in a perturbation expansion. Once the velocity fields in the viscous boundary layer are known, the viscous stresses and their contributions to the torque about the desired axis of symmetry are calculated from standard laminar-flow theory.

Calculations have also been done for circular cylinders and spheres. In general, the time-averaged torque about the axis of symmetry (the z axis) is given by the nonlinear terms in the perturbation expansion for the torque. The physical significance is that the torque is proportional to the acoustic energy dissipated in the viscous boundary layer.

*This work was done by Fritz Busse and Taylor Wang of Caltech for NASA's Jet Propulsion Laboratory. For further information, Circle 46 on the TSP Request Card. NPO-15413*



**Acoustic/Viscous Torque** was calculated and measured for a disk 1 inch (2.54 cm) in diameter. Acoustic plane waves of wavelength 10 inches (25.4 cm) are incident along the x and y axes; torque is measured about the z axis. The data points are the experimental values. The theory is indicated by the solid and dashed lines.

## Adhesive-Bonded Tab Attaches Thermocouples to Titanium

The mechanical strength of the titanium is preserved by attaching tab-mounted thermocouples with a thermosetting adhesive.

*Dryden Flight Research Center, Edwards, California*

The mechanical strength of titanium-alloy structures that support thermocouples is preserved by first spotwelding the thermocouples to titanium tabs and then attaching the tabs to the titanium with a thermosetting adhesive. The method was adapted from a similar technique that has been used with success to bond strain gages to metal surfaces. In contrast to spot welding, a technique previously used for thermocouples, the fatigue strength of the titanium is unaffected by adhesive bonding. The technique is also gentler than soldering or attaching the thermocouples with a tap screw, two other often-used approaches.

In one application, in which a thermocouple is fastened to the flight surface of a research aircraft, engineers selected a conducting adhesive that could withstand the 600° F (315° C) temperatures expected during a flight. The resin is spread over the area where the tab is to be attached, the tab with the spotwelded thermocouple is applied with pressure, and the adhesive is cured with a large soldering iron or heat gun. Typical heat-application times (for this adhesive) are 2 to 5 minutes. The adequacy of the bond is verified by measuring the resistance between the tab and the underlying titanium structure. Resistance readings under 5

ohms are considered acceptable.

In comparison tests on adhesive-bonded thermocouples and spotwelded thermocouples, both attached to titanium-alloy structures, the thermocouple temperature measurements agreed within 1 percent. The tests were run up to 1,000° F (538° C). In tests conducted at 1,000° F to determine the shear strength of the adhesive bond, the thermocouple wire broke before the adhesive bond failed.

*This work was done by Clarence E. Cook of Dryden Flight Research Center. For further information, Circle 47 on the TSP Request Card. FRC-11017*

# Interferometer Accurately Measures Rotation Angle

Interference fringes are used to determine angular displacement and velocity.

*Goddard Space Flight Center, Greenbelt, Maryland*

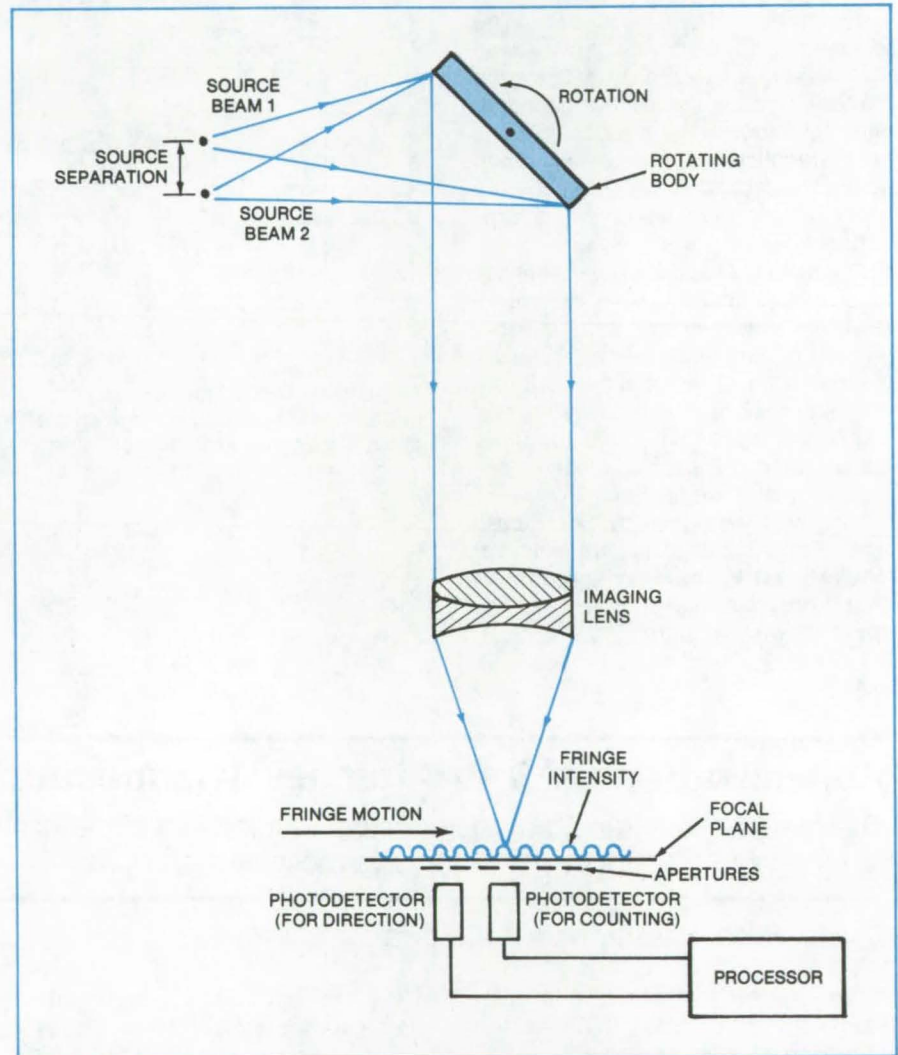
The rotation of a reflecting part is measured accurately and without mechanical contact by an optical interferometer. The apparatus senses the movement of interference fringes formed by twin beams reflected from the rotating part and uses the movement to calculate the angular velocity or angular displacement. The measurement does not interfere with the rotation, and the accuracy is unaffected by translation of the part with respect to the apparatus.

The measurement is based on the principle that monochromatic and coherent light beams create interference fringes (Young's fringes) when they are superimposed. The two beams in the new instrument are reflected from the rotating part and pass through an imaging lens having a very long focal length. The fringes appear at the lens focal plane.

A photodetector behind an aperture on the central axis of the image plane senses the bright lines of the pattern and sends an electrical pulse to a signal processor every time a bright line passes. The processor counts the fringes in a fixed time period and calculates the angular speed of rotation from the fringe count, the light wavelength, and the separation of the sources. Another photodetector determines the direction of motion of the fringes and hence the rotational direction of the body.

The two beams have the requisite coherence and monochromaticity if they are derived from the same source, for example, a laser. The beam from a helium/neon laser (wavelength 6,328 Å) is directed into the lens and passes through a pinhole in the focal plane. A beam-splitter and mirror system divide the beam into two parallel branches of equal intensity. For greater mechanical stability, the beam optics can be constructed entirely of prisms bonded to a fused-silica base.

Increasing the distance between the beam sources increases the number of fringes counted for a given angle and thus increases the accuracy. For exam-



**Interference Fringes From Superimposed Beams** move across a photodetector, creating electrical pulses. The frequency of the pulses is a direct measure of the angular velocity of the rotating body. If the separation of the sources changes, it affects the separation of all the fringes equally and does not affect the angular velocity measurement.

ple, a beam separation of 6.328 mm corresponds to an accuracy within about 1 microradian. Increasing the separation to 63.28 mm makes the measurements accurate to less than 1 microradian; however, accuracy is eventually limited by mechanical, optical, and thermal noise.

*This work was done by Peter O. Minott of Goddard Space Flight Cen-*

**ter.** For further information, Circle 48 on the TSP Request Card.

*This invention is owned by NASA, and a patent application has been filed. Inquiries concerning nonexclusive or exclusive license for its commercial development should be addressed to the Patent Counsel, Goddard Space Flight Center [see page A5]. Refer to GSC-12614.*



# Ultrasonic Transducer Analyzer

Transducer beam is characterized by analyzing echoes from a point reflector.

*Marshall Space Flight Center, Alabama*

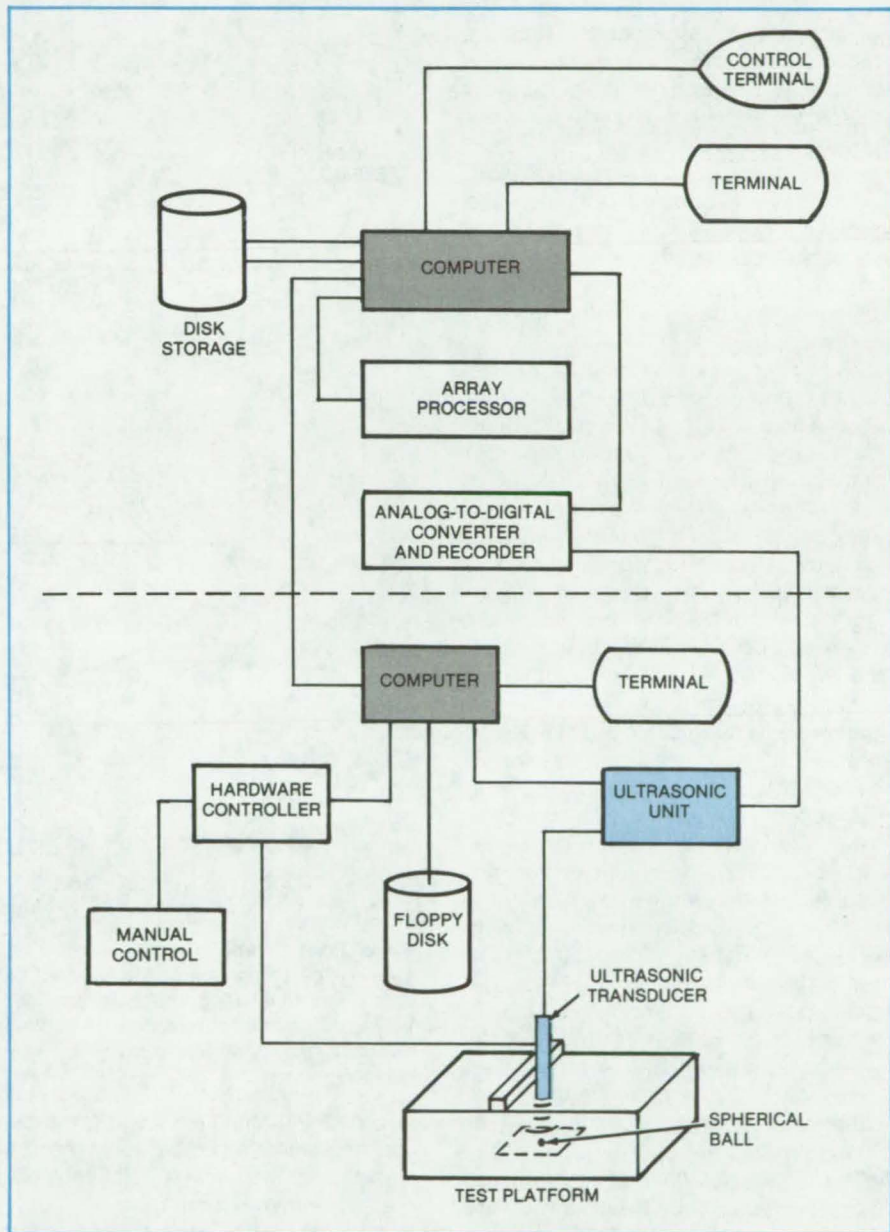
Ultrasonic transducer-beam-intensity distributions are determined by analyzing echoes from a spherical ball. Computers control the equipment and process the data. Important beam characteristics, such as the location of best beam focus and the beam diameter at focus, can be determined quickly from an extensive set of plots generated by the apparatus. (A previous transducer-characterization method using schlieren optics was more difficult to set up, produced fewer quantitative results, and did not characterize the beam in detail.)

The mathematical analysis of a scattering process is simplest when the scattering center is as simple as possible. In this case, the transducer beam strikes a small spherical ball approximating a point-scattering center. Part of the beam reflects back to the transducer, producing an echo signal the intensity of which depends on the beam intensity at the ball and on the distance to the ball.

The hardware configuration is shown in the figure. To start the measurement process, the operator helps the program locate the ball by identifying the primary echo on a CRT display. Then, under computer control, the transducer steps through a three-dimensional lattice of positions. At each depth, a 1-inch (25-mm) square is scanned in 0.01-inch (0.25-mm) steps. Depth increments range from 1/8 to 1 inch (3 to 25 mm). Echo intensity at each position is recorded digitally for later analysis.

The transducer-characterization task is divided into two phases: data acquisition and data processing governed by programs called PACT and PEARL, respectively. Both programs are flexible, containing options to be selected by the user to custom-fit the system to the particular application.

A digital-filtering option in PEARL reduces noise in the plots. The system can also spot flaws in metal plates, once the transducer has been analyzed.



In the **Ultrasonic Transducer Analyzer Hardware**, the equipment below the dashed line operates the test platform. The equipment above digitizes, stores, and analyzes the transducer echo signals.

*This work was done by Michael K. Grounds of M&S Computing, Inc., for Marshall Space Flight Center. For further information, including documentation on PACT and PEARL, Circle 49 on the TSP Request Card.*

*Inquiries concerning rights for the commercial use of this invention should be addressed to the Patent Counsel, Marshall Space Flight Center [see page A5]. Refer to MFS-25410.*

## Far-Field Antenna Pattern From a Near-Field Test

The shape of the beam from an antenna is found by series expansion of polar-scan data taken in a plane.

*NASA's Jet Propulsion Laboratory, Pasadena, California*

Testing the far-field radiation pattern of large directive antennas, such as those carried into space by the Space Shuttle, is inherently difficult. The field intensity must be sampled over very large areas and distances.

In the past, techniques have been developed for calculating the far-field pattern from near-field test data. Although these methods allow the tests to be run in a conventional anechoic chamber, the test geometry may not be simple.

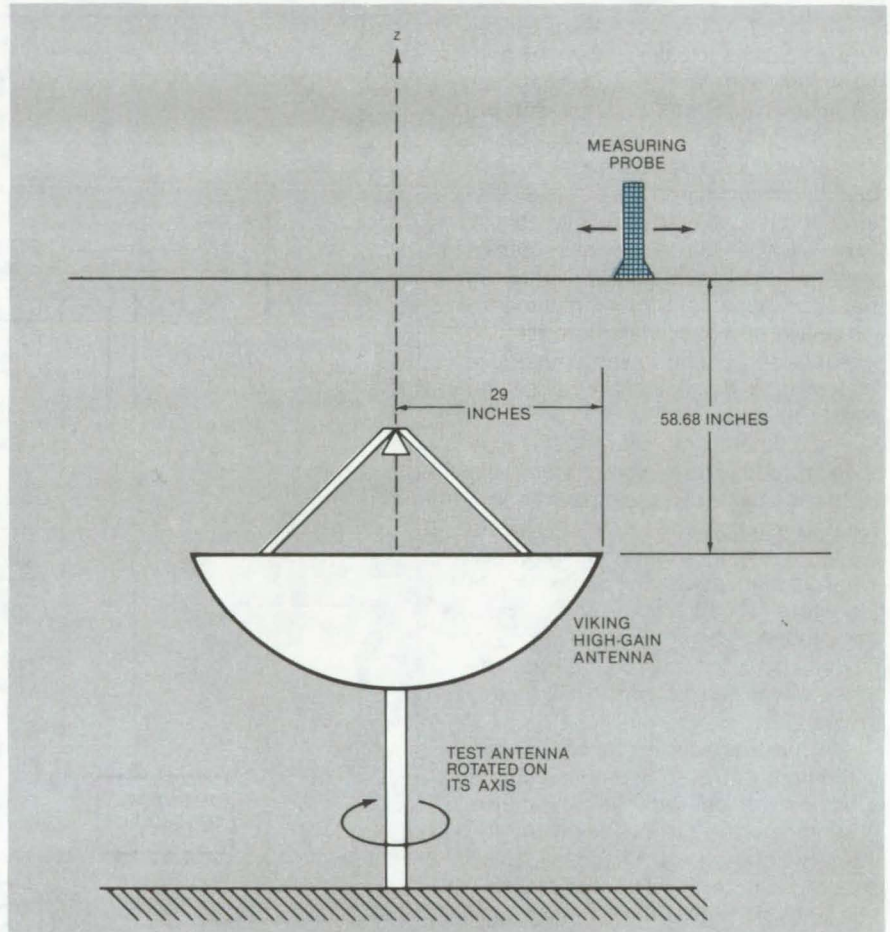
A new technique for determining the far-field pattern uses data derived from a near-field polar scan in a plane. Scan data are obtained from a sampling probe that moves linearly in front of the antenna while the antenna is rotated on its axis. The far-field pattern is constructed by using a Jacobi-Bessel series-expansion algorithm.

As can be seen in the figure:

- Only a single line of motion is required for the probe, while the test antenna is rotated around the z-axis for the other dimension of motion.
- The antenna points in a fixed direction. Moreover, this direction can be vertical, which may be important for light antennas that are subject to deformation by gravity.

The Jacobi-Bessel series expansion is suited for constructing beam-shaped patterns and is compatible with the plane/polar measurement. In addition:

- Plane/polar data are used directly without interpolation to a rectangular grid (needed in a previous technique that used a probe scanning a rectangular geometry).
- The number of data points required can be reduced by taking advantage of rotational symmetry.
- The integration involved can be performed piecewise over the aperture plane without any additional complexity. In fact, it may be performed as the measurement progresses. Thus, large quantities of data can be handled readily if necessary.



**Plane/Polar Geometry** simplifies the measurement of near-field data for this antenna and allows a determination of the far-field pattern by Jacobi-Bessel series expansion of the data. The measuring probe is an undersized, dielectrically loaded and open-ended waveguide with a far-field pattern similar to that of a small magnetic dipole in its forward direction, making it unnecessary to rotate the probe in a direction similar to the antenna rotation.

- Once the far field has been computed at one point, it can be determined at any other point with relatively little effort and computer time.
- With little extra computational effort, the field can be computed as close as several diameters from the antenna. This Fresnel-zone computation serves as an excellent check of the accuracy of the measurement and the far-field computation.

This method was applied to the Viking high-gain parabolic reflector an-

tenna. The radius of the antenna dish is 29.00 inches (73.66 cm), and the X-band signal wavelength is 1.40 inches (3.56 cm).

For the tests, the measuring probe was in a plane only 58.68 inches (149.05 cm) from the antenna aperture; it was moved from the axis to a radius of 60.00 inches (1.524 meters), where the amplitude of the near field was 35 to 40 dB below the on-axis value. At every radial position, the data were sampled at  $0.5^\circ$  intervals as

the antenna rotated. The total number of measured data points consisted of 720 points in each of 150 rings.

The far-field pattern constructed from the data was a good approximation of the actual far-field patterns

measured 5 years earlier. The data-point spacing and the radius of the scan area affected the match of the constructed pattern with the actual pattern.

This work was done by Yahya Rahmat-Samii and Victor Galindo-

Israel of Caltech and Raj Mittra of the University of Illinois for NASA's Jet Propulsion Laboratory. For further information, including details of the computational technique, Circle 50 on the TSP Request Card. NPO-14905

## Heat Pipe Blocks Return Flow

A metal-foil reed valve shuts off a heat pipe if the sink is warmer than the source.

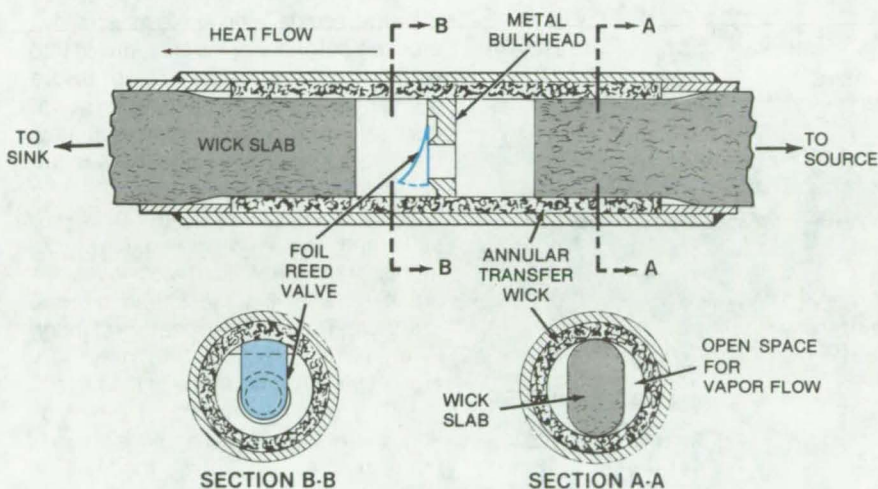
Ames Research Center, Moffett Field, California

A metal-foil reed valve in a heat pipe now being tested limits heat flow to one direction only, as electric current is limited by a diode. It is intended for applications (e.g., the cooling of electronic components) where heat is to be transported in one direction only—from source to sink. If the sink gets warmer than the source, the diode heat pipe turns off and acts as an insulator.

The fluid in a heat pipe vaporizes at the warm end of the pipe, absorbing heat. It flows to the cooler end (where the pressure is lower) and condenses, releasing the transported heat to the sink. A wick transports the condensed fluid back to the source by capillary action.

The diode heat pipe (see figure) includes wick slabs, an annular wick, a foil reed valve, and a fluid. The reed valve lets vapor pass in one direction only. In the conducting direction of flow, the reed flexes open at a pressure differential that is small compared to the capillary pressure limit of the wick. Returning liquid from the condenser bypasses the valve bulkhead through the annular transfer wick and returns to the evaporator.

In the reverse or insulating direction, when the sink temperature exceeds the source temperature, the pressure differential across the valve quickly causes the reed to close off the opening. When the pressure reaches the capillary pressure limit of the wick, which occurs rapidly, liquid flows from the high-pressure side of the valve, through the annular wick, to the low-



**A Metal-Foil Reed Valve** in a conventional slab-wick heat pipe limits heat flow to one direction only. With the sink warmer than the source, the reed is forced closed, and the fluid returns to the source side through the annular transfer wick. When this occurs, the wick slab on the sink side of the valve dries out, and the heat pipe ceases to conduct heat.

pressure side. The region that was the condenser in the forward mode dries out, and the region that was the evaporator floods with liquid. With the wicking dry on the condenser side, the heat pipe immediately ceases to conduct.

Satisfactory valve operation and wick dryout were observed visually during tests simulating the pressure and flow conditions of an actual heat pipe. In these tests a reed valve assembly made entirely of type 304 stainless steel was mounted in a glass tube. The vapor phase of the fluid was simulated with helium; the liquid phase, with ace-

tone. For a wide range of gas flow rates, the reed deflected smoothly without flapping. The reed foil used was 0.00025 inch (0.0064 mm) thick.

This work was done by James E. Enginger of TRW, Inc., for Ames Research Center. Further information may be found in NASA CR-152183 [N78-33379/NSP], "Extended Development of Variable Conductance Heat Pipes" [\$8]. A copy may be purchased [prepayment required] from the National Technical Information Service, Springfield, Virginia 22161. ARC-11285



## Nozzle Modification Suppresses Flow Transients

Fluctuations in boundary-layer flow would be reduced by flaring the nozzle exit.

Marshall Space Flight Center, Alabama

A proposal for steadying the flow from the rocket nozzle on the Space Shuttle main engine could be applied to other large-area-ratio contoured nozzles. Oscillations and pulsations in

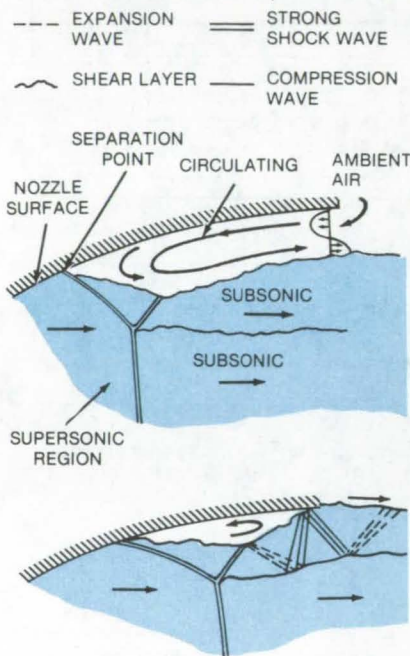


Figure 1. Supersonic Flow in a Nozzle may exhibit boundary-layer instability. In the flow shown at the top, the shear layer is detached. In oscillatory flow, the shear layer alternates between attachment, as shown at the bottom, and detachment.

the boundary-layer flow would be reduced by flaring the nozzle exit. Transient side loads on the nozzle would be suppressed.

The steady flow in a conventional nozzle is shown at the top of Figure 1. Since the flow pressure is lower than the ambient pressure, mass circulates into and out of the separation layer.

If the nozzle exit angle is shallow, then the outer shear layer is forced into contact with the wall by pressure gradients in the main flow, as shown at the bottom of Figure 1. Consequently, mass is pumped back into the separation bubble.

When the pressure in the bubble is sufficiently high, the shear layer detaches from the wall. This relieves the pressure, allowing the shear layer to reattach. The cycle repeats, resulting in an oscillatory flow that may vary around the circumference of the nozzle.

In the pulsatory mode of unsteady flow, the reattachment angle is steeper than in the oscillatory mode. The pressure in the expanded flow is greater than ambient, giving rise to faster mass accumulation than in the oscillatory case. The higher pressure also obstructs the outflow, causing the pressure in the separation bubble to be uniform around the circumference and to build rapidly. The result is a more violent "pulsatory" expansion.

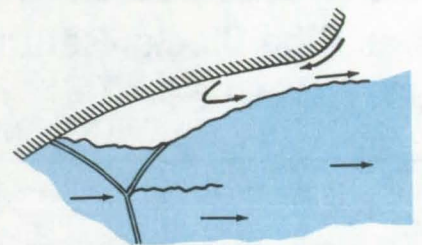


Figure 2. Supersonic Flow in the Modified Nozzle features a shallower reattachment angle. As shown here, the flow remains fully detached and stable.

By reducing the reattachment angle with a rounded corner, as shown in Figure 2, the reverse flow would be reduced or eliminated. Large pressure gradients and eddies that can lead to fluctuations are suppressed. The exact radius of curvature of the corner would depend on the shear-layer thickness.

This work was done by G. V. R. Rao of Rockwell International Corp. for Marshall Space Flight Center. For further information, Circle 51 on the TSP Request Card.

Inquiries concerning rights for the commercial use of this invention should be addressed to the Patent Counsel, Marshall Space Flight Center [see page A5]. Refer to MFS-19567.

## Microcomputer Checks Butt-Weld Accuracy

Electrical gage and microcomputer eliminate time-consuming manual measurements.

Marshall Space Flight Center, Alabama

The alignment and angle of the plates on either side of a butt weld are measured and recorded automatically by a hand-held gage and a desk-top microcomputer. The gage/microcomputer quickly determine whether a weld is within dimensional tolerances or whether reworking is needed.

The microcomputer prints out the measurements while an operator moves the gage from point to point along the weld. Out-of-tolerance measurements are marked by an asterisk on the printout.

The system replaces a mechanical curve tracer that employs a comblike

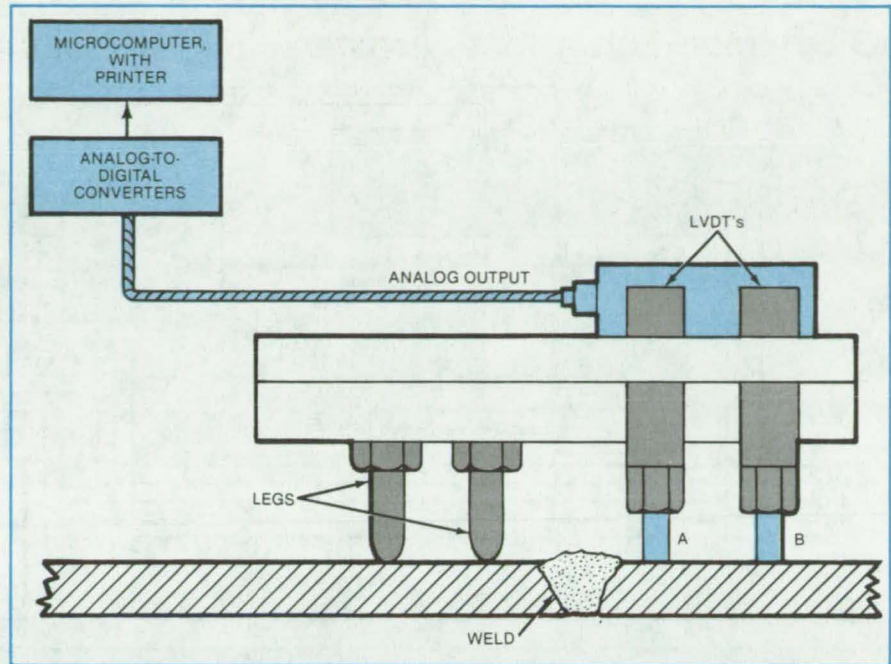
device to transfer the outline of a weld to paper. An operator had to measure the intersecting angles (peaking angles) of the two plates and the offset of their surfaces (mismatch), using a protractor and an optical comparator.

The operator of the new system positions the measuring unit so that it

is supported by its legs on one side of the weld, and its two linear-variable differential transformers (LVDT's) are on the other side (see figure). When the operator presses a small thumb-actuated switch on the unit, the extension of the LVDT's is sensed electronically. The computer uses the extension values to calculate the peaking and mismatch at that location from programmed geometric and trigonometric relations. The operator repeats the procedure for a series of locations along the weld.

Before using the gage, the operator types pertinent information into the computer via the keyboard; for example, operator name, date, weld identification number, measurement interval [1 ft or 6 in. (30.5 or 15.2 cm)], and tolerance values for peaking and mismatch. After the operator has checked the calibration of the instrument by inserting gage blocks under the LVDT's, the measurements can proceed.

The instrument will be integrated into an automatic weld-inspection system. It can improve the efficiency and productivity of welding for liquid-natural-gas containers, tank cars, high-pressure tank trailers, storage vessels, nuclear reactors, and similar structures. Preliminary tests on a



**Straddling a Butt Weld**, a gage produces displacement signals from linear-variable differential transformers. A microcomputer converts the displacement measurements, A and B, into peaking and mismatch values from trigonometric formulas.

production line indicate a saving of 50 percent with a significant increase in accuracy.

*This work was done by V. Clisham, W. Garner, C. Cohen, J. Beal, R.*

*Polen, and J. Lloyd of Martin Marietta Aerospace for Marshall Space Flight Center. For further information, Circle 52 on the TSP Request Card. MFS-25557*

## Self-Correcting Electronically-Scanned Pressure Sensor

High-data-rate sensor automatically corrects for temperature variations.

*Langley Research Center, Hampton, Virginia*

The inherent sensitivity to temperature changes of semiconductor pressure sensors has discouraged their widespread use. Errors caused by such sensitivity, which affects the sensor calibration and zero offset, can be reduced by compensating elements or in situ calibration, but only at the expense of size, cost, or complexity. The compensating elements are often larger than the pressure-sensing elements and require extensive calibration of the pressure sensors. In situ calibration mechanisms are as large as the pressure-sensing module, requiring pneumatic multiplexing and automatic data-processing equipment to compute and store the calibration coefficients.

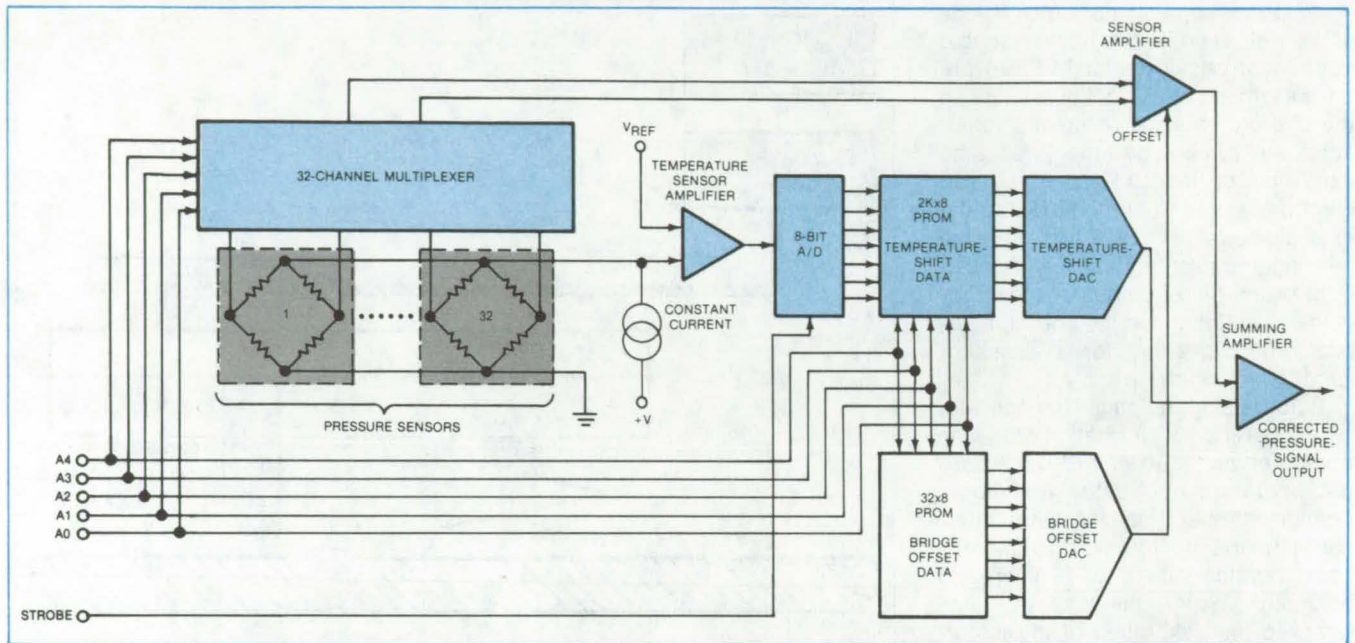
A new multichannel, self-correcting pressure sensor can be used in wind tunnels, aircraft, process controllers, and automobiles. It offers data rates approaching 100,000 measurements per second with inaccuracies due to temperature shifts held below 0.25 percent (nominal) of full scale over a temperature span of 55° C. The system consists of solid-state sensors, signal-multiplexing electronics to address each sensor electronically, and digital circuitry to correct automatically for the inherent thermal sensitivity of the pressure sensors and the electronics.

A 32-channel system is shown in the figure. Pressure sensors 1 to 32 have their analog outputs connected to a 32-

channel multiplexer that allows any of the pressure sensors to be digitally addressed. The electrical output of the addressed sensor is amplified by the sensor amplifier and applied to the input of the summing amplifier.

The sensor address is also applied to a programmable read-only memory (PROM) along with a digital address corresponding to the temperature of the pressure sensors. The temperature address is generated by the output of an analog-to-digital converter that derives its input signal from the sensor excitation voltage as it changes with temperature.

The output of the PROM is applied to a digital-to-analog converter (DAC),  
(continued on next page)



The **Error-Correction Circuit** sums the signal from 1 of 32 semiconductor pressure sensors with temperature-shift data obtained from a previous calibration. Zero-offset error is corrected by applying a signal to the offset input of the sensor amplifier.

which generates a signal at the input of the summing amplifier. Stored in the PROM are digital values obtained from a previous calibration. When addressed by the pressure-sensor address lines and an address corresponding to an arbitrary temperature scale, the calibration data generate a voltage that corrects the thermal-shift zero errors when summed with the sensor output voltage.

Tests were made with the zero-offset error measured at 25° C and given as percent of full-scale output (FSO). The thermal shift error was

measured over a 25°-to-80° C temperature interval in five equal temperature steps. Before compensation, the average zero-offset error was 2.5 percent of FSO, and the maximum error was 11.12 percent of FSO. After compensation, these errors were reduced to 0.05 percent of FSO and 0.12 percent of FSO, respectively. Similarly, the average and maximum temperature-shift errors were reduced from 4.84 percent and 7.85 percent of FSO before compensation to 0.14 percent and 0.31 percent of FSO, respectively, after compensation. The approach can be

expanded to include digital error correction for changes in sensitivity with temperature and for differences in sensitivity from sensor to sensor.

*This work was done by Chris Gross and Thaddeus Basta, Jr., of Langley Research Center. For further information, Circle 53 on the TSP Request Card.*

*Inquiries concerning rights for the commercial use of this invention should be addressed to the Patent Counsel, Langley Research Center [see page A5]. Refer to LAR-12686.*

## Lacquer Reveals Impact Damage in Composites

Brittle lacquer unveils effects normally visible only by ultrasonic inspection.

*Langley Research Center, Hampton, Virginia*

A coating of brittle lacquer on composite laminated panels reveals hidden internal damage. The lacquer coating measures the spread of cracking and delamination in graphite/epoxy panels subjected to cyclic compression loads after impact damage.

Ordinarily smooth and glossy, the lacquer flakes and scales on the exterior surface adjacent to the internal damage (see Figure 1). Ultrasonic in-

spection confirms that the area of the spalled lacquer correlates very well with the size and shape of the damage, as illustrated by the data plotted in Figure 2. The lacquer thus traces the gradual deterioration of the panel.

Graphite/epoxy composite panels are affected by impact even if the impacting object does not penetrate the panel. For example, a 48-ply test panel hit by a small aluminum ball traveling at

300 ft/s (91.4 m/s) failed under compression at only half the strain at which an undamaged panel would fail. Even when the strain is kept very low, the internal damage spreads under cyclical compression load.

The lacquer coating is used in tests at Langley Research Center to indicate initial impact damage as well as spreading damage. A test specimen is coated with lacquer on the side oppo-

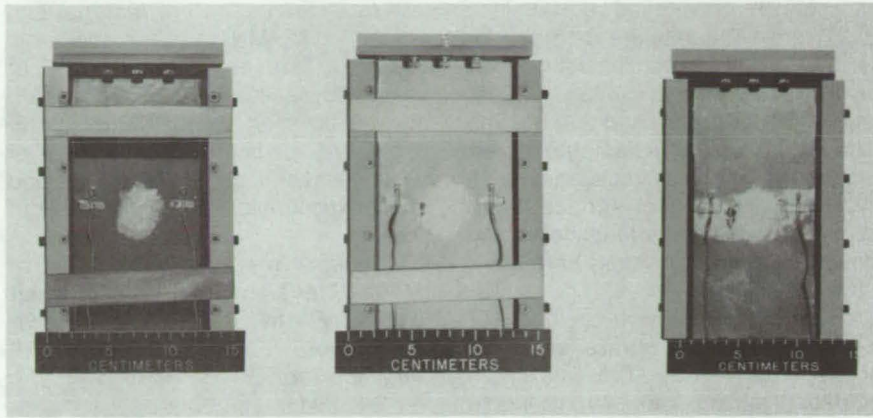


Figure 1. **Spalled Brittle Lacquer** (white blotch) shows the progression of a damaged area under the surface of a graphite/epoxy composite panel. The panel was subjected to cyclic compression in which the maximum strain was 0.0025. The photograph on the left is the panel after being hit by a projectile; the panel is shown at the center after 140,000 compression cycles and, at the right, after failure at 173,000 cycles.

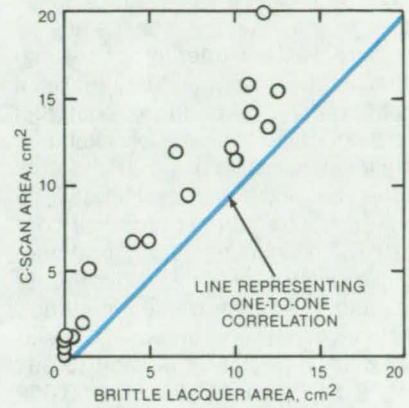


Figure 2. **Ultrasonic C-Scan and Spalled-Lacquer Areas Are Compared.** The data lie above and very close to the line representing one-to-one correlation.

site the surface at which a projectile will be fired. The spalled area shows the effect of the impact without the specimen having to be removed from the test fixture.

This work was done by Marvin D. Rhodes and Jerry G. Williams of **Langley Research Center.** For further information, Circle 54 on the TSP Request Card.

Inquiries concerning rights for the commercial use of this invention should be addressed to the Patent Counsel, Langley Research Center [see page A5]. Refer to LAR-12700.

## Measuring Cyclic-Stress Properties of Pressure Vessels

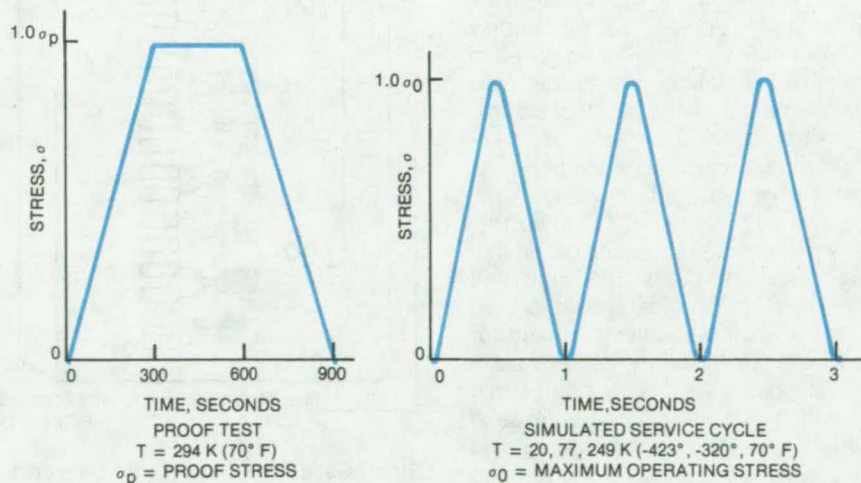
Cyclical fracture data augment static pressure testing.

### Marshall Space Flight Center, Alabama

An inexpensive method of evaluating the life expectancy of pressure vessels subjects small samples of the vessel material to stress cycles that simulate actual service conditions (see figure). Developed for thin-gage aluminum alloy vessels on spacecraft, the method would be useful for commercial thin-wall vessels as well.

The procedure reveals faults that may be masked in full-scale "proof testing," in which completed vessels are subjected to static pressure. It is possible for a vessel to survive a proof test with a deep flaw that could develop into a leak when the vessel is exposed to pressure cycles during operation. In fact, the cyclic life of proofed vessels with deep flaws was found to be about 35 percent less than that of unproofed vessels. Apparently flaws grow during proof testing to the point where they represent incipient failures.

(continued on next page)



**Simulated-Service Cycle Differs** from a conventional proof-test cycle in that a specimen is subjected to a sine-wave variation of stress instead of a prolonged steady stress. Simulated-service testing is performed at low and high temperatures as well as at room temperature. (Flaws initiated by the severe stresses of proof testing can later develop into leaks during service, thus effectively reducing useful service life.)



The simulated-service data can be used to estimate the service life of pressure vessels after proof testing. Often, application of the data makes it unnecessary to perform postproof nondestructive testing (for example, ultrasonic inspection).

The method has been used to determine fracture properties for 2219-T87 aluminum parent material, welded material, repair-welded material, and mismatch-welded material. Data have been recorded for specimen thicknesses of 0.032 inch (0.081 cm), 0.043 inch (0.109 cm), 0.062

inch (0.157 cm), and 0.100 inch (0.254 cm). The data are recorded for various temperatures, including cryogenic temperatures:  $-423^{\circ}$ ,  $-320^{\circ}$ , and  $+70^{\circ}$  F (20, 77, and 294 K). The data cover tensile tests, proof tolerance tests, and simulated-service cycling-to-leak tests on surface flaws, as well as fracture-toughness and simulated-service cycling-to-fracture tests on through flaws.

The simulated-service cycle was a sinusoidally varying stress at a frequency of 1 Hz. The maximum operating stress was 40 ksi (276

MN/m<sup>2</sup>) for the parent material and 25 ksi (172 MN/m<sup>2</sup>) for the weld material. The service life (number of cycles to cause malfunction by leak) was established for both virgin flaws that have not been exposed to proof testing and critical flaws that have had proof exposure and are on the verge of leaking.

*This work was done by C. F. Fiftal of Martin Marietta Corp. for Marshall Space Flight Center. For further information, Circle 55 on the TSP Request Card.*  
MFS-23734

## Matching of Apparent-Strain Characteristics

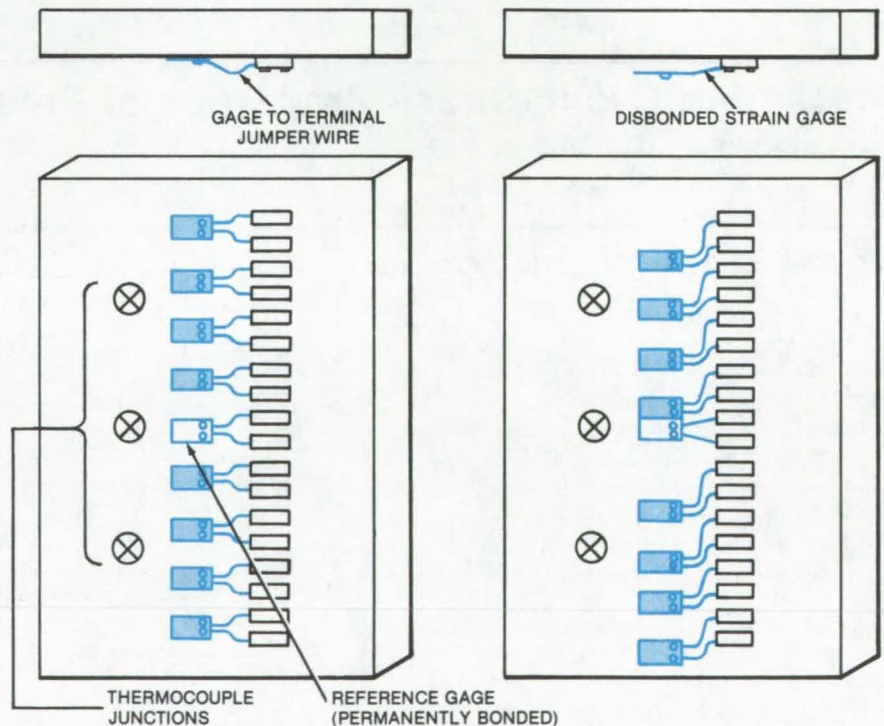
Strain gages for cryogenic use are matched prior to installation on transducers.

*Langley Research Center, Hampton, Virginia*

Inherent differences exist in the apparent-strain curves of transducer strain gages. Since the differences are magnified at cryogenic temperatures, a resultant apparent strain arises when four arbitrarily chosen strain gages are wired in a four-active-arm Wheatstone bridge circuit. It is preferable, therefore, in developing transducers with four-arm strain-gage bridges, to use strain gages for which the individual apparent-strain curves are accurately predetermined and matched to each other. This matching is achieved by a new "temporary bonding" technique.

Previously, corrections for apparent strain were made using a temperature-sensitive wire placed internally in the Wheatstone bridge circuit. The correction wire has inherent problems, in that long lengths are often required and physical space on most transducers is limited; therefore, sufficient space for the wire is not always available. In addition, long pieces of this apparent-strain correction wire are difficult to place in intimate contact with the strain-gaged surface and can cause erroneous loop data.

Temporary bonding and matching of strain gages significantly reduce the length of the correction wire. The method requires a test block on which the gages are temporarily bonded, an adequate number of strain gages to choose from, thermocouples for moni-



**Strain Gages Are Temporarily Bonded** to the surface of a test block (left). Apparent strain is recorded in an excursion to  $-190^{\circ}$  C; and the gages are disbonded (right) following heating to elevated temperature.

toring temperature, and a data-acquisition system for recording apparent strain.

First, several strain gages are bonded to a test block (see figure) using a bonding agent that disintegrates at

$170^{\circ}$  C. Second, the gages are wired to the data-acquisition system, and data are taken during a predetermined temperature excursion from ambient temperature to  $-190^{\circ}$  C. Next, the test block is heated to an elevated tempera-



ture; the strain gages become disbonded, and the bonding agent flakes off. Finally, the strain gages are unsoldered, pumiced, and cleaned. They are then selected for use on transducers.

Matching strain gages for cryogenic use has several advantages. Initial accuracy for cryogenic transducers is greatly improved, less apparent-strain

correction wire is required, and there are smaller errors due to loop data caused by long pieces of correction wire. A decrease in nonlinearity as well as apparent strain is possible when a temperature excursion from ambient temperature to  $-190^{\circ}\text{C}$  and back is plotted and the strain gages are matched at points along the excursion

as well as at the endpoint.

*This work was done by Thomas C. Moore of Langley Research Center. No further documentation is available.*

*Inquiries concerning rights for the commercial use of this invention should be addressed to the Patent Counsel, Langley Research Center [see page A5]. Refer to LAR-12743.*

## Pressure Switch Is a Low-Cost Battery Indicator

Printed-circuit switch would indicate the charge state.

*Goddard Space Flight Center, Greenbelt, Maryland*

A conventional pressure switch, fabricated by printed-circuit manufacturing techniques, can indicate when the charge on a battery departs from a preset level. A membrane on the switch is exposed to the internal pressure of the battery, which varies according to the stored charge. When the pressure varies from the preset level, the switch can turn on a light-emitting diode or similar indicator to warn the user that the battery is low. The pressure switch might also be suitable for other applications in which an economical, mass-producible, pressure-threshold sensor is needed.

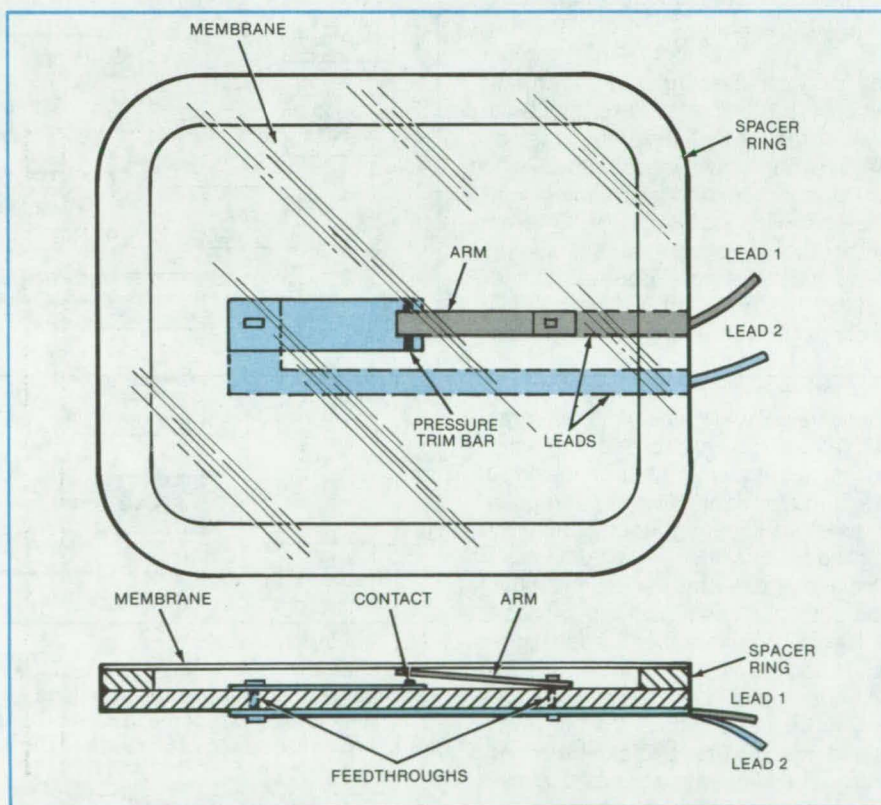
As shown in the figure, the flexible membrane is held by a spacer ring above a substrate. Two electrical contacts within the ring are separated by a spring arm. Normally open, the spring arm is moved toward the substrate by the membrane as pressure outside the membrane increases. The leads and contacts are formed on the substrate by printed-circuit techniques.

The switch is designed for a given turn-on pressure by selection of the height of the ring, the extensibility of the membrane, and the spring constant of the arm. The turn-on pressure for a given geometry and materials selection will vary because of tolerances normally encountered in production runs. Each switch may be adjusted (trimmed) for the desired

**Pressure on the Membrane** forces it into the recess defined by the spacer ring. The membrane thus presses the spring arm against an adjustable contact and sets up a continuous electrical path between leads 1 and 2.

turn-on pressure by positioning a trim bar that sets the contact spacing. The switch interior can be pressurized so that it reacts to a required pressure differential.

*This work was done by J. L. Abita of Johns Hopkins University for Goddard Space Flight Center. No further documentation is available. GSC-12679*



# Pulsed Phase-Locked-Loop Strain Monitor

A high-resolution, fully-automated strain monitor

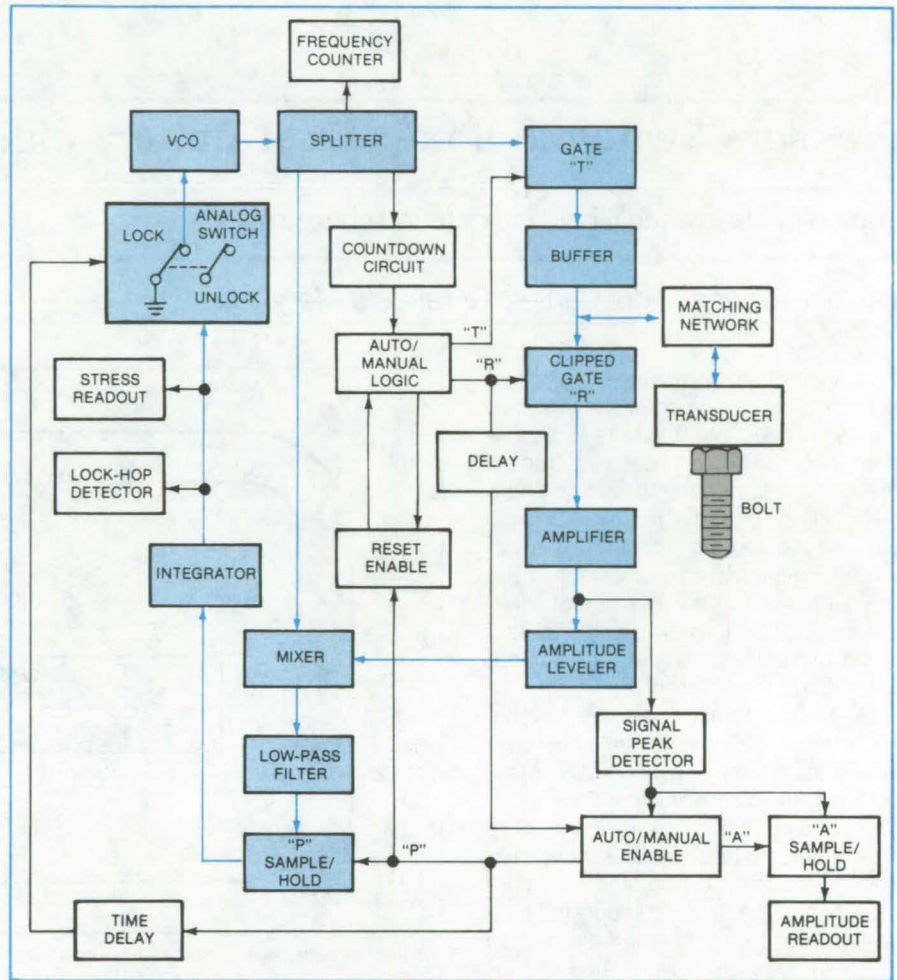
Langley Research Center, Hampton, Virginia

A new strain monitor uses a pulsed phase-locked loop ( $P^2L^2$ ) to measure accurately the elongation or strain in any solid material under load, for example, in a bolt during an assembly operation. The monitor is expected to have broad application in materials testing, structural design, fabrication, and assembly.

The  $P^2L^2$  circuit (see figure) transmits a gated radio-frequency (RF) acoustic wave into a sample. The acoustic wave propagates through the material, reflecting from an interface such as the end of the sample boundary, and returns to the transducer. The phase of the electrical signal produced at the transducer by the acoustic wave is compared with that of the continuously-running voltage-controlled oscillator (VCO) from which the initial driving signal was gated. A feedback loop is closed, locking the VCO to a fixed phase relationship with respect to the reflected signal.

When the sample is loaded, the sound-velocity dependence on strain causes an acoustic phase shift, producing a frequency shift in the VCO. The frequency shift divided by frequency ( $\Delta F/F$ ) is linearly proportional to the applied load. Included in the design is a "lock-hop" detector that signals faulty operation such as a  $2\pi$  jump in phase.

The  $P^2L^2$  instrument has higher resolution (parts in  $10^7$ ) and appears to be more reliable than other devices now in use. In addition, it is fully automated, easy to use, and can be configured with two transducers, if necessary. The readout could be coupled to a microprocessor to calculate actual  $\Delta F/F$  values from the frequency counter and convert them into stress in MPa or psi, including proper calibration for the acoustic stress constant or geometry of the sample. Other physical parameters that change the total phase



The  $P^2L^2$  Strain Monitor measures strain by monitoring the change in phase of an acoustic signal that passes through a stressed sample. The phase change causes a shift in the frequency of the VCO. As with other monitors of this type, the instrument is only accurate in the elastic range of the material.

shift (i.e., that change the sound velocity or sample length) can also be monitored with the  $P^2L^2$ .

This work was done by Joseph S. Heyman and Francis D. Stone of Langley Research Center. For further information, Circle 56 on the TSP Request Card.

This invention is owned by NASA, and a patent application has been filed. Inquiries concerning nonexclusive or exclusive license for its commercial development should be addressed to the Patent Counsel, Langley Research Center [see page A5]. Refer to LAR-12772.

## Strain-Gaged Bolts Are Easily Prepared

A simple workbench procedure simplifies the installation of strain gages in structural bolts.

Lyndon B. Johnson Space Center, Houston, Texas

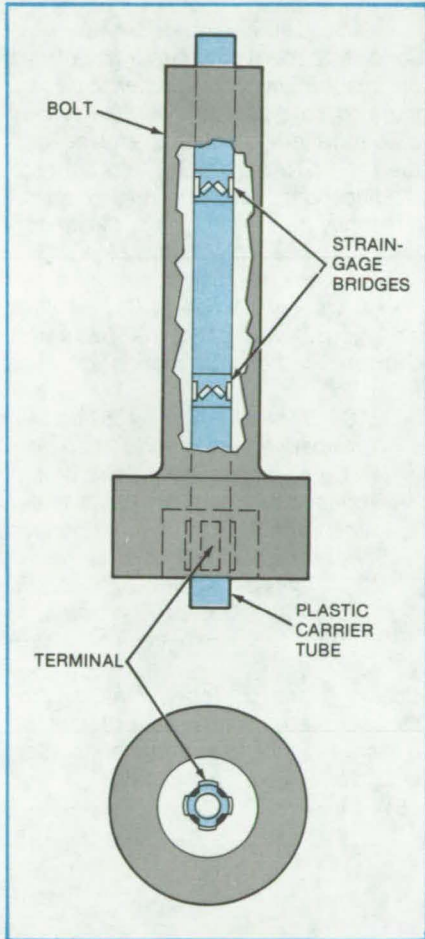


Figure 1. This Bolt Is Instrumented for Shear Measurements by strain gages that are mounted on a plastic carrier tube. Shear at two points on the bolt is measured with this arrangement.

A new method for installing strain gages in structural bolts is implemented as a standard workbench procedure. Rather than potting the gages in a hole along the axis of the bolt, as in conventional strain-gaged bolts, the gages are first installed on the outside of a plastic carrier tube. The tube is then epoxied in the axial hole.

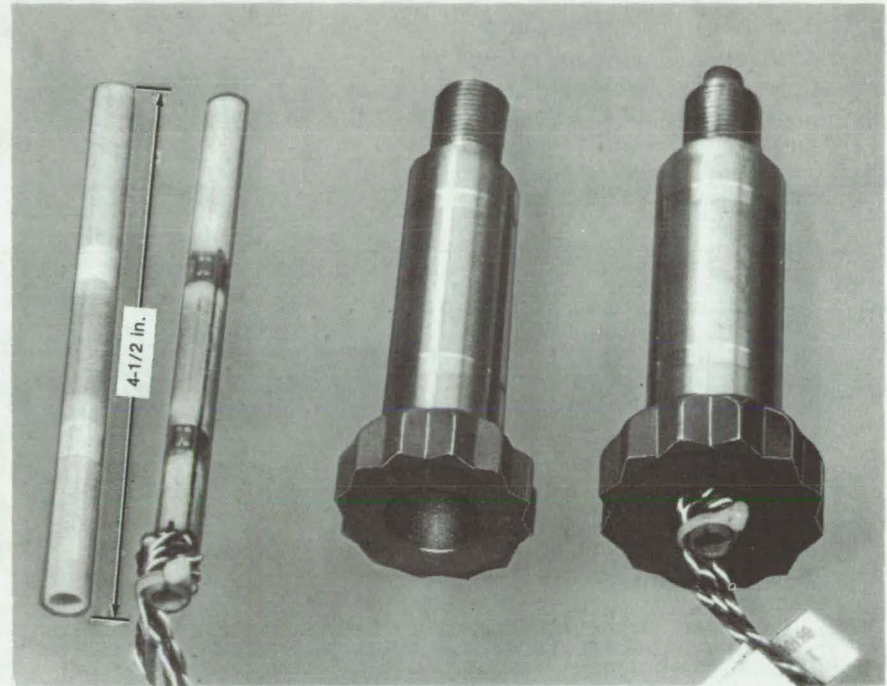


Figure 2. The Stages of Assembly for the bolt instrumentation are seen here. Recesses and grooves are cut into the fiberglass/epoxy carrier tube, the strain gages are mounted and wired, and the completed carrier is bonded into the bolt.

The new procedure can be used to prepare gages to monitor bolt tension, shear, or torsion. Since the strain gages are installed on the outside of the carrier tube rather than on the inside of the hole, the installer has better access to the work. In addition, more gages are mounted in a given volume, and there is more room for trimming and temperature-compensation circuitry. Overall temperature stability of a full-bridge installation is improved because all the gages are located close to each other.

In one application of the new procedure (see Figure 1), the x and y components of shear are measured in two cross-sectional planes through a bolt. Eight shear half bridges are used. By changing the orientation of the bridges, axial or torsional strains could also be measured. The fiberglass/

epoxy carrier tube has very low shear modulus and low strength, so it does not affect the stress in the bolt.

The carrier tube has four longitudinal grooves to carry connecting wires to terminals outside of the bolt shaft. After the gages and wires have been recessed into the carrier, a protective and insulating coat of epoxy is applied. Then, when all of the gage bridges are verified as operative and having proper shear sensitivity, the carrier tube is bonded into the bolt (Figure 2). Completed bolts are calibrated for shear and checked for crosstalk.

This work was done by Robert R. Walker of Rockwell International Corp. for Johnson Space Center. For further information, including drawings and parts list, Circle 57 on the MSC-18823

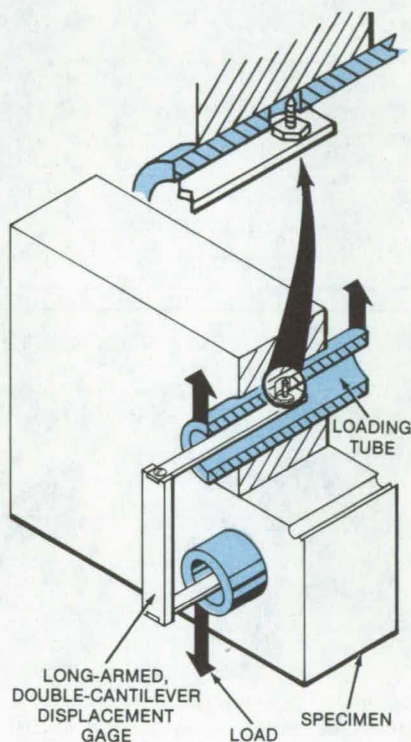
## Load-Displacement Measurement on Pin-Loaded Specimens

Load applied with tubes rather than pins allows a more accurate measurement of displacement.

Lewis Research Center, Cleveland, Ohio

A number of material-evaluation methods require a determination of the energy imparted to a specimen as load is applied to it. This requirement results in the need for accurate measurement of the relative displacement of the points of load applications. Measurements of the displacement at a location other than in the center of the area of load application on the specimen include extraneous displacement fractions. If not accounted for, these extraneous fractions result in errors in the determination of the actual energy imparted to the specimen. Accounting for the error can involve complex data-analysis procedures.

A means was devised for determining the load point displacement accurately. The method is depicted in the figure. Load is applied with tubes rather than with pins. Sharp points at the ends of a long-armed, double-cantilever displacement gage protrude through holes in the loading-tube walls and register on the specimen in the center of the area of load application. No extraneous displacement fraction is present in the measurement, and data-correction procedures are unnecessary.



**Tubes Apply a Load** as the displacement is registered by a long-armed, double-cantilever gage. Sharp points at the ends of the arms protrude through holes in the tube walls and contact the center of the area of load application.

Users of the innovation are cautioned that there must be sufficient wall thickness in the loading tubes to equate them to solid-pin behavior. Guidelines on determining thickness are found in the report NASA TM-81379, and gage modifications for individual applications may be aided by gage design formulas provided in the report NASA TN-D-3724, both referenced below.

This work was done by D. M. Fisher and R. Buzzard of **Lewis Research Center**. Further information may be found in:

NASA TM-81379 [N80-13513/NSP], "Comparison Tests and Experimental Compliance Calibration of the Proposed Standard Round Compact Plane Strain Fracture Toughness Specimens" [\$5.50]; and NASA TN-D-3724 [N67-10749/NSP], "Design and Use of Displacement Gage for Crack-Extension Measurements" [\$5].

Copies of these reports may be purchased [prepayment required] from the National Technical Information Service, Springfield, Virginia 22161. LEW-13624

## Computer Programs

These programs may be obtained at very reasonable cost from COSMIC, a facility sponsored by NASA to make new programs available to the public. For information on program price, size, and availability, circle the reference letter on the COSMIC Request Card in this issue.

### Heat-Energy Analysis for Solar Receivers

A general heat-transfer program with specific features for analyzing solar receivers

The heat-energy analysis program (HEAP) solves general heat-transfer problems, with some specific features that are "custom-made" for analyzing solar receivers. It can be utilized not only to predict receiver performance under varying solar flux, ambient temperature, and local heat-transfer rates but also to detect the locations of hotspots and metallurgical difficulties and to predict performance sensitivity of neighboring component parameters.

HEAP models the physical system with a relatively-simple mathematical

description. Its basic methodology is a nodal, finite-difference approach to the heat-transfer calculations. The receiver is partitioned in space by nodes or zones and in time by time increments. Between any two arbitrary nodes, the differential heat-transfer-rate equations are expressed with all modes of heat transfer included. The net energy stored in each node is calculated using the first law of thermodynamics including the energy exchange to and from neighboring nodes. For steady-state solutions, a Newton-Raphson iteration

solution is used to solve for the temperature distribution of the equilibrium nodes and the net energy stored at the source/sink nodes. For transient solutions, a forward-marching finite-difference numerical technique is used to solve for the nodal temperature histories.

Inputs to HEAP consist of solar flux distributions, optical and physical properties, fluid flow rates, and boundary conditions. The radiation view factors are supplied by a built-in subroutine. Outputs generated by HEAP include temperature distribution, fluid outlet conditions, accumulated energy extracted, receiver efficiency, and heat losses.

HEAP is written in FORTRAN IV for batch execution and has been implemented on a UNIVAC 1100-series computer with a central memory requirement of approximately 47K of 36-bit words. It was developed in 1979.

*This program was written by Fikry L. Lansing of Caltech for NASA's Jet Propulsion Laboratory. For further information, Circle B on the COSMIC Request Card.*  
NPO-14835

## Program for Analysis and Resizing of Structures

An efficient code for resizing large- or small-scale finite-element models subject to constraints

The Program for Analysis and Resizing of Structures (PARS) determines optimum resizing of structures subject to stress, displacement, and flutter constraints. It is an efficient code for sizing large- or small-scale finite-element models in the presence of strength, thermal, and aeroelastic constraints with minimum and maximum bounds on structural dimensions.

Based on the SPAR finite-element system, PARS is composed of individual processors that are executed in a logical sequence to perform analysis or synthesis. The processors communicate directly and automatically with a data complex that contains the information generated by each processor.

PARS can resize structures modeled with truss, beam, and shear-panel elements and triangular or quadrilateral membranes or plates. All elements

except the beams may be resized.

PARS uses an optimization procedure based on a mathematical programming method. The method employs the sequence of unconstrained minimization technique, in which design requirements are incorporated using an extended interior-penalty-function approach. Approximate analysis, design-variable linking, constraint deletion, and approximate expressions for constraint-function second derivatives are used in conjunction with Newton's method to reduce computation time and increase the size of the solvable structural-design problem. This optimization technique may be automatically invoked for both static and flutter optimizations.

In addition, PARS automatically obtains a fully stressed design when the structure is subject only to stress constraints. The user has the option of developing his/her own optimization loops by calling the processors in a user-defined sequence.

Input to PARS consists of the SPAR finite-element model of the structure, the design constraints, and the PARS control parameters. Output from PARS includes a sized finite-element model, optimization history, and selected structural parameters.

PARS is written in FORTRAN IV for batch execution and has been implemented on a CDC CYBER 170-series computer under control of NOS 1.3. PARS has a central memory requirement of approximately 70K (octal) of 60-bit words. The PARS user must have access to the SPAR system. PARS was developed in 1979.

*This program was written by R. T. Haftka, B. Prasad, and U. Tsach of the Illinois Institute of Technology for Langley Research Center. For further information on PARS and SPAR, Circle C on the COSMIC Request Card.*  
LAR-12704

## Unsteady Subsonic Loadings Due to Control-Surface Motion

Program yields aerodynamic pressures and other effects of wing and control-surface motion.

The RHOIV computer program predicts the unsteady lifting-surface loadings caused by motions of leading edge and trailing-edge control surfaces

having sealed gaps at hinge lines and side edges. The analysis is based on linear, subsonic, potential-flow theory using the kernel function method. Linear combinations of pressure distributions are used that are continuous except at planform edges and hinge lines. The loading solution is obtained by downwash collocation for the deflection or motion of the main wing and control surfaces. Deflection-mode data are input for specified points, with surface deflections being obtained by surface spline interpolations for the main surface and individual control surfaces.

RHOIV offers the user several features to enhance the usability and flexibility of the program:

- The planform leading and trailing edges may consist of from one to nine straight-line segments, with each control-surface hinge line being a single straight-line segment.
- Two kinds of rounding are provided for leading-edge and trailing-edge
- Each half span may include from zero to six controls.
- The analysis may employ either spanwise symmetry or antisymmetry of loading and motion.
- Two types of vertical gust downwash can be handled — a gust sinusoidally distributed in the flight direction and a gust that would be produced by vertical translation (heaving).
- The effects of airfoil thickness are approximated by inputting a chordwise distribution of streamwise velocity ratios for a steady airfoil.

The user also has options in specifying the output to be generated by the program. Optional printed outputs include lifting pressures, section generalized forces, total generalized forces, aerodynamic C-matrices, and various interpolated deflection-mode data. Points for listing pressure solutions and span stations for generalized forces may be either user-specified or allowed to default to program selection. The user may save for subsequent reuse or postprocessing the deflection-mode input data, the aerodynamic C-matrices (a major fraction of the computing cost), the lifting pressures and section generalized forces (for example, for plotting), and the total generalized forces (for example, for flutter analysis). Comparisons of RHOIV-calculated results with experimental data show accurate

(continued on next page)



theoretical pressure distributions for many different control-surface configurations.

RHOIV is written in FORTRAN IV and COMPASS for batch execution. It has been implemented on a CDC CYBER 70-series computer with a central memory requirement of approximately 56K (octal) of 60-bit words. The RHOIV program was originally developed in 1975 and was last updated in 1979.

*This program was written by William S. Rowe of The Boeing Co. for Langley Research Center. For further information, Circle D on the COSMIC Request Card. LAR-12802*

## **Aerodynamics of Sounding-Rocket Geometries**

Program computes the theoretical aerodynamics of slender, axisymmetric finned vehicles.

The theoretical aerodynamics program TAD predicts the aerodynamic characteristics of vehicles with sounding-rocket configurations. These slender, axisymmetric finned vehicles have a wide range of aeronautical applications from rockets to high-speed armament. Over a given range of mach numbers, TAD computes the normal-force-coefficient derivative, the center of pressure, the roll-forcing-moment-coefficient derivative, the roll-damping-moment-coefficient derivative, and the pitch-damping-moment coefficient derivative of a sounding-rocket-configured vehicle.

The vehicle may consist of a sharp-pointed cone or tangent-ogive nose cone and up to nine other body divisions with shapes of conical shoulder, conical boattail, or circular cylinder. It can have fins of trapezoid planform shape with constant cross section and either three or four fins per fin set. The characteristics computed by TAD are accurate to within

10 percent of experimental data in the supersonic region.

TAD calculates the characteristics of separate portions of the vehicle, calculates the interference between the portions, and then combines the results to form a total vehicle solution. Also, TAD can calculate the characteristics of the body or fins separately, as an aid in the design process.

Inputs to TAD consist of simple descriptions of the body and fin geometries and the mach range of interest. Outputs include the aerodynamic characteristics of the total vehicle, or user-selected portions, at specified points over the mach range.

TAD is written in FORTRAN IV for batch execution and has been implemented on an IBM 360 computer with a central memory requirement of approximately 123K of 8-bit bytes. The TAD program was originally developed in 1967 and was last updated in 1972.

*This program was written by J. S. Barrowman of Goddard Space Flight Center. For further information, Circle E on the COSMIC Request Card. GSC-12680*

## **Aeroelastic Analysis for Rotorcraft**

Program considers the aeroelastic stability of the coupled rotor and airframe.

The testing of rotorcraft, either in flight or in a wind tunnel, requires a consideration of the coupled aeroelastic stability of the rotor and airframe or of the rotor and support system. Even if the primary purpose of a test is to measure rotor performance, ignoring the question of dynamic stability introduces the risk of catastrophic failure of the aircraft.

An aeroelastic-analysis computer program incorporates an analytical model of the aeroelastic behavior of a wide range of rotorcraft. Such an analytical model is desirable for both pretest predictions and posttest correlations. The program can be applied

in investigations of isolated rotor aeroelasticity and helicopter-flight dynamics and could be employed as a basis for more-extensive investigations of aeroelastic behavior, such as automatic control system design.

The equations of motion are derived by using an integral Newtonian method, which provides considerable insight into the blade inertial and aerodynamic forces. The rotor model includes coupled flap-lag bending and blade-torsion degrees of freedom and is applicable to articulated, hingeless, gimbaled, and teetering rotors with an arbitrary number of blades. The aerodynamic model is valid for both high and low inflow and for both axial and nonaxial flight. Rotor rotational speed dynamics, including engine inertia and damping, and perturbation inflow dynamics are included in the aerodynamic model.

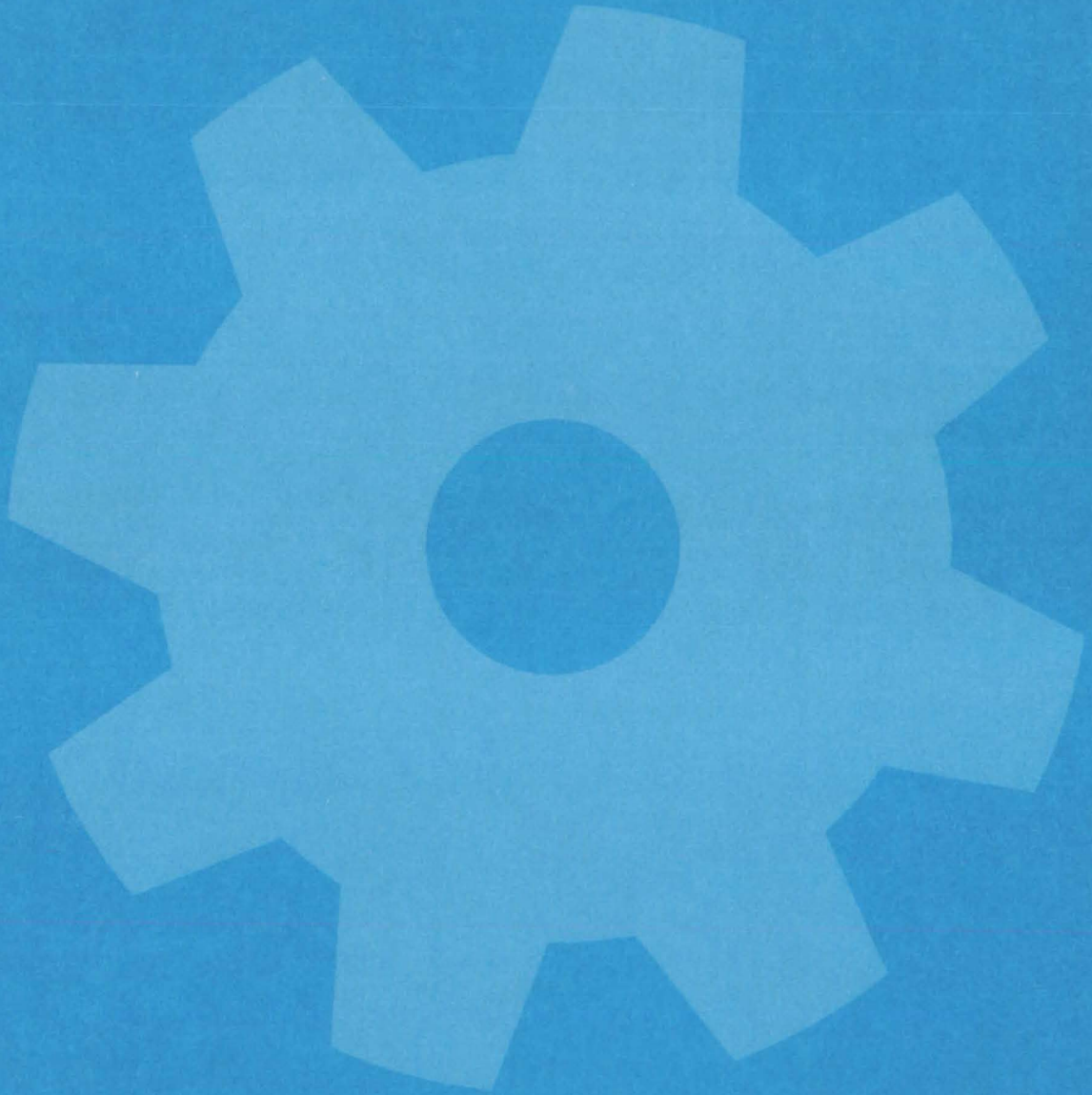
For a rotor on a wind-tunnel support, a normal-mode representation of the test module, strut, and balance is used. The aeroelastic analysis for rotorcraft in flight applies to a general two-rotor aircraft, including single main-rotor and tandem helicopter configurations, and to side-by-side or tilting-proprotor aircraft configurations. The rotor model includes rotor/rotor aerodynamic interference and ground effect.

The aircraft model includes rotor/fuselage/tail aerodynamic interference, engine dynamics, and control dynamics. A constant-coefficient approximation is used for nonaxial flow, and a quasi-static approximation is used for the low-frequency dynamics. The coupled system dynamics results in a set of linear differential equations that are used to determine the stability and aeroelastic response of the system.

This program is written in FORTRAN IV for batch execution and has been implemented on an IBM 360-series computer with a central memory requirement of approximately 624K of 8-bit bytes. It was developed in 1977.

*This program was written by Wayne Johnson of Ames Research Center. For further information, Circle F on the COSMIC Request Card. ARC-11150*

# Machinery



## **Hardware, Techniques, and Processes**

- 75 Dynamic Isolation for Cryogenic Refrigerators
- 76 Constant-Pressure Hydraulic Pump
- 77 Adhesives Mixer/Applicator
- 77 Automatic Collection of Rock and Soil Samples
- 78 Aerodynamics Improve Wind Wheel
- 79 Lathe Attachment Finishes Inner Surface of Tubes
- 80 Blind Fastener Is Easy To Install
- 81 Resistance Heater Helps Stirling-Engine Research
- 82 Ball-and-Socket Joint Can Be Disassembled
- 82 Integrated Structural and Cable Connector
- 84 Device Acquires, Orients, and Clamps

## **Books and Reports**

- 84 Advances in Turbine-Engine Technology



# Dynamic Isolation for Cryogenic Refrigerators

Total vibration isolation and pressure compensation are provided between mechanical cooler and sensitive instrument elements.

Langley Research Center, Hampton, Virginia

Mounting hardware now under test at Langley Research Center provides virtually total vibration isolation between a mechanical cryogenic refrigerator and the sensitive instrument elements that are being cryogenically cooled. One such system — a prototype housing for tunable diode lasers (TDL's) — is shown in Figure 1. Peak-to-peak motions measured at the TDL are less than 1 micron (0.04 mil) in all axes. TDL heterodyne modes with a CO<sub>2</sub> laser (P26, 28.141-THz) demonstrate 2 MHz frequency stability with no evidence of vibration. In addition, the mounting provides an evacuated Dewar housing for the detectors. It is fully pressure-compensated for all ambient pressures from sea level to vacuum. The system also isolates the refrigerator from its mounting surface, which would typically be an instrument structural element or housing.

As shown in Figure 2, the mechanical cooler is dynamically isolated from both the TDL mount and the instrument platform. The instrument bellows and the reaction bellows work together to provide the "soft" suspension necessary to isolate cooler vibrations and at the same time compensate for ambient pressure changes. External forces due to unbalanced pressure are absorbed by the reaction bracket and housing and are reacted through the instrument platform with no effect on the vibration isolation or on the instrument optical alignment.

Previous devices for vibration isolation of a cryogenically cooled TDL from a mechanical refrigerator have several limitations. The most basic is that they address only the problem of direct transmission from the cold tip to the diode mount. While this is the most critical path for vibration transmission, it accounts possibly for only 60 to 90 percent of the total vibration problem, since mechanical motion can be transmitted through the mounting frame, vacuum shroud, and diode mounting. This secondary vibration, which can be particularly serious as instrument resolution is improved, is compensated for

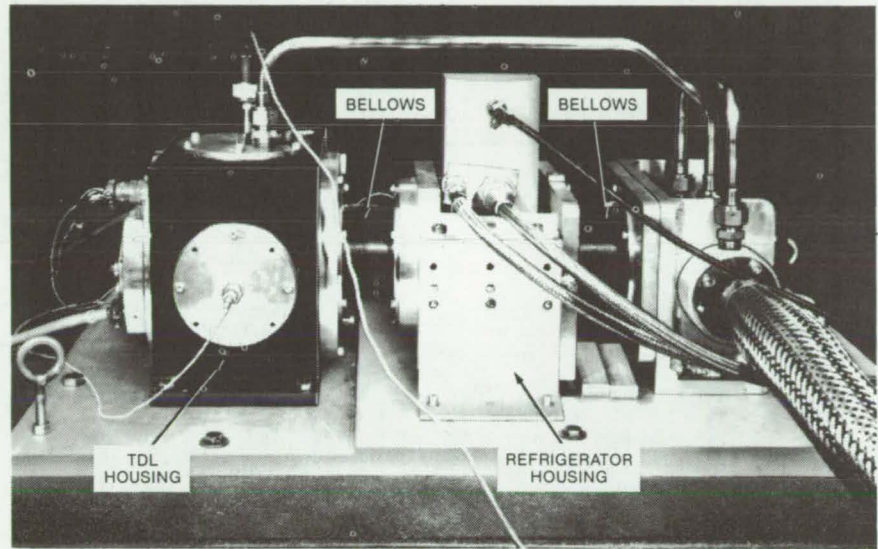


Figure 1. The prototype **Pressure-Compensated Mounting** isolates a TDL housing from mechanical vibration. The mounting is being tested as part of a Langley Research Center program for the development of highly sensitive instruments that remotely measure the important chemical constituents of the atmosphere. The instruments typically have a requirement for cryogenic cooling of the sensitive detectors and components that are necessary to detect the presence of the tenuous constituents of the atmosphere.

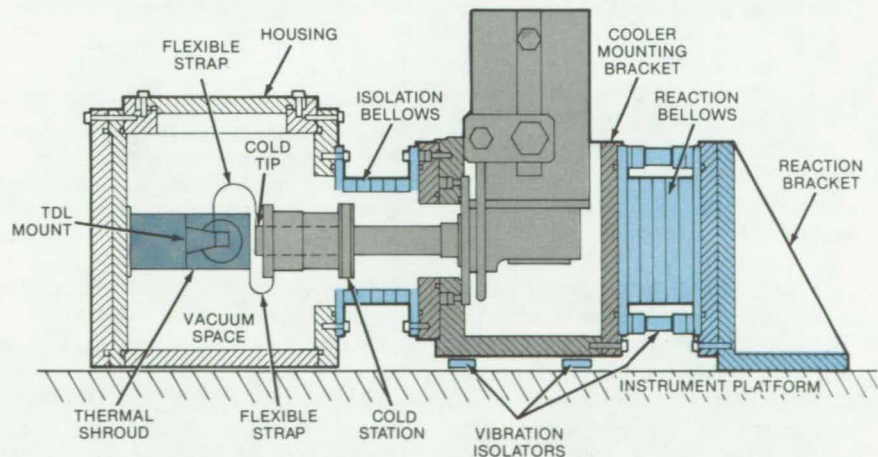


Figure 2. The **Key Elements of the Mounting** are the two bellows, the reaction plate, flexible straps, and the vibration isolators. Together they form a dynamically soft suspension that isolates the TDL from all possible vibration paths to the cryogenic refrigerator.

in the new dual-bellows mounting. Previous systems were also limited by their sensitivity to atmospheric pressure and because they did not isolate the refrigerator from its mounting. This is particularly serious for a flight instrument,

where the housing is flexible and lightweight.

Further vibration compensation or dynamic tuning is achieved by mounting selected vibration isolators between the cooler mounting bracket and  
(continued on next page)

the reaction bracket as illustrated in Figure 2. This feature permits the concept to be used with different types of coolers that may have different dynamic performance. Isolation of the cooler

mounting bracket and mechanical cooler provides an additional advantage in that external vibration inputs to the cooler, such as may be transmitted through compressor lines or leads, are isolated from the instrument platform.

This work was done by Robert D. Averill and Edward A. Crossley, Jr., of Langley Research Center. No further documentation is available. LAR-12728

## Constant-Pressure Hydraulic Pump

Higher efficiency and constant output pressure are made possible by a unique gas-to-hydraulic power converter.

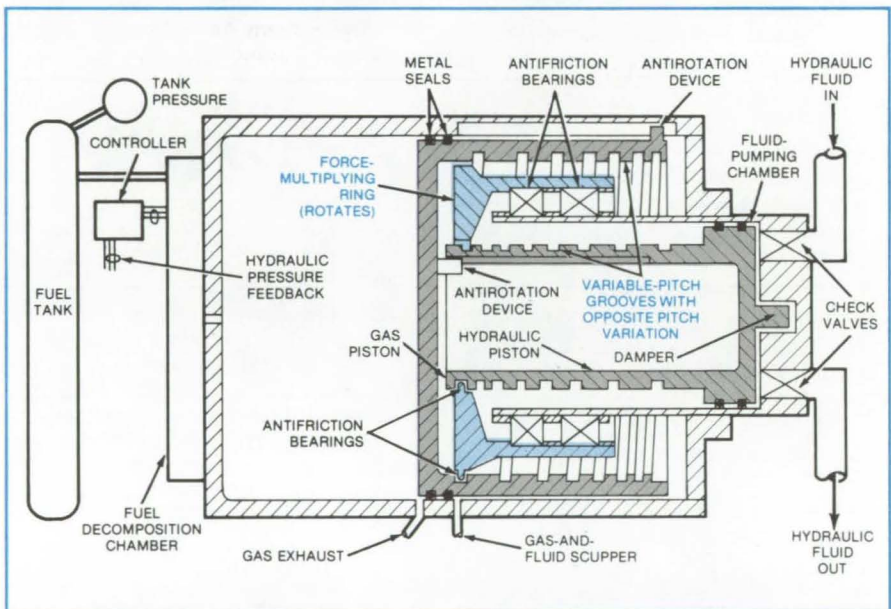
Lyndon B. Johnson Space Center, Houston, Texas

Constant output pressure in a gas-driven hydraulic pump would be assured in a new design for a gas-to-hydraulic power converter. With a force-multiplying ring attached to the gas piston, the expanding gas would apply constant force on the hydraulic piston even though the gas pressure drops. As a result, the pressure of the hydraulic fluid remains steady, and the power output of the pump does not vary.

The multiplier would make gas/hydraulic pumps equal in efficiency to hot-gas-turbine-driven hydraulic pumps, yet it would be smaller and lighter. The gas/hydraulic pump should also be more reliable because it does not require rotary shaft seals.

In the new design (see figure), gas at high pressure forces a piston to travel the length of a cylinder. The gas-driven piston drives a rotating force-multiplier ring that in turn drives a hydraulic piston, which pushes the hydraulic fluid out of a fluid-pumping chamber at high pressure. The hydraulic pressure capability is determined by the gas-to-hydraulic-piston-area ratio and the initial gas pressure.

Constant hydraulic-piston force (for constant hydraulic power) is produced by the force-multiplying ring. The force multiplier transmits the motion of the gas piston to the hydraulic piston through variable-pitch annular grooved tracks machined on the inside of the gas piston and the outside of the hydraulic piston. As the gas piston translates, the force multiplier rotates and imparts translational motion to the hydraulic piston. With constant hydraulic flow, the gas piston speeds up as the gas pressure drops, due to the



The **Force-Multiplier Ring** rotates and rides in variable-pitch grooves in the gas and hydraulic pistons as the gas piston is pushed by expanding gas. The pitch variation of the hydraulic piston is opposite to that of the gas piston. In this illustration, the pressure is supplied by fuel that decomposes into a hot gas; however, cold gas can also be used, with no need for a decomposition chamber.

varying pitch of the grooved tracks, which ensures that the hydraulic piston applies constant pressure to the hydraulic fluid.

As the gas piston approaches the end of its travel, it uncovers a port through which the low-pressure spent gas can be exhausted. The low pressure in the exhaust gas can be used to bring the gas and hydraulic pistons back to their starting positions.

It is estimated that the unit would provide low-flow hydraulic power at pressures up to 10,000 psi ( $6.9 \times 10^7 \text{N/m}^2$ ). For greater power, addi-

tional sets of pistons can be used. For additional weight savings, the pump could be built as an integral part of a hydraulic actuator.

This work was done by Charles W. Galloway of Johnson Space Center. For further information, Circle 58 on the TSP Request Card.

This invention is owned by NASA, and a patent application has been filed. Inquiries concerning nonexclusive or exclusive license for its commercial development should be addressed to the Patent Counsel, Johnson Space Center [see page A5]. Refer to MSC-18794.

## Adhesives Mixer/Applicator

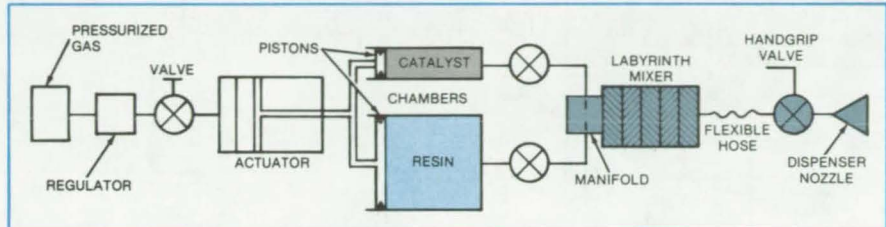
Pneumatic pressure mixes and dispenses a two-component adhesive.

*Lyndon B. Johnson Space Center, Houston, Texas*

Two-part adhesives such as an epoxy resin and its catalyst, are stored, mixed, and dispensed by an applicator originally developed for use aboard the Space Shuttle orbiter. Compressed gas furnishes the energy for mixing and dispensing. An operator needs only to open the pressure valve and to pull a trigger on the dispenser nozzle to apply the adhesive.

The unit (see figure) mixes the components of the adhesive thoroughly and in the correct ratio, even though they have widely different viscosities. For example, the viscosity of the catalyst may be similar to that of water (1 poise), while the viscosity of the resin may range from that of thick molasses (400 poises) to that of "nonflowing" putty (15,000 poises). For epoxy, the components are combined in the precise ratio of 1 part catalyst to 10 parts resin.

The adhesive components are stored in concentric chambers, shown as separate for clarity in the illustration. A compressed-nitrogen tank on the unit supplies gas pressure to a pair of concentric pistons, which force the components from the chambers. (To furnish the 1:10 volumetric ratio, the piston-surface areas are in the ratio of 1:10. The pistons can be made in other ratios as necessary.)



**Two-Component Adhesives** are stored, metered, mixed, and dispensed in a self-contained portable unit. The combined volume of the catalyst and resin chambers is 400 in.<sup>3</sup> (6,550 cm<sup>3</sup>). The pistons are shaped to conform to the head end of the chambers so that there is little waste. A small-volume (100-in.<sup>3</sup>, or 1,640-cm<sup>3</sup>) throwaway applicator was also developed.

The components extruded from the chambers enter a commercially-available, static labyrinth-path mixer, where they combine into a homogeneous paste as they flow through interlaced passages. The mixture then flows through a double-braided hose to the dispensing nozzle. By squeezing a handgrip on the nozzle, the operator applies gas pressure to the mixture, thereby releasing the adhesive. The operator stops the flow by releasing the grip. It is not necessary to use the full contents of the storage chambers at once; the unmixed components can be saved for later use. However, the mixer, hose, and nozzle must be replaced unless they are flushed to remove the mixed adhesive before it hardens.

The nitrogen tank is made of lightweight titanium. It stores nitrogen at 3,000 psi (20x10<sup>6</sup> N/m<sup>2</sup>) in its 34-in.<sup>3</sup> (555-cm<sup>3</sup>) volume. A gage on the tank indicates the internal pressure to the operator. As the gas enters the piston chambers and the dispenser nozzle, regulator reduces the pressure to 250 psi (1.7x10<sup>6</sup> N/m<sup>2</sup>). A pressure-relief valve, which vents at 450 psi (3.1x10<sup>6</sup> N/m<sup>2</sup>) assures that the application cannot be overpressurized.

*This work was done by Daniel O. Ramos and Kenneth E. Werner of General Electric Co. for Johnson Space Center. For further information, Circle 59 on the TSP Request Card.*  
MSC-18916

## Automatic Collection of Rock and Soil Samples

Proposed machine would gather specimens without human intervention.

*Lyndon B. Johnson Space Center, Houston, Texas*

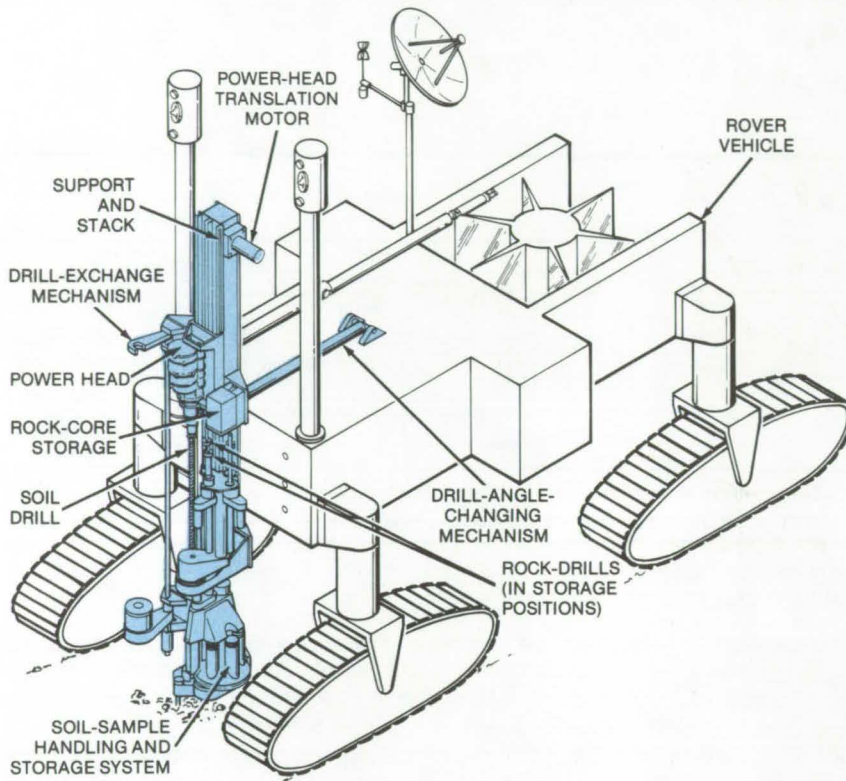
A proposed machine would sample rock or soil automatically. Originally intended as a tool for the unmanned exploration of planets, the new machine concept may also be useful in terrestrial agricultural and geologic surveys.

The machine, mounted on a wheeled or tracked vehicle, positions a drill for a cut at any angle from horizontal to vertical, moves the power head to drive the drill into the cut, and stores the drilled core in a container. The machine uses different

drills for rock and soil and changes from one to the other as necessary. It even holds small rocks to prevent them from spinning when they are drilled.

The sampling-machine power head moves on a track on a beam that is the  
(continued on next page)





The **Automatic Sample Collector** drills a vertical sample. The 1-m-long soil drill is being used; the shorter rock drill is stowed away. The machine contains duplicates of each type of drill as spare parts.

primary structural support for the drill (see figure). The beam is rotated by a pivot mechanism to the required drilling angle. A motor-operated chain drive moves the power head along the track.

Separate mechanisms and areas are used to store rock samples and soil samples. For the collection of soil, the 1-m-long soil drill is driven to a

depth of 10 cm. The machine raises the drill and moves a container under the drill, and the drill is rotated to shake a 10-cm<sup>3</sup> portion of the soil it has collected into the container. The excess soil spills over the side. The soil in the container is compacted under a packing mechanism, and the machine moves the container away from the drill.

The drill is driven to a depth of 20 cm so that it collects another 10-cm-thick sample, which is also deposited in the container. The drilling and filling procedure is repeated, building up layers in the sample container in the reverse order of their occurrence in the ground.

A soil container can hold ten 10-cm<sup>3</sup> samples. When a container is filled, the machine caps it, stores it on a turret, and moves a new container into position.

To take rock samples, the machine removes the soil drill and replaces it with one designed for penetrating rock. The rock drill is advanced to a predetermined depth into the rock (usually somewhat deeper than the 10-cm individual soil samples) and accepts a solid rock core. After being drilled, the core is forced from the interior of the drill and transferred to a 5-by-5 array of storage tubes. Each tube is capped as it is filled.

The power head can travel as much as 135 cm along its track. It can apply a force equal to the weight of the vehicle to the drill. The operation of the machine is controlled by a stored program and by data gathered by the vehicle sensors.

*This work was done by Gilbert M. Kyriasis of Martin Marietta Corp. for Johnson Space Center. To obtain a report that presents a preliminary design study of the core-sampling system, Circle 60 on the TSP Request Card.*

MSC-18868

## Aerodynamics Improve Wind Wheel

Aerodynamic refinements are proposed to increase efficiency.

*Marshall Space Flight Center, Alabama*

Modifications based on aerodynamic concepts would raise the efficiency of a wind-wheel electric-power generator. The changes smooth the airflow, to increase the power output, without increasing the size of the wheel.

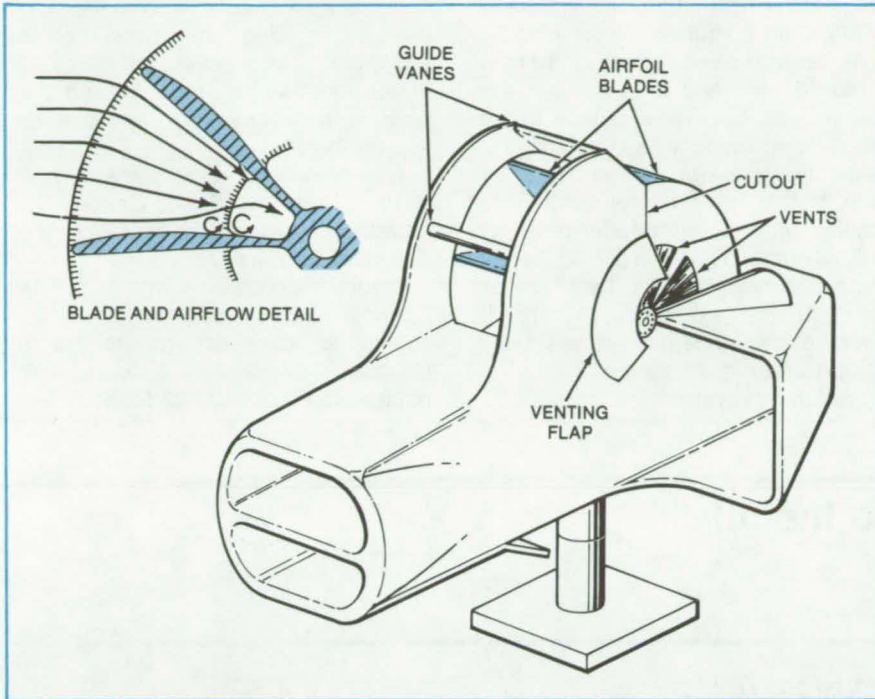
The original wind wheel is described in "Wind-Wheel Electric-Power Generator" (MFS-23515) on p. 276 of *NASA Tech Briefs*, Vol. 3, No. 2. It resembles a water wheel in appearance and opera-

tion. Ducting directs the wind at the exposed blades. The improved version, shown in the figure, differs from the original in four significant respects:

- Airfoil profiling is used on all duct and wheel edges exposed to the wind. The airfoil is more effective than other types of edge rounding in keeping the boundary-layer airflow attached to the duct walls. This reduces the deceleration of the wind, resulting in increased

mass flow through the turbine and therefore increased power.

- Airfoil wheel blades replace the simple cambered-plate blades. Airfoil blades are superior because at typical windspeeds and windmill dimensions, they operate during a portion of the rotation in a lift mode, instead of the drag mode of cambered plates.
- The wheel is vented near the axis. Venting flaps on the duct guide the



The **Improved Wind Wheel** features streamlined ducting and airfoil blades to smooth the airflow and thereby increase efficiency.

outside airflow away from the cutout section, creating a suction. The suction, along with the venturi pressure gradients near the blade vertex, accelerates the airflow along the blades.

- Guide vanes direct the wind onto the blades. The vanes act like airfoil leading-edge flaps to increase the camber of the blades behind them, enabling them to operate in the lifting mode at later stages in the rotation, where they would otherwise revert to the drag mode. The guide vanes have airfoil shapes.

Any of the modifications alone would improve the efficiency of the machine. However, the combined changes are synergistic. Significant improvements in efficiency are therefore anticipated without any increase in size or in the number of moving parts and without departing from the simplicity of the original design.

This work was done by Vernon W. Ramsey of the National Research Council for **Marshall Space Flight Center**. For further information, Circle 61 on the TSP Request Card.

Inquiries concerning rights for the commercial use of this invention should be addressed to the Patent Counsel, Marshall Space Flight Center [see page A5]. Refer to MFS-25506.

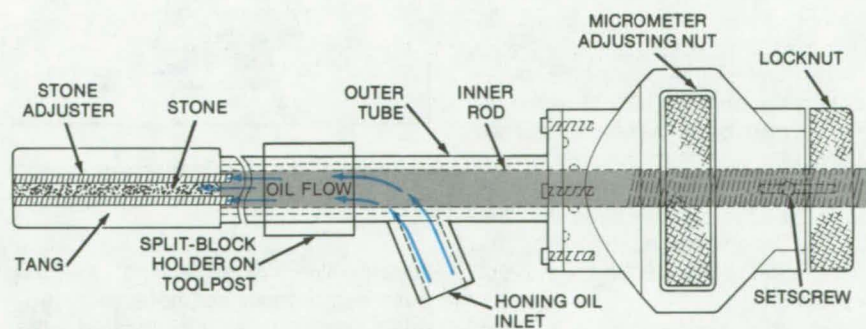
## Lathe Attachment Finishes Inner Surface of Tubes

Inexpensive tool produces smooth surfaces to within 1 microinch.

*Lyndon B. Johnson Space Center, Houston, Texas*

Extremely smooth finishes, to within 1 microinch (25 nm), are machined on the inside surfaces of tubes by a new attachment for a lathe. The relatively inexpensive accessory, called a "microhone," holds a honing stone against the workpiece by rigid tangs instead of by springs as in conventional honing tools. The conventional tools produce surfaces that are comparatively rough, varying by 8 to 10 microinches (200 to 250 nm) in smoothness.

Microhoning removes surface irregularities and imparts a low-friction, high-gloss finish. It can be done with either the microhone or the workpiece (continued on next page)



The **Inner Rod Permits Adjustment of the Microhoning Stone**, while the outer tube supports the assembly. The outer tube is held between split blocks on a lathe toolpost. In this arrangement, the workpiece rotates around the honing stone.



moving and the other member stationary. When the microphone is stationary, the workpiece is placed in a long-bed lathe with one end in a chuck and the other end, the one with the bore to be honed, in a center rest.

The honing stone, held by tangs brazed to a long rod, is mounted on the lathe toolpost by a split block. The two halves of the block are placed around an outer tube surrounding the rod (see figure) and fastened to the toolpost. The lathe operator inserts the stonehead in the bore and presses it

into position against the inner surface by adjusting a knurled micrometer.

As the workpiece rotates, the stone is moved back and forth through the bore, honing the inside surface to the specified dimensions. As each pass is made, the operator compensates for wear of the stone by readjusting its position with the micrometer nut.

Oil is pumped into the outer tube via an inlet on the side of the tube. The oil flows to the workpiece, where it lubricates the stone and washes away the grit created by honing. The oil is filtered and recycled.

If the workpiece is held stationary, the stone-holding tube is mounted in the chuck of an electric drill. The drill motor rotates the stone around the bore. In this case, oil is fed directly into the bore.

This work was done by Alfred J. Lancki of **Johnson Space Center**. For further information, Circle 62 on the TSP Request Card.

Inquiries concerning rights for the commercial use of this invention should be addressed to the Patent Counsel, Johnson Space Center [see page A5]. Refer to MSC-18780.

## Blind Fastener Is Easy To Install

Fingers expand to grip parts, contract to release them.

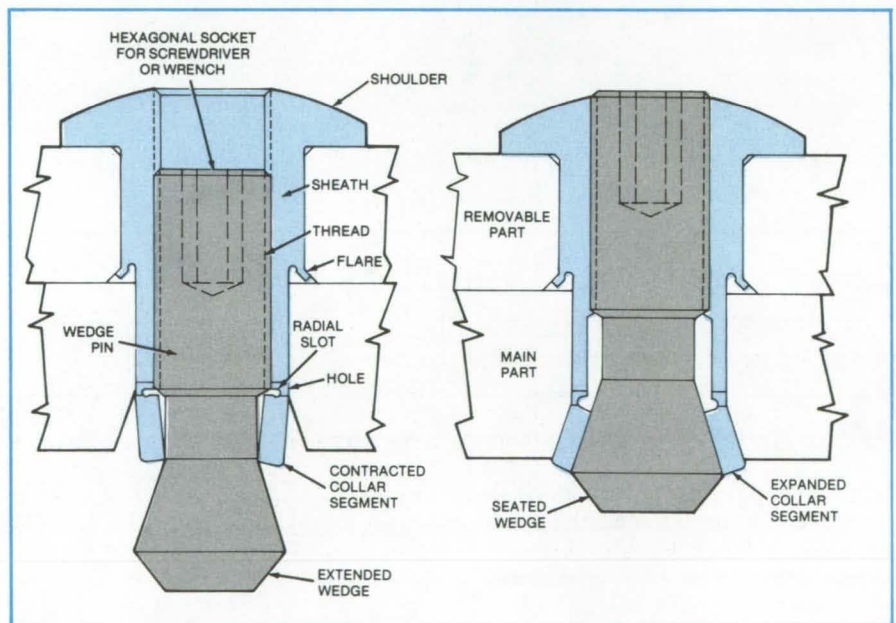
Lyndon B. Johnson Space Center, Houston, Texas

Panels, sheets, doors, and other structures could be easily attached and removed from a mating part by a proposed new fastener. This would be possible even if one side of the assembly is accessible and the other is blind. The new hardware could be reused repeatedly to join and release the mated parts, and it could carry substantial loads in both shear and tension.

The fastener is permanently anchored in the removable part only. Its protruding end is inserted into a hole in the mating part. When a wedge pin is screwed tightly closed, a segmented collar is pressed against the bottom surface of the assembly, clamping the two parts together. The installation has no loose parts, and no rear nut is needed.

As shown in the figure, the outer sheath of the fastener is held on the removable part by its shoulder and an undercut flare at its midsection, which rests against a countersunk surface. With the wedge extended (so that the collar segments are contracted), the fastener can be inserted in the hole of the mating part.

When the wedge pin is rotated counterclockwise by a screwdriver or key wrench, it is retracted into the



A Segmented Collar Contracts or Expands to release parts (left) or to grip them (right). The wedge-pin cone angle is  $30^{\circ} \pm 15^{\circ}$ .

sheath. The wedge end of the pin pushes the collar segments outward, until, when it is fully seated, the segments are pressed against the side of the tapered hole.

To disengage the parts, the wedge pin is screwed clockwise (again, a screwdriver or key wrench is inserted from the removable-part side) until the wedge is extended from the sheath

and the collar segments have contracted. The removable part is then released from the main part, still holding the fastener.

The collar has six or more equal segments separated by radial slots that terminate in holes drilled through the body wall. The holes and slots improve the

flexibility of the collar over hundreds of attachment cycles.

The hole in the mating part is tapered at the back (blind) face so that it can accommodate the fingerlike collar segments. In another version of the fastener, both outer surfaces of the mating parts are countersunk so that the hardware does not protrude on either side.

*This work was done by Scott A. Peterson of Rockwell International Corp. for Johnson Space Center. No further documentation is available.*

*Inquiries concerning rights for the commercial use of this invention should be addressed to the Patent Counsel, Johnson Space Center [see page A5]. Refer to MSC-18742.*

---

## Resistance Heater Helps Stirling-Engine Research

Reliability and measurability of performance are improved.

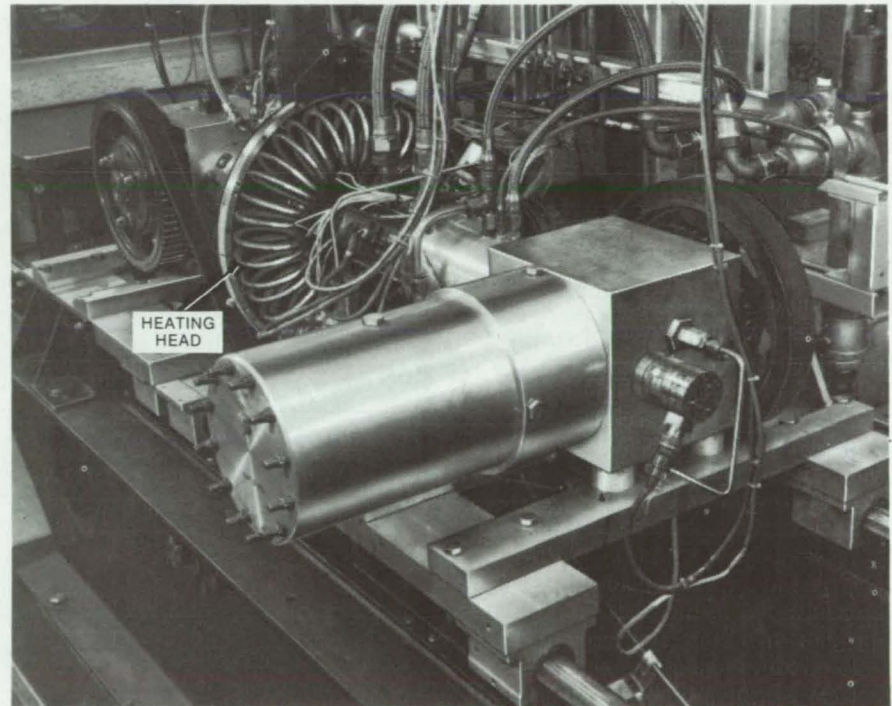
---

*NASA's Jet Propulsion Laboratory, Pasadena, California*

An electrical-resistance heater is an effective way to heat the working gas of an experimental Stirling engine. The heating element is made of Nichrome (or equivalent) heating wire embedded in highly-compacted magnesium oxide insulation and a coaxial metal outer sheath. The outer surface of the metal sheath is welded or brazed directly to the tubes through which the engine working gas flows (see figure).

An electrically powered heater is used in the experimental engine, instead of more-conventional sources (such as combustion and solar), so that the engine input energy can be measured and the engine thermal efficiency and thermodynamic balance determined. A previous electrical-heater head for a research Stirling engine had the voltage supplied directly to the body of the heat-exchanger tubes so that the tube became the electrical resistance element of the heater. However, the low-resistance tubes require currents of thousands of amperes to generate sufficient resistance heating. Because the temperature coefficient of many high-performance alloys reverses at high temperatures, instabilities of the heater power supply could be induced with an ensuing burnout of one or more heater tubes. Also, safety must be considered when applying a voltage directly to the engine case.

The heating element is fabricated by starting with a large-diameter tubular sheath that contains the insulated Nichrome wire. It is then swaged and



The Stirling Engine Heater Head consists of 18 double-turn coils of tubing, each of which is tightly wrapped with a resistance-heating element, through which the working gas flows. These coils form a toroid about the periphery of the heater-head body. In operation, the heater elements reach 1,500° F (815° C).

drawn to a very small diameter. In the process the insulation becomes compacted. The heater element is flexible enough to be wound spirally on the tubes.

With the new resistance heater, the total circuit resistance can be selected independently of the tube geometry by simply changing the size of the wires and/or the number of wire wraps

around each tube. This simplifies the power-supply requirements. It is unlikely that a failure of a resistance element would cause failure of the tube and loss of the working gas.

*This work was done by Frank W. Hoehn of Caltech for NASA's Jet Propulsion Laboratory. For further information, Circle 63 on the TSP Request Card.  
NPO-14928*



## Ball-and-Socket Joint Can Be Disassembled

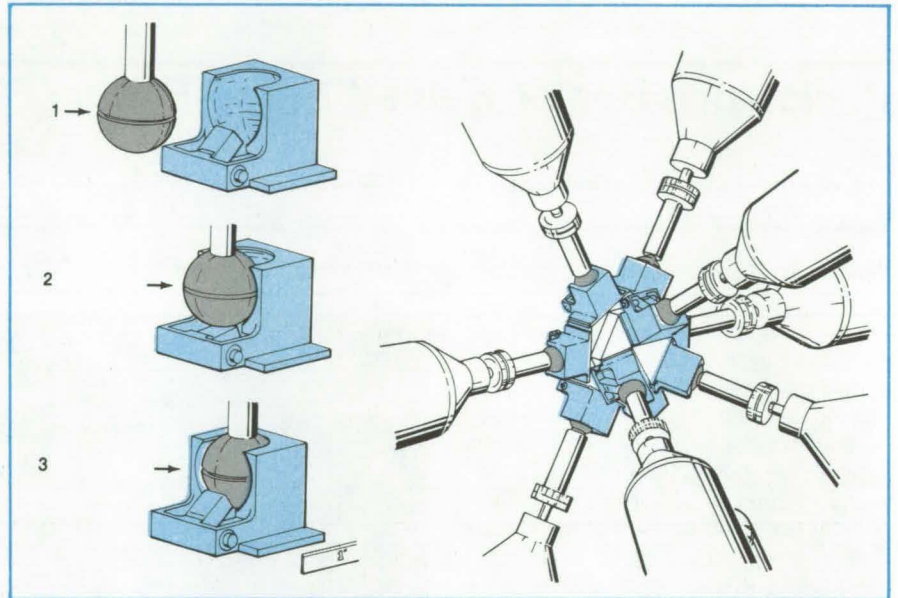
Self-contained coupling requires no tools or additional hardware.

*Langley Research Center, Hampton, Virginia*

A ball-and-socket joint originally developed for the construction of large platforms in zero g could be used in such Earth-based temporary structures as scaffolding, camping equipment, tent posts, trade shows, and displays. It is a quick connect/disconnect coupling that is easily engaged and disengaged yet is rigid and structurally sound when assembled.

The new joint consists of a socket mounted on a central hub or union and a ball-ended bolt or fitting mounted at the end of a column or any structural member. The central hub can be tubular or configured to specific geometric shapes, such as the tetrahedral geometry shown in the figure. A spring-loaded latch in the socket retains the ball. The coupling is disengaged simply by depressing the latch and extracting the ball. If a locknut that bears against the socket face once the ball is engaged is added, the joint can be made rigid.

The unit is self-contained and requires no loose hardware. It is engaged and disengaged without tools manually, or remotely by a manipulator. It is reusable over a long period of time, is universal, and can accommo-



A **Ball-and-Socket Joint** is assembled in the three-step sequence shown at the left. An assembled tetrahedral node for a truss is shown at the right.

date varied structural configurations, such as tetrahedron, pentahedron, hexahedron, etc. Lateral entry of the ball into the socket means that standardized attachments, including closeout attachments, may be used.

*This work was done by Raymond S. Totah of Rockwell International Corp. for **Langley Research Center**. For further information, Circle 64 on the TSP Request Card. LAR-12770*

## Integrated Structural and Cable Connector

A quick-connect structural coupling also makes electrical or fiber-optic connections.

*Langley Research Center, Hampton, Virginia*

The ball-and-socket coupling described in the preceding article has been modified to join electrical or fiber-optic cable connectors remotely. It is a quick-connect/disconnect coupling that has application in hazardous environments, such as space, undersea, and nuclear installations.

A perspective view of the integrated-structure/cable connector is shown in Figure 1. The column end fitting and ball are joined by a hollow shaft. An actuation sleeve and cone on the shaft slide in opposite directions. Lockpins hold the cone until the sleeve is moved.

Projecting from the sleeve are three cam-actuator pins (only one is shown) that pass through longitudinal slots in the shaft to a cylindrical-shell translation cam. Inside the cam is a slide driven by three cam-follower pins (only one is shown). Splines on the slide and shaft allow only axial



movement. A cable-receptacle housing carried within the slide rotates freely on ball bearings.

The first step in making the structural connection is to insert the ball into the socket, as shown in Figure 2a. It is important to note the position of the lockpins and the locking ball between them. Only one set of three pairs of lockpins is shown. The long pins fastened to the cone move with it, and the short pins are attached to the sleeve. A locking ball between the pins is holding the cone against a compressed coil spring.

Pulling the sleeve away from the cone allows the ball to slip into a groove in the short pin, locking the sleeve and releasing the cone. The coil spring forces the cone against a conical depression on the socket face, making the joint rigid. This position is shown in Figure 2b. Note that when the sleeve was pulled, the cam moved the cable receptacle an equal distance toward the plug.

When the cone is seated firmly against the socket, the long lockpin has released the locking ball. The sleeve is pulled to the end of its travel, where it is held by a detent and spring. This also moves the cable receptacle into the plug to make the connection, as shown in Figure 2c.

A bayonet pin on the receptacle slides along the surface of a helical alignment cam surrounding the plug to orient the connectors. The bayonet pin enters an axial slot, assuring precise orientation of the mated plug and receptacle.

*This work was done by Raymond S. Totah of Rockwell International Corp. for Langley Research Center. For further information, Circle 65 on the TSP Request Card.*

*Inquiries concerning rights for the commercial use of this invention should be addressed to the Patent Counsel, Langley Research Center [see page A5]. Refer to LAR-12769.*

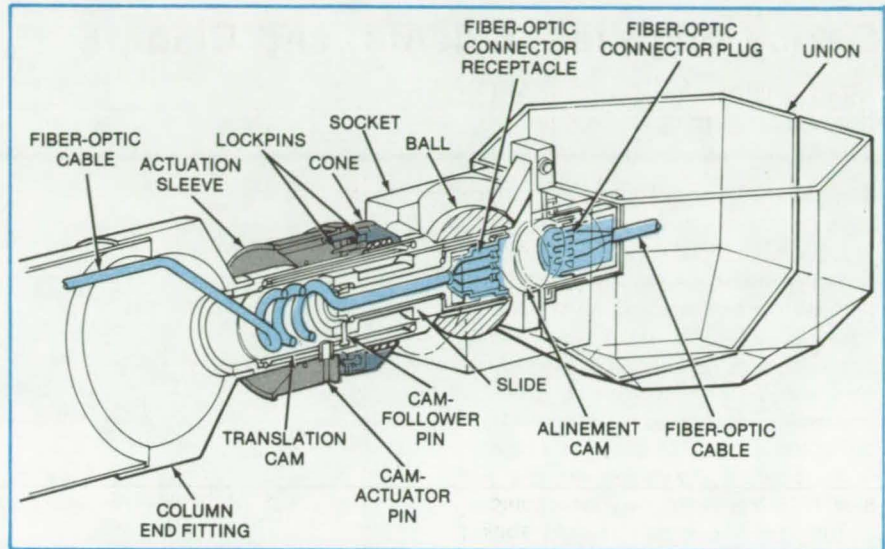


Figure 1. A **Ball-and-Socket Coupling** includes a fiber-optic cable. The cable in the ball is coupled to the cable in the socket, in the sequence shown in Figure 2.

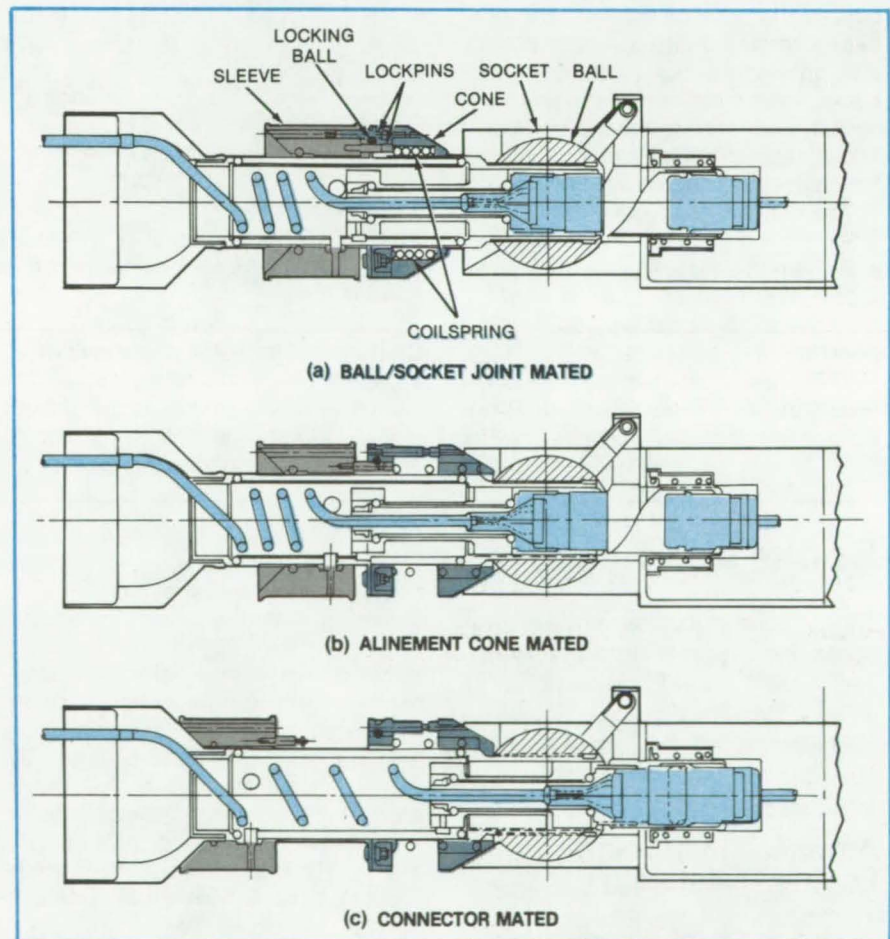


Figure 2. **Three Steps** couple the two parts of the fiber-optic cable. In (a), the ball has been inserted in its socket. The cone has been released in (b), and the cable has moved toward the plug. In (c), the sleeve has been pulled to the end of its travel on the left, and the cable and plug have mated.

## Device Acquires, Orients, and Clamps

Mechanism aligns an object as it hooks up to it.

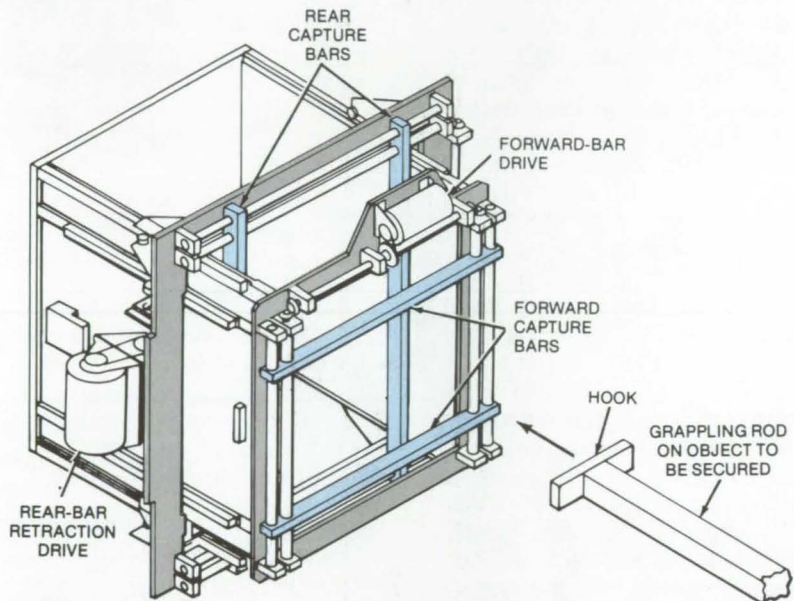
Marshall Space Flight Center, Alabama

A proposed mechanism secures an object in three stages: initial acquisition, alignment, and clamping. Originally developed to aid Space Shuttle crews in retrieving satellites, the concept may also be useful in undersea work or as a machine-tool attachment for quick changes of tools.

As shown in the figure, the mechanism is a box with two motor-driven pairs of bars, one pair at right angles to the other. A grappling rod on the object to be retrieved enters the open face of the box, and the two pairs of bars gently close on the rod. The rear pair is retracted into the box, pulling the rod into the box by its grappling hook. As the rod is pulled, the bars align it, correcting the roll, pitch, yaw, and offset of the object. Latches in the box then clamp the object in position.

The concept was developed for a grappling rod 24.75 in. (62.9 cm) long with a 1-inch-square (2.54-cm-square) cross section. It could be built from readily available gears, pillow blocks, bearings, and solenoids.

This work was done by Edwin C. Pruet and Kem B. Robertson of Essex Corp. for Marshall Space Flight



**Attachment Device** will align and clamp the grappling rod after it is acquired. A guide added to the front of the mechanism would assist the initial entry of the hook into the box.

**Center.** No further documentation is available.

This invention is owned by NASA, and a patent application has been filed. Inquiries concerning nonexclu-

sive or exclusive license for its commercial development should be addressed to the Patent Counsel, Marshall Space Flight Center [see page A5]. Refer to MFS-25403.

## Books and Reports

These reports, studies, and handbooks are available from NASA as Technical Support Packages (TSP's) when a Request Card number is cited; otherwise they are available from the National Technical Information Service.

### Advances in Turbine-Engine Technology

A status report on advanced technologies for aircraft turbine engines

A report has been published that describes major advances in high-temperature materials, coatings, and turbine-blade coating technology for aircraft turbine engines.

Advanced materials, coatings, and cooling technology are the keys to achieving improved turbine-engine performance via high-cycle operating temperatures, lighter structural components, and adequate resistance to various environmental factors associated with aircraft turbine engines. By increasing the strength of intermediate-temperature materials used for turbine disks, increased rotor speeds and a reduced number of turbine stages can be achieved with resultant savings in engine weight and cost. Increases in allowable turbine-blade and stator temperatures will permit operation at higher cycle temperatures and/or reduced cooling air.

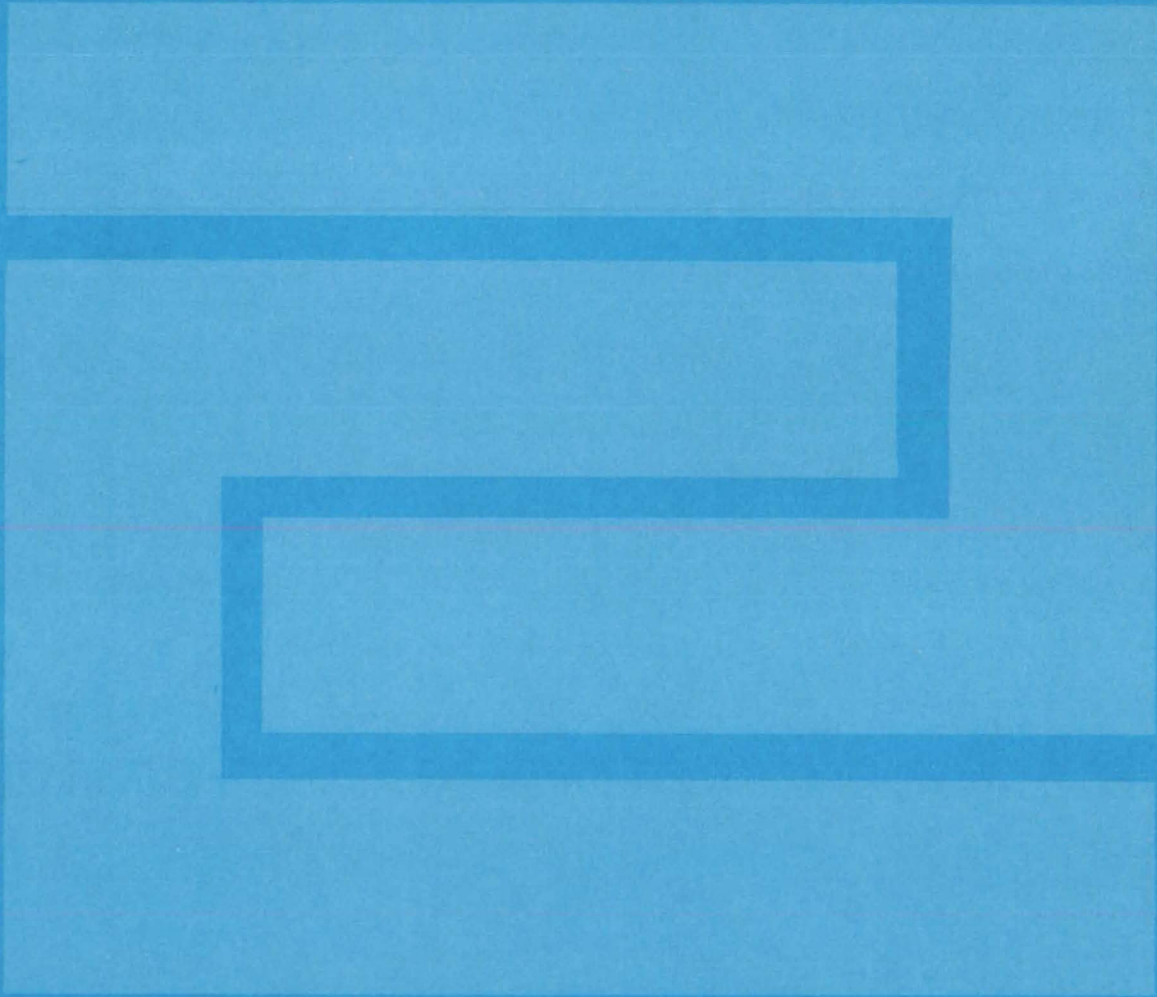
Another important aspect is the development of coatings. Significant progress has been made in providing coating protection against oxidation,

hot corrosion, and erosion for high-temperature turbine components by the industrial community, the department of defense (DOD), and NASA.

Advances in material categories described include metal-matrix composites, superalloys, directionally solidified eutectics, and ceramics, as well as coatings and turbine-cooling developments.

This work was done by John C. Freche and G. Mervin Ault of Lewis Research Center. Further information may be found in NASA TM-X-73628 [N77-33159/NSP], "Progress in Advanced High Temperature Turbine Materials, Coatings, and Technology" [\$6.50]. A copy may be purchased [prepayment required] from the National Technical Information Service, Springfield, Virginia 22161. LEW-13672

# Fabrication Technology



## Hardware, Techniques, and Processes

- 87 Improved Clothing for Firefighters
- 88 Gravity-Feed Growth of Silicon Ribbon
- 89 Heat-Exchanger Method of Crystal Growth
- 89 Removing Defects From Silicon Ribbon
- 90 Ceramic for Silicon-Shaping Dies
- 91 Recharging the Silicon Crucible in a Hot Furnace
- 91 Crucible Grows Wide Silicon Ribbon
- 92 Refractories Keep Silicon Crystals Pure
- 93 Improved Facility for Producing Silicon Web
- 94 Automatic Control of Silicon Melt Level
- 94 Temperature-Controlled Support for a Seed Crystal
- 95 Fiber-Reinforced Slip Castings
- 96 Fluxless Brazing of Large Structural Panels
- 97 Weatherproof Crimp Connector
- 98 Capacitively-Heated Fluidized Bed
- 99 Shaping Transistor Leads for Better Solder Joints
- 100 Metallic Panels Would Insulate at 2,700° F
- 101 Wire EDM for Refractory Materials
- 101 Heat Lamps Solder Solar Array Quickly
- 102 High-Temperature Seal for Sliding-Gate Valve
- 103 Structural Modules Would Contain Transmission Lines
- 104 IC Capacitors on Groups III-to-V Substrates
- 105 Levitator for Containerless Processing
- 106 Sprayed Coating Renews Butyl Rubber
- 106 Metal Sandwich Panel With Biaxially Corrugated Core
- 108 Ultra-Thin-Film GaAs Solar Cells
- 108 Sealed Strip Line for Extreme Temperatures
- 109 Wire Whip Keeps Spray Nozzle Clean

## Books and Reports

- 110 Materials Processing in Space

---

## Improved Clothing for Firefighters

The application of space technology should reduce the incidence of injuries, heat exhaustion, and fatigue.

---

### *Marshall Space Flight Center, Alabama*

Improved protective gear for firefighters against heat, flame, moisture, impact, and penetration has emerged from a joint NASA and U.S. Fire Administration program to develop and field-test improved firefighter protective clothing and equipment. Using the advanced materials and design concepts of aerospace technology, protective gear (see figure) was fabricated and tested for the head, face, torso, hand, and foot. In the tests, it was found that the new gear protects better than conventional firefighter gear, weighs 40 percent less, and reduces the wearer's energy expenditure by 25 percent. A comparison of the hazards and protection afforded firefighters by the new gear and by current gear is shown in the table.

Protecting the head and ears are a helmet and a detachable inner liner or hood. The helmet outer shell is made of high-temperature epoxy resin reinforced with one layer of glass and one layer of aramid fabric. The liner is made of polyurethane heat-resistant foam. Attached to the torso protection, the hood prevents debris or water from reaching the neck. The front peak of the helmet keeps debris and water away from the face and protects the face shield when it is retracted.

The face protector is a full visor fabricated from high-temperature-resistant thermoplastic (polyethersulfone). It covers the eyes, nose, and cheeks down to the upper lip. When not in use, the visor is stowed inside the helmet.

Two configurations make up the torso protection. One consists of a short jacket and bib pants, and the other is a longer coat and pants without a bib. This protection does not depend on the garment worn underneath. Padding at the knees and elbows adds impact protection.

The outer shell of the torso protection is flame and heat resistant. It is made either of polybenzimidazole (PBI) or of a blend of aramid fiber and a mixture of aramid fiber and paper. A waterproof, breathable fabric liner helps to



**Protective Gear for Firefighters** is an integrated ensemble for the head, torso, and extremities. Two different pant-and-coat configurations are shown. The new gear will be performance-tested by selected municipal firefighting organizations. Also being developed for firefighters are lighting, communications, and personal cooling systems.

reduce metabolic-heat buildup; it prevents liquids from passing through but does not block air and water vapor. To work with the foot protection, the pant legs have an adjustable seal in the trousers.

An outer glove shell and a wristlet are worn to protect the hand and wrist.

The wristlet, which is attached to the torso protector, protects against heat, puncture, and cuts and prevents debris and water from entering the sleeve. The glove shell comes in two versions: One is a high-temperature latex-dipped waterproof glove; the other is a nonwaterproof leather-palmed glove.

(continued on next page)

For the foot and ankle, a light, molded polyurethane boot 11 in. (28 cm) high offers heat and arch-penetration protection. The boots, which weigh less than 4 lb (1.8 kg), have a steel toecap, a steel midsole, and an aluminum arch protector.

This work was done by Fred J. Abeles of Grumman Aerospace Corp. for Marshall Space Flight Center. Further information may be found in:

NASA CR-161529 [N80-32098/NSP], "Project FIRES, Volume 1: Program Overview and Summary, Phase 1B" [\$6];

NASA CR-161530 [N80-32586/NSP], "Project FIRES, Volume 2: Protective Ensemble Performance Standards, Phase 1B" [\$10];

NASA CR-161531 [N80-32100/NSP], "Project FIRES, Volume 3: Protective Ensemble Design and Procurement Specification, Phase 1B" [\$10]; and

NASA CR-161532 [N80-32099/NSP],

Hazard	Protection		Areas Improved*
	Current	Prototype	
Impact	< 10 ft-lb at 250° F (< 13.5 N-m at 120° C)	150 ft-lb at 485° F (203.4 N-m at 250° C)	Head/Ear
Penetration	< 10 ft-lb at 250° F	100 ft-lb at 485° F (135.6 N-m at 250° C)	Head/Ear
	10 to 20 lb (4.5 to 9.1 kg)	400 lb (180 kg)	Foot/Ankle (Arch)
Heat	25 lb (11.3 kg)	50 lb (23 kg)	Hand/Wrist
	Sags at 300° F (150° C) < 5 min	> 5 min at 485° F (250° C)	Head/Ear
(Radiation, Convection)	Head > 100° F (38° C) Exposed Areas	Head < 100° F (38° C) Full Coverage	Torso/Limb (Neck, Wrist)
Heat (Conduction)	250° F (120° C) < 2 min	250° F (120° C) > 5 min	Torso/Limb (Knees, Elbows)
Cut	< 20 lb (9.1 kg)	> 20 lb (9.1 kg)	Hand/Wrist
	< 1 lb (0.4 kg)	> 4 lb (1.8 kg)	Face/Eye
Scratch	< 1 lb (0.4 kg)	> 4 lb (2 kg)	Face/Eye
Water	Exposed Areas	Full Coverage	Torso/Limb (Neck) Hand/Wrist (Wrist)

\*For those areas not listed, protection is at least equal to current gear.

### Comparison of Prototype and Current Firefighting Protective Gear

"Project FIRES, Volume 4: Prototype Protective Ensemble Qualification Test Report, Phase 1B" [\$10]. Paper copies of these reports may be purchased [prepayment required] from the National Technical Information Ser-

vice, Springfield, Virginia 22161. The reports are also available on microfiche at no charge. To obtain microfiche copies, Circle 66 on the TSP Request Card.

MFS-25546

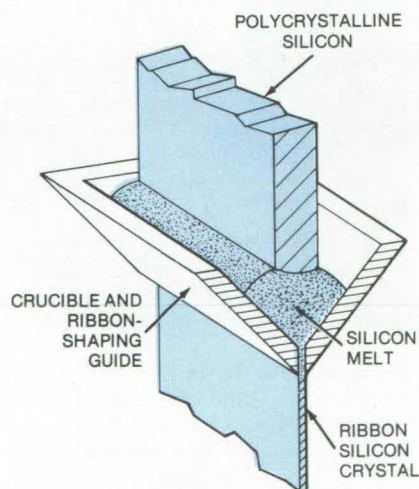
## Gravity-Feed Growth of Silicon Ribbon

Liquid pressure forces melted silicon through the slot in a vee-shaped crucible.

NASA's Jet Propulsion Laboratory, Pasadena, California

In the inverted Stepanov apparatus now under development for NASA's Jet Propulsion Laboratory, silicon is melted in a vee-shaped crucible that has a long narrow slot at the bottom of the vee (see figure). Molten silicon flows from the slot at a rate controlled by fluid pressure; as it emerges, it cools and solidifies to form a continuous ribbon.

To eliminate surface-tension effects, the crucible walls are made of (or lined with) a material that liquid silicon does not wet. The pressure necessary to force silicon out of the slot is applied by the liquid head — i.e., the amount of melted silicon in the crucible. The liquid level is precisely controlled by simply feeding the molten pool with a solid silicon rod.



The Pressure of Melted Silicon in the crucible determines the rate at which the silicon crystal ribbon grows in this inverted Stepanov technique. In the conventional Stepanov apparatus, silicon is pulled up through a die floating on the melt.

The vee configuration allows the trough of the crucible to be lined with flat plates. This simple geometry makes it easy to test different liner materials. It also should lower the cost of a production system. Further development is needed to reduce the chemical reactivity of the liner material and to understand the specific conditions for ribbon growth when the melt does not wet the edge of the die.

[Also see the related article, "Improved Inverted Stepanov Apparatus" (NPO-14297), on page 234 of NASA Tech Briefs Vol. 4, No. 2.]

This work was done by Glenn W. Cullen of RCA Corp. for NASA's Jet Propulsion Laboratory. For further information, Circle 67 on the TSP Request Card.

NPO-14967

## Heat-Exchanger Method of Crystal Growth

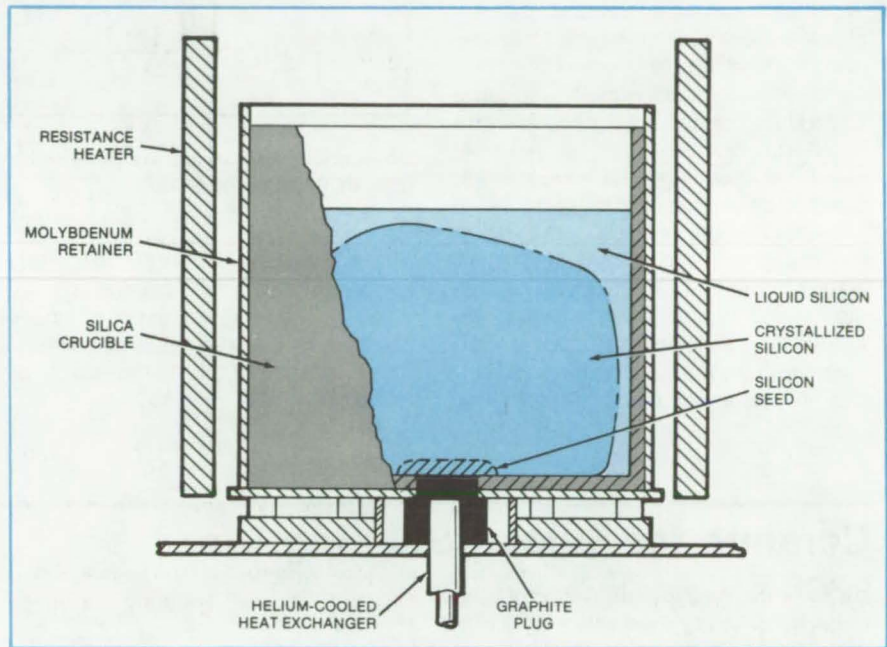
A large, silicon crystal grows in a crucible with no moving parts.

NASA's Jet Propulsion Laboratory, Pasadena, California

Large crystals of silicon are grown from the melt, in either a vacuum or a pressurized atmosphere, without moving the crucible, furnace, or anything else. A seed crystal is mounted on a helium-cooled heat exchanger, which prevents the seed from melting when the furnace melts the rest of the silicon material in the crucible; the heat exchanger draws off heat from the melt so that a solid ingot grows outward from the seed in a regular crystal structure. The bottom of the crucible is insulated so that the heat exchanger cools only the seed.

The figure shows the silicon seed mounted on a graphite plug that is flush with the inside bottom surface of the silica crucible. (During heatup the seed attaches to the graphite through the formation of silicon carbide and therefore does not float in the melt.) The helium-cooled heat exchanger fits inside the graphite plug. The crucible is inside a cylindrical heating chamber with a resistance heater. It is surrounded by a cylindrical molybdenum retainer and rests on a molybdenum disk that is supported by graphite rods on a graphite plate.

After loading, the furnace is evacuated, and the temperature is raised to above the melting point of the silicon stock. Once the stock is melted, the temperature is reduced to slightly above the melting point, so that the melt starts to cool and solidify on the seed. The figure shows the ingot partially solidified. The solid/liquid interface has advanced from the seed so that there is a thin annulus of liquid be-



In **Crystal Growth** by the heat-exchanger method, the heat-conducting graphite plug improves heat transfer from the melt to the heat exchanger. The crystal grows outward from the seed.

tween it and the crucible wall. There is also liquid above the ingot. When substantially all of the liquid has solidified, the temperature of the crucible wall is allowed to drop below the silicon melting temperature, and the crucible and ingot are cooled.

Previously, it has been necessary to use a purge gas (typically, argon) to suppress crucible decomposition through the reaction  $\text{Si} + \text{SiO}_2 \rightarrow 2\text{SiO}$ . The heat-exchanger method minimizes turbulence in the melt, suppressing crucible decomposition and therefore al-

lowing operation in a vacuum. Vacuum operation minimizes convective currents and thus improves thermal symmetry in the furnace. It also improves the quality of the crystal by lowering its oxygen content and removing volatile impurities.

*This work was done by Chandra P. Khattak and Frederick Schmid of Crystal Systems, Inc., for NASA's Jet Propulsion Laboratory. For further details, Circle 68 on the TSP Request Card.*

NPO-14819

## Removing Defects From Silicon Ribbon

In a proposed process, the surface is bombarded by ion clusters, gettered, and annealed.

NASA's Jet Propulsion Laboratory, Pasadena, California

A new proposal for removing impurities from silicon ribbon and sheet could be developed into an automated production-line process. The new tech-

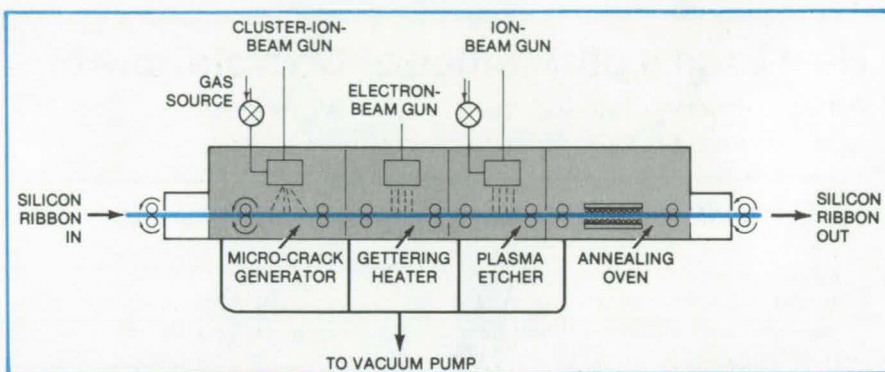
nique, which combines ion-cluster bombardment, electron-gun heating, and plasma etching, could be a key step in fabricating inexpensive solar-

cell arrays. Silicon sheets and ribbons treated this way could have the enhanced carrier lifetimes necessary for  
(continued on next page)

satisfactory solar-cell performance.

The figure shows the elements of the proposed system. Silicon ribbon or sheet is fed into the processor continuously, passing through an air lock into a partially evacuated chamber. A gas such as xenon is metered into the chamber for the generation of a cluster-ion beam from an ion gun. The energy of the ion beam is adjusted so that the clustered ions strike the ribbon surface (the intended back surface of the solar cell to be fabricated) with enough force to produce minute fractures. The gun must emit clustered ions because unclustered ions might not have enough mass to cause microfracturing.

Gettering occurs as the ribbon passes through the second chamber. An electron beam heats the ribbon, causing the impurities to move to the microcracks. The processed surface is then plasma-etched in a third evacuated chamber, where it passes through a resistance-heated chamber by an ion beam that removes



**Impurities and Defects Are Removed** from silicon ribbon in a continuous process as it moves through the system.

the surface layer containing gettered material. Finally, the ribbon is annealed in a fourth evacuated chamber, where it passes through a resistance-heated oven to remove all mechanical imperfections.

*This work was done by Katsunori Shimada of Caltech for NASA's Jet Propulsion Laboratory. For further information, Circle 69 on the TSP Request Card. NPO-14772*

## Ceramic for Silicon-Shaping Dies

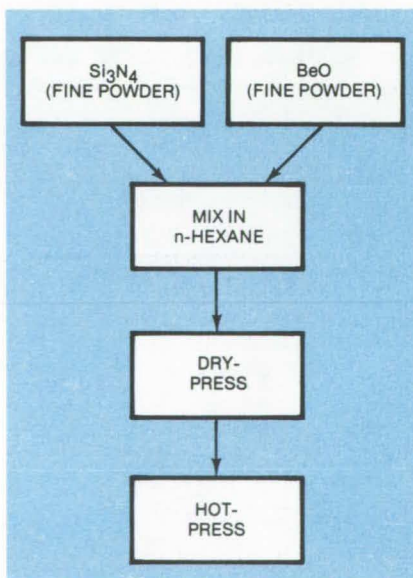
SiBON is strong, stable, and resistant to molten silicon.

*NASA's Jet Propulsion Laboratory, Pasadena, California*

Silicon beryllium oxynitride (SiBON) is a promising candidate material for the manufacture of the shaping dies used in fabricating ribbons or sheets of silicon. It is extremely stable, resists thermal shock, and has excellent resistance to molten silicon.

For the low-cost production of solar cells, it is desirable to grow silicon crystals as ribbon or sheet. Such crystals can be produced by extruding silicon through a ceramic die; however, the die must be chemically stable because even a slight contamination of the silicon degrades the performance of the photovoltaic cells.

SiBON is a solid solution of beryllium silicate in beta-silicon nitride. The preparation of the material (see figure) starts with 4 hours of ball milling a mixture of ultrafine powders of  $\text{Si}_3\text{N}_4$  and BeO in n-hexane, either with or without the addition of silica. (The proportion of BeO is the minimum that produces material of the desired quality.) Alumina milling equipment causes undue con-



**The Preparation of Silicon Beryllium Oxynitride Dies** requires mixing, milling, and pressing. The result is a strong ceramic that is resistant to molten silicon.

tamination, so PTFE-coated equipment is being studied.

After the removal of the n-hexane medium, the powder is dry-pressed, loaded into graphite dies coated with boron nitride, and hot-pressed at  $1,750^\circ\text{C}$  ( $3,182^\circ\text{F}$ ) for 1 hour at  $5,000$  to  $10,000\text{ lb/in.}^2$  ( $35 \times 10^6$  to  $70 \times 10^6\text{ N/m}^2$ ). It is important to exclude any materials that might volatilize Be out of the mixture during hot pressing.

This procedure produces a fine-grained, dense, single-phase, strong ceramic. Preliminary tests in contact with molten silicon in an argon atmosphere show that the SiBON is extremely resistant to chemical attack. The beryllium content of the silicon sample after this contact is less than 10 parts per million.

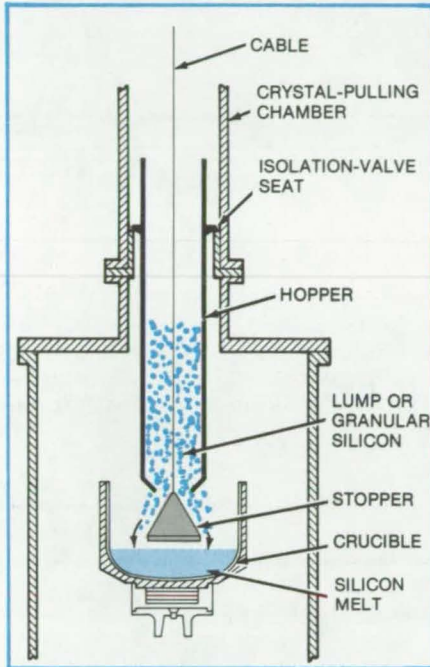
*This work was done by Ibrahim Sekercioglu and Roger R. Wills of Battelle Memorial Institute for NASA's Jet Propulsion Laboratory. For further information, Circle 70 on the TSP Request Card. NPO-14783*



## Recharging the Silicon Crucible in a Hot Furnace

A hopper suspended in the crystal-pulling chamber does not disturb the melt temperature or atmosphere.

NASA's Jet Propulsion Laboratory, Pasadena, California



**A Fresh Charge of Silicon** is added to the melted material in a hot crucible. By eliminating the cooldown and heatup periods for the refilling of the crucible, this technique increases furnace productivity and reduces the cost of silicon crystals for such applications as solar cells.

A "melt recharger" adds raw silicon to the crucible in a crystal-growing furnace without disturbing the inert-gas atmosphere or significantly lowering the temperature of the melt. In contrast to a previous design, which could only handle silicon rod, the new recharger accepts silicon in lump, granule, or powder form.

As the figure shows, the crucible-refill hopper is lowered into the hot zone of the crystal-pulling chamber through an isolation valve. The cable that supports the hopper is fastened to a cone-shaped stopper in the bottom of the hopper.

The hopper rests on the seat of the isolation valve. If the cable is re-

leased, the stopper moves out of the opening in the hopper, allowing part of the polysilicon charge to drop into the crucible. (The crucible is positioned so that the silicon is released at the right height to prevent the spilling of lumps or splashing of the melt.)

By increasing the efficiency of the production of silicon crystals, this process can reduce their cost. Several satisfactory recharge runs have been performed with the hopper/recharger.

This work was done by Richard L. Lane of Kayex Corp. for **NASA's Jet Propulsion Laboratory**. For further information, Circle 71 on the TSP Request Card.  
NPO-14980

### Strain-Gaged Bolts Are Easily Prepared

Strain gages are easily installed in bolts by a simple workbench procedure. The gages are mounted on the outside of a plastic-carrier tube and epoxied into a hole in the bolt. The external mounting on the carrier is superior to epoxying the bare gage in the hole.

(See page 69.)

### Blind Fastener Is Easy To Install

Joining panels, sheets, doors, and other structures to a mating part when only one side of the assembly is accessible would be easy with a proposed new fastener. The fastener is permanently anchored to the removable part only. A wedge pin attaches and releases the assembly.

(See page 80.)

## Crucible Grows Wide Silicon Ribbon

Oval shape and slotted lid produce the required temperature distribution.

NASA's Jet Propulsion Laboratory, Pasadena, California

The inexpensive manufacture of solar cells may require quality silicon ribbon crystals. One way to produce them is by growing wide dendritic webs, which can be very long and have high structural perfection. Dendrites grow from a supercooled melt, however, so the width of the ribbon depends on how wide a region of supercooled molten sil-

icon can be maintained in the crucible. A special crucible assembly has produced long dendritic ribbons over 4 cm wide.

The figure shows the crucible with the web forming as a thin liquid-silicon film supported by surface tension between two wirelike silicon dendrites that are growing from the melt. (Be-

cause the drawing is cut away, only one of the dendrites is shown.) The induction coils that heat the susceptor are not shown, but the elongated shape of the assembly is clearly seen. The shape of the slot in the lid above the melt modifies the temperature on the surface of the melt to generate the desired temperature profile, and the rectangular

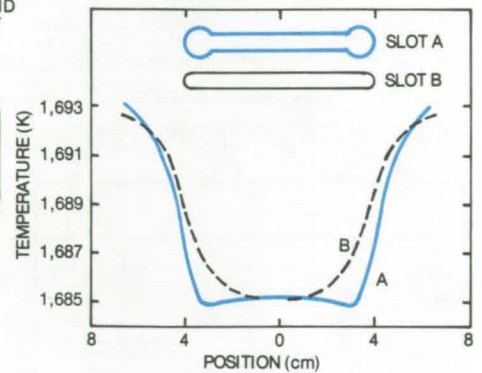
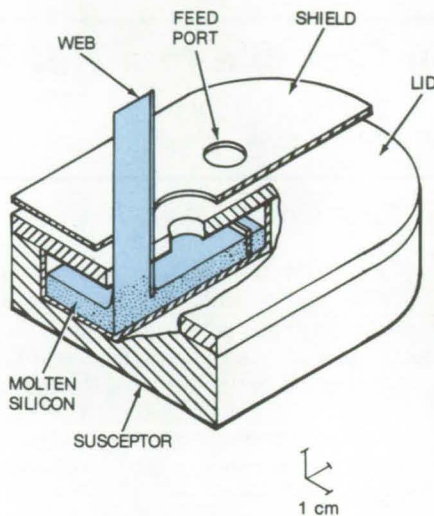
(continued on next page)

crucible minimizes thermal convection to promote temperature stability.

The results of temperature modeling for two slot designs are also shown in the figure. To have the supercooled silicon relatively stable, so that it will not freeze spontaneously, it must be confined to only a portion of the whole melt; the liquid silicon in contact with the container must be above the melting temperature (1,693 K) to avoid nucleation and freezing.

Slot A generates a supercooled temperature profile that is flat over a distance greater than 6 cm. This is verified by temperature probes of the melt and by the fact that dendritic web more than 4.2 cm wide has been grown from this slot. The web was still increasing in width when growth was terminated.

This work was done by Ray Seidensticker of Westinghouse Electric Corp. for NASA's Jet Propulsion Laboratory. For further information, Circle 72 on the TSP Request Card. NPO-14859

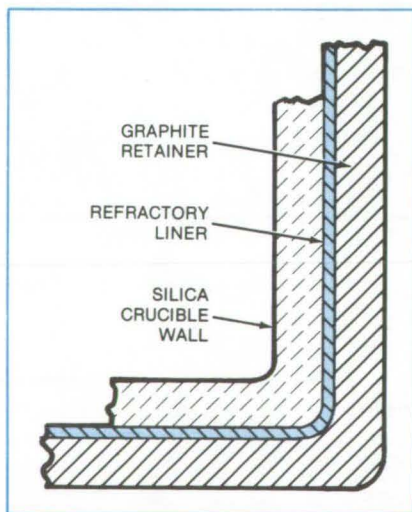


**The Elongated Geometry** of the susceptor/crucible/lid assembly allows molten silicon to supercool — a necessary condition for the growth of dendritic crystal ribbon. The curves at the right show how the surface temperature of the melted silicon depends on the shape of the slot in the lid. Crystals 4.2 cm wide were grown from this crucible, whereas the upper limit on width for a previous round susceptor was 2.5 cm.

## Refractories Keep Silicon Crystals Pure

Substitution of other refractories for graphite prevents the formation of silicon carbide.

NASA's Jet Propulsion Laboratory, Pasadena, California



**The Formation of Carbon Monoxide Gas** (which gives rise to silicon carbide impurities in the melt) is prevented by a liner of refractory material that is free of elemental carbon. For pressures above about 4 torr, silicon carbide can be used as the refractory liner.

In the vacuum growth of silicon crystals using the Czochralski method or the heat-exchanger method, unwanted silicon carbide impurities may contaminate the silicon crystals. This contamination is prevented by substituting other refractory materials for the graphite elements in contact with silica elements.

The crucible containing the silicon melt is generally made of silica (silicon dioxide). The support for the crucible and the retainer around it are generally made of graphite. When silica and carbon are in contact or close proximity at about 1,700 K, as in silicon crystal growth, carbon monoxide is generated by the reactions



The carbon monoxide gas, however produced, can travel from the region where it is produced to the silicon melt. There, silicon carbide is formed by the reaction



since silicon carbide is more stable

than carbon monoxide.

The replacement of graphite elements in close proximity to the silica crucible with other refractories, such as molybdenum, tantalum, or tungsten, prevents the generation of carbon monoxide gas. The same result is effected by coating the outside of the silica crucible or the inside of the graphite retainer and support with one of these refractories, as shown in the figure.

The problem of carbide contamination can arise in the crystal growth of any material that forms a carbide more stable than carbon monoxide. The prevention of carbide contamination in such cases is possible by using noncarbon refractories in place of graphite.

This work was done by Frederick Schmid and Chandra P. Khattak of Crystal Systems, Inc., for NASA's Jet Propulsion Laboratory. For further information, Circle 73 on the TSP Request Card.

NPO-14820

## Improved Facility for Producing Silicon Web

New equipment produces a fourfold increase in the width of a continuous dendritic silicon web.

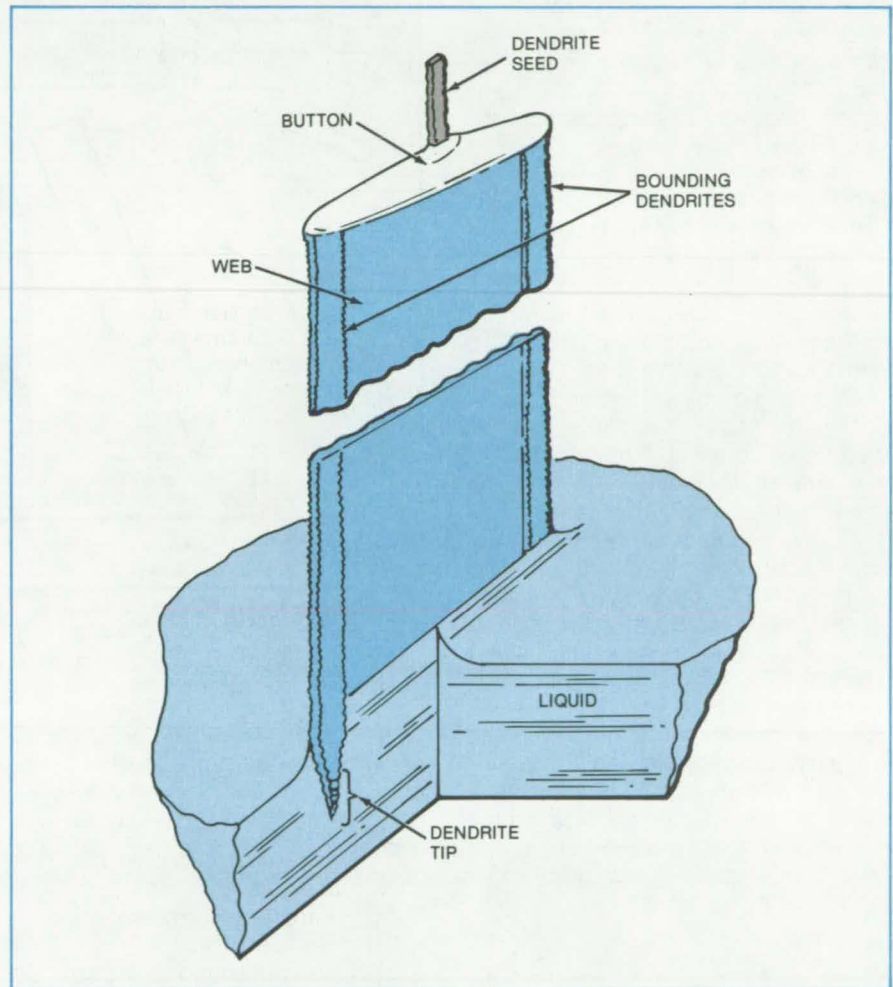
*NASA's Jet Propulsion Laboratory, Pasadena, California*

Facilities developed for NASA's Jet Propulsion Laboratory grow continuous silicon dendritic web that is up to 5 cm wide instead of only 1.3 cm as in the past. The silicon web or ribbon crystal may be used to make inexpensive solar cells and other solid-state devices. It is formed by the freezing of supercooled liquid silicon supported between two needlelike dendritic crystals, as shown in the figure.

Growth takes place in a work chamber filled with argon gas. As the web grows, it is drawn out of the chamber through a duct and guided to a storage reel. (Argon flows out of the web-withdrawal duct to prevent the diffusion of air into the growth chamber.) There are several hermetic penetrations into the chamber — for electrical power, cooling water, temperature sensors, heating-coil positioner, and web positioner. Viewports are also built in, to let the equipment operator watch the growth process.

Because growth of the wide web requires a large susceptor and crucible, the induction heating coil (work coil) is located inside the chamber for efficient electromagnetic coupling. Having the coil in the argon atmosphere, however, makes it necessary to use a low frequency for the heating (10 kHz instead of 450 kHz) to avoid corona and voltage breakdown in the argon.

The new apparatus has the capability for ribbon widths as great as 5 cm in one version, and as great as 10 cm in another design. The 5-cm version has been constructed and has thus far produced web 4.1 cm wide. The 10-cm design has not been constructed.



This Section of Silicon Dendritic Web Growth shows the formation of the web between two needlelike dendrite rods.

*This work was done by C. S. Duncan of Westinghouse Electric Corp. for NASA's Jet Propulsion Laboratory.*

*For further information, Circle 74 on the TSP Request Card. NPO-14860*

### Plasma Deposition of Amorphous Silicon

Strongly adhering films of silicon are deposited directly on glass and aluminum substrates by a nonequilibrium plasma jet. The amorphous silicon films are formed by the decomposition of silicon tetrachloride or trichlorosilane in the plasma. (See page 42.)

### Ball-and-Socket Joint Can Be Disassembled

A new ball-and-socket joint is disassembled simply by depressing a latch. Nonetheless, it is rigid and structurally sound when assembled. It can be modified to incorporate electrical or optical cables. Possible applications are in assembling scaffolds and other temporary structures. (See page 82.)

### Improved Fire-Resistant Resins for Laminates

Composites fabricated with new phosphorus-containing resins resist heat, fire, solvents, and chemicals. The mechanical properties of composite laminates can be varied by using different components for the resins, which can be used as adhesives and as matrix materials. (See page 56.)

## Automatic Control of Silicon Melt Level

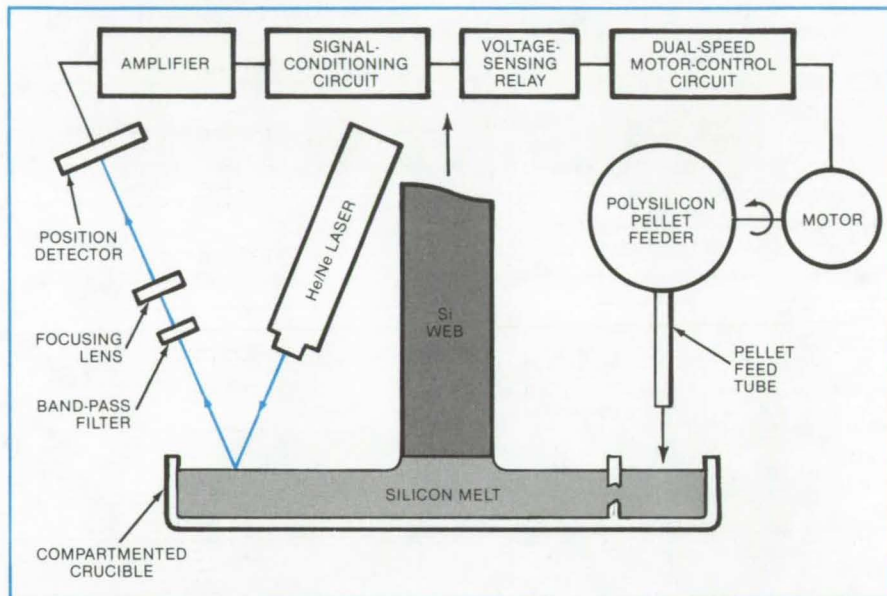
Maintaining a constant level during the growth of a dendritic web improves growth speed and web quality.

NASA's Jet Propulsion Laboratory, Pasadena, California

Automatic control of the melt level can reduce costs in dendritic-web growth of ribbon silicon crystals. The rate of growth, growth quality, and labor costs are all dependent on the melt level.

When combined with a melt-replenishment system and a melt-level sensor, a new circuit offers continuous closed-loop automatic control of the melt level during web growth. Shown in the accompanying block diagram, the circuit installed on a silicon-web furnace controls the melt level to within 0.1 mm for as long as 8 hours. It automatically selects either of two predetermined melt-replenishment rates, as required, to hold the melt level constant. One rate is less than the expected web-growth rate and the other is greater.

The circuit includes a manual signal-level adjustment, which adjusts the sensitivity of the system, and a manual offset adjustment, which furnishes a reference level to match the speed-selecting relay. A modified commercial motor-speed regulator controls a dc shunt motor that drives a pellet feeder. An interlock between the circuit and the clutch switch in the web drive stops melt replenishment if web growth is stopped.



This **Closed-Loop Circuit**, shown as a block diagram, controls the level of the silicon melt to within 0.1 mm during the growth of dendritic silicon web, thus improving growth rate and web quality. The level is sensed by monitoring the position of a laser beam reflected from the surface of the molten silicon.

In addition to affording greater area growth rate and higher web quality, automatic melt-level control also allows semiautomatic growth of the web over long periods. The semiautomatic operation can greatly reduce costs.

This work was done by C. S. Duncan and W. B. Stickel of Westinghouse Electric Corp. for NASA's Jet Propulsion Laboratory. For further information, Circle 75 on the TSP Request Card. NPO-15487

## Temperature-Controlled Support for a Seed Crystal

A mounting assembly has thermoelectric modules that determine the temperature of the seed during crystal growth.

Marshall Space Flight Center, Alabama

A rodlike structure has been proposed for supporting a seed crystal at the center of a body of saturated fluid and for controlling the temperature/time profile of the seed for experiments on crystal growth. The support is called a sting, taking its name from the thin rod used for mounting an aerodynamic test model in a wind tunnel. It was originally conceived for growing triglycine sulfate crystals in space.

The sting assembly consists of a gold-covered copper tip surrounded by a sheath of inert polymer such as tetrafluoroethylene (TFE), thermoelectric modules, a copper heat sink, platinum temperature sensors, a tubular heat pipe, and copper cooling fins (see figure). The thermoelectric modules pump heat away from the sting tip or to it, depending on the direction of current flow. The seed crystal is at-

tached to the temperature-controlled tip by an adhesive that has high thermal conductivity. The heat sink, heat pipe, and cooling fins offer a thermally conducting path for dissipating heat drawn from the tip by the thermoelectrics.

The sheath around the sting tip has low thermal conductivity and tends to assume the temperature of the surrounding solution. Therefore the seed

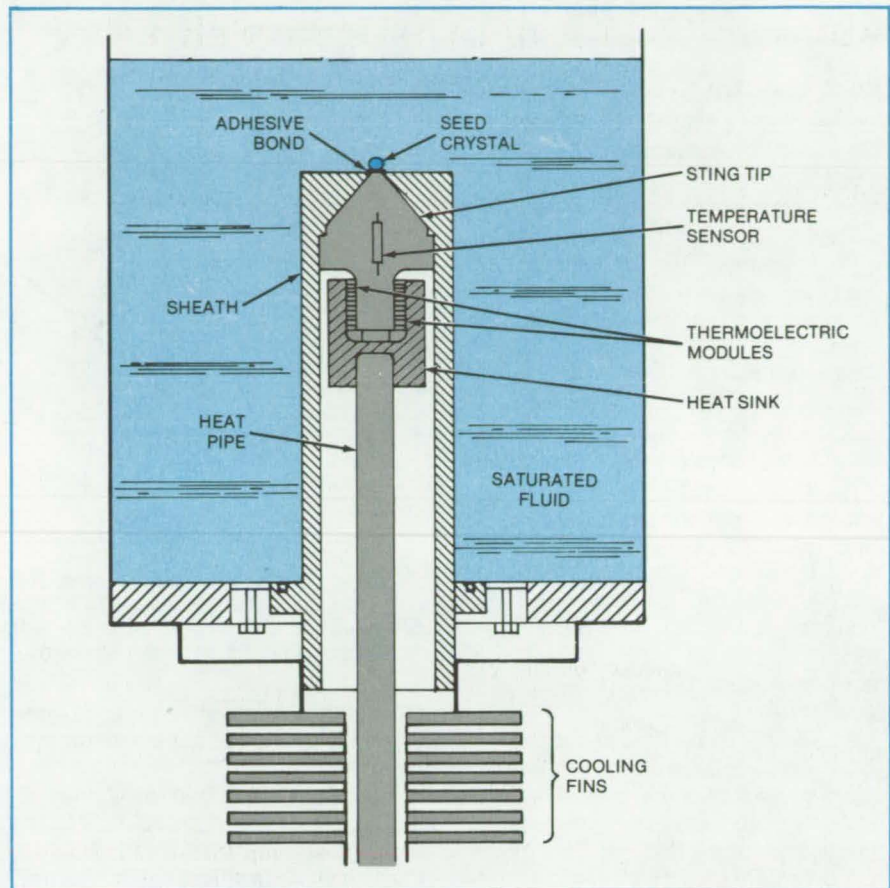
crystal attached to the tip is the only cold spot in the saturated fluid mass, which is a sufficient condition for crystal growth. The warmer sheath tends to suppress the nucleation of unwanted crystals near the seed crystal.

The temperature of the seed, and of the growing crystal, is monitored by the platinum temperature sensors. For triglycine sulfate, the temperature range is from 25° to 60° C, with an accuracy of  $\pm 0.1^\circ$  C. Heat is removed to maintain the crystal-seed temperature 5° C below the fluid temperature. For some conditions, a sting temperature as much as 50° C below the crystal-surface temperature is required.

The proposed circuitry for the sting consists of the sensors, two analog-to-digital converters (ADC's), and drivers for the thermoelectric modules. The ADC's convert the sensor outputs to a binary number that is compared to predetermined temperature profiles. The temperature error is compensated for by a control algorithm that commands the drivers to adjust the power to the thermoelectric modules.

*This work was done by James L. Reeve of TRW, Inc., for Marshall Space Flight Center. For further information, Circle 76 on the TSP Request Card.*

*Inquiries concerning rights for the commercial use of this invention should be addressed to the Patent Counsel, [see page A5]. Refer to MFS-25341.*



The **Seed Crystal** is cooled or heated by thermoelectric modules while the surrounding sheath remains at solution temperature. Heat is withdrawn to the cooling fins by the heat pipe, which replaces a solid copper rod in a previous design.

## Fiber-Reinforced Slip Castings

The addition of hyperpure silica fibers eliminates cracking and reduces shrinkage in thick ceramic castings.

*Ames Research Center, Moffett Field, California*

The addition of silica fibers greatly reduces shrinkage and cracking during the casting of ceramics. Fiber-reinforced slip-cast silica ceramics are also tougher and have lower dielectric loss. The fiber-reinforcement method was originally developed for the thick heat shield of a Jupiter probe. It is potentially applicable to radomes, heat reflectors, furnace parts, and laboratory ware.

The silica fibers are hyperpure material containing only 1 part per million total metal-ion impurities. The

hyperpure fibers ensure high reflectance (important in the space probe) and allow the casting to be fired at a temperature greater than 2,200° F (1,204° C) without a loss of strength from devitrification.

The hyperpure silica is commercially available as a loose wool consisting of extremely long fibers ranging in diameter from 3 to 7 micrometers. The wool is chopped in a blender to an average fiber length of 0.050 inch (0.127 centimeter). To prevent the introduction of metallic

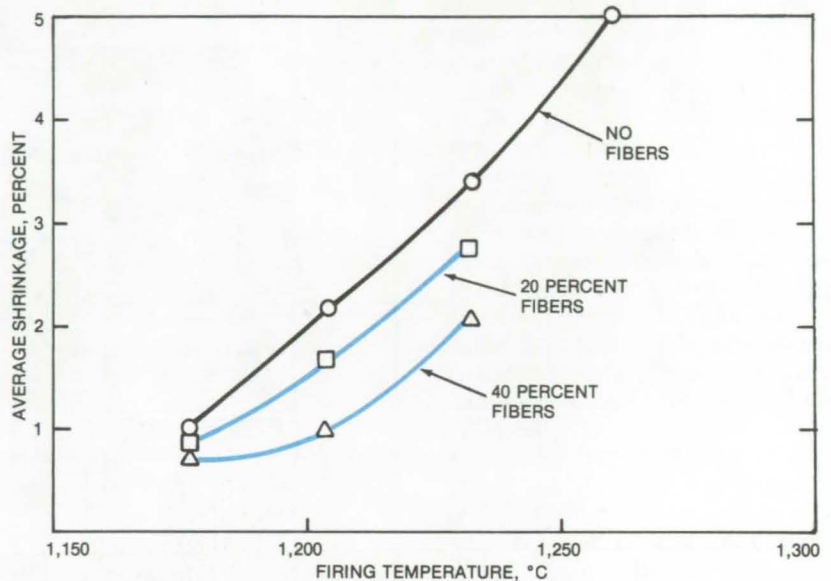
impurities into the fibers, the inside surfaces of the stainless-steel blender cup and lid are coated with polytetrafluoroethylene, and a plastic blade is substituted for the standard stainless-steel blade. A batch of 30 g of fiber is chopped in 2,000 g of deionized water for 20 seconds. The wet chopped fibers are spread out as a cake on a nylon screen and dried at 1,000° F (540° C) to drive off organic contaminants.

(continued on next page)

Next, the chopped fibers are added to a previously prepared slip (a suspension of uniformly-sized silica grains in water). So that the fibers can be adequately wet and dispersed in the slip, it is necessary to add them in small increments (5 percent of the grain solids weight) to a dilute (50-percent) suspension of the grains in water. Because the chopped fibers are extremely fluffy, the slip becomes viscous and lumpy (like cottage cheese) after each fiber addition. When all the fibers are wet, the slip returns to a smooth viscous state.

After the fibers have been added, water is evaporated from the slip to bring it to 78 percent solids content, the proper composition for casting. As much as 50 percent of fiber reinforcement by weight can be added. The shrinkage of a casting (and its tendency to crack) decreases substantially as the fiber content is increased up to the 50-percent level (see figure).

An alternative method of decreasing shrinkage — by adding large-grain silica instead of silica fibers — was found to be unsatisfactory because it produces a brittle casting. The fiber-reinforcement method increased casting toughness 2.6 times because of



**Shrinkage Is Reduced** as more silica fibers are added to a silica grain suspension. The fibers also increase the strength and toughness of the casting.

the higher ultimate strength and higher strain to failure of the fiber-reinforced material.

This work was done by James C. Blome, David N. Drennan, and Harlow M. Keeser of McDonnell Douglas Corp. for **Ames Research Center**. Further information, may be found in

NASA CR-152117 [N79-29333], "Development, Fabrication, and Test of a High Purity Silica Heat Shield," [\$11]. A copy may be purchased [prepayment required] from the National Technical Information Service, Springfield, Virginia 22151. ARC-11279

## Fluxless Brazing of Large Structural Panels

High quality, heat-treated aluminum assemblies are produced without fluxes or heat-treat fixtures.

*Langley Research Center, Hampton, Virginia*

Fluxless brazing is used in fabricating aluminum structural panels that withstand high internal pressure. Aluminum sheet of structural thickness (e.g., 0.032 inches or 0.81 mm) with 4045 aluminum/silicon-braze-alloy cladding is brazed to corrugated "fin stock" [e.g., 0.005-inch, (0.1-mm) aluminum alloy] having channels 0.001 inch (0.03 mm) high by the same width. The process is carried out in an inert (argon) atmosphere in a retort furnace. Filler bars are used in some channels to prevent the fin stock from collapsing as pressure is applied (see

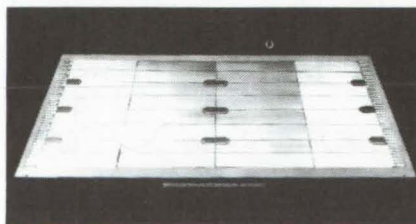


Figure 1. **Prior to Brazing**, fin stock is positioned on cover stock. Filler bars run the length of the panel to hold the fin stock in place. The comblike areas at the ends of the plate admit coolant to the panel passages.

Figure 1). Supporting edge stringers and structural supports could also be part of the panel design, and brazing to these elements would be done in the same operation.

Aluminum brazing is often used when fabricating assemblies with many large joints. Two brazing methods have been used: The first, salt-bath brazing, has the disadvantage that the salt is highly corrosive to aluminum if even a minute amount is left on the assembly, and extensive care in post-braze cleaning is essential. The second method, commonly

referred to as fluxless brazing, generally consists of brazing aluminum assemblies without using corrosive fluxes. Fluxless brazing is usually preferred where in-service inspection is not possible or where corrosion could cause catastrophic failure.

The sandwich assembly is brazed at approximately 1,055° to 1,095° F (570° to 590° C) at a pressure of from 150 to 200 psi ( $1.0 \times 10^6$  to  $1.4 \times 10^6$  N/m<sup>2</sup>). Braze tooling is isolated from the panel by thin wafers of oxidized stainless steel at all areas of contact. Thus, the tooling is easily removed from the panel without "parting" agents, which can contaminate the structure.

After brazing, panels are heat treated by quenching in a solution of 76 percent water and 24 percent UCON-A (Registered trademark of Union Carbide Corp.) or equivalent. The latter is a polymer that helps to provide a more uniform flow of heat from the article being quenched, thereby minimizing warping and distortion caused by thermal stresses. No

heat-treat fixture is necessary for this operation.

After quenching, the panel is kept at a low temperature (typically by packing in dry ice) until the top elements are welded to the coolant manifolds. Prior to the welding of the top elements, the bottom manifold elements are stressed so as to oppose the thermal-stress caused by the welding heat.

After welding is complete, machining or straightening may be required to compensate for warping and distortion not prevented by prestressing the weld

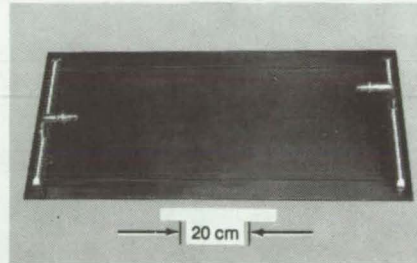


Figure 2. A Completed Panel with coolant manifolds affixed is shown here. Panels are aged to T-6 temper.

area. A completed panel, which was aged to the T-6 temper, is shown in Figure 2.

The process fabricates heat-treated panels without using fluxes or heat-treat fixtures. Maintaining the material at low temperature from the time of heat treatment until after final welding increases the quality of the final welds. Prestressing the areas of final weldment to counter normal warping eliminates the need for high-pressure fixtures or excessive machining of welded areas, while resulting in panels that conform closely to design specifications.

This work was done by Charles S. Beuyukian of Rockwell International Corp. for Langley Research Center. Further information may be found in NASA CR-3159 [N79-31628/NSP], "Actively Cooled Plate Fin Sandwich Structural Panels for Hypersonic Aircraft" [\$14]. A copy may be purchased [prepayment required] from the National Technical Information Service, Springfield, Virginia 22161. LAR-12519

## Weatherproof Crimp Connector

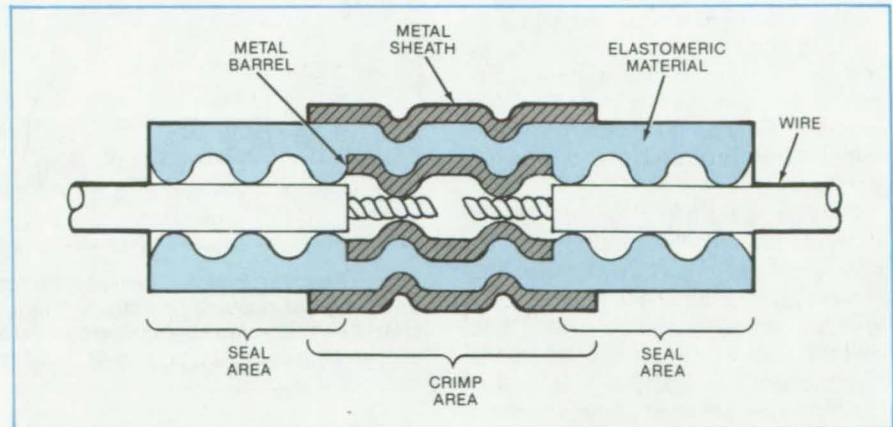
Proposed electrical connector would be inexpensive, easy to install, and durable.

NASA's Jet Propulsion Laboratory, Pasadena, California

A concept for an electrical connector combines the environmental durability of a sealed connection with the simplicity and economy of a crimped connection. The device should provide convenient and reliable outdoor electrical connections — for example, between an array of photovoltaic solar cells and a dwelling.

The connector includes a malleable metal barrel covered with an elastomer such as neoprene or silicone (see figure). The tubelike elastomer fits tightly around wires inserted at either end, providing a weathertight seal.

The center portion of the connector is crimped to create an electrical path between the inserted wires through the metal barrel. A sheath of thin-gage metal on the outside of the elastomer



**Environmental Durability and Crimpability** are ensured by the elastomer tube and metal barrel. An external metal sheath protects the elastomer from damage during crimping.

tube protects the elastomer from being pierced by the crimping tool.

This work was done by Frank J. Mosna of Motorola, Inc., for NASA's

**Jet Propulsion Laboratory.** For further information, Circle 77 on the TSP Request Card. NPO-15497

## Capacitively-Heated Fluidized Bed

Preferential heating of seed particles aids silicon production.

NASA's Jet Propulsion Laboratory, Pasadena, California

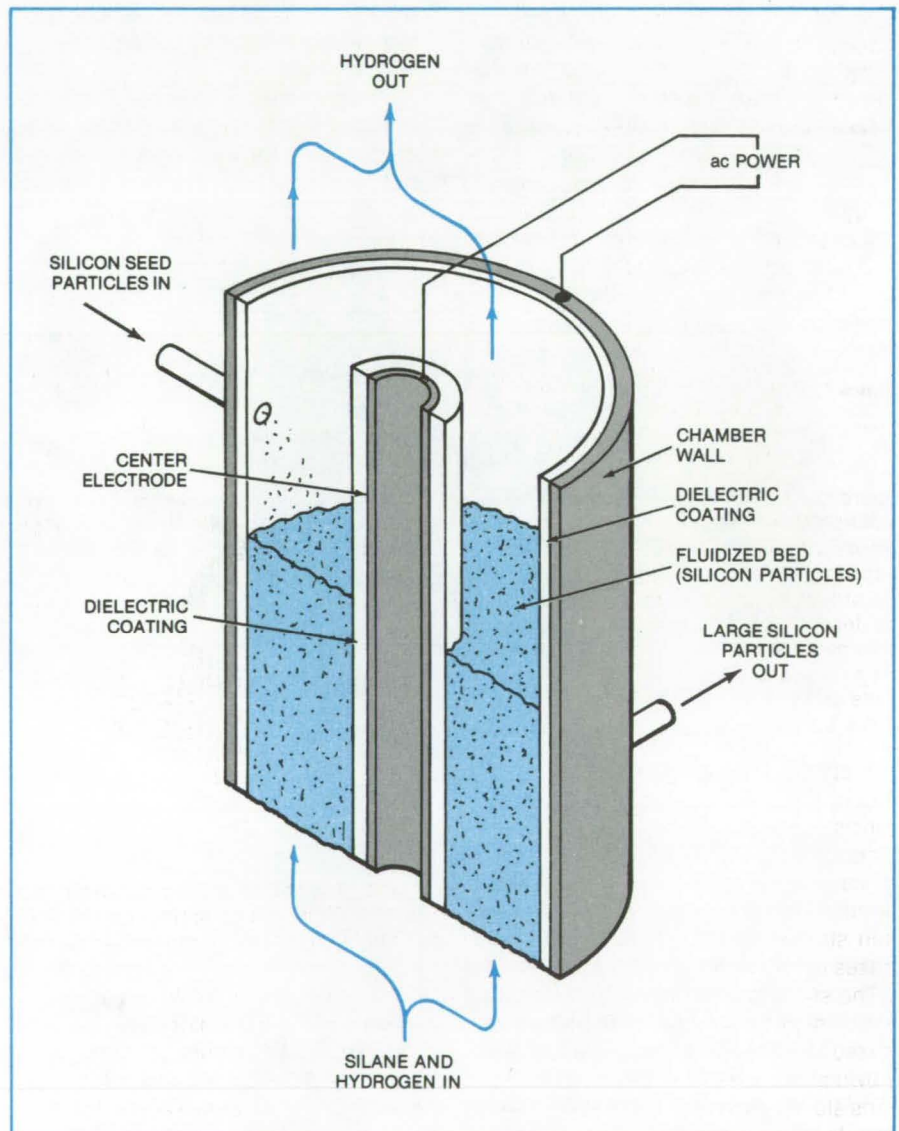
A fluidized-bed chamber in which the particles in the bed are capacitively heated produces high yields of polycrystalline silicon for semiconductor devices. The deposition of unrecoverable silicon on the chamber wall is reduced, and the amount of recoverable silicon depositing on seed particles in the bed is increased. Moreover, the particles have a size and density suitable for direct handling without consolidation, unlike the silicon dust produced in heated-wall chambers.

As in other silicon fluidized-bed chambers, a stream of silane ( $\text{SiH}_4$ ) and hydrogen flows through a mass of silicon particles, suspending and agitating them so that they form a fluidlike bed. The particles are heated to a temperature between  $550^\circ$  and  $1,000^\circ$  C. The silane decomposes, depositing silicon on the hot silicon particles. The heavier particles with deposited layers are continuously withdrawn from the chamber, and the seed particles are continuously replenished.

The particles in the new chamber (see figure) are maintained at the reaction temperature by capacitive heating. The chamber wall and a central electrode are connected to an alternating-current supply. Both the wall and the central electrode are coated with a dielectric material such as quartz or alumina. The alternating potential between the central electrode and the wall creates alternating currents within the particles, and the currents heat the particles.

Previously, the particles were heated indirectly, through the chamber wall, by an external gas or electrical heater. Silicon was deposited on the hot chamber wall, as well as on the seed particles, and the silicon on the wall was lost to the process. In addition, the silane tended to decompose homogeneously without a particle or wall substrate and to form a silicon powder that was too light and fine for further processing.

While the heavier silicon particles are removed from the bottom of the fluidized bed, hydrogen gas flows from the top of the bed. This gas is a mixture of the hydrogen that entered the bed with the silane (and diluted it to the re-



**Silicon Seed Particles Are Heated Preferentially** by capacitively-coupled alternating currents. Typical operating conditions during one test run were:  $350 \text{ cm}^3$  of silicon particles piled 15.8 cm deep, fluidization pressure of 9.2 in.  $\text{H}_2\text{O}$  ( $2,300 \text{ N/m}^2$ ), 44 volts at 75 kHz, and inlet gas temperature  $487^\circ$  C. The particle temperature was raised to  $785^\circ$  C by capacitive heating.

quired chemical concentration) and the hydrogen released by the decomposition of the silane to silicon. The gas is recycled to the fluidized bed, and some of it may be extracted for other uses, such as the preparation of silane feedstock.

As alternatives to silane, halosilanes, such as tetrachlorosilane, may be used

as reactants. These compounds are cheaper than silane, but release corrosive gases when they decompose.

This work was done by E. J. McHale of Union Carbide Corp. for NASA's Jet Propulsion Laboratory. For further information, Circle 78 on the TSP Request Card. NPO-14912



# Shaping Transistor Leads for Better Solder Joints

A handtool steps the leads without stressing the connections to the ceramic package.

Lyndon B. Johnson Space Center, Houston, Texas

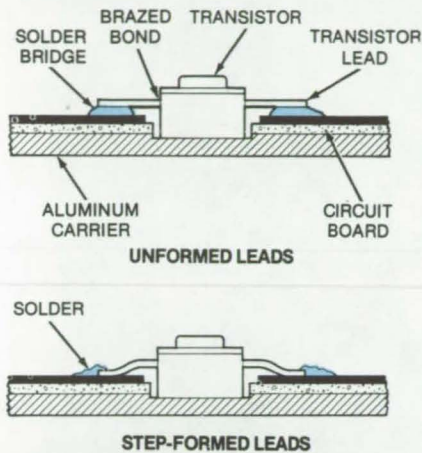


Figure 1. **Reliable Solder Connections** between transistor leads and circuit boards are made possible by forming steps in the leads. The steps also relieve the strain for the brazed joint between the leads and the transistor package. Unformed leads and poor solder connections are shown at the top; formed leads and good connections are shown at the bottom.

A special lead-forming tool puts a step in the leads of microwave power transistors without damaging the braze joints that fasten the leads to the package. The stepped leads are soldered to circuit boards more reliably than straight leads, and stress on the brazes is relieved.

The straight flat leads of a metal/ceramic high-frequency transistor are brazed to the ceramic package as shown at the top of Figure 1. When the transistor is installed, the leads generally do not make contact with the soldering areas on the circuit board but clear them by 0.005 to 0.020 inch (0.1 to 0.5 mm). In the past, the leads were attached by a solder bridge; however, the solder joints failed after thermal cycling, and the brazed lead-to-ceramic bonds often cracked.

To minimize the solder gap between the leads and the board and to relieve strain at the lead brazes, the stepped lead and improved solder joint shown at the bottom of the figure are used. The new tool forms the step without

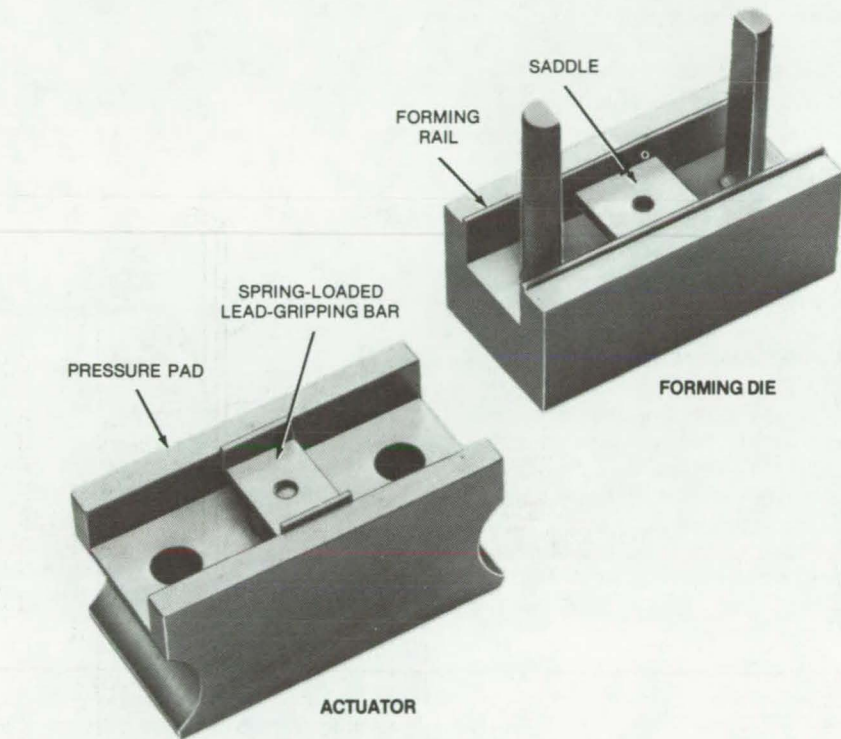


Figure 2. The **Lead-Forming Handtool** has two parts: a forming die, shown at the right, and an actuator. The spring-loaded saddle is adjusted so that when the transistor package is placed on it, the leads rest on the forming rails.

straining the braze joint where the lead is bonded in the transistor package.

As shown in Figure 2, the tool consists of an actuator and a forming die with an adjustable saddle for the transistor. Both the saddle and the actuator are spring-loaded to prevent bending, twisting, or pulling of the transistor leads.

The first step in using the lead-forming tool is measuring the seating of the transistor in the saddle and measuring the lead position on the forming rail. The tool is adjusted, using the screw on the base of the forming die, so that the transistor leads are just seated on the form rails. The actuator is then placed over the forming die and transistor.

Thumb pressure is applied to form the step in the leads. The body of the transistor is supported in the saddle so that the leads are gripped and then formed without being peeled, twisted, or pulled. After forming the leads, the actuator is removed, and the transistor is carefully removed. In tests of transistors for the Space Shuttle payload-interrogator power amplifier, no failures occurred in the solder joints or in the brazed bonds when the stepped leads were soldered.

This work was done by Harold Mandel and John E. Dillon of TRW, Inc., for Johnson Space Center. For further information, including photographs and detailed drawings of the forming tool, Circle 79 on the TSP Request Card.  
MSC-18837

## Metallic Panels Would Insulate at 2,700° F

Insulation under development for the Space Shuttle could have other applications.

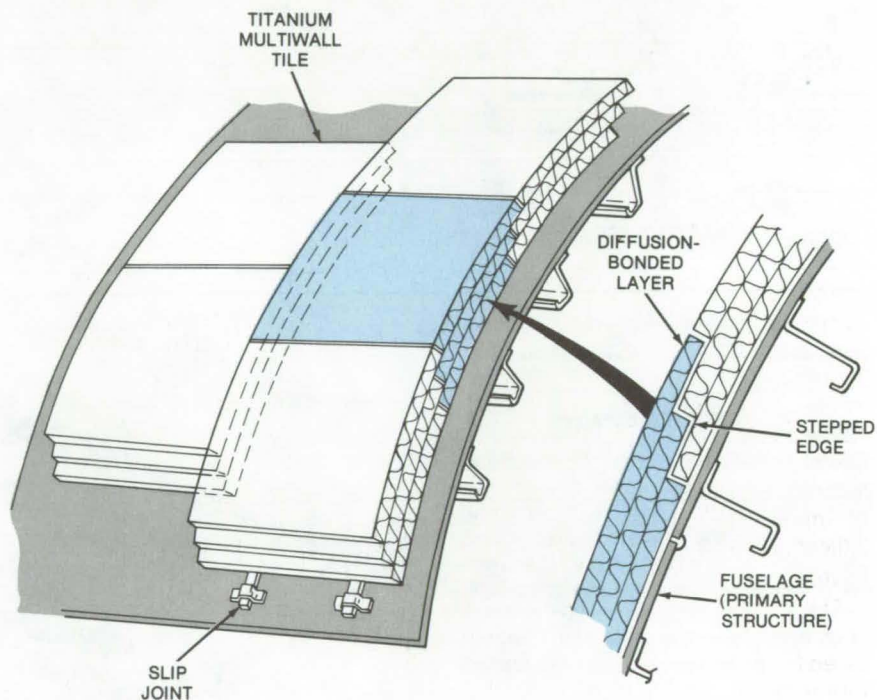
*Langley Research Center, Hampton, Virginia*

Multiwall metallic panels now under development as replacements for the ceramic surface-insulation tiles of the Space Shuttle could eventually be used in other aircraft and possibly even as thermal protection in ground-based applications. Various configurations of the basic multilayer sandwich are expected to protect against temperatures ranging from 700° to 2,700° F (370° to 1,480° C). With assistance from heat-pipe cooling, the panels should withstand temperatures to 3,500° F (1,930° C); however, the heat pipes would not exceed 1,600° F (870° C).

A major objective for the new panels is to survive the expected 100-mission lifetime of the Space Shuttle. They should be more durable than the fibrous or ceramic tiles, which have to be carefully monitored for surface fraying, erosion, and cracking. The new metal panels should withstand thermal and mechanical stresses better, without adding to the weight of the vehicle.

Each panel attaches to the primary structure with a bayonet mounting at its corners (see figure). This simple slip joint allows for expansion to relieve thermal stress. Furthermore, each panel is isolated from the strains of the primary structure, with adequate space for thermal expansion and mechanical tolerances. To prevent vibration, felt strips are compressed at the edges of the panels. Each panel is vented to the local static pressure through a hole in the felt strip at the trailing edge on the cooler surface.

The insulating panels have different structures, depending on the local temperature to be encountered. For the temperature range from 700° to 900° F (370° to 480° C), multiwall metal (usually titanium) panels consist of alternating flat and dimpled sheets, joined at dimple crests as shown in the figure. Heat conduction through these panels is minimal because the layers touch only at the dimple crests,



**Insulating Panels** are attached to a surface to protect the interior from high temperatures. In this illustration, the panels are multiwall in which layers of dimpled foil alternate with smooth ones, forming thousands of small cells within the panel.

resulting in a contact area less than 0.2 percent of the surface area. The long conduction path and low heat conductivity of titanium contribute to the thermal barrier. Radiative heat transfer is inhibited by the multiple layers, each of which is a radiation barrier. Heat transfer by convection is avoided by keeping the cells small. Gaseous conduction can be eliminated by evacuating the cells and sealing them; however, when vented they are weight-competitive with the ceramic tile system.

For the temperature range from 900° to 1,600° F (480° to 870° C), a metallic enclosure supports a fibrous insulating filling. The pressure loads are supported by either an outer foil-gage superalloy dimple-core sandwich or a superalloy honeycomb sandwich and an inner titanium

sandwich, joined by beaded edge seals.

For the range from 1,600° to 1,900° F (870° to 1,040° C), the outer sandwich is a superalloy honeycomb sandwich with a thicker facesheet to resist oxidation.

In the range of 1,900° to 2,200° F (1,040° to 1,200° C), the outer layer is a flanged waffle of oxidation-dispersion-strengthened alloy, which has excellent oxidation resistance.

At 2,200° to 2,700° F (1,200° to 1,480° C), the outer layer is a coated refractory-metal-flanged waffle or a rib-stiffened advanced-carbon/carbon panel. While the carbon/carbon is lighter in weight, the refractory metal panels may last longer due to better resistance to damage.

Nickel-alloy heat pipes can be used where localized heating may produce

temperatures as high as 3,500° F. The heat pipe would transfer the heat to a large, cooler area, from which it can be radiated; and the heat pipes operate at about 1,600° F for long life.

The basic technology required to produce the panels has been or is being developed, and models have

been built. They await large-scale testing of assemblies on representative structures.

This thermal protection system was conceived by L. Robert Jackson of **Langley Research Center**. For further information, Circle 80 on the TSP Request Card.

This invention is owned by NASA, and a patent application has been filed. Inquiries concerning nonexclusive or exclusive license for its commercial development should be addressed to the Patent Counsel, Langley Research Center [see page A5]. Refer to LAR-12620.

## Wire EDM for Refractory Materials

Computer-controlled wire electric-discharge machining yields high-quality surfaces.

*Lewis Research Center, Cleveland, Ohio*

Fabrication of such materials as high-strength/high-temperature alloys, carbides, and ceramics to small tolerances is generally a time-consuming and expensive operation. These materials usually require the use of broaching, milling, or grinding techniques. As strength requirements of materials increase, fabrication difficulties and costs usually keep pace.

The turbine blades and rotors of jet engines are one instance of parts fabricated from high-strength/high-temperature materials. In this application, precise matching of turbine blade roots and disks is necessary for optimum performance (see Figure 1).

In an attempt to reduce fabrication time and costs, the Wire Electrical Discharge Machine (Wire EDM) method was investigated as a tool for fabricating matched blade roots and disk slots. Eight high-strength nickel-base superalloys were used in this investigation. The computer-controlled Wire EDM technique provided high-quality surfaces with dimensional tolerances of  $\pm 0.005$  inch (0.1 mm) — see Figure 2. Fabrication cost of the experimental

blades and disks was also reduced by about 70 percent from that of standard fabrication techniques. Thus, the Wire EDM method offers the potential for substantial reductions in fabrication costs for "hard-to-machine" alloys and electrically conductive materials in specific high-precision applications.

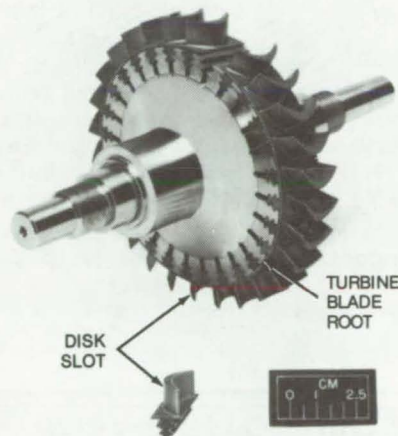


Figure 1. Turbine Blade Roots and Disk Slots are examples of jet-engine parts that are matched by Wire EDM.

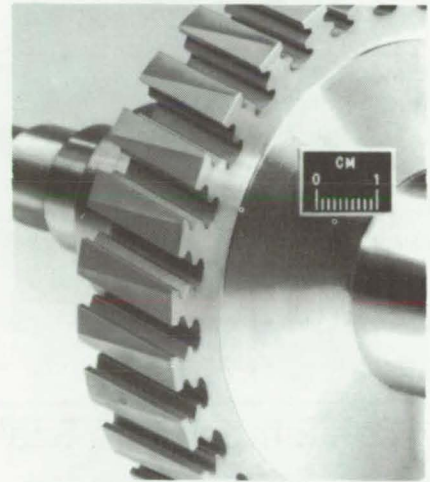


Figure 2. Dimensional Tolerances of 0.005 inch (0.1 mm) in high-strength, high-temperature material parts, such as turbine blade roots are possible with the Wire Electrical Discharge Machine method.

This work was done by G. R. Zellars, F. E. Harris, C. E. Lowell, W. M. Pollman, V. J. Rys, and R. J. Wills of **Lewis Research Center**. No further documentation is available. LEW-13460

## Heat Lamps Solder Solar Array Quickly

Heat lamps reflow-solder a solar-cell array held on a compliant vacuum platen.

*NASA's Jet Propulsion Laboratory, Pasadena, California*

All the interconnection tabs in a nine-solar-cell array have been soldered simultaneously with radiant heat. The cells and tabs are held in position for

soldering by sandwiching them between a compliant silicone-rubber vacuum platen and a transparent polyimide sealing membrane (see figure). Heat

lamps warm the cells, producing smooth, flat solder joints of high quality.

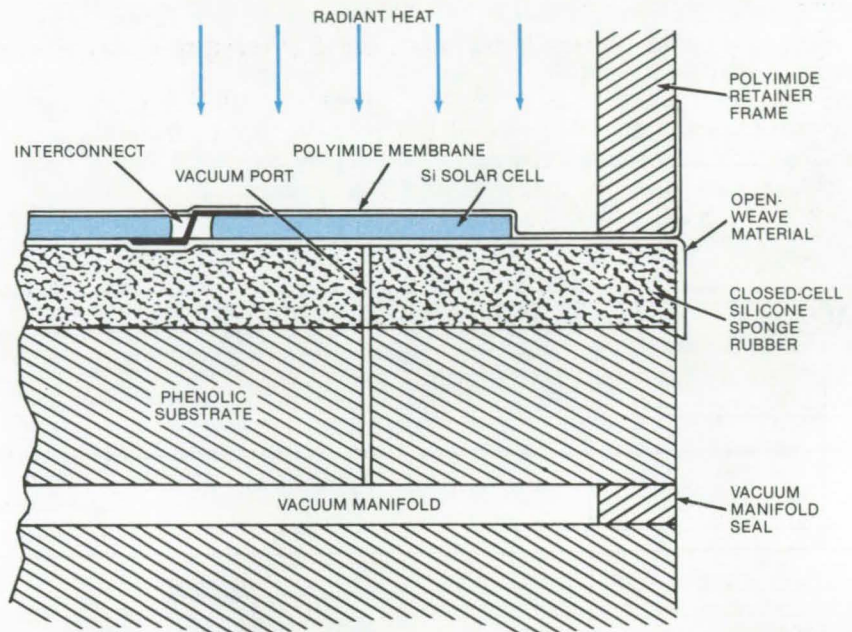
Development of the new radiant-heat soldering technique was motivated by

the excessive time and energy required by a conductive method previously used. Cells heated conductively are clamped between a silicone sponge-rubber pad and a heated aluminum plate. However, it takes about 4 minutes to heat the plate to soldering temperature. In addition, small solder lumps on the cells inhibit thermal contact and cause some of them to crack when clamped against the rigid plate. The faster radiant-heating method is preferable also because the silver/glass-frit screen-printed metalizations must be soldered quickly to prevent silver dewetting.

The antireflection coatings on the cells help the radiant-heating process. On exposure to the infrared lamps, the temperature rose from ambient to the 200° C soldering temperature in 45 seconds. Uncoated cells took five times longer to reach soldering temperature.

The new method is proposed for continuous manufacturing of 4-foot-square (1.2-meter-square) solar arrays. The arrays would pass under a bank of heat lamps at the rate of one every 45 seconds.

This work was done by Peter J. Coyle and Marvin S. Crouthamel of RCA



The **Radiant-Heat Mass-Soldering Fixture** for a nine-cell array has a 1-ft<sup>2</sup> (0.09-m<sup>2</sup>) sponge-rubber platen. A vacuum port is located under the center of each cell. Seven 375-W reflector heat lamps arranged in a close-packed hexagon 2.75 in. (7 cm) above the array heat the cells uniformly. The open-weave mesh, which could be stainless steel or aluminum, spreads the vacuum across the area under the cells.

Corp. for **NASA's Jet Propulsion Laboratory**. For further information, Circle 81 on the TSP Request Card.  
NPO-14866

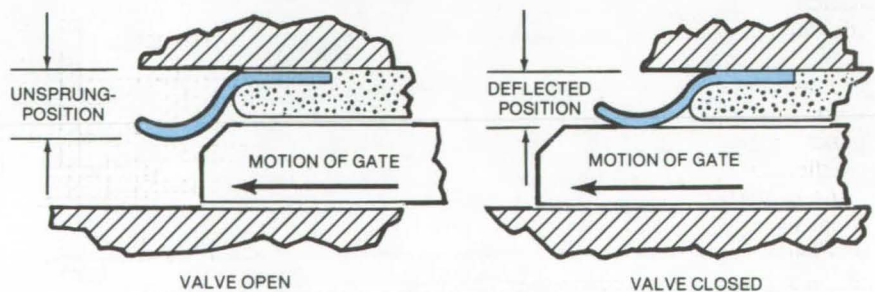
## High-Temperature Seal for Sliding-Gate Valve

A Belleville-spring seal operates reliably between -400° and +1,100° F.

Marshall Space Flight Center, Alabama

A sliding-gate valve originally developed for rocket exhaust-gas ducts is sealed by a Belleville spring. It is simple, compact, and operates over a wider range of temperatures — from about -400° to +1,100° F (-250° to +600° C) — than conventional O-ring-sealed valves.

As shown in the figure, the spring is not loaded when the gate is open. When the valve is closed, the beveled leading edge of the gate picks up the spring and deflects it; this loads the spring and thus seals the valve. The seal retains the advantages of slide valves: quick opening and closing, unobstructed flow, and low operating torque.



The **Spring Seal** on this sliding-gate valve applies a high unit loading to the gate with small spring deflection.

This work was done by Randall G. Leonard of Rockwell International

Corp. for **Marshall Space Flight Center**. No further documentation is available.  
MFS-19607

## Structural Modules Would Contain Transmission Lines

Electrical, fluid, and other lines would be encapsulated in proposed load-bearing elements.

Goddard Space Flight Center, Greenbelt, Maryland

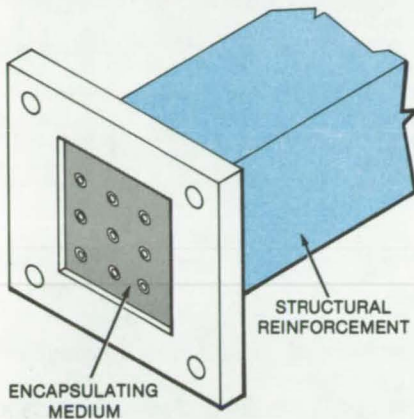


Figure 1. **Structural Reinforcement**, encapsulating medium, and wires would be common to members and fittings used for bearing structural loads.

The weight and cost of aircraft, ships, ground vehicles, and buildings could be reduced by incorporating as a part of the mechanical structure such hardware as electric wires, pneumatic lines, fiber optics, and hollow tubes for acoustic transmission. For example, an automobile could include wires, fuel lines, and heating and coolant lines all in one load-supporting structure.

The new proposal, originally suggested for spacecraft, is a set of uniformly-sized mass-producible modular structural elements that contain electric, fluid, and other transmission lines. Since the lines are encapsulated, they are less likely to be damaged. The module shell could be solid metal, sheet metal, honeycomb, fiberglass, plastic, composites, or wood.

An example of this proposal is electrical wiring integrated into structural elements (see Figure 1). Two types of modular elements are used: members and fittings. The members carry electrical signals from one location in a structure to another. Cross sections of the members are almost any shape, and they are either hollow or solid. The fittings transmit electrical signals from member to member and to external devices and sources; they interface with equipment platforms, vehicles, (continued on next page)

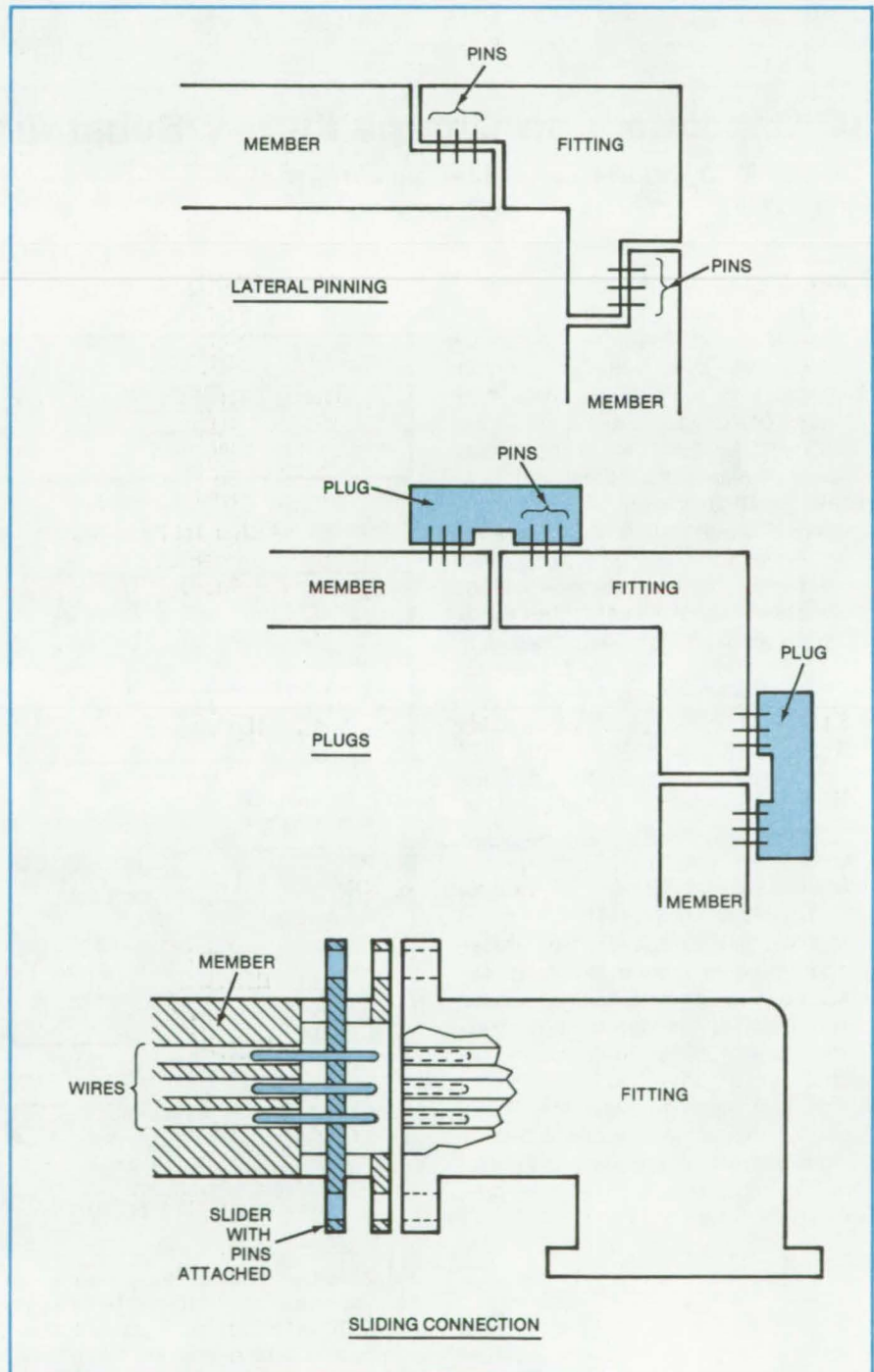


Figure 2. **Members and Fittings** could be connected in different ways. An advantage of using plugs is that wiring can be rerouted by simply changing a plug.

and base structures. To connect members and fittings mechanically, flanges and bolts, bonding, welding, soldering, riveting, and quick disconnects may be used.

Members and fittings both include wires, encapsulating material, and structural reinforcement. Connections for members and fittings include lateral pins, plugs, and sliding con-

nections, as well as straight couplings (see Figure 2). These all allow members and fittings to be replaced without having to physically move any adjacent structure.

In a straight connection, wires would run from one end of a member to the other and terminate at each end in a recessed socket. Adjacent modules would be connected electrically

through conducting pins. The recess would prevent electrical contact other than through the pins. Nonconducting pins, inserted in the remaining sockets, would add mechanical support.

*This work was done by William A. Leavy of Goddard Space Flight Center. For further information, Circle 82 on the TSP Request Card.*  
GSC-12523

## IC Capacitors on Groups III-to-V Substrates

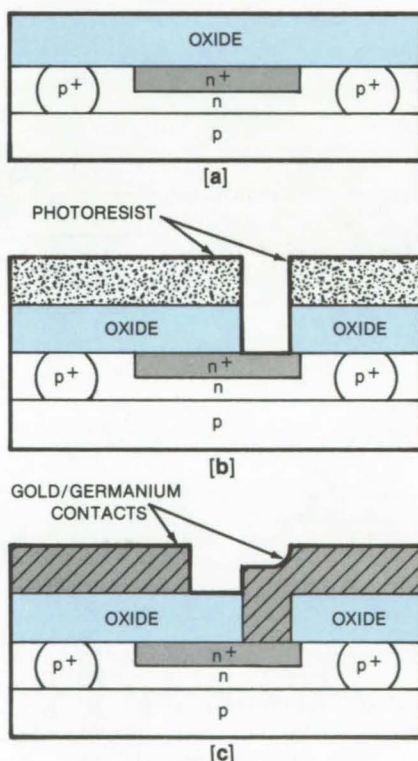
Dielectric layers are formed on gallium arsenide and indium phosphide by spin deposition.

*Goddard Space Flight Center, Greenbelt, Maryland*

Oxides applied by a "spin-on" process have been used to fabricate capacitors on gallium arsenide and indium phosphide substrates; they might also be used with other compounds of elements in groups III to V of the periodic table. The III-to-V materials are attractive for integrated circuits because they offer responses potentially six times faster than silicon.

In conventional silicon IC's, oxide layers for capacitors are thermally grown — that is, they are formed by exposing the silicon substrate to water vapor at a high temperature. This method is not practical for the III-to-V semiconductors because they decompose at temperatures required for the reaction (more than 600° C). Although oxides can be grown on III-to-V materials by electrochemical reaction at moderate temperature, such "anodic" dielectric layers are unstable, porous, and break down at low voltages. The commercially-available spin-on oxides are cured at 200° C, well below harmful temperature levels.

To fabricate a capacitor (see figure), the oxide suspension is applied at room temperature to the top



### NOTES:

1. p+ = ISOLATION REGION
2. n+ = BOTTOM CAPACITOR ELECTRODE
3. GOLD/GERMANIUM CONTACT AT THE LEFT IS THE TOP CAPACITOR ELECTRODE

**A "Spin-On" Oxide Suspension Is Formed** on a group III-to-V substrate, as in (a). After the oxide layer has been cured, a pit is etched in the oxide layer where it is not covered by a protective photoresist (b). Gold/germanium conductors are then deposited by photoresist etching to form capacitor electrodes (c).

surface of a substrate in which an electrode and isolation junctions have already been formed by ion-implantation. After the substrate is spun to distribute the suspension uniformly, the oxide is cured at 200° C so that it becomes a hard, firmly attached layer. Finally, a gold/germanium electrode and a contact to the substrate electrode are deposited by conventional photolithography.

Since various oxides can be used — for example, those of silicon, phosphorus, boron, aluminum, or titanium, with or without dopants — and since the oxides can be deposited in a range of thicknesses from less than 100 Å to greater than 5,000 Å, capacitances can be varied from very low to ultra high (about 580 pF). By choosing a spin-on oxide with a coefficient of expansion that matches that of the substrate, thermal stress and possible device failure are reduced.

*This work was done by George E. Alcorn and Robert Jones of Goddard Space Flight Center and Charles Leinkram of Bowie State College. For further information, Circle 83 on the TSP Request Card.*  
GSC-12543

## Levitor for Containerless Processing

Aerodynamic forces support objects while they are processed.

*Marshall Space Flight Center, Alabama*

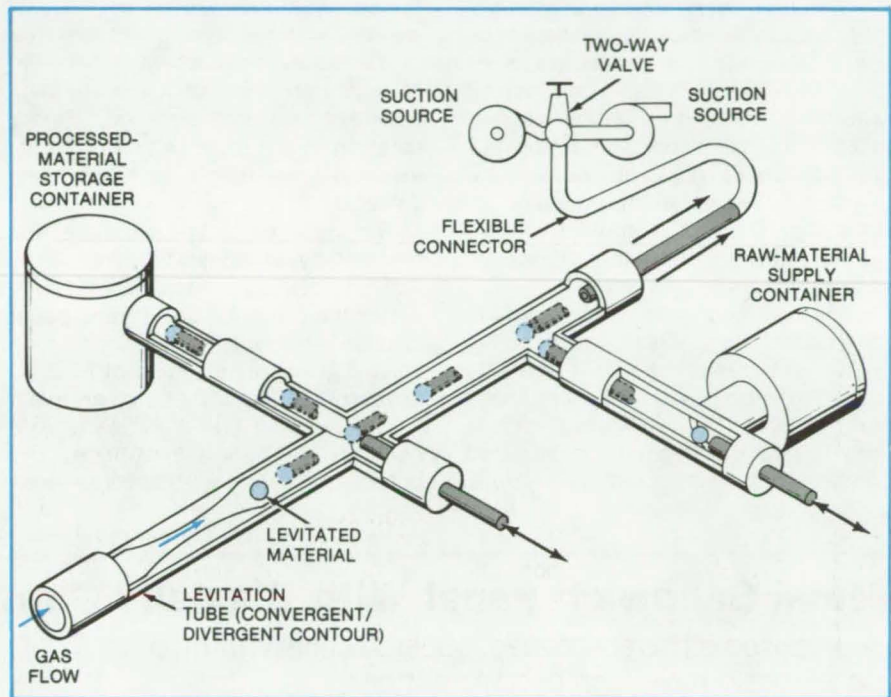
Objects are levitated by aerodynamic forces in an apparatus originally developed for space research but just as effective on Earth. Unlike previous designs for containerless materials processing, the new levitor is orientation-independent. It also works equally as well whether or not gravity is present.

Small spheres of glass 2 mm in diameter have already been processed at temperatures up to 1,200° C in a prototype levitor. When fully developed it will melt, mix, solidify, and even store materials. The levitated object could be a sphere or cylindrical solid, a powder, or a liquid; and it may be either electrically conducting or insulating.

The levitor is a tube containing identical converging and diverging sections on the upstream and downstream sides of a constriction (see figure). The flow and pressure are regulated so that the aerodynamic forces hold material at the downstream end of the diverging section. It is the unique shape of the tube that makes the aerodynamic forces in any direction greater than the weight of the object.

A tube in the downstream section sucks gas from the main tube or blows gas into it to influence the position of the material. Powders could be introduced through the internal tube to form alloys or to create multiple layers of immiscible materials on a fluid sphere. Slots can be added to the downstream section to remove or introduce gas for regulating or changing the position of the material.

Gas entering the convergent/divergent section must be free of turbulence and must have a uniform velocity distribution to create the aerodynamic environment for stable levitation. A series of antivortex



The **Levitation Apparatus** supports a sphere by aerodynamic forces from the gas flowing through the convergent/divergent section. The concentric inner tube is moved along the axis of the cylindrical housing. It is used to inject the sphere into the levitation volume, to introduce other raw material, and to apply suction or pressure to control the levitation. Only the levitation section has thus far been successfully tested.

screens could be placed in a stilling chamber preceding the levitor entrance, and flow-directing vanes could be placed in the upstream volume to modify the gas flow.

A pushrod would inject raw material from a supply container. Processed material would be ejected into another container. Powders or granular materials would be introduced by a ram or a revolving screw, and drops of liquid material would be inserted by a drop-forming nozzle. The gas flow would be reduced during drop injection so that the drop could be captured and stabilized.

The material can be heated to processing temperature by heating the flowing gas or by energy from an induction coil. Cooling gas can be injected through a slot.

*This work was done by L. H. Berge, W. A. Oran, and John M. Theiss of Marshall Space Flight Center. For further information, Circle 84 on the TSP Request Card.*

*Inquiries concerning rights for the commercial use of this invention should be addressed to the Patent Counsel, Marshall Space Flight Center [see page A5]. Refer to MFS-25509.*

## Sprayed Coating Renews Butyl Rubber

A sprayed coating renews worn butyl rubber products.

*John F. Kennedy Space Center, Florida*

Damaged butyl rubber products are renewed by a spray technique originally developed for protective suits worn by NASA workers. A commercial two-part adhesive (Stadhesive, or equivalent) is mixed with Freon-113 (or equivalent) trichlorotrifluoroethane to obtain the optimum viscosity for spraying. The mix is applied with an external-air-mix spray gun (Binks, or equivalent, with S-66 nozzle).

The method was developed to extend the service life of the protective butyl rubber suits worn by workers handling hypergolic (self-igniting) fuels and oxidizers. The suits in inventory are frequently repaired for localized abrasion, butyl thinning, and tears.

Previously, there was no economical way to coat large areas or entire suits.

The spray process is limited to replacing rubber worn off through extended use and cleaning. Before spraying, a suit must be free of holes, exposed inner fabric, or other basic defects.

The surfaces of the suits are first cleaned by abrading them with dry 320- to 360-grit sandpaper, then wiping them with Freon-113 and paper towels. The butyl mixture is then applied at a spray pressure of 70 to 80 psig (480,000 to 550,000 N/m<sup>2</sup>) with the nozzle held 1 to 3 inches (3 to 8 centimeters) from the surface. The optimum viscosity is 45 to 60 seconds

in a No. 4 Zahn cup. Sticky butyl cobwebs form if the nozzle is held too far from the surface.

Five of the suits were sealed, inflated, and given three coats each at half-hour intervals. They were then cured for 72 hours and field-tested in routine hypergolic operations. Only one minor defect, caused by inadequate surface preparation, was noted. No failures of the butyl coating were observed.

*This work was done by Robert B. Martin of Boeing Services International for Kennedy Space Center. No further documentation is available. KSC-11198*

## Metal Sandwich Panel With Biaxially Corrugated Core

A proposed diffusion-bonded, superplastically formed panel would have high bending stiffness.

*Dryden Flight Research Center, Edwards, California*

A biaxially-corrugated sandwich core, formed by concurrent diffusion bonding and superplastic deformation, would make a proposed sandwich panel unusually strong and stiff. The new panel should be useful in vehicle and other applications where a light-weight panel that resists bending is needed. [In diffusion bonding, component sheets are joined under pressure at high temperature without melting or the use of bonding agents. Superplasticity is the ability of a material such as titanium alloy to undergo large plastic deformations (up to 1,000 percent) at high temperatures without localized thinning or necking.]

Sandwich panels usually consist of two thin high-strength face sheets bonded to a relatively-thick low-density core. A common aerospace sandwich panel has a honeycomb core bonded to the face sheets along the lines of contact between them.

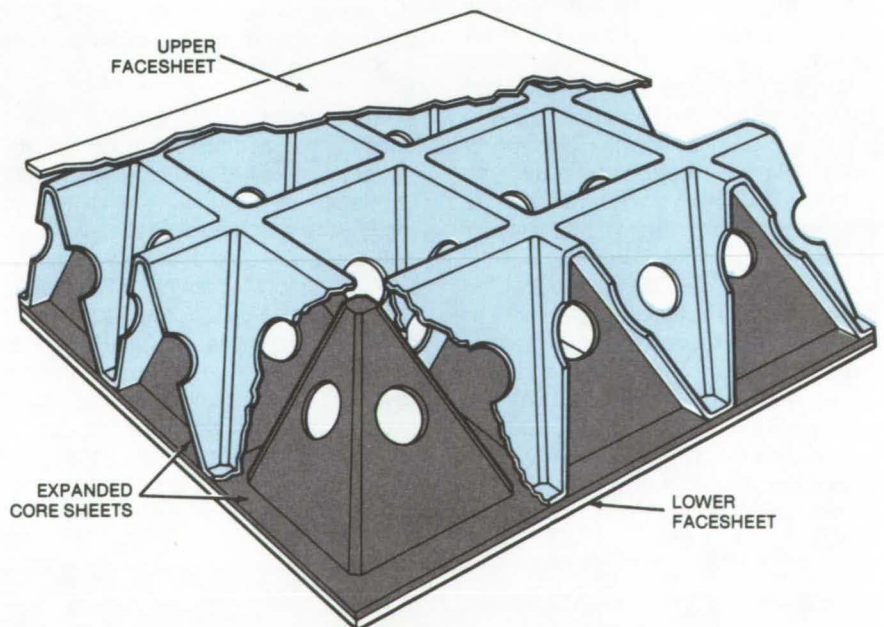


Figure 1. The **Metal Sandwich Panel** would have an internal core consisting of a multitude of hollow, truncated pyramids. The four layers of the panel would be diffusion-bonded at all contacting areas. The holes in the core are needed during the forming of the panel, as in Figure 2.



The new panel (see Figure 1) would consist of a biaxially corrugated core made of two titanium-alloy sheets sandwiched between facesheets of the same material. Each core sheet has a series of hollow, truncated, square pyramids made by superplastic expansion. The component sheets are diffusion-bonded to each other along their contacting areas. Since each rippled surface braces or stiffens the other, the resulting structure resists bending better than a single corrugated structure. Moreover, the bonded areas between the core sheets and the surface sheets are less prone to failure than are the lines of contact in honeycomb sandwich panels.

The sandwich panel would be formed from four flat titanium-alloy sheets (see Figure 2). A stopoff coating is applied to the square areas on the component sheets that are not to be diffusion-bonded. The component sheets pack is clamped in a die that is heated under high pressure to cause diffusion bonding along the linear surfaces between the stoppoff squares. While the component-sheets pack is still hot, an inert gas such as argon is injected by a gas jet at about 100 psi ( $6.9 \times 10^5 \text{ N/m}^2$ ). The gas passes through holes in the core sheets and presses the two facesheets into the die cavity. As the top facesheet rises, it draws the diffusion-bonded core sheets along with it.

*This work was done by William L. Ko of Dryden Flight Research Center. For further information, Circle 85 on the TSP Request Card.*

*This invention is owned by NASA, and a patent application has been filed. Inquiries concerning nonexclusive or exclusive license for its commercial development should be addressed to the Patent Counsel, Dryden Flight Research Center [see page A5]. Refer to FRC-11026.*

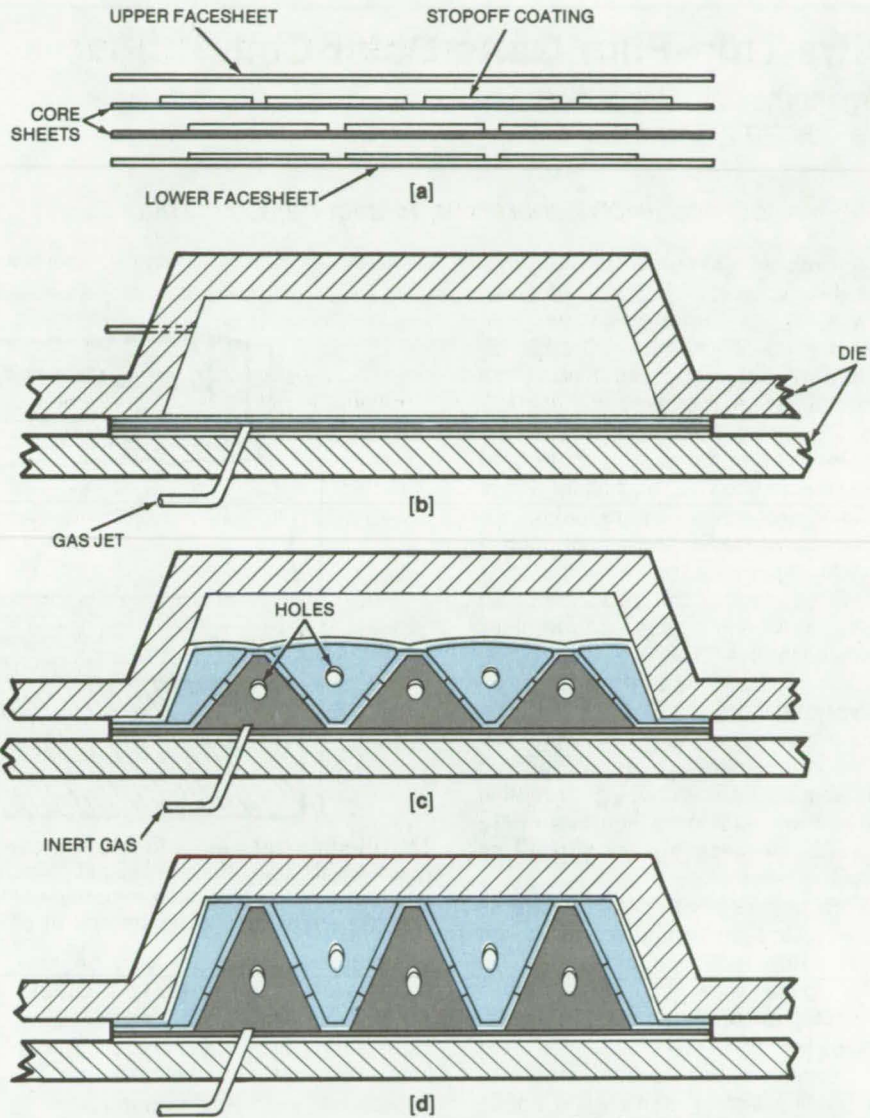


Figure 2. Panel Forming begins (a) with the stacking of the four component sheets of the sandwich. Stopoff coatings have been applied to the component sheets in areas that are not to be bonded. In (b), the component-sheets pack is clamped in a die that is heated under high pressure to cause diffusion bonding between layers in uncoated areas. With the titanium alloy used, both diffusion bonding and superplastic deformation occur at  $1,700^\circ \text{ F}$  ( $930^\circ \text{ C}$ ). In (c), the core of the panel undergoes superplastic deformation as it is expanded by an inert gas. The gas passes through the holes, which are also shown in Figure 1. In (d), the two surface sheets of the panel are flattened by the die, as the panel assumes its final form.

### Detecting Cracks on Inner Surfaces

Microscopic cracks and pores in visually inaccessible areas of a workpiece, such as the inside of a reamed or drilled hole, are detected with a silicone mold that picks up fluorescent dye from the defect. Ultraviolet light makes the absorbed dye glow. The intensity of the fluorescence indicates the defect depth. (See page 56.)

### Microcomputer Checks Butt-Weld Accuracy

A quick determination of whether or not a weld is within dimensional tolerances is made automatically by a hand-held gage linked to a desk-top microcomputer. The alignment and angle of the plates on either side of a butt weld are measured, and out-of-tolerance measurements are indicated by an asterisk on the printout. (See page 62.)

### Elastomer-Toughened Polyimide Adhesives

Rubber-modified addition polyimides that can withstand long-term exposures at elevated temperatures are now available for bonding composite materials and such metals as titanium. The adhesives incorporate small amounts of commercially available elastomers into the polymer matrix to modify the polymer toughness. (See page 38.)

## Ultra-Thin-Film GaAs Solar Cells

Organometallic deposition can lower the cost of GaAs solar cells.

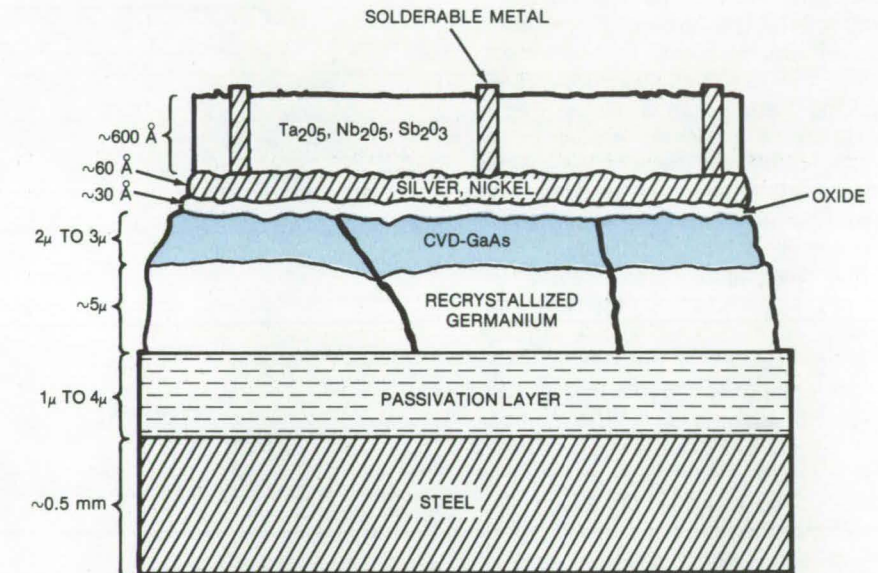
NASA's Jet Propulsion Laboratory, Pasadena, California

A process based on the organometallic chemical vapor deposition (OM/CVD) of trimethyl gallium with arsine forms economical ultrathin (2- to 6- $\mu\text{m}$ ) GaAs epitaxial films. This process has higher potential for low manufacturing cost and large-scale production compared with more-conventional halide CVD and liquid-phase epitaxy processes. By reducing the thickness of GaAs and substituting a low-cost substrate for the single-crystal GaAs wafer, the process could make GaAs solar cells commercially more attractive.

Ultrathin GaAs films were grown on polycrystalline germanium and on single-crystal GaAs surfaces. The films were made in an RF-heated quartz-tube reactor using trimethyl gallium and arsine as sources of Ga and As, respectively, and  $\text{H}_2\text{S}$  as n-type dopant.

Film samples with both substrates were tested on antireflection-coated metal-oxide-semiconductor (AMOS) solar cells (see figure). Samples deposited on single-crystal GaAs substrates had solar-cell efficiencies up to 17 percent, which is comparable to cells using films grown by the halide process. Films grown on laser-recrystallized poly-Ge had 5.7 percent cell efficiency.

Since film thicknesses and process parameters were not optimized, the performance of single-crystal GaAs



The **Ultrathin GaAs Layer** in this antireflection metal-oxide-semiconductor solar cell is only 2 to 3  $\mu\text{m}$  thick. It is deposited by an organometallic chemical-vapor-deposition process that uses trimethyl gallium as a source. The thinness of the layer cuts cost by reducing the amount of gallium in the cell.

film test cells is already very promising. Laser-recrystallized Ge substrate samples can be further improved by eliminating the diffusion of metal impurities from the steel substrate by appropriate passivating coatings.

The use of the laser-recrystallized Ge film method looks promising from several points. First, the steel substrate is low-cost. Second, the Ge layer provides a low-resistance ohmic

back contact. Third, it can be a stress-relief layer between the substrate and the GaAs film to compensate for the difference in thermal expansion between the two layers.

*This work was done by Ke-Li Wang, Bok K. Shin, Yea-Chuan M. Yeh, and Richard J. Stirn of Caltech for NASA's Jet Propulsion Laboratory. For further information, Circle 86 on the TSP Request Card.*  
NPO-14930

## Sealed Strip Line for Extreme Temperatures

Hermetic structure for microwave antenna feeds is strong, light, and inexpensive.

Lyndon B. Johnson Space Center, Houston, Texas

The feed circuits that carry signals to and from the S-band communication antennas on the Space Shuttle must withstand temperatures ranging from  $-300^\circ$  to  $+600^\circ$  F ( $-185^\circ$  to  $+315^\circ$  C). They must be strong, light,

and weatherproof and must have good electrical characteristics. Strip transmission lines that satisfy all of these requirements have been made inexpensively by a plating technique.

The new strip-line circuit consists of an inner conductor, a dielectric, and

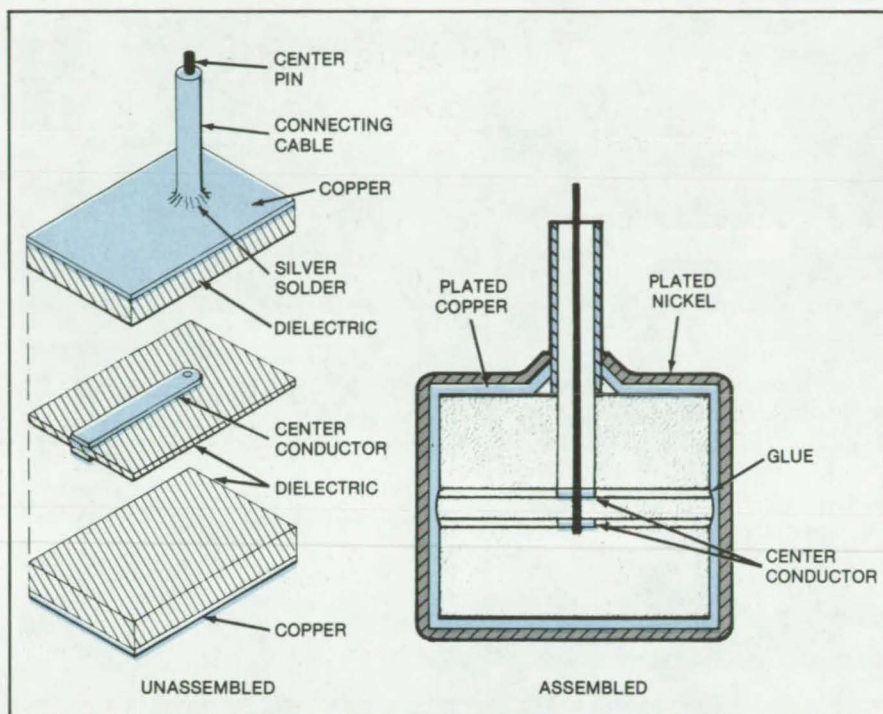
an outer conductor, in a structure similar to a coaxial transmission line. The outer conductor is plated around the dielectric on all four sides, producing a unibody construction that is hermetically sealed. Commercially-available dielectric material and epoxy

rated to withstand the extreme temperatures are used in the construction.

As shown in the figure, three layers of copper-clad dielectric are sandwiched to form the core of the structure. The center conductor consists of a pair of strips etched on a thin layer of double-clad dielectric material. That layer is glued between the two thicker pieces of dielectric, which have copper on only the outer sides, to hold the parts together during plating. The outer jackets of the connecting cables or connectors are silver-soldered to the top or bottom copper cladding, and the center pins are silver-soldered to the twin center conductor.

The edges of the dielectric assembly are sealed with epoxy, and for added strength, the top and bottom dielectric boards are electroless-plated with 0.003 inch (0.008 cm) of copper. A bead of silver solder (not shown) is placed around the margin where the inner and outer boards meet. In the final step, the entire unit is plated with 0.010 inch (0.025 cm) of copper and 0.015 inch (0.038 cm) of nickel to form the hermetic outer conductor.

A proposed alternative structure would use the same twin center conductor on the thin dielectric board, but the board would be suspended in an air-filled cavity. To construct such a unit, a wax block would be molded



An **Enclosed Strip-Line Feed** for microwave antennas is made by plating the exterior of an assembly of etched copper-clad dielectric boards.

around the center board, plated to form the outer conducting enclosure, and then melted away. The new strip line could be used in airborne-radar front ends and feed networks. It could also be adapted for underwater applications.

*This work was done by George C. Sargent of Watkins-Johnson Co. for Johnson Space Center. For further information, including details of materials and construction, Circle 87 on the TSP Request Card. MSC-16994*

## Wire Whip Keeps Spray Nozzle Clean

A wire whip prevents the buildup of spray-on foams while the spray gun is in use.

### Marshall Space Flight Center, Alabama

The buildup of spray-on foam insulation on a spray-gun nozzle is prevented by an air-turbine-driven wire (see Figure 1). Without affecting the spray, the wire cuts and removes the foam buildup. The technique should be useful in other spray applications.

To remove the material as it builds up, an air turbine, such as dentists use, swings a length of piano wire or

fishline (nylon, acrylic, or tetrafluoroethylene) at 10,000 rpm against the nozzle face. The centrifugal force and whip flexure sling any foam off the wire while removing any accumulated material from the nozzle face. The air turbine is remotely controlled by the spray-gun operator. Two lengths of wire are used for balance and to increase the cleaning action.

Also, an aerodynamic method has been suggested to prevent material from clogging the nozzle. In the proposed method, the purge flow is increased, and vortex-generating grooves are cut in the nozzle and inside the spray cap. As shown in Figure 2, the nozzle has a spray cap that imposes a purge flow over the small rounded nozzle face. By cutting  
(continued on next page)

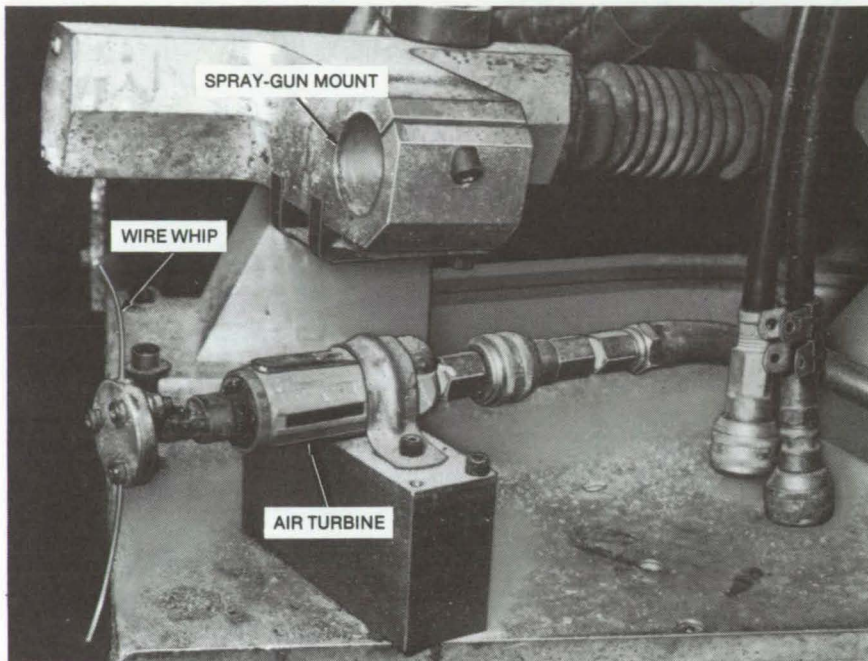


Figure 1. An Air-Turbine-Driven Wire Whip is clamped near the spray-gun mount. When the spray gun is installed, the wire whip is in position to remove foam buildup from the nozzle face. Two lengths of wire 1 to 2 inches (2.5 to 5 cm) long and about 0.03 inch (0.8 mm) in thickness are used.

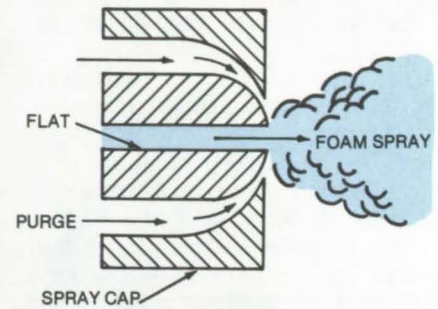


Figure 2. Foam Spray would be prevented from accumulating on the nozzle face by increasing the purge flow and by cutting vortex-generating grooves inside the cap and on the nozzle flats.

grooves inside the cap and also on the nozzle flats, buildup would be prevented. The vortexes would also assist mixing, would disperse the material fan, and would reduce wavy patterns on the surface being sprayed.

This work was done by Harry R. Carroll of Martin Marietta Corp. for Marshall Space Flight Center. No further documentation is available. MFS-25175

## Books and Reports

These reports, studies, and handbooks are available from NASA as Technical Support Packages (TSP's) when a Request Card number is cited; otherwise they are available from the National Technical Information Service.

### Materials Processing in Space

#### Research on processing in a low-gravity environment

A new 193-page report describes investigations of materials processing in a low-gravity environment. Ultimately, the research could lead to new commercially-applicable materials and processes and to an understanding of the constraints imposed by gravity. The NASA-supported work, carried out in 46 academic, industrial, and Government laboratories, covers six broad areas:

- Crystal Growth;
- Metals, Alloys, and Composites;

- Glasses, Ceramics, and Refractory Materials;
- Fluids, Transport, and Chemical Processes;
- Ultra-High-Vacuum and Containerless Processing Technologies; and
- Bioprocessing.

The investigations focused on promising areas revealed in research of the past decade. These areas include crystal growth, directional solidification of metals, containerless processing of reactive materials, the synthesis and separation of biological materials, and the identification of high-vacuum characteristics of an orbiting wake shield.

There is special emphasis on factors affecting the design of hardware for gravity-free applications. Examples of hardware being studied are high-gradient furnaces and heat pipes that take advantage of a lack of convection; acoustic, electromagnetic, and electrostatic modules for containerless processing; and devices for electrophoretic separation. Research is being

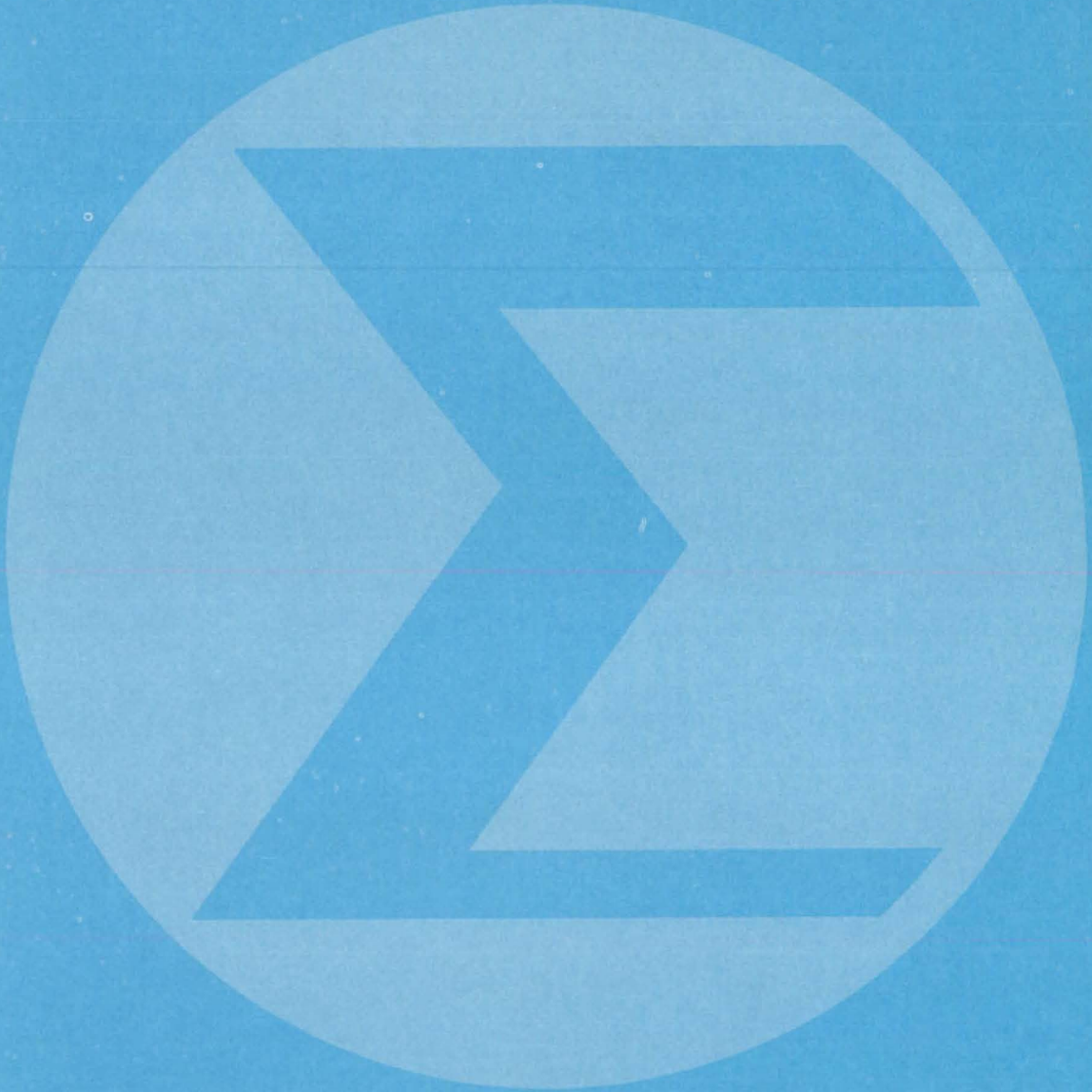
directed toward such commercial products as infrared detector crystals, inertial-confinement fusion targets, electrolytes with dispersoids, and ferromagnets.

For each of over 100 tasks described in the report, an overview is given of their objective and current state of development. Also, most of the task descriptions include a list of recent publications on the task findings.

This work was done by R. J. Naumann of Marshall Space Flight Center. Further information may be found in NASA TM-78294 [N80-31418/NSP], "Materials Processing in Space: Program Tasks" [\$12]. A paper copy may be purchased [prepayment required] from the National Technical Information Service, Springfield, Virginia 22161. The report is also available on microfiche at no charge. To obtain a microfiche copy, Circle 88 on the TSP Request Card.

MFS-25544

# Mathematics and Information Sciences



## Computer Programs

113 Linear-Algebra Programs

113 I/O Error Analyzer (UNIVAC 1108 Version)

## Computer Programs

These programs may be obtained at very reasonable cost from COSMIC, a facility sponsored by NASA to make new programs available to the public. For information on program price, size, and availability, circle the reference letter on the COSMIC Request Card in this issue.

### Linear-Algebra Programs

Thirty-eight FORTRAN-callable subroutines for performing the operations of linear algebra

The Basic Linear Algebra Subprograms (BLAS) library is a collection of 38 FORTRAN-callable routines for performing the basic operations of numerical linear algebra. The BLAS library is a portable and efficient source of basic operations for designers of programs involving linear algebraic computations.

The subprograms available in the library cover the operations of dot product, the addition of a vector and a scalar times a vector, Givens transformation, modified Givens transformation, copy, swap, Euclidean norm, the sum of magnitudes, the multiplication of a scalar times a vector, and locating an element of largest magnitude. Since these subprograms are to be used in an ANSI FORTRAN context, the cases of single precision, double precision, and complex data are provided for. All of the subprograms have been thoroughly tested and give consistent results even when transported from machine to machine.

The BLAS library is supplied in portable FORTRAN and in Assembler code versions for IBM 370, UNIVAC 1100, and CDC 6000-series computers. The Assembler versions offer extra efficiency in operations involving

large vectors. The BLAS library was developed in 1979. [For a more complete description, see the ACM Transactions on Mathematical Software, Vol. 5, No. 3, September 1979, pp. 308-325.]

*This program was written by Charles L. Lawson, Fred T. Krogh, and S. Singletary Gold of Caltech; D. R. Kincaid, J. Sullivan, and E. Williams of the University of Texas; R. J. Hanson and Karen Haskell of the Sandia Laboratories; J. Dongarra of the Argonne National Laboratory; and C. B. Moler of the University of New Mexico for NASA's Jet Propulsion Laboratory. For further information, Circle G on the COSMIC Request Card.*

NPO-15108

### I/O Error Analyzer (UNIVAC 1108 Version)

A program for gaging the performance of I/O peripherals

IOALZ4 is an Assembly-language utility program for the UNIVAC 1108, operational under level 33 of the EXEC 8 operating system. It scans user-selected portions of the system log file, whether located on tape or mass storage, searching for and processing I/O error entries. Several different kinds of information are returned by the analyzer to assist the installation manager and systems programmers in assessing system performance, gaging overall peripheral activity, and distinguishing marginal media from faulty equipment.

The three types of output produced are:

1. Type I output — consisting of individual summaries of the contents of each I/O error packet encountered during processing, with the entry information sorted by subcode/equipment type/subsystem/unit;
2. Type II output — consisting of "synoptic matrices" for each subcode/equipment pair and tabulating fault/status conditions occurring for each subsystem/unit during the analysis of the user-specified portion of the log file — row totals (the number of fault/status occurrences for each subsystem/unit) and column totals (the number of occurrences of each fault/status type) are the output for each synoptic matrix; and
3. Type III output — consisting of such equipment-independent statistics as mean-time-to-error, average error per unit time, average references per unit time, average references per error, and the variance of error — for convenience in comparing the performance of similar devices, this information is arranged in separate tables for each subcode/equipment pair.

IOALZ4 is written in Assembler (~95 percent) and FORTRAN IV (~5 percent) for batch or demand execution. It has been implemented on a UNIVAC 1108 computer, with a central memory requirement of approximately 39K of 36-bit words. The IOALZ4 program was developed in 1976 and modified in 1978.

*This program was written by Edwin T. Vaughan of Goddard Space Flight Center and Dan-Lai Lee of Computer Science Corp. For further information, Circle H on the COSMIC Request Card.*

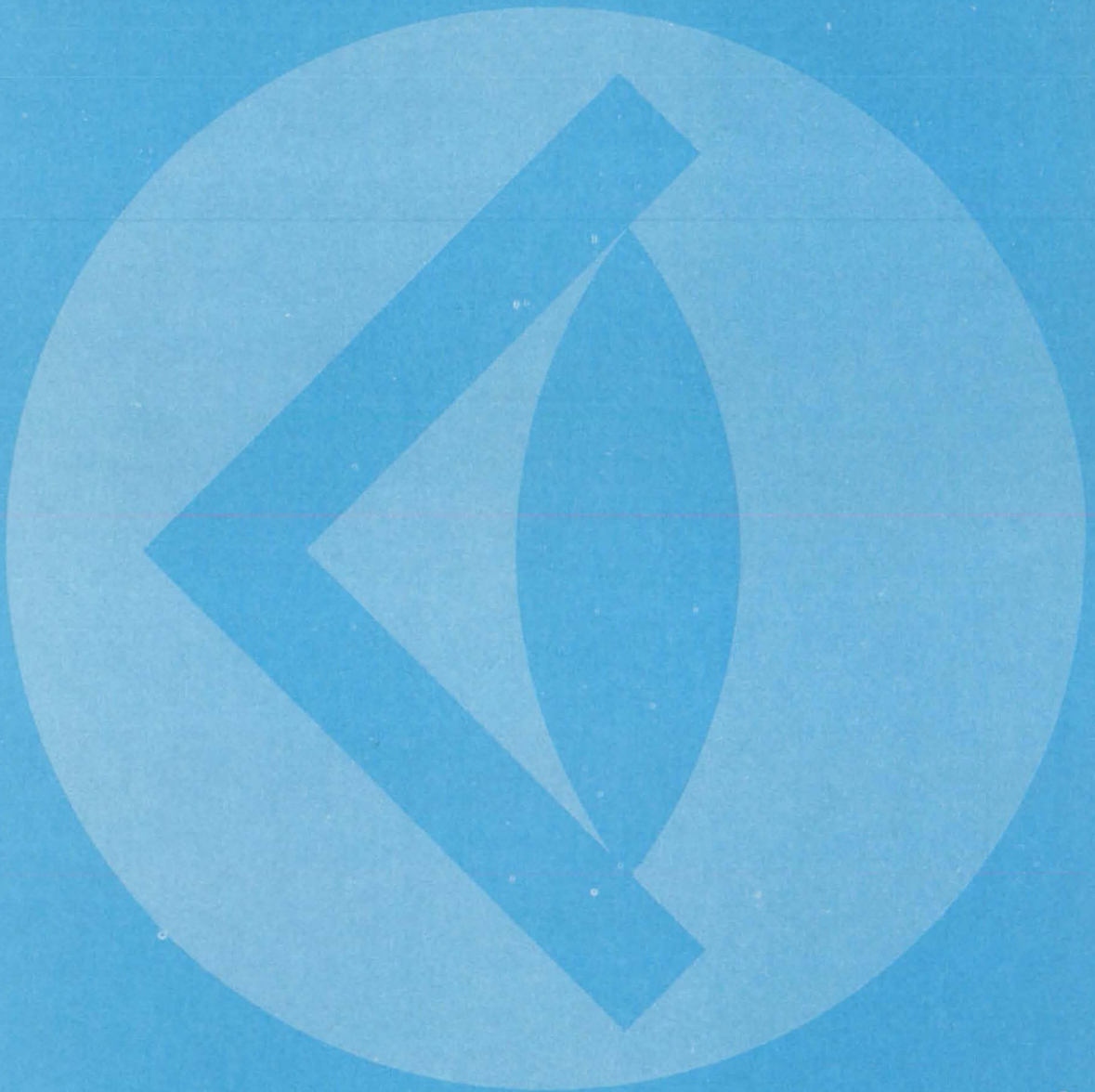
GSC-12621







# SUBJECT INDEX



<b>ACCELERATED LIFE TESTS</b>			
Improved model for MOS breakdown page 8	NPO-14850		
<b>ACOUSTIC STREAMING</b>			
Viscous torques on a levitating body page 56	NPO-15413		
<b>ADHESIVES</b>			
Adhesives mixer/applicator page 77	MSC-18916		
Elastomer-toughened polyimide adhesives page 38	LAR-12775		
<b>AERODYNAMIC CHARACTERISTICS</b>			
Aerodynamics improve wind wheel page 78	MFS-25506		
Aerodynamics of sounding-rocket geometries page 72	GSC-12680		
Aeroelastic analysis for rotorcraft Page 72	ARC-11150		
Subsonic loadings due to control-surface motion page 72	LAR-12802		
<b>AEROELASTICITY</b>			
Aeroelastic analysis for rotorcraft page 72	ARC-11150		
<b>AIRCRAFT DESIGN</b>			
Advanced technologies for commercial airplanes page 20	MSC-18982		
<b>AIRFOIL PROFILES</b>			
Aerodynamics improve wind wheel page 78	MFS-25506		
<b>ALGEBRA</b>			
Linear-algebra programs page 113	NPO-15108		
<b>ALGORITHMS</b>			
Algorithms could automate cancer diagnosis page 45	MSC-18764		
New algorithms manage fourfold redundancy page 16	MSC-18498		
<b>AMPLIFIER DESIGN</b>			
Log-output signal processor scans eight decades page 11	ARC-11293		
<b>ANEMOMETERS</b>			
High-speed laser anemometer page 52	LEW-13527		
<b>ANGULAR VELOCITY</b>			
Interferometer accurately measures rotation angle page 58	GSC-12614		
<b>ANISOTROPY</b>			
Deformation-induced anisotropy of polymers page 41	NPO-15325		
<b>ANTENNAS</b>			
Compact dual-mode microwave antenna page 6	LAR-12784		
<b>ANTENNA RADIATION PATTERNS</b>			
Far-field antenna pattern from near-field test page 60	NPO-14905		
<b>AUTOMATIC GAIN CONTROL</b>			
Spike-free automatic level control page 8	KSC-11170		
<b>AVIONICS</b>			
Advanced technologies for commercial airplanes page 20	MSC-18982		
<b>BAFFLES</b>			
Baffle keeps solar energy in receiver page 27	NPO-15387		
<b>BALLS</b>			
Ball-and-socket joint can be disassembled page 82	LAR-12770		
<b>BATTERY CHARGERS</b>			
Pressure switch is a low-cost battery indicator page 67	GSC-12679		
<b>BEAM SPLITTERS</b>			
Beam splitter intensities are preselected page 23	MFS-25312		
<b>BITS</b>			
Optical memory stores $10^{12}$ bits page 15	MFS-25456		
<b>BOLTS</b>			
Strain-gaged bolts are easily prepared page 69	MSC-18823		
<b>BOUNDARY LAYER FLOW</b>			
Nozzle modification suppresses flow transients page 62	MFS-19567		
<b>BRAZING</b>			
Fluxless brazing of large structural panels page 96	LAR-12519		
<b>BUTT JOINTS</b>			
Microcomputer checks butt-weld accuracy page 62	MFS-25557		
<b>CANCER</b>			
Algorithms could automate cancer diagnosis page 45	MSC-18764		
Compact dual-mode microwave antenna page 6	LAR-12784		
<b>CAPACITORS</b>			
IC capacitors on groups III to V substrates page 104	GSC-12543		
<b>CASTINGS</b>			
Fiber-reinforced slip castings page 95	ARC-11279		
<b>CELLS [BIOLOGY]</b>			
Algorithms could automate cancer diagnosis page 45	MSC-18764		
<b>CHEMICAL REACTORS</b>			
Capacitively-heated fluidized bed page 98	NPO-14912		
<b>CLAMPS</b>			
Device acquires, orients, and clamps page 84	MFS-25403		
<b>CLEANING</b>			
Wire whip keeps spray nozzle clean page 109	MFS-25175		
<b>COAXIAL CABLES</b>			
Sealed strip line for extreme temperatures page 108	MSC-16994		
<b>COLOR TELEVISION</b>			
Graphics-system color-code interface page 17	LAR-12646		
<b>COMBUSTION CHAMBERS</b>			
Two-stage combustor reduces pollutant emissions page 40	NPO-14911		
<b>COMMUNICATION CABLES</b>			
Integrated structural and cable connector page 82	LAR-12769		
<b>COMPOSITE MATERIALS</b>			
Lacquer reveals impact damage in composites page 64	LAR-12700		
<b>COMPUTER GRAPHICS</b>			
Graphics-system color-code interface page 17	LAR-12646		
<b>COMPUTER PROGRAMS</b>			
I/O error analyzer (UNIVAC 1108 version) page 113	GSC-12621		
<b>COMPUTER STORAGE DEVICES</b>			
Optical memory stores $10^{12}$ bits page 15	MFS-25456		
<b>CONTAINERLESS MELTS</b>			
Levitor for containerless processing page 105	MFS-25509		
Materials processing in space page 110	MFS-25544		
<b>CONTAMINATION</b>			
Refractories keep silicon crystals pure page 92	NPO-14820		
Removing defects from silicon ribbon page 89	NPO-14772		
<b>CONTROL EQUIPMENT</b>			
Spike-free automatic level control page 8	KSC-11170		
<b>CONTROL SURFACES</b>			
Subsonic loadings due to control-surface motion page 72	LAR-12802		
<b>CORE SAMPLING</b>			
Automatic collection of rock and soil samples page 77	MSC-18868		
<b>CORRUGATED PLATES</b>			
Metal sandwich panel with biaxially corrugated core page 106	FRC-11026		
<b>COST ANALYSIS</b>			
Energy-systems economic analysis page 32	NPO-15097		
<b>COUPLINGS</b>			
Ball-and-socket joint can be disassembled page 82	LAR-12770		
Blind fastener is easy to install page 80	MSC-18742		
<b>CRACKS</b>			
Detecting cracks on inner surfaces page 56	MFS-19575		
<b>CROP GROWTH</b>			
Chemical-growth regulators for guayule plants page 48	NPO-15213		
Portable radiometer monitors plant growth page 47	GSC-12412		
<b>CRUCIBLES</b>			
Crucible grows wide silicon ribbon page 91	NPO-14859		
Gravity-feed growth of silicon ribbon page 88	NPO-14967		
Heat-exchanger method of crystal growth page 88	NPO-14819		
Recharging the silicon crucible in a hot furnace page 91	NPO-14980		
<b>CRYOGENIC EQUIPMENT</b>			
Dynamic isolation for cryogenic refrigerators page 75	LAR-12728		
Fiber-optic, semiconductor temperature gage page 55	MSC-18627		
<b>CRYSTAL GROWTH</b>			
Automatic control of silicon melt level page 94	NPO-15487		
Ceramic material for silicon-shaping dies page 90	NPO-14783		
Crucible grows wide silicon ribbon page 91	NPO-14859		
Gravity-feed growth of silicon ribbon page 88	NPO-14967		
Heat-exchanger method of crystal growth page 88	NPO-14819		
Improved facility for producing silicon web page 93	NPO-14860		
Levitor for containerless processing page 105	MFS-25509		
Materials processing in space page 110	MFS-25544		
Recharging the silicon crucible in a hot furnace page 91	NPO-14980		
Removing defects from silicon ribbon page 89	NPO-14772		
Temperature-controlled support for a seed crystal page 94	MFS-25341		
<b>DEFECTS</b>			
Removing defects from silicon ribbon page 89	NPO-14772		
<b>DEFORMATION</b>			
Deformation-induced anisotropy of polymers page 41	NPO-15325		
<b>DENDRITIC CRYSTALS</b>			
Automatic control of silicon melt level page 94	NPO-15487		

Crucible grows wide silicon ribbon page 91	NPO-14859		
Improved facility for producing silicon web page 93	NPO-14860		
<b>DESTRUCTIVE TESTS</b>			
Lacquer reveals impact damage in composites page 64	LAR-12700		
<b>DETONATORS</b>			
Sequential impulse generator uses fiber optics page 24	NPO-14939		
<b>DIAGNOSIS</b>			
Algorithms could automate cancer diagnosis page 45	MSC-18764		
Compact dual-mode microwave antenna page 6	LAR-12784		
<b>DIES</b>			
Ceramic material for silicon-shaping dies page 90	NPO-14783		
<b>DISPENSERS</b>			
Adhesives mixer/appliator page 77	MSC-18916		
<b>DISPLACEMENT MEASUREMENT</b>			
Load-displacement measurement on pin loaded specimens page 70	LEW-13624		
<b>DRILLING</b>			
Automatic collection of rock and soil samples page 77	MSC-18868		
<b>ECONOMIC ANALYSIS</b>			
Energy-systems economic analysis page 32	NPO-15097		
<b>ELASTOMERS</b>			
Elastomer-toughened polyimide adhesives page 38	LAR-12775		
Preparation of perfluorinated imidoamidoxime polymers page 35	ARC-11267		
<b>ELECTRIC CONNECTORS</b>			
Weatherproof crimp connector page 97	NPO-15497		
<b>ELECTRIC CONTACTS</b>			
Multilayer, front-contact grid for solar cells page 10	LAR-12613		
<b>ELECTRICAL FAULTS</b>			
Improved model for MOS breakdown page 8	NPO-14850		
Short-circuited power networks page 20	MSC-18977		
<b>ELECTROSTATIC PROBES</b>			
Correcting for background density in plasma measurements page 53	NPO-15332		
<b>ENERGY CONVERSION EFFICIENCY</b>			
Aerodynamics improve wind wheel page 78	MFS-25506		
Baffle keeps solar energy in receiver page 27	NPO-15387		
Energy-systems economic analysis page 32	NPO-15097		
Load-responsive motor controller page 4	MFS-25560		
New energy-saving technologies use induction generators page 25	MFS-25513		
Power-factor controller with regenerative braking page 5	MFS-25477		
Three-phase power-factor controller page 3	MFS-25535		
<b>ENGINE DESIGN</b>			
Advances in turbine-engine technology page 84	LEW-13672		
<b>EPOXY RESINS</b>			
Adhesives mixer/appliator page 77	MSC-18916		
<b>ERROR DETECTION CODES</b>			
I/O error analyzer (UNIVAC 1108 version) page 113	GSC-12621		
<b>EXTINGUISHING</b>			
Synthesis of fire-extinguishing dawsonites page 36	ARC-11326		
<b>FAILURE</b>			
New algorithms manage fourfold redundancy page 16	MSC-18498		
<b>FAR FIELDS</b>			
Far-field antenna pattern from near-field test page 60	NPO-14905		
<b>FASTENERS</b>			
Blind fastener is easy to install page 80	MSC-18742		
<b>FIBER OPTICS</b>			
Fiber-optic, semiconductor temperature gage page 55	MSC-18627		
<b>FIELD MEASUREMENTS</b>			
Far-field antenna pattern from near-field test page 60	NPO-14905		
<b>FIRE FIGHTING</b>			
Protective clothing for firefighters page 87	MFS-25546		
<b>FIREPROOFING</b>			
Fire-resistant resins for laminates page 37	ARC-11321		
Synthesis of fire-extinguishing dawsonites page 36	ARC-11326		
<b>FLAWS</b>			
Detecting cracks on inner surfaces page 56	MFS-19575		
<b>FLOW MEASUREMENT</b>			
High-speed laser anemometer page 52	LEW-13527		
<b>FLUIDIZED BED PROCESSORS</b>			
Capacitively-heated fluidized bed page 98	NPO-14912		
<b>FLUXES</b>			
Fluxless brazing of large structural panels page 96	LAR-12519		
<b>FOAMS</b>			
Wire whip keeps spray nozzle clean page 109	MFS-25175		
<b>FOLDING</b>			
Weatherproof crimp connector page 97	NPO-15497		
<b>FRACTURE STRENGTH</b>			
Measuring cyclic-stress properties of pressure vessels page 65	MFS-23734		
<b>FUEL COMBUSTION</b>			
Two-stage combustor reduces pollutant emissions page 40	NPO-14911		
<b>GALLIUM ARSENIDES</b>			
Ultra-thin-film GaAs solar cells page 108	NPO-14930		
<b>GENERATORS</b>			
New energy-saving technologies use induction generators page 25	MFS-25513		
<b>GRAPHICS</b>			
Graphics-system color-code interface page 17	LAR-12646		
<b>GUIDANCE [MOTION]</b>			
Less-costly inertial guidance page 51	ARC-11257		
<b>HEAT EXCHANGERS</b>			
Heat-exchanger method of crystal growth page 88	NPO-14819		
<b>HEAT PIPES</b>			
Heat pipe blocks return flow page 61	ARC-11285		
<b>HEAT SHIELDING</b>			
Metallic panels would insulate at 2,700° F page 100	LAR-12620		
<b>HEAT TRANSFER</b>			
Heat-energy analysis for solar receivers page 70	NPO-14835		
<b>HEATING EQUIPMENT</b>			
Motel DHW retrofit — Dallas, Texas page 28	MFS-25580		
Pyramidal-reflector solar heater Page 27	MFS-25571		
Solar-cooled classroom building — Columbus, Ohio page 30	MFS-25597		
Solar-energy system for a commercial building — Topeka, Kansas page 29	MFS-25609		
Solar-heated and cooled office building — Columbus, Ohio page 30	MFS-25608		
Solar-heated public library — Troy, Ohio page 30	MFS-25601		
Solar-heated water at a motel — Mobile, Alabama page 29	MFS-25603		
Solar hot water for an industrial laundry — Fresno, California page 31	MFS-25550		
Solar hot water for motor inn — Texas City, Texas page 29	MFS-25614		
Solar-water-heater design package page 31	MFS-25574		
Solar water heater installation package page 28	MFS-25573		
<b>HELICOPTER DESIGN</b>			
Aeroelastic analysis for rotorcraft page 72	ARC-11150		
<b>HIGH TEMPERATURE ENVIRONMENTS</b>			
High-temperature seal for sliding-gate valve page 101	MFS-19607		
Sealed strip line for extreme temperatures page 108	MSC-16994		
<b>HONEYCOMB STRUCTURES</b>			
Metallic panels would insulate at 2,700° F page 100	LAR-12620		
<b>HYDRAULIC EQUIPMENT</b>			
Constant-pressure hydraulic pump page 76	MSC-18794		
<b>INDUCTION MOTORS</b>			
Three-phase power-factor controller page 3	MFS-25535		
Load-responsive motor controller page 4	MFS-25560		
New energy-saving technologies use induction generators page 25	MFS-25513		
Power-factor controller with regenerative Braking page 5	MFS-25477		
<b>IMPACT TESTS</b>			
Lacquer reveals impact damage in composites page 64	LAR-12700		
<b>IMPULSE GENERATORS</b>			
Sequential impulse generator uses fiber optics page 24	NPO-14939		



**INERTIAL GUIDANCE**

Less-costly inertial guidance  
page 51 ARC-11257

**INSPECTION**

Lacquer reveals impact damage in composites  
page 64 LAR-12700

**INTEGRATED CIRCUITS**

IC capacitors on groups III to V substrates  
page 104 GSC-12543

**INTERFACES**

Graphics-system color-code interface  
page 17 LAR-12646

**INTERFEROMETERS**

Beam splitter intensities are preselected  
page 23 MFS-25312

Interferometer accurately measures rotation  
angle  
page 58 GSC-12614

**ION DENSITY**

Correcting for background density in  
plasma measurements  
page 53 NPO-15332

**JOINTS [JUNCTIONS]**

Ball-and-socket joint can be disassembled  
page 82 LAR-12770

**LACQUERS**

Lacquer reveals impact damage in composites  
page 64 LAR-12700

**LAMINATES**

Fire-resistant resins for laminates  
page 37 ARC-11321

**LASER APPLICATIONS**

Dual-laser schlieren system  
page 54 MFS-25315

High-speed laser anemometer  
page 52 LEW-13527

**LASER HEATING**

Sequential impulse generator uses fiber optics  
page 24 NPO-14939

**LATHES**

Lathe attachment finishes inner surface of tubes  
page 79 MSC-18780

**LEVITATION**

Levitor for containerless processing  
page 105 MFS-25509

**LIGHT BEAMS**

Beam splitter intensities are preselected  
page 23 MFS-25312

**LINEAR CIRCUITS**

Resistors improve ramp linearity  
page 7 GSC-12635

**LINEAR EQUATIONS**

Linear-algebra programs  
page 113 NPO-15108

**LOAD TESTS**

Load-displacement measurement on pin  
loaded specimens  
page 70 LEW-13624

**LOGARITHMIC RECEIVERS**

Log-output signal processor scans eight decades  
page 11 ARC-11293

**LOW GRAVITY MANUFACTURING**

Levitor for containerless processing  
page 105 MFS-25509

**MACHINING**

Lathe attachment finishes inner surface  
of tubes  
page 79 MSC-18780

Wire EDM for refractory materials  
page 101 LEW-13460

**MECHANICAL PROPERTIES**

Load-displacement measurement on pin  
loaded specimens  
page 70 LEW-13624

**METABOLISM**

Constraint-free measurement of metabolic  
rate  
page 46 MSC-18885

**METAL BONDING**

Fluxless brazing of large structural panels  
page 96 LAR-12519

**METAL OXIDE SEMICONDUCTORS**

Improved model for MOS breakdown  
page 8 NPO-14850

**MICROWAVE EQUIPMENT**

Compact dual-mode microwave antenna  
page 6 LAR-12784

Sealed strip line for extreme temperatures  
page 108 MSC-16994

**MIXING**

Adhesives mixer/appliator  
page 77 MSC-18916

**MODULES**

Integrated structural and cable connector  
page 82 LAR-12769

**MOUNTING**

Dynamic isolation for cryogenic refrigerators  
page 75 LAR-12728

**MULTIPLEXING**

Self-correcting electronically-scanned  
pressure sensor  
page 63 LAR-12686

**NETWORK ANALYSIS**

Short-circuited power networks  
page 20 MSC-18977

**NONDESTRUCTIVE TESTING**

Strain-gaged bolts are easily prepared  
page 69 MSC-18823

**NOZZLE DESIGN**

Nozzle modification suppresses flow transients  
page 62 MFS-19567

**OPTICAL EQUIPMENT**

Beam splitter intensities are preselected  
page 23 MFS-25312

**OPTICAL MEMORY [DATA STORAGE]**

Optical memory stores  $10^{12}$  bits  
page 15 MFS-25456

**OSCILLATORS**

High-frequency gated oscillator  
page 12 MSC-18634

**OXIDE FILMS**

IC capacitors on groups III to V substrates  
page 104 GSC-12543

**PANELS**

Metal sandwich panel with biaxially  
corrugated core  
page 106 FRC-11026

**PARABOLIC ANTENNAS**

Far-field antenna pattern from near-field test  
page 60 NPO-14905

**PERFLUORO COMPOUNDS**

Preparation of perfluorinated imidoylamidoxime  
polymers  
page 35 ARC-11267

**PHASE LOCKED SYSTEMS**

Improved phase-lock detector  
page 19 MSC-18797

Pulsed phase-locked-loop strain monitor  
page 68 LAR-12772

**PLANTS [BOTANY]**

Chemical-growth regulators for guayule plants  
page 48 NPO-15213

Portable radiometer monitors plant growth  
page 47 GSC-12412

**PLASMA DIAGNOSTICS**

Correcting for background density in plasma  
measurements  
page 53 NPO-15332

**PLASMA JETS**

Plasma deposition of amorphous silicon  
page 42 NPO-14954

**POLLUTION CONTROL**

Two-stage combustor reduces pollutant emissions  
page 40 NPO-14911

**POLYETHER RESINS**

Synthesis of perfluorinated polyethers  
page 36 ARC-11241

**POLYIMIDES**

Elastomer-toughened polyimide adhesives  
page 38 LAR-12775

**POLYMER PHYSICS**

Deformation-induced anisotropy of polymers  
page 41 NPO-15325

Viscoelastic properties of polymer blends  
page 39 NPO-14924

**POSITIONING**

Device acquires, orients, and clamps  
page 84 MFS-25403

**POWER CONDITIONING**

Load-responsive motor controller  
page 4 MFS-25560

Power-factor controller with regenerative braking  
page 5 MFS-25477

Three-phase power-factor controller  
page 3 MFS-25535

**POWER SUPPLY CIRCUITS**

Solar-powered supply is light and reliable  
page 18 MFS-25430

**PRESSURE REGULATORS**

Constant-pressure hydraulic pump  
page 76 MSC-18794

**PRESSURE SENSORS**

Pressure switch is a low-cost battery indicator  
page 67 GSC-12679

Self-correcting electronically-scanned pressure  
sensor  
page 63 LAR-12686

**PRESSURE VESSELS**

Measuring cyclic-stress properties of pressure  
vessels  
page 65 MFS-23734

**PROTECTIVE CLOTHING**

Protective clothing for firefighters  
page 87 MFS-25546

Sprayed coating renews butyl rubber  
page 106 KSC-11198

**PUMPS**

Constant-pressure hydraulic pump  
page 76 MSC-18794

**PURITY**

Refractories keep silicon crystals pure  
page 92 NPO-14820

**RADIANT HEATING**

Heat lamps solder solar array quickly  
page 101 NPO-14866

**RADIO FREQUENCY HEATING**

Capacitively-heated fluidized bed  
page 98 NPO-14912

Compact dual-mode microwave antenna  
page 6 LAR-12784

**RADIOMETERS**

Portable radiometer monitors plant growth  
page 47 GSC-12412

<b>REDUNDANCY</b>					
New algorithms manage fourfold redundancy					
page 16	MSC-18498				
<b>REFRACTIVITY</b>					
Dual-laser schlieren system					
page 54	MFS-25315				
<b>REFRACTORY MATERIALS</b>					
Refractories keep silicon crystals pure					
page 92	NPO-14820				
<b>REFRACTORY METAL ALLOYS</b>					
Wire EDM for refractory materials					
page 101	LEW-13460				
<b>REINFORCING FIBERS</b>					
Fiber-reinforced slip castings					
page 95	ARC-11279				
<b>RESISTANCE HEATING</b>					
Resistance heater helps Stirling-engine					
research					
page 81	NPO-14928				
<b>ROCKS</b>					
Automatic collection of rock and soil samples					
page 77	MSC-18868				
<b>ROTATING SHAFTS</b>					
Rotary transformer seals power in					
page 9	GSC-12595				
<b>ROTATION</b>					
Interferometer accurately measures rotation angle					
page 58	GSC-12614				
<b>RUBBER</b>					
Sprayed coating renews butyl rubber					
page 106	KSC-11198				
<b>SAMPLERS</b>					
Automatic collection of rock and soil samples					
page 77	MSC-18868				
<b>SCHLIEREN PHOTOGRAPHY</b>					
Dual-laser schlieren system					
page 54	MFS-25315				
<b>SEALING</b>					
High-temperature seal for sliding-gate valve					
page 101	MFS-19607				
<b>SHORT CIRCUITS</b>					
Short-circuited power networks					
page 20	MSC-18977				
<b>SIGNAL DETECTORS</b>					
Improved phase-lock detector					
page 19	MSC-18797				
Log-output signal processor scans eight decades					
page 11	ARC-11293				
<b>SIGNAL GENERATORS</b>					
High-frequency gated oscillator					
page 12	MSC-18634				
<b>SIGNAL TRANSMISSION</b>					
Rotary transformer seals power in					
page 9	GSC-12595				
<b>SILICON</b>					
Automatic control of silicon melt level					
page 94	NPO-15487				
Capacitively-heated fluidized bed					
page 98	NPO-14912				
Ceramic material for silicon-shaping dies					
page 90	NPO-14783				
Crucible grows wide silicon ribbon					
page 91	NPO-14859				
Gravity-feed growth of silicon ribbon					
page 88	NPO-14967				
Heat-exchanger method of crystal growth					
page 88	NPO-14819				
Improved facility for producing silicon web					
page 93	NPO-14860				
Plasma deposition of amorphous silicon					
page 42	NPO-14954				
Recharging the silicon crucible in a hot furnace					
page 91	NPO-14980				
Refractories keep silicon crystals pure					
page 92	NPO-14820				
Removing defects from silicon ribbon					
page 89	NPO-14772				
<b>SIZE DETERMINATION</b>					
Program for analysis and resizing of structures					
page 71	LAR-12704				
<b>SMOOTHING</b>					
Lathe attachment finishes inner surface of tubes					
page 79	MSC-18780				
<b>SOIL SCIENCE</b>					
Automatic collection of rock and soil samples					
page 77	MSC-18868				
<b>SOLAR CELLS</b>					
Heat lamps solder solar array quickly					
page 101	NPO-14866				
Multilayer, front-contact grid for solar cells					
page 10	LAR-12613				
Ultra-thin-film GaAs solar cells					
page 108	NPO-14930				
<b>SOLAR ENERGY</b>					
Baffle keeps solar energy in receiver					
page 27	NPO-15387				
Heat-energy analysis for solar receivers					
page 70	NPO-14835				
Motel DHW retrofit — Dallas, Texas					
page 28	MFS-25580				
Pyramidal-reflector solar heater					
page 27	MFS-25571				
Solar-cooled classroom building — Columbus, Ohio					
page 30	MFS-25597				
Solar-energy system for a commercial building — Topeka, Kansas					
page 29	MFS 25609				
Solar-heated and cooled office building — Columbus, Ohio					
page 30	MFS-25608				
Solar-heated public library — Troy, Ohio					
page 30	MFS-25601				
Solar-heated water at a motel — Mobile, Alabama					
page 29	MFS-25603				
Solar hot water for an industrial laundry — Fresno, California					
page 31	MFS-25550				
Solar hot water for motor inn — Texas City, Texas					
page 29	MFS-25614				
Solar water heater installation package					
page 28	MFS-25573				
Solar-water-heater design package					
page 31	MFS-25574				
Temperature controller for a solar furnace					
page 26	NPO-15388				
<b>SOLAR FURNACE</b>					
Temperature controller for a solar furnace					
page 26	NPO-15388				
<b>SOLAR GENERATORS</b>					
Solar-powered supply is light and reliable					
page 18	MFS-25430				
<b>SOLDERING</b>					
Heat lamps solder solar array quickly					
page 101	NPO-14866				
Shaping transistor leads for better solder joints					
page 99	MSC-18837				
<b>SOUNDING ROCKETS</b>					
Aerodynamics of sounding-rocket geometries					
page 72	GSC-12680				
<b>SPACE LABORATORIES</b>					
Materials processing in space					
page 110	MFS-25544				
<b>SPARK MACHINING</b>					
Wire EDM for refractory materials					
page 101	LEW-13460				
<b>SPIROMETERS</b>					
Constraint-free measurement of metabolic rate					
page 46	MSC-18885				
<b>SPRAY NOZZLES</b>					
Wire whip keeps spray nozzle clean					
page 109	MFS-25175				
<b>SPRAYED COATINGS</b>					
Sprayed coating renews butyl rubber					
page 106	KSC-11198				
<b>SPRINGS [ELASTIC]</b>					
High-temperature seal for sliding-gate valve					
page 101	MFS-19607				
<b>STRAIN GAGES</b>					
Matching of apparent-strain characteristics					
page 66	LAR-12743				
Pulsed phase-locked-loop strain monitor					
page 68	LAR-12772				
Strain-gaged bolts are easily prepared					
page 69	MSC-18823				
<b>STRESS ANALYSIS</b>					
Measuring cyclic-stress properties of pressure vessels					
page 65	MFS-23734				
Program for analysis and resizing of structures					
page 71	LAR-12704				
<b>STRESS RELIEVING</b>					
Shaping transistor leads for better solder joints					
page 99	MSC-18837				
<b>STIRLING CYCLE</b>					
Resistance heater helps Stirling-engine research					
page 81	NPO-14928				
<b>STRIP TRANSMISSION LINES</b>					
Sealed strip line for extreme temperatures					
page 108	MSC-16994				
<b>STRUCTURAL MEMBERS</b>					
Blind fastener is easy to install					
page 80	MSC-18742				
Fluxless brazing of large structural panels					
page 96	LAR-12519				
Integrated structural and cable connector					
page 82	LAR-12769				
Program for analysis and resizing of structures					
page 71	LAR-12704				
Structural modules would contain transmission lines					
page 103	GSC-12523				
<b>SUBSONIC FLOW</b>					
Subsonic loadings due to control-surface motion					
page 72	LAR-12802				
<b>SUPPORTS</b>					
Temperature-controlled support for a seed crystal					
page 94	MFS-25341				
<b>SURFACE CRACKS</b>					
Detecting cracks on inner surfaces					
page 56	MFS-19575				
<b>SWEEP CIRCUITS</b>					
Resistors improve ramp linearity					
page 7	GSC-12635				
<b>TEMPERATURE CONTROL</b>					
Heat pipe blocks return flow					
page 61	ARC-11285				
Motel DHW retrofit — Dallas, Texas					
page 28	MFS-25580				
Pyramidal-reflector solar heater					
page 27	MFS-25571				
Solar-cooled classroom building — Columbus, Ohio					
page 30	MFS-25597				
Solar-energy system for a commercial building — Topeka, Kansas					
page 29	MFS-25609				



Solar-heated and cooled office building —  
Columbus, Ohio  
page 30 MFS-25608

Solar-heated public library — Troy, Ohio  
page 30 MFS-25601

Solar-heated water at a motel —  
Mobile, Alabama  
page 29 MFS-25603

Solar hot water for an industrial laundry —  
Fresno, California  
page 31 MFS-25550

Solar hot water for motor inn —  
Texas City, Texas  
page 29 MFS-25614

Solar water heater installation package  
page 28 MFS-25573

Solar-water-heater design package  
page 31 MFS-25574

Temperature-controlled support for a seed  
crystal  
page 94 MFS-25341

Temperature controller for a solar furnace  
Page 26 NPO-15388

**TEMPERATURE MEASUREMENT**  
Fiber-optic, semiconductor temperature gage  
page 55 MSC-18627

**THERMAL INSULATION**  
Metallic panels would insulate at 2,700° F  
page 100 LAR-12620

**THERMOCOUPLES**  
Tab attachment of thermocouples to titanium  
page 57 FRC-11017

**THIN FILMS**  
Ultra-thin-film GaAs solar cells  
page 108 NPO-14930

**TITANIUM ALLOYS**  
Tab attachment of thermocouples to titanium  
page 57 FRC-11017

**TORQUE**  
Viscous torques on a levitating body  
page 56 NPO-15413

**TOUGHNESS**  
Elastomer-toughened polyimide adhesives  
page 38 LAR-12775

**TRANSDUCERS**  
Matching of apparent-strain characteristics  
page 66 LAR-12743

Ultrasonic transducer analyzer  
page 59 MFS-25410

**TRANSFORMERS**  
Rotary transformer seals power in  
page 9 GSC-12595

**TRANSISTORS**  
Shaping transistor leads for better solder joints  
page 99 MSC-18837

**TRANSMISSION LINES**  
Structural modules would contain transmission  
lines  
page 103 GSC-12523

**TURBINE ENGINES**  
Advances in turbine-engine technology  
page 84 LEW-13672

**ULTRASONIC WAVE TRANSDUCERS**  
Ultrasonic transducer analyzer  
page 59 MFS-25410

**VALVES**  
High-temperature seal for sliding-gate valve  
page 101 MFS-19607

**VAPOR JETS**  
Plasma deposition of amorphous silicon  
page 42 NPO-14954

**VECTOR SPACES**  
Linear-algebra programs  
page 113 NPO-15108

**VIBRATION ISOLATORS**  
Dynamic isolation for cryogenic refrigerators  
page 75 LAR-12728

**VISCOELASTICITY**  
Viscoelastic properties of polymer blends  
page 39 NPO-14924

**VISCOUS DRAG**  
Viscous torques on a levitating body  
page 56 NPO-15413

**VOLTAGE CONVERTERS [DC TO DC]**  
Solar-powered supply is light and reliable  
page 18 MFS-25430

**WEATHERPROOFING**  
Weatherproof crimp connector  
page 97 NPO-15497

**WELD TESTS**  
Microcomputer checks butt-weld accuracy  
page 62 MFS-25557

**WINDMILLS [WINDPOWERED MACHINES]**  
Aerodynamics improve wind wheel  
page 78 MFS-25506

**WINDPOWERED GENERATORS**  
New energy-saving technologies use  
induction generators  
page 25 MFS-25513

National Aeronautics and  
Space Administration

Washington, D.C.  
20546

Official Business  
Penalty for Private Use \$300

SPECIAL FOURTH-CLASS RATE  
BOOK

FOURTH-CLASS MAIL  
POSTAGE & FEES PAID  
NASA  
WASHINGTON, D.C.  
PERMIT No. G 27

**NASA**

*The technology of heated transparent materials, used in the helmet faceplates of Apollo astronauts and other NASA projects, has found several nonaerospace applications. Among them is this overbed canopy that provides a controlled thermal environment for burn victims. [See page A1.]*

